

**UCSF**

**UC San Francisco Electronic Theses and Dissertations**

**Title**

Representatins of electrical and acoustic cochlear stimulation in cat primary auditory cortex

**Permalink**

<https://escholarship.org/uc/item/5cj7h1nb>

**Author**

Raggio, Marcia Witte

**Publication Date**

1992

Peer reviewed|Thesis/dissertation

Representations of Electrical and Acoustic Cochlear Stimulation  
in Cat Primary Auditory Cortex

by

Marcia Witte Raggio

DISSERTATION

Submitted in partial satisfaction of the requirements for the degree of

DOCTOR OF PHILOSOPHY

in

Speech and Hearing Science

in the

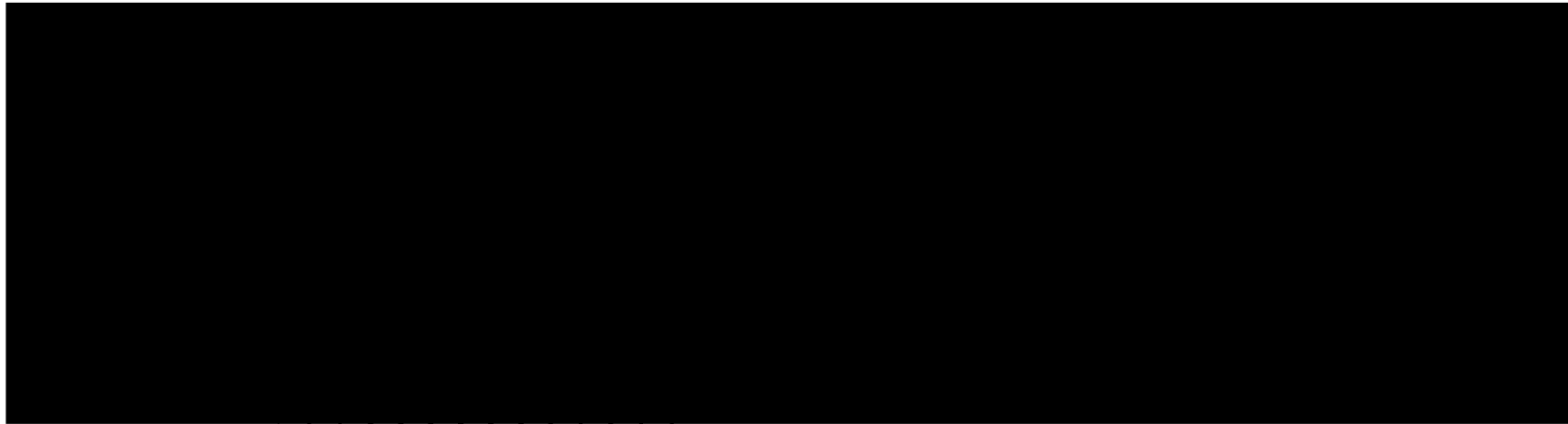
GRADUATE DIVISION

of the

UNIVERSITY OF CALIFORNIA

San Francisco

UCSF LIBRARY



Date

University Librarian

Degree Conferred: . . . 12-31-92 . . . . .



UNIVERSITY OF MICHIGAN

Copyright 1992  
by  
Marcia Witte Raggio

## **DEDICATION**

I dedicate this dissertation to Dr. Christoph Schreiner. Due to his unwavering dedication to excellence in science, I was most fortunate to be the recipient of his ever-present inspiration, knowledge, and guidance during this endeavor. His encouragement, patience, and humor were truly priceless commodities when I felt overwhelmed by the task. I can only hope that I will one day be as fine a mentor as Dr. Schreiner with his consummate scientific curiosity and his unsurpassed generosity of spirit.

UNIVERSITY OF MICHIGAN

## **ABSTRACT**

### **Representations of Electrical and Acoustic Cochlear Stimulation in Cat Primary Auditory Cortex**

**by**

**Marcia Witte Raggio**

Cochlear implant technology has been applied experimentally and clinically in the treatment of profound deafness. Early investigations of the consequences of electrical stimulation concentrated on peripheral neural units. The present studies represent preliminary steps in investigating 1) how the primary auditory cortex (AI) represents peripheral electrical stimulation, and 2) how central neuronal responses to electrical stimulation compare to those for normal acoustic stimulation. The findings of these studies may provide a working hypothesis for explaining varying cochlear implant patient performance.

Two experimental series were undertaken in which the responses of single neurons and multiple neuron clusters were evaluated in AI of the cat using acoustic and electrical pulsatile stimuli. Electrical stimuli were delivered using a four bipolar pair scala tympani electrode. In the first experimental series, a number of physiological neuronal response parameters were investigated including rate/level, latency/level, and temporal repetition coding. In the second experimental series, the distribution of several acoustic parameters were mapped in AI. Following acoustic mapping, animals were implanted and the distribution of threshold for electrical stimuli was determined using each of four radial electrode pairs and one longitudinal electrode pair at the same or nearly the same locations.

UNIVERSITY OF CALIFORNIA LIBRARY

The results of the first experimental series revealed two major relationships for electrical stimulation: response thresholds were positively correlated with response latency and negatively correlated with firing rate. This was not observed for acoustic stimulation. The second experimental series revealed two systematic distributions for electrical threshold across AI: 1) differential stimulation of each radial electrode pair revealed an area of greatest sensitivity at a cochleotopically-appropriate location in the cortex; 2) electrical threshold distribution in the isofrequency domain of AI revealed a dorsal and a ventral area of low response thresholds separated by a central area with high response thresholds. This distribution was negatively correlated with the threshold distribution for acoustic stimulation. The results of both series are consistent with the hypothesis that temporally highly coherent peripheral electrical stimulation results in stronger inhibitory effects on cortical neurons than those observed with acoustic stimulation.

Michael M Merzenich  
Committee Chairman

APR 17 1999

# TABLE OF CONTENTS

TITLE	1
1. INTRODUCTION	2
2. METHODS AND MATERIALS	14
3. RESULTS	34
3.1 Experimental Series One: Electrical and Acoustic Neuronal Response Properties	34
3.1.1 Auditory & Electrical Brainstem Response Audiometry	34
3.1.2 Response Parameters for Rate, Latency and Temporal Coding	37
3.1.3 Rate/Level Functions: Properties	38
3.1.4 Correlations of Rate/Level Function Parameters	54
3.1.5 Latency/Level Functions: Properties	58
3.1.6 Correlations of Latency/Level Function Parameters	71
3.1.7 Temporal Repetition Coding: Modulation Transfer Functions	73
3.1.8 Temporal Repetition Coding: Entrainment	87
3.1.9 Correlations of Temporal Coding Parameters	96
3.1.10 Intercorrelations of Rate, Latency, and Temporal Repetition Parameters	101
3.2 Experimental Series Two: Spatial Distribution of Electrical Response Threshold	107
3.2.1 Rostral-caudal Distributions: Cochlear Place Domain	107
3.2.2 Dorsal-ventral Distributions: Isofrequency Domain	128

UNIVERSITY OF TORONTO LIBRARY

3.2.3 Control Animals	133
3.2.3.1 Control: Implantation Two Weeks Prior to Mapping	133
3.2.3.2 Control: Deafened Three Years, Unstimulated	136
3.2.3.3 Control: Inferior Colliculus	139
3.2.4 Summary	142
3.3 Experimental Series Two: Spatial Distribution of Acoustic Response Properties	143
3.3.1 Characteristic Frequency (CF)	144
3.3.2 Intensity Parameters	146
3.3.2.1 Acoustic Threshold	146
3.3.2.2. Best Level/Strongest Response Level	151
3.3.2.3 Monotonicity of Rate/Level Functions	151
3.3.3 Bandwidth Parameters: Q10dB and Q40dB	154
3.3.4 Temporal Parameters: Latency	159
3.3.5 Binaural Interaction	159
3.3.6 Summary	164
3.4 Experimental Series Two: Comparison of Acoustic and Electrical Response Properties and Distributions	167
3.4.1 Equalization of Acoustic & Electrical Stimulus Domain	169
3.4.2 Correlation Analysis	169
3.4.3 Principal Component Analysis	186
3.4.4 Summary	197
4. DISCUSSION	201
4.1 Experimental Series One: Neuronal Response Properties	203
4.1.1 Rate/Level Functions	203

ANNEX 1 (2007)

4.1.2 Latency/Level Functions	207
4.1.3 Temporal Repetition Coding: Modulation Transfer Functions	211
4.1.4 Intercorrelation of Rate, Latency, and Temporal Repetition Parameters	215
4.2 Experimental Series Two: Spatial Distributions of Acoustic & Electrical Responses	224
4.2.1 Caudal-Rostral Domain	224
4.2.2 Ventral-Dorsal Domain	225
4.3 Comparison of Electrical Stimulations Effects in Other Auditory Stations	231
4.3.1 Auditory Nerve	231
4.3.2 Cochlear Nucleus	233
4.3.3 Inferior Colliculus	234
4.3.3.1 Response Types	234
4.3.3.2 Threshold	235
4.3.3.3 Rate/Level Functions	237
4.3.3.4 Latency	237
4.3.3.5 Spatial Tuning	239
4.4 Implications for Cochlear Implant Design & Performance	242
4.5 Summary and Conclusions	246
5. BIBLIOGRAPHY	248

## LIST OF TABLES

Table 1	Rate/Level Function Parameters	52
Table 2	Correlations of Rate/Level Function Parameters	57
Table 3	Latency/Level Function Parameters	69
Table 4	Correlations of Latency/Level Parameters	72
Table 5	Temporal Repetition Coding Parameters	86
Table 6	Correlations of Temporal Repetition Coding Parameters	99
Table 7	Correlations of Rate/Level Parameters with Latency/Level and Temporal Coding Parameters	103
Table 8	Correlations of Latency/Level Parameters with Temporal Coding Parameters	105
Table 9	Electrical Threshold Values: All Pairs, All Cases	124
Table 10	Acoustic Parameter Values: All Cases	145
Table 11	Correlations of Acoustic Parameters and Electrical Thresholds: Case by Case	170
Table 12	Correlations of Acoustic Parameters and Electrical Thresholds: All Cases Combined	185
Table 13	Principal Component Analysis for Acoustic Parameters	187
Table 14	Principal Component Analysis Including Electrical Threshold	191

ANNEX 100

## LIST OF FIGURES

Figure 1	Illustration of cochlear implant in situ	21
Figure 2	Four bipolar pair cochlear electrode	23
Figure 3	Acoustic and electrical ABR	36
Figure 4	Single unit PSTHs for electrical and acoustic click stimulation	40
Figure 5	Rate/level functions for electrical stimulation	42
Figure 6	Comparative rate/level functions for electrical and acoustic stimulation for single units	46
Figure 7	Normalized rate/level functions for electrical and acoustic stimulation	49
Figure 8	Distribution histograms of rate/level function parameters for acoustic and electric stimulation	51
Figure 9	Correlations of intensity parameters	56
Figure 10	Comparative latency/level functions for electrical and acoustic stimulation for single units	61
Figure 11	Normalized latency/level functions	63
Figure 12	Distribution histograms of latency parameters	66
Figure 13	Distribution histograms of latency/level function parameters for acoustic and electric stimulation	68
Figure 14	Repetition rate PSTHs for acoustic & electrical stimulation	76
Figure 15	Period histograms for 8Hz repetition rate	78
Figure 16	Temporal modulation transfer functions	81
Figure 17	Normalized temporal modulation transfer functions	83

ANNEX 7 (2007)

<b>Figure 18</b>	<b>Distribution histograms of temporal modulation transfer function parameters</b>	<b>85</b>
<b>Figure 19</b>	<b>Entrainment functions</b>	<b>90</b>
<b>Figure 20</b>	<b>Comparative entrainment functions</b>	<b>92</b>
<b>Figure 21</b>	<b>Distribution histograms of entrainment function parameters</b>	<b>94</b>
<b>Figure 22</b>	<b>Correlations of temporal parameters</b>	<b>98</b>
<b>Figure 23</b>	<b>Schematic representations of recording locations in AI</b>	<b>110</b>
<b>Figure 24</b>	<b>Reconstruction method for spatial distributions</b>	<b>112</b>
<b>Figure 25</b>	<b>3D reconstructions of electrical threshold distributions in AI: frontal view (C163)</b>	<b>114</b>
<b>Figure 26</b>	<b>3D reconstructions of electrical threshold distributions in AI: side view (C166)</b>	<b>117</b>
<b>Figure 27</b>	<b>3D reconstructions of electrical threshold distributions in AI: side view (C194)</b>	<b>120</b>
<b>Figure 28</b>	<b>Spatial tuning for electrical stimulation</b>	<b>126</b>
<b>Figure 29</b>	<b>Electrical threshold distribution along isofrequency domain</b>	<b>130</b>
<b>Figure 30</b>	<b>3D reconstructions of electrical threshold distributions in AI: side view (C163)</b>	<b>132</b>
<b>Figure 31</b>	<b>Electrical threshold distribution two weeks post-implantation</b>	<b>135</b>
<b>Figure 32</b>	<b>Electrical threshold distribution three years post-neonatal deafening</b>	<b>138</b>
<b>Figure 33</b>	<b>Electrical threshold distribution in IC</b>	<b>141</b>
<b>Figure 34</b>	<b>Characteristic Frequency distribution in AI</b>	<b>148</b>

UNIVERSITY OF TORONTO LIBRARY

<b>Figure 35</b>	<b>Tone threshold distribution in AI</b>	<b>150</b>
<b>Figure 36</b>	<b>Strongest response level distribution in AI</b>	<b>153</b>
<b>Figure 37</b>	<b>Slope of HLS distribution in AI</b>	<b>156</b>
<b>Figure 38</b>	<b>Q10dB distribution in AI</b>	<b>158</b>
<b>Figure 39</b>	<b>Q40dB distribution in AI</b>	<b>161</b>
<b>Figure 40</b>	<b>Onset latency distribution in AI</b>	<b>163</b>
<b>Figure 41</b>	<b>Binaural interaction distribution in AI</b>	<b>166</b>
<b>Figure 42</b>	<b>Spatial correlation of acoustic and electrical response threshold</b>	<b>175</b>
<b>Figure 43</b>	<b>Spatial correlation between electrical threshold and acoustic strongest response level</b>	<b>177</b>
<b>Figure 44</b>	<b>Spatial correlation between electrical threshold and Q40dB</b>	<b>180</b>
<b>Figure 45</b>	<b>Spatial correlation between electrical threshold and slope of HLS</b>	<b>182</b>
<b>Figure 46</b>	<b>Spatial correlation between electrical threshold and binaural interaction</b>	<b>184</b>
<b>Figure 47</b>	<b>Principal component analysis: acoustic parameters</b>	<b>190</b>
<b>Figure 48</b>	<b>Principal component analysis: electrical parameters</b>	<b>193</b>
<b>Figure 49</b>	<b>Spatial distribution of electrical and acoustic intensity factors</b>	<b>196</b>
<b>Figure 50</b>	<b>Principal component analysis of acoustic and electrical parameters</b>	<b>199</b>

**Representations of Electrical and Acoustic Cochlear Stimulation  
in Cat Primary Auditory Cortex**

**by**

**Marcia Witte Raggio**

UNIVERSITY OF MICHIGAN LIBRARY

## 1. INTRODUCTION

Cochlear implants are electrical stimulation devices that provide sound sensation to profoundly deaf individuals. This family of electrical stimulation appliances has proved to be a viable treatment for profound deafness by providing improved lipreading ability, environmental sound awareness, and various degrees of speech understanding without visual cues, i.e. open speech reception. Although many cochlear implant patients are able to understand open speech at significant levels of intelligibility, many other patients remain unable to understand more than minimal speech or none at all. Still others require long periods of experience with cochlear implant stimulation before they begin to gain open (auditory only) speech understanding. Poor or delayed speech understanding may be explained by issues involving electrode design, speech coding strategies, stimulus characteristics, anatomical limitations, patterned cochlear stimulation or limitations in central nervous system processing capacities or any combination of these or other factors. The present study was undertaken as an initial effort to provide some understanding of the central auditory nervous system representation of cochlear electrical stimulation, in particular, in the primary auditory cortex (AI), as a beginning for the evaluation of its contributions to and possible limitations for speech understanding in cochlear implant patients. Primarily, these initial studies evaluated the questions: 1) how are inputs from cochlear implant stimulation channels represented in the primary auditory cortical field? And 2) how does their representation relate to that of simple acoustic stimuli?

AMMATTI 1001

## A Brief History of Cochlear Implants

Djourno and Eyries (1957) first reported direct electrical stimulation of the auditory nerve in a totally deaf individual. A monopolar electrode was placed on the auditory nerve, with a ground electrode placed in the temporalis muscle. Stimulation with 100Hz pulsed stimuli resulted in a percept described as sounding like "crickets". The patient initially reported that his greatest benefit was an increase in lipreading ability, but was later able to understand "a few, simple words" (see Luxford and Brackmann, 1985 for review).

Three California otolaryngologists, William F. House, F. Blair Simmons, and Robin P. Michelson, working independently in the 1960s, began investigating the effects of peripheral electrical stimulation on auditory perception (e.g. House and Urban, 1973; Simmons, 1966; Michelson, 1971). These physicians and their many co-investigators began to evaluate issues such as the effects of electrical stimulus waveforms and intensity on auditory sensation, site of stimulation such as promontory versus scala tympani, tissue tolerances and safety, number of electrodes and channels, biomedical compatibility of materials, and many other efficacy issues involving the fostering of speech discrimination. At the same time, advances in electronics as a function of space technology provided smaller and better circuitry that could be incorporated into cochlear implant designs.

In the 1970s, small groups of pre- and postlingually deafened, adult patients were implanted and studied. Most patients reported experiencing an inoffensive sound sensation that helped with lipreading as well as a general awareness and even identification of some environmental sounds

UCSF LIBRARY

(Bilger, 1977).

The focus of investigation during that decade and the next was on configuring electrode designs and stimulation schemes that would provide the best stimulation of the known distributed representations of speech sounds by auditory spiral ganglion. In particular, investigations engaged issues such as the representation of place and periodicity pitch, dynamic range, and carrier and envelope timing. The efficacy of the resulting designs, across many implant centers, has not resulted in a clear consensus regarding the number of electrodes or the number of stimulator channels necessary for normal or near-normal speech understanding as significant performance has been demonstrated using multi-channel/multi-electrode (Dowell, et al., 1986; Dankowski, et al., 1988; Schindler and Kessler, 1989; Doyle, et al., 1991), single channel/multi-electrode (Owens, et al., 1983), and even single channel/single bipolar electrode (Gantz, et al., 1989; Doyle, et al., 1991) designs. However, it has become clear that bipolar electrode stimulation that allows for more discrete stimulation of auditory nerve fibers is superior for speech understanding than is monopolar, single electrode stimulation (Theilemeir, 1983).

To date, there are many clinical cochlear implant patients with a substantial ability to understand open speech, using a variety of implant designs and speech coding strategies (Dowell, et al., 1986; Schindler and Kessler, 1987; Dankowski, et al., 1988; Schindler and Kessler, 1989; Wilson, et al., 1989; Wilson, et al., 1991; Doyle, et al., 1991). Of particular interest, however, is the finding that the implant patient described in 1957 (see above) was eventually able to understand a few words. In addition, a large number of new implant patients who do not experience initial open speech understanding develop the ability to understand speech

UNIVERSITY OF CALIFORNIA LIBRARY

to some extent over the ensuing weeks, months, and even years. Schindler and Kessler (1987) evaluated the open speech understanding of eighteen multi-channel patients (UCSF/Storz device) initially after implantation, and sequentially at 6-8 weeks post-implantation, 6 months post-implantation, and one year post-implantation. The results of this investigation on open speech items from the Minimal Auditory Capabilities Battery (MAC) (Owens, et al.,1985) revealed steady improvements in open-set spondee recognition, monosyllabic words, and sentences ranging from 16% to 72%, 2% to 32%, and 9% to 64%, respectively. Spivak and Waltzman (1990) found similar results for fifteen patients using the Nucleus 22-channel cochlear implant who were evaluated at three months post-implantation, and then at one, two, and three years post-implantation. Using the same MAC Battery subtests, they demonstrated that the greatest improvement in speech understanding occurred within the first three months post-implantation, but that many patients continued to improve over the ensuing three years. Mean percent improvement for all open set speech tests was 8% for patients who had no open set speech understanding at 3 months post-implantation and 41% for patients who did have some open speech understanding at three months post-implantation.

Of note is the fact that none of the patients in either longitudinal study underwent directed auditory training. Therefore, these improvements in speech understanding were the result of everyday, experiential listening with their cochlear implants. This suggests that everyday exposure to sound stimuli and in particular to speech stimuli with a cochlear implant may lead to functional adjustments in the central auditory system that allows for the conversion of distorted speech perceptions into salient stimuli, i.e. to a measurable improvement in open speech understanding over time. The cerebral cortex has been identified as a site that exhibits

UCSF LIBRARY  
APR 17 1997



Robertson and Irvine (1989) evaluated the effects of discrete basilar membrane lesions on the representation of the lesioned frequencies in the rostral auditory cortical field of the guinea pig. Approximately one month after peripheral lesioning, auditory cortical mapping studies revealed that cortical neuron clusters with initial characteristic frequencies (CF) in the range of the peripheral lesion subsequently exhibited CFs slightly higher or lower, with nearly normal thresholds. That is, there was a neuronal loss of sensitivity in the cortical area originally responsive to the lesioned frequencies with a concomitant expansion of the representation of the lesion margin frequencies that completely or almost completely occupied that area. In control studies in which the cortex was mapped within a few hours after peripheral lesions, it was found that the lesioned frequencies were still represented cortically, but with much higher thresholds. These results indicate a gradual rather than a sudden emergence of the low-threshold representation of the margin CFs.

In another class of experiments, auditory cortical plasticity has been demonstrated by classical conditioning studies (Thompson, et al., 1972; Disterhof and Stuart, 1976; Kitzes, et al., 1978; Weinberger, et al., 1984; Diamond and Weinberger, 1986, 1989; Weinberger and Diamond, 1987). The results of these experiments show significant increases or decreases in discharge activity in auditory cortical cells following the associative pairing of an acoustic conditioned stimulus (CS) with an unconditioned stimulus (US). Since the extent of these physiological changes did not occur during sensitization, or when the two stimuli were unpaired, it is clear that the associative process played the most salient role in discharge plasticity. In two studies, in particular, (Diamond and Weinberger, 1986; Weinberger and Diamond, 1987) learning-induced changes to a conditioned stimulus revealed that discharge plasticity is not

1987 1989  
1984 1986 1987

simply the result of general changes in cellular excitability, but rather, results from alterations in the signal processing that are specific to the stimulus. That is, experiments in cats revealed changes in the frequency receptive fields of single auditory cortical neurons that were specific to the frequency (or narrow band of frequencies) of the CS. Thus, learning can cause specific changes in the distributed cortical representations of sound stimuli that have acquired significance, i.e. classical conditioning results in a substantial increase or decrease in the evoked activity of single neurons to a CS of a particular frequency or narrow band of frequencies. These findings suggest that auditory cortical neurons function adaptively and are able to alter their functional selectivity with alterations of inputs or when the stimulus bears particular significance.

In a third class of plasticity experiments, Recanzone and colleagues (1993) used operant conditioning techniques to train owl monkeys in a frequency same/different discrimination task. The animals were required to discriminate between tones of differing frequencies. Following two to three months of training, the animals demonstrated marked improvement in their discrimination performance. After the training period, mapping experiments were undertaken in the primary auditory cortices of these animals that revealed a several-fold increase in the cortical area devoted to the trained frequencies relative to the area normally allocated to them. The representational expansion was not seen in control animals that received equivalent exposure to the experimental stimuli, but were not required to attend to them. Therefore, it can be concluded that behavioral relevance is a key factor in the invocation of cortical reorganization.

Along with the investigation of the central representation of cochlear electrical stimulation, a further goal of the present study is to begin to

UNIVERSITY OF TORONTO LIBRARY

understand the mechanisms of cortical adaptability that may underlie the conversion (or the lack of conversion) of distorted speech perceptions into understandable speech stimuli over time.

### Topography of Physiological Parameters in Primary Auditory Cortex

Before central topographic response distributions using peripheral electrical stimulation can be fully appreciated, they must be evaluated with regard to the distributions of physiological parametric responses using acoustic stimulation in the same neuronal population. Several studies have been conducted in the primary auditory cortex of cats that reveal the distributions of a number of physiological response parameters. Microelectrode studies of AI neurons (Merzenich, et al., 1975; Reale and Imig, 1980) have revealed an orderly representation of characteristic frequency across the rostrocaudal dimension of AI with lowest frequencies represented caudally and highest frequencies represented rostrally. Orthogonal to this rostrocaudal dimension are roughly straight, parallel isofrequency contours aligned successively across the width of the primary field, i.e. a given frequency is represented along several millimeters of cortical space.

A number of other physiological response distributions in the primary auditory cortex of cats have also been investigated. Studies of the functional distribution of excitatory bandwidth (Q10dB and Q40dB) using multiple unit recordings have been undertaken (Schreiner and Cynader, 1984; Schreiner and Mendelson, 1990). Pure tone stimuli were used to determine the spectral range that produced an excitatory response of AI neurons. The range of frequencies generating an excitatory response at 10 and 40dB above threshold provides an estimate of the sharpness of the

UCLA LIBRARY

frequency tuning for a given neuron. The spatial distribution of Q10dB and Q40dB values revealed neurons in an area of central AI running orthogonal to the isofrequency gradient with relatively high values or sharp tuning bordered by areas of relatively low values or broader tuning on the ventral and dorsal sides. In summary, the topographic distribution of excitatory bandwidth response across AI was not uniform with an area of sharp tuning in central AI surrounded on the ventral and dorsal sides by neurons with relatively broad tuning.

In another study by Schreiner and Sutter (1992), the distribution of excitatory bandwidth at 10dB and 40 dB above threshold was determined for single and multiple unit neuronal recordings in AI. The results of this study concurred to some extent with those above in that the spatial distribution of sharpness of tuning of multiple units along the dorsoventral extent of AI revealed an area of sharpest tuning in central AI with areas of broader tuning in the ventral and dorsal regions. For single neurons, however, the non-uniformity in the bandwidth distribution was not a V-shaped phenomenon as noted above. Rather, the dorsal half of this distribution was similar to that for multiple units (broad tuning), but neurons in the ventral half showed relatively sharp tuning similar to that previously noted in central AI. The Q10dB distribution for single units was markedly different, showing no clear systematic spatial distribution across the dorsoventral extent of AI. An explanation for the difference in tuning behavior in ventral AI between multiple and single units may be found in the influence of CF scatter. The center of AI is sharply tuned for both single and multiple units and, therefore, the single unit CF scatter at any given location must be small. However, in the dorsal, and particularly in the ventral regions, the local scatter must be large to result in broad multiple unit tuning while maintaining sharp single unit tuning. Therefore,

UNIVERSITY  
OF CALIFORNIA  
LIBRARY

broadly tuned multiple units can emerge in the face of sharply tuned single units as representing the total integrated excitatory response of the entire recording site (Schreiner and Mendelson, 1990).

The spatial distribution of a number of tone intensity parameters in AI has also been investigated in multiple unit studies by Schreiner, Mendelson, and Sutter (1992). The distribution of response thresholds to contralateral stimulation of CF tones along the dorsoventral extent revealed an area of lowest threshold in the central region of AI with relatively higher thresholds in the ventral and dorsal regions. The spatial distribution of monotonic or non-monotonic growth of firing rate as a function of intensity reveals a similar segregation of values such that a region in central AI contains neurons that are highly non-monotonic with more monotonic neurons found in the dorsal and ventral regions (Phillips et al., 1985). In addition, a second region of highly non-monotonic neurons is found in the most dorsal extent of AI (Schreiner et al., 1992). Best level or strongest response values, or the stimulus level producing the highest firing rate for a CF tone, revealed a segregation not unlike those already mentioned for response threshold and monotonicity. That is, an area in central AI revealed recording locations with the lowest best levels that increased systematically toward the ventral and dorsal regions, suggesting that AI contains a systematic representation of sound intensity.

Other response parameters that appear to be non-randomly distributed across AI are onset latency to tone stimulation and preference for the speed of frequency sweeps. The shortest onset latencies and a preference for slow frequency sweeps were found near the dorsal half of the center of AI with increasing latencies and a preference for faster frequency sweeps toward the dorsal and ventral boundaries (Schreiner, et al., 1988;

UNIVERSITY OF CALIFORNIA LIBRARY

Mendelson, et al., 1993).

A final physiological response distribution to be discussed is that of binaural interaction type. Microelectrode studies have revealed elongated spatial aggregates of neurons oriented orthogonally to the isofrequency axis in AI that respond with an excitatory response with stimulation of either ear (excitatory-excitatory or EE, binaural summation), or with an excitatory response to stimulation of the contralateral ear but with an inhibitory response with stimulation of the ipsilateral ear (excitatory-inhibitory or EI, binaural suppression) (Imig and Adrian, 1977; Middlebrooks, et al., 1980).

To summarize, the studies of the topographic response distributions of a variety of physiological parameters in primary auditory cortex, have revealed systematic organizational constructs across the ventral-dorsal isorepresentational domain of this functional area. Using acoustic stimulation, neurons in the central sector of AI respond with sharper frequency tuning, lower thresholds, lower best levels, and relatively sharper intensity tuning, i.e. high non-monotonicity. The ventral and dorsal regions generally respond with near-opposite responses. This confluence of response parameters in the central region, that differs from the response parameters in the dorsal and ventral regions, suggests that there are at least three distinctly different functional areas across the dorsal-ventral extent of AI.

### Specific Aims

The spatial distributions of physiological responses in primary auditory cortex using acoustic stimulation offer a very complex yet systematic

1987 1991  
LIBRARY



## 2. METHODS and MATERIALS

Neuronal responses in the auditory cortex evoked by acoustical and/or electrical stimulation of the cochlea were recorded from the right hemisphere of twelve healthy, adult cats (*felis catus*). Animals were obtained from a breeding colony at University of California at San Francisco. Inspection of the outer ear canals and the tympanic membranes revealed no signs of abnormalities. Minimum response thresholds of click-evoked auditory brainstem responses (ABRs) and of cortical neurons were within normal range. In two animals, responses were exclusively obtained for contralateral electrical cochlear stimulation. In six animals, acoustic responses from the ear contralateral to the studied hemisphere were obtained prior to the implantation of the cochlear electrode array. In four animals, acoustically-evoked responses from the ipsilateral ear were obtained in the course of recording responses resulting from contralateral cochlear electrode stimulation. In one of these cases, electrically evoked responses were also obtained in the central nucleus of the inferior colliculus.

### Experimental Series One: Neuronal Response Properties

#### Experimental Protocol

In this series, a number of response properties of auditory cortical neurons were evaluated for electrical pulse as well as acoustical click stimulation. Electrical stimulation was delivered via intracochlear electrodes. Acoustical stimulation was delivered via head-mounted

UNIVERSITY OF CALIFORNIA LIBRARY

earphones to the ipsilateral ear. Monaural or binaural deafening occurred at varying procedural intervals for the different experimental protocols used in this series. Two electrical stimulating conditions were investigated, one using the "best radial electrode pair", i.e. the pair with the lowest threshold (depending upon cortical location), and the second using a longitudinal electrode pair comprised of one apical-most and one basal-most electrode contact. Microelectrode recordings of single and multiple unit activity was undertaken for a range of stimulus parameters. Response profiles for electrical and acoustical stimulating conditions were reconstructed and compared.

### Deafening Procedures

Prior to implantation of the intracochlear electrode and recording from cortical cells, the animals were deafened using one of three procedures: 1) acutely by electrode insertion; 2) acutely by intrascalar injection of neomycin sulfate (20% solution, 25 $\mu$ l); 3) chronically, by a series of daily intramuscular injections of neomycin sulfate beginning 24 hours after birth for 16-21 days at 50mg/kg/day. The progressive decrement in hearing was tracked using click-evoked auditory brainstem response audiometry either daily for the animals deafened by systemic injection, or for approximately one hour beginning immediately after intrascalar injection. Animals were tracked until no ABR responses could be recorded for levels below 100 dB SPL. In animals presumably deafened by electrode insertion, an electrically evoked ABR (EABR) was measured after insertion, but the EABR was not tracked over time since earlier studies (Snyder, et al., 1990) found that there was no difference in the physiological behavior

UNIVERSITY

or EABR thresholds or waveform of inferior colliculus neurons between animals that had been acutely deafened and implanted and those that had not been deafened, but acutely implanted.

### Anesthesia and Surgery

Six adult cats were used in the initial series of experiments. Animals were initially sedated with an intramuscular injection of a 4:1 mixture of Ketamine hydrochloride (10 mg/kg) and acepromazine maleate (0.10 mg/kg). While sedated, animals' heads and forelimb surfaces were shaved and an intravenous catheter inserted into the cubital vein. Sterile Ringer's solution was continuously infused through the catheter. After venous cannulation, an initial dose of sodium pentobarbital (40 mg/kg) was administered. Anesthesia was maintained at areflexic levels with supplementary intravenous injections of sodium pentobarbital, and during experimental procedures with a continuous infusion of sodium pentobarbital (2mg/kg/hr) in lactated Ringer's solution (infusion volume 3.5 ml/h). The animals were also administered dexamethasone sodium phosphate (0.14 mg/kg) to prevent brain edema, atropine sulphate (0.5cc IM) to reduce salivation, and prophylactic antibiotic treatment (Penicillin G100K units). Following the initial dose of sodium pentobarbital, a tracheotomy was performed and a tracheal tube placed to ease breathing, and to reduce breathing noises. The body temperature of the animals was maintained at 37.5C by means of a heated water blanket with feedback control.

1981  
LIBRARY

### Surgical Exposure of the Cortex

The animal's head was mounted in a standard mouth-bar head holder leaving the external meati unobstructed. The temporalis muscle was then retracted and the right lateral cortex was exposed by craniotomy and dural reflection. Since the area of the basilar membrane subtended by the scala tympani electrode was restricted to the most basal 8mm, only the presumed central and rostral-most sectors of primary auditory cortex were exposed and mapped. The exposed cortical region was covered with silicone oil and a video image of the surface vasculature obtained with a CCD camera, an image capture board (Data Translation DT2255) and capture software (Image 1.4, NSCA). Electrode penetration sites were marked on drawing layers mounted over these images of the cortical surface vasculature in a display program (Canvas, Deneba).

### Implant Surgery

Following the craniotomy, experimental animals underwent acute deafening using intrascalar injections of neomycin sulfate. Two control animals in which electrical stimulation was the sole stimulating condition, were either chronically deafened, or were functionally deafened by electrode insertion. All animals then underwent acute cochlear implantation under non-sterile conditions. An elliptical incision was made through the scalp and a posterior temporalis muscle flap created. The bulla was then exposed and opened, thereby exposing the round window. The round window membrane was opened and the intracochlear electrode inserted into the scala tympani. Once in place, the silastic electrode

UNIVERSITY OF CALIFORNIA LIBRARY

carrier was secured to the promontory and under the temporalis flap using a butyl cyanoacrylate adhesive (Histoacryl®).

### Electrical Auditory Brainstem Responses (EABR)

Prior to the response measurements for electrical stimulation, EABRs were recorded for each electrode pair. EABRs were recorded, differentially amplified (100,000x), and bandpass filtered 100 Hz to 3 kHz. Recordings were made using silver wires inserted through the skin. The active electrode was placed at the vertex and the reference placed just below the stimulated ear. The ground was located at the nape of the neck or under the contralateral ear. Responses were averaged for 500 presentations of 20pps at several stimulus levels.

### Electrode Design

The electrodes used in these studies consisted of eight PyreML® coated, platinum-iridium wires (90%:10%) embedded in a silastic carrier and each of which ended in a modified ball contact (100µm diameter). The contacts were arranged in four near-radial pairs. The individual ball contacts of each radial pair were approximately 0.25mm wide with a separation between radial pair contacts of 0.25 to 0.5mm. The separation between electrode pairs was typically 2mm, however, individual cases had a separation range of 1.5 to 3mm. Commonly, the total separation between the apical- and basal-most pairs was 6mm. The electrode was designed such that when fully inserted, the apical-most pair reached an insertion depth of approximately eight millimeters from the round window,

UNIVERSITY  
LIBRARY

approximately 12 mm from the extreme cochlear base. Since the carrier extended approximately 1 mm beyond the apical pair, the entire carrier length was approximately 9 mm. The orientation of the electrodes in situ was such that one contact of each pair was located just below the habenula while the other, radially-oriented contact was rotated 90 degrees toward the modiolus at the level of the spiral ganglion (see Figure 1). Figure 2 shows a schematic drawing of the electrode with Pair 1,2 located at the most apical end of the carrier and Pair 7,8 at the most basal end. The electrode design for two control animals differed from the above description in the number of electrode contacts, the radial electrode contact separation, and the overall length of the carrier, i.e. three pairs or six contacts with a radial separation of 1 mm and an insertion depth of approximately 10 mm from the basal extreme of the cochlea (Snyder, et al., 1990).

### Stimulus Generation

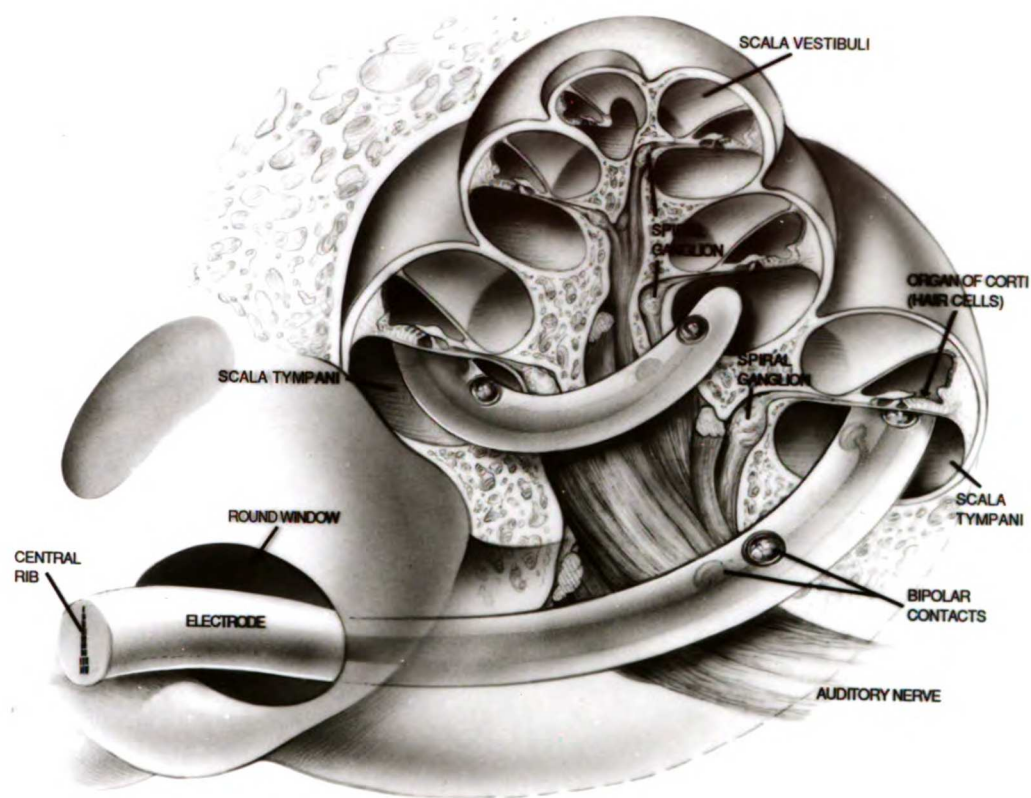
Electrical and acoustical pulse stimuli were generated and controlled by a signal processing computer (TMS32010) and converted to an analog signal by a 16 bit digital-to-analogue converter running at a 60 kHz sampling rate. A low impedance attenuator was used to control electrical current in a range from 1  $\mu$ Amp to 30 mAmps. After attenuation, electrical stimuli were delivered via a specially designed stimulus isolation voltage-to-current amplifier calibrated to deliver a 100  $\mu$ Amp output for an input of one Volt into an output impedance of up to 100 k $\Omega$  (Vureck et al., 1981). Stimuli were then delivered to an electrode pair switch box connected by cable to the electrode connector at the animal's

UNIVERSITY OF TORONTO LIBRARY

**Figure 1. Illustration of a multiple bipolar electrode cochlear implant in situ in a right human cochlea. The electrode is introduced into the scala tympani through the round window.**

AMERICAN LIBRARY

FIGURE 1



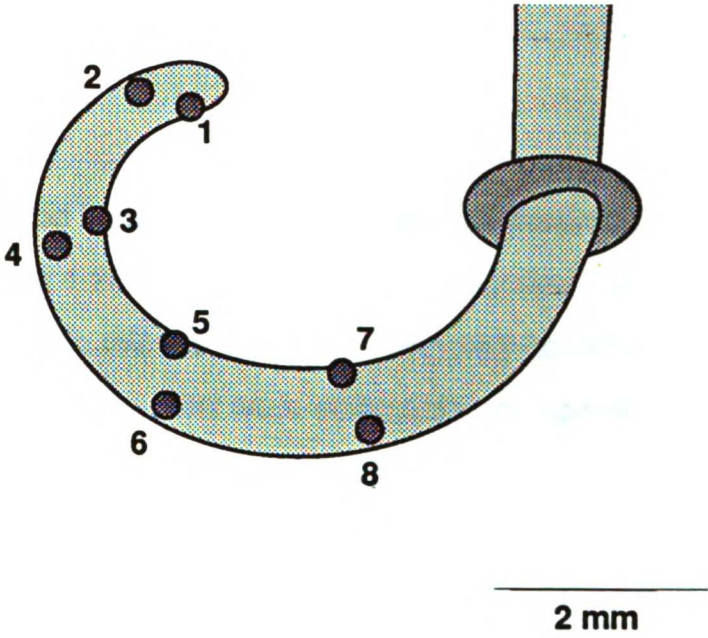
UCSF LIBRARY

**Figure 2. Schematic illustration of a model four bipolar pair cochlear electrode. Electrode contacts are numbered 1 through 8 from apical to basal arranged in four radial or near radial pairs. Stimulation of contact 1 and 7 or 1 and 8 serve as a longitudinal electrode pair. The cuff around the electrode serves as an anchor that is secured to the temporal bone at the round window.**

1957 LIBRARY

FIGURE 2

**Schematic Representation of a Four Bipolar Pair Feline Cochlear Implant Electrode**



UCSF LIBRARY

head that allowed for discrete stimulation of each pair independently. Typically, electrical stimuli consisted of capacitively coupled, charge balanced, biphasic square wave pulses (200 $\mu$ s/phase), delivered at 1-2 pps and with an interstimulus interval of 500 to 1000 ms. For one set of measurements, interstimulus intervals were systematically varied between 500ms (2Hz) and 26.3ms (38Hz). Electrical current levels were expressed in dB re 100 $\mu$ A. Acoustic pulse stimuli were identical to the electrical pulse stimuli in terms of duration and intervals. Sound intensity for pulses was calibrated in dB SPL with the sound level meter (Bruel and Kjaer) in fast impulse mode.

### Recording Procedure

Parylene-coated tungsten microelectrodes (Microprobe) with impedances of 0.8 to 1.2Mohm at 1kHz were introduced into the auditory cortex with an hydraulic microdrive (KOPF) remotely controlled by a stepping motor. All penetrations were essentially orthogonal to the brain surface. The recordings reported here were obtained from 24-100 penetrations per case, and were made at intracortical depths ranging from 600-1200 $\mu$ m as determined by the microdrive setting. Activity of single neurons and small clusters of neurons were amplified, band-pass filtered, and monitored on an oscilloscope and an audio monitor. Spike activity was sought using various stimulus intensities while advancing the recording electrode. Spike activity was isolated from the background noise with a window discriminator (BAK DIS-1) using action potential amplitude and waveform criteria. The number of spikes per presentation and the arrival time of each spike were recorded and stored in a computer (DEC 11/73).

UNIVERSITY OF CALIFORNIA LIBRARY

The recording window had a duration of 320-1200 ms.

### Parametric Response Measurements

The following parametric response measurements were made for single unit recordings:

**Rate/Level Functions:** A measure of firing rate as a function of increasing stimulus intensity. For most cases, firing rate was measured serially for a stimulus intensity level range of 25dB in steps of two to three dB. These measurements were made using the 'best' radial pair (the pair with the lowest response threshold, i.e. dependent on recording location in cortex), the longitudinal pair (Pair 1,7 or 1,8), and for ipsilateral acoustic click stimulation when possible. From these functions the following measurements were made:

***threshold level (dB):*** the level at which the firing rate exceeded spontaneous firing rate by two spikes/30 signal presentations.

***transition point (dB):*** a subjectively determined level at which the low-level segment of the rate/level function, exhibiting a rapidly growing firing rate, changes into a high-level segment with slower growth, saturation or decline of firing rate for increases in stimulus level.

***transition point rate:*** the firing rate at the point of transition.

***dynamic range (dB):*** the difference in level between the threshold and the

1987 LIBRARY

transition point.

*low level segment slope (%/dB):* in rate/level functions that display a transition point, the rate of change in firing rate of the low-level segment, the slope from threshold to transition point, is estimated by linear regression.

*high level segment slope (%/dB):* estimation of the rate of change in firing rate for higher level values, i.e. the slope from the transition point to the highest stimulus intensity applied.

Latency/Level Functions: A measure of the peak response latency as a function of level. Peak response latency is the latency at which the highest spike activity occurred, and was measured serially at stimulus intensity levels of 5 to 28dB. These measurements were made using the 'best' radial pair, the longitudinal pair (Pair 1,7 or 1,8), and ipsilateral acoustic click stimulation when possible. From these functions, the following measurements were made: minimum latency, latency at the transition point between the two segments of the response function, average latency of the high level segment, the latency standard deviation of the high level segment ('latency coherence'), the slope of the low level segment, the slope of the high level segment, and the transition point level.

Temporal Repetition Coding: A measure of the frequency following or stimulus repetition following capacity of cortical neurons was obtained by presenting one second trains of pulses with different interpulse intervals.

UNIVERSITY OF TORONTO LIBRARY

Between each pulse train was a pause of one second. Constructions of temporal repetition or temporal modulation transfer function (tMTF) involved the measurement of firing rate at serial stimulus repetition frequencies ranging from 2 to 38Hz. These measurements yield a typical function that allowed an estimation of the range and type of repetition coding at a cortical location, e.g. band-pass or low-pass types with high or low limiting repetition frequencies. Typically, stimuli were delivered at 5-15 dB above response threshold. These measurements were made using the 'best' radial pair, the longitudinal pair (Pair 1,7 or 1,8), and ipsilateral acoustic click stimulation when possible. From these functions the following response characteristics were obtained:

*best modulation frequency (BMF):* repetition rate producing the maximum firing rate.

*high and low cut-off frequency:* the repetition rates at response magnitudes of -6dB from BMF (50% of maximum firing rate) on the high and low sides of the tMTF.

*entrainment:* the number of spikes occurring per stimulus pulse.

*entrainment cut-off (6dB):* the repetition rate for entrainment 6dB below maximum entrainment.

*entrainment cut-off (0.25):* the repetition rate for entrainment of 0.25 spikes per pulse (spp).

AMM 17 1997

## Data Representation

One method of data representation throughout these studies is the use of three-dimensional reconstructions that represent the spatial distributions of parametric responses across the primary auditory cortical surface. These reconstructions were performed with a software package (Surfer® Golden Software) using standard methods for pseudo-three dimensional representation applied in geological studies to represent terrain. The methods are based on an interpolation algorithm that weights the ten nearest neighboring points according to an inverse distance law, and calculates the values necessary for a complete description of the mapped area. The actual spatial locations of the recording sites were used to generate a two-dimensional grid of the represented area by projecting the actual sites to the nearest grid point. A third dimension, elevation of the grid, corresponds to the spatially averaged local magnitude of a functional parameter at a given site.

## Experimental Series Two: Spatial Response Distributions

### Experimental Protocol

Six additional animals were used in these studies in which each experiment consisted of two parts. The initial objective was to determine the spatial distributions of physiological response characteristics in the primary auditory cortex (AI) of the adult cat using contralateral acoustic stimulation. This was accomplished by sampling multiple unit neuronal responses at depths of 850 to 950 microns at 50 to 90 cortical locations.

UNIVERSITY OF CALIFORNIA LIBRARY



allowing a 3-bit amplitude resolution at the lowest level used. Additional attenuation was provided by a pair of passive attenuators (Hewlett Packard). Stimuli up to 110 dB SPL could be delivered through the speaker system. The duration of each tone burst was usually 50 ms, except when it was extended to 85 ms for cortical locations with long-latency responses. The rise/fall time of the tone bursts was 3 ms. The interstimulus interval was 400-1000 ms.

### Frequency Response Areas

Frequency response areas (FRAs) were obtained at each penetration site. To generate an FRA, we delivered 675 different tone bursts. Tone bursts were presented in a pseudorandom sequence of different frequency-level combinations selected from 15 level values and 45 frequency values. Steps between levels were 5dB resulting in a sampled dynamic range of 75dB.

The frequency range covered by the 45 frequency steps was centered around the estimated characteristic frequency (CF) of the recording site and covered between two and five octaves, depending upon the estimated width of the frequency tuning curve. Stimulus frequencies were chosen so that the 45 presented frequencies were spaced an equal fraction of an octave over the entire range. For most cases this provided a 0.067-octave resolution over a total of three octaves. Usually each stimulus parameter combination was presented only once. Occasionally, a second or third complete presentation of the stimulus set was necessary to derive consistent FRAs.

UNIVERSITY OF CALIFORNIA LIBRARY



***Best Level/Strongest Response:*** the stimulus level at which the highest firing rate occurs.

***Q-10, Q-40dB:*** CF divided by the bandwidth of an FRA 10dB or 40dB above minimum threshold.

***Monotonicity:*** slope of the high-level segment of rate-level functions, i.e. for levels above the transition point.

***Latency:*** the minimum latency at CF.

***Binaural Interaction Class:*** the magnitude of the spike response from stimulation of the contralateral ear was comparatively evaluated with the addition of stimulation of the ipsilateral ear using audiovisual criteria. Excitatory-excitatory (EE) neurons showed an excitatory response for stimulation of either ear and often showed an increase in contralateral response level/activity with addition of stimulation of the ipsilateral ear. Excitatory-Inhibitory (EI) neurons showed a decrease in contralateral response/activity with the addition of stimulation of the ipsilateral ear. Usually, the ipsilateral stimulus alone did not produce an excitatory response. Monaural responses (EO) showed no contralateral change with the addition of stimulation of the ipsilateral ear and the ipsilateral stimulus did not produce an evoked response on its own.

#### **Parametric Response Measurements: Electrical Stimulation**

Threshold mapping was the singular goal of electrical stimulation in

1001 LIBRARY



### **3. RESULTS**

The results of the present study will be described in four primary sections that encompass the findings from Experimental Series One and Two: 1) electrical and acoustic neuronal response properties in terms of rate/level functions, latency/level functions, and temporal repetition coding including correlation analyses (Experimental Series One); 2) spatial distributions of electrical response threshold in AI (Experimental Series Two); 3) spatial distributions of acoustic response properties in AI (Experimental Series Two); 4) comparison of acoustic and electrical response properties and distributions (Experimental Series Two).

#### **3.1 Experimental Series One: Electrical and Acoustic Neuronal Response Properties**

##### **3.1.1 Auditory and Electrical Brainstem Response Audiometry**

Auditory (ABR) and electrical brainstem responses (EABR) were used in this study to 1) monitor progressive intracochlear deafening, and 2) evaluate the effectiveness of electrode placement. Figure 3 (A) shows auditory brainstem responses for an animal that had been deafened using an intrasclerous injection of neomycin sulfate. At 65dB SPL stimulation intensity using auditory click stimuli, a robust response can be seen prior to neomycin administration. At 2 minutes post-neomycin administration, a clear decrement in amplitude with minimal changes in latency was observed. Essentially no response was observable at 10 minutes post-neomycin administration.

Figure 3 (B) and (C) are examples of electrical auditory brainstem

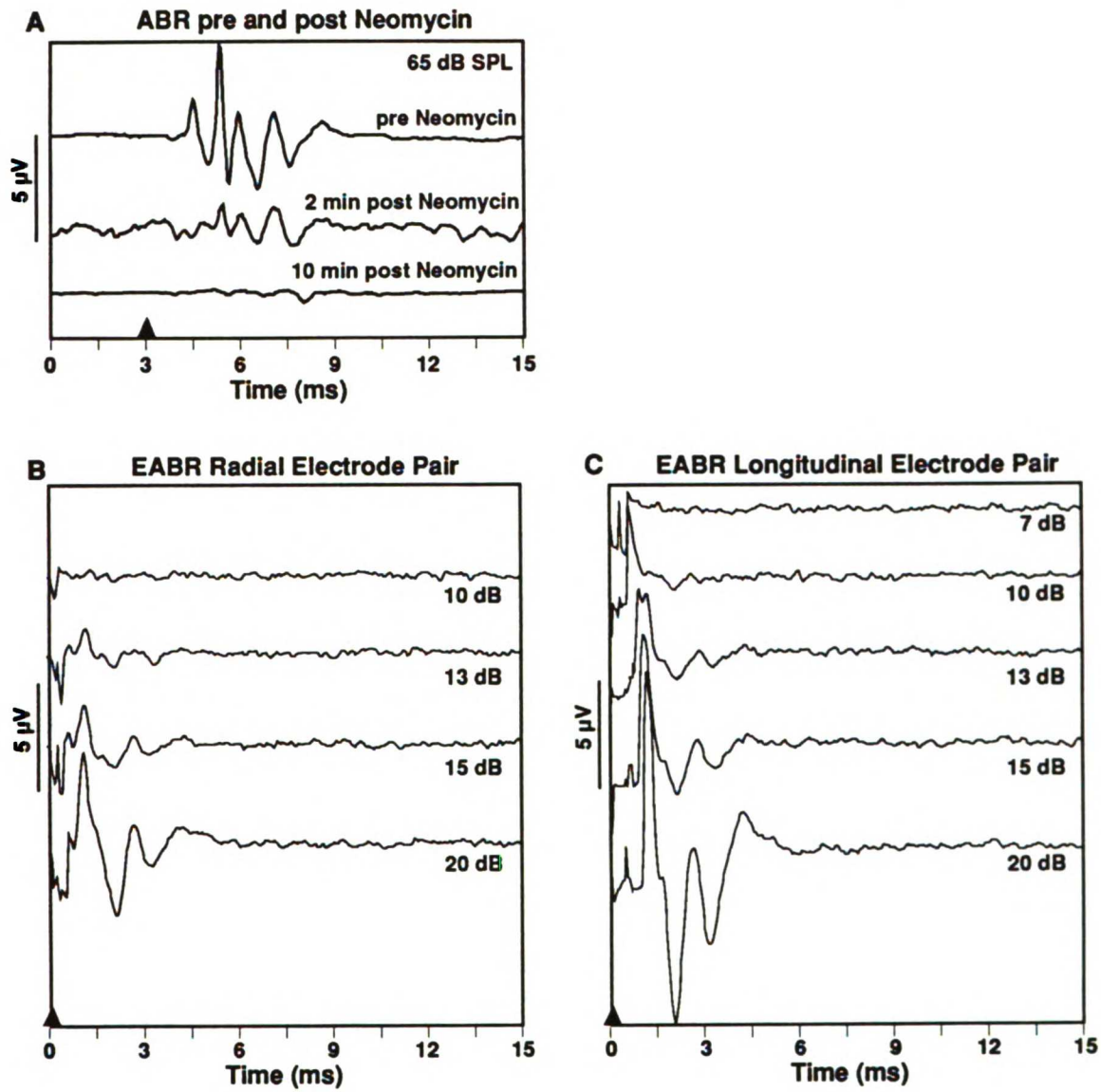
LIBRARY  
UNIVERSITY OF CALIFORNIA  
SAN DIEGO

**Figure 3. Acoustic and electrical auditory brainstem responses (ABRs). A) Acoustically evoked ABRs pre- and post-neomycin sulfate scalar injection are shown. B) and C) Exemplary intensity series for electrical ABRs (EABRs) evoked with a radial and longitudinal electrode pair are seen. All traces are averages of 500 stimulus presentations (0.5ms/phase, 20pps).**

UNIVERSITY OF CALIFORNIA LIBRARY

FIGURE 3

Acoustically and Electrically Evoked Brainstem Response



UCSF LIBRARY

responses using pulsed stimulation (0.5ms/phase, 20 pulses/second) for a radial and a longitudinal electrode pair. The EABRs for the longitudinal pair (C) showed slightly lower thresholds and higher response magnitudes than those for the radial electrode pair (B). The range of EABR thresholds across all cases was 5 to 20dB for the best radial pair and 3 to 15dB for the longitudinal pair. The other radial pairs showed thresholds that were typically within 5dB of these values for the best radial.

### 3.1.2 Response Parameters for Rate, Latency, and Temporal Coding

Response of 89 single units and 32 multiple units to contralateral, bipolar cochlear stimulation with short pulses were recorded in the primary auditory cortex of six animals. In addition, responses were recorded for ipsilateral acoustic click stimulation for the same neurons. These measurements were made primarily for two electrode stimulation configurations, a radial pair and a longitudinal pair. Since little is known about the physiological behavior of primary auditory cortical neurons in response to peripheral electrical stimulation, a large number of parameters were measured and examined. The primary goals of this evaluation were: 1) to determine physiological response characteristics of these central neurons and compare them in terms of functional, stimulating mode-specific similarities and differences, and 2) to determine which descriptive parameters revealed the most significant information and which could be eliminated due to minimal information or redundancy.

Rate versus level, latency versus level, and temporal repetition rate functions were also determined for the same neurons for an acoustic click stimulus presented ipsilaterally to the studied cortical hemisphere.

UNIVERSITY  
LIBRARY

However, since either only a limited number of neurons responded to ipsilateral acoustic stimulation with action potentials, or for a number of samples contact with the neuron was lost before acoustic stimulation could be presented. Therefore, only about a third of sampled neurons contributed to the acoustic response data. It should be noted that some parametric values of acoustic and electrical rate/level functions are not directly comparable without intensity scale corrections, due to the differences in the intensity scales for those two conditions. In spite of this limitation, the overall shapes and parametric relationships of these rate/level functions are consistent across different modes of stimulation, justify the initial inclusion of the acoustic parameters in this comparison, and provide a basis for making an intensity scale correction.

### 3.1.3 Rate/Level Functions: Properties

Representative examples of post-stimulus time histograms (PSTHs) for the radial and longitudinal electrical stimulation and for acoustic click stimulation are shown for one neuron in Figure 4. For all three conditions, a clear phasic response with a short response latency was seen in response to pulsatile stimulation. In some cases, a second, late response was also present. From the PSTHs, rate/level functions were constructed by measuring the firing rate of the initial response (20ms recording window width).

Figure 5 shows exemplary rate/level functions for two single units (A,B) and two multiple units (C,D) for all four radial electrode pairs, and for one longitudinal electrode pair. An analysis of these rate/level functions reveals a number of common cortical physiological characteristics. Different electrode configurations have different

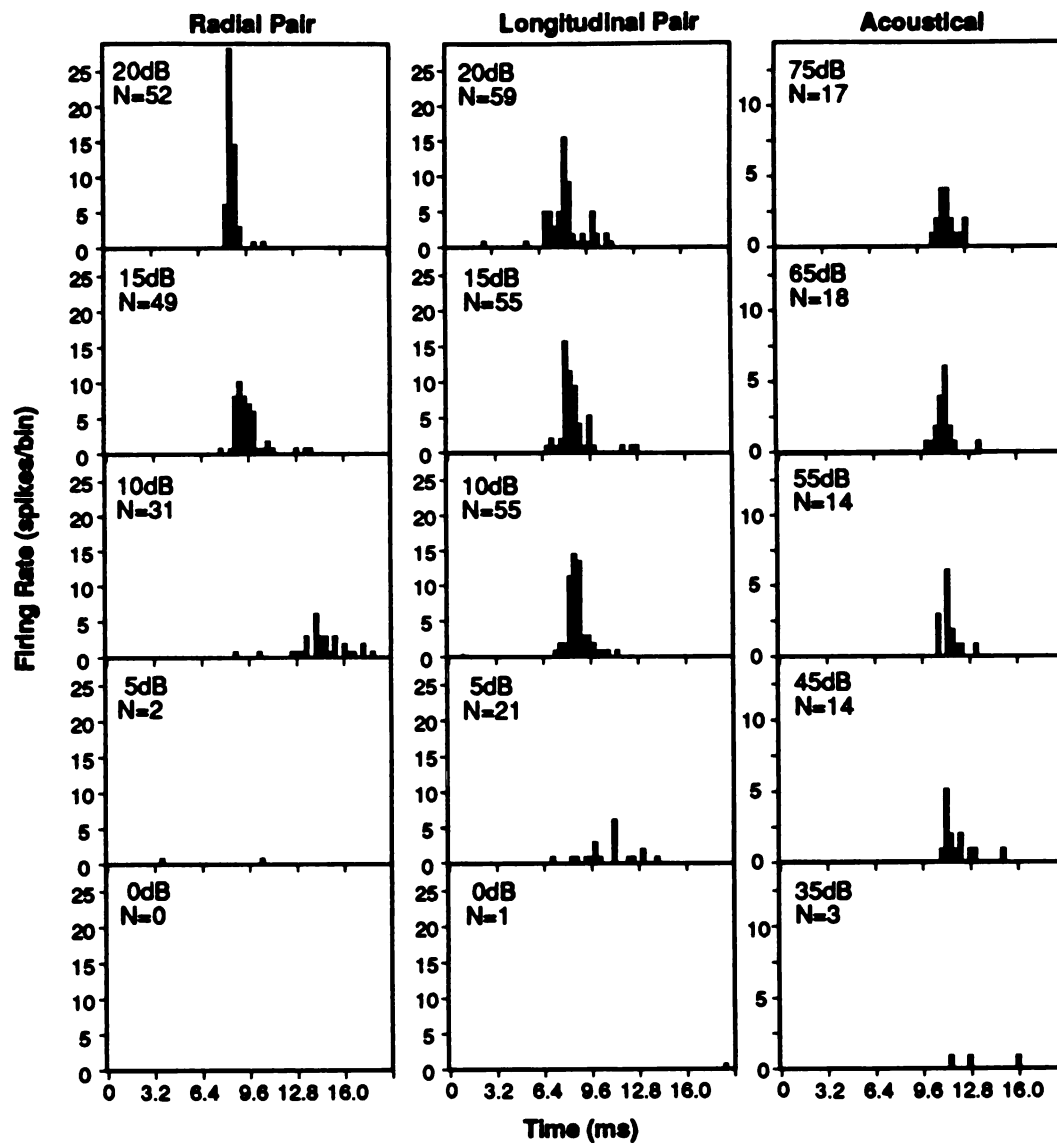
1987  
LIBRARY

**Figure 4. Post-stimulus time histograms recorded for a single neuron in primary auditory cortex. Histograms were recorded from the same neuron for a radial electrode pair, a longitudinal electrode pair, and for acoustic click stimulation. Each signal was repeated 50 times. The binwidth is 0.32 ms.**

1981 LIBRARY

FIGURE 4

Rate/Level Post-Stimulus Time Histograms



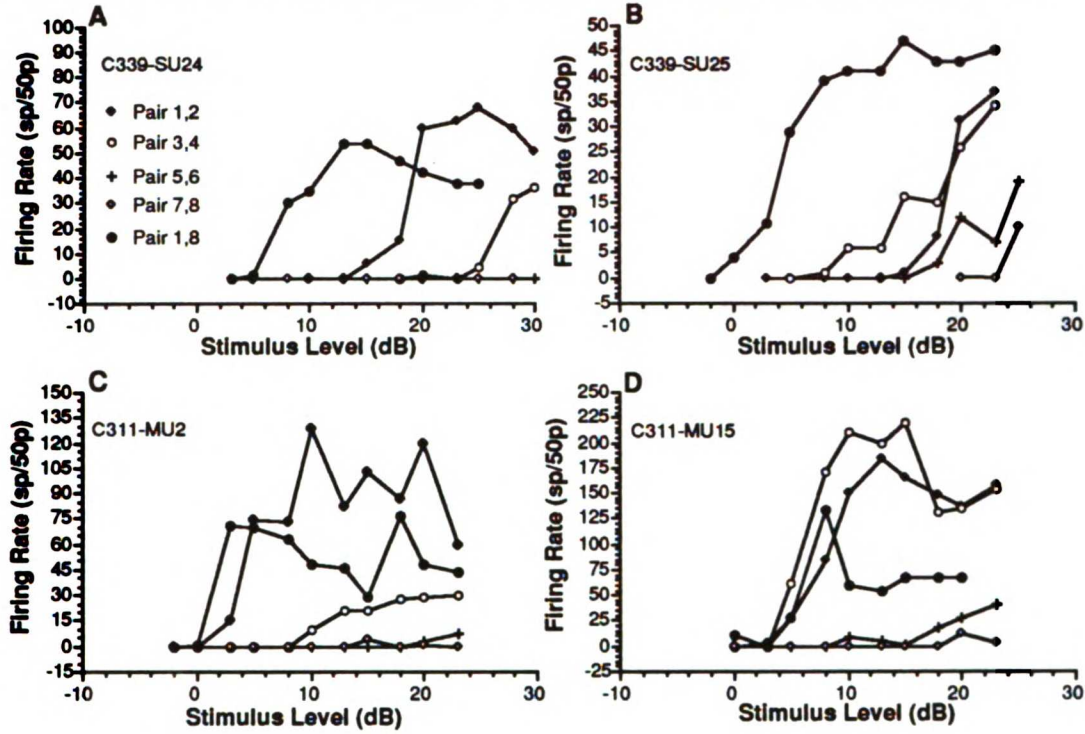
ACCEPTED MANUSCRIPT

**Figure 5. Rate/level functions for intracochlear electrical stimulation. Four radial electrode pairs (1-2,3-4,5-6,7-8) and one longitudinal electrode pair (1-8) were used. Firing rate is measured in spikes/50 pulses for two single units (A, B) and two multiple units (C,D).**

LIBRARY  
UNIVERSITY OF TORONTO

FIGURE 5

Rate-Level Functions for Radial and Longitudinal Bipolar Electrical Stimulation



UNIVERSITY OF CALIFORNIA LIBRARY

thresholds as well as different response growth behavior for both single and multiple units. In addition, most effectively excites individual and multiple neurons. Stimulation of a particular electrode pair, for example neuron SU24 shows a relatively lower threshold for apical Pair 1,2, while neuron SU25 has a lower threshold for the more basal Pair 3,4. In Figure 5C, the multiple unit MU2 shows a lower threshold for Pair 1,2, while MU15 (Fig. 5D) has a lower threshold for Pair 3,4. Pairs 5,6 and 7,8, have relatively higher thresholds for all four exemplary neuronal samples. When considering these electrode preferences, it is important to note that most of the data from this portion of the study was collected for units located near the caudal-rostral center of the ectosylvian gyrus where the more apical cochlear electrodes consistently produce relatively better responses than the more basal electrode pairs. Stimulation of longitudinal Pair 1,8 consistently showed the lowest threshold of any electrode configuration for both single and multiple units at these or any other locations. Since stimulation of some electrode pairs resulted in consistently lower thresholds, such pairs typically yielded more complete rate/level data since the highest applied current was limited (maximum current: 3162  $\mu$ Amp or 30dB). Therefore, all subsequent data descriptions are presented a) only for the radial electrode pair with the lowest response threshold, usually Pair 1,2, b) the longitudinal Pair 1,8, and c) for acoustic click stimulation.

In addition to the descriptive threshold data already discussed in Figure 5, the rate/level functions for all pairs showed other common features. These features include a rapidly rising segment for intensities just above response threshold (low level segment or LLS), and a second, typically more shallow segment (high level segment or HLS). The juncture of the low and high level segments (transition point or TP) is characterized by a

UNIVERSITY OF CALIFORNIA LIBRARY

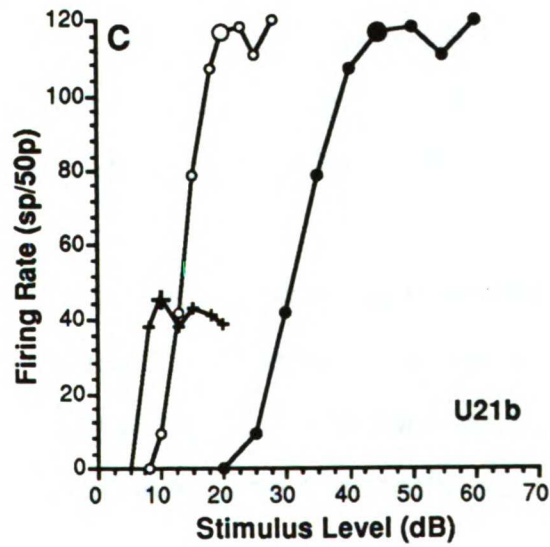
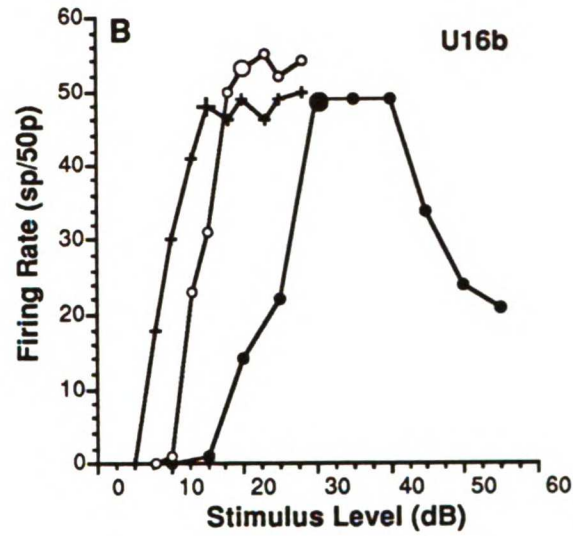
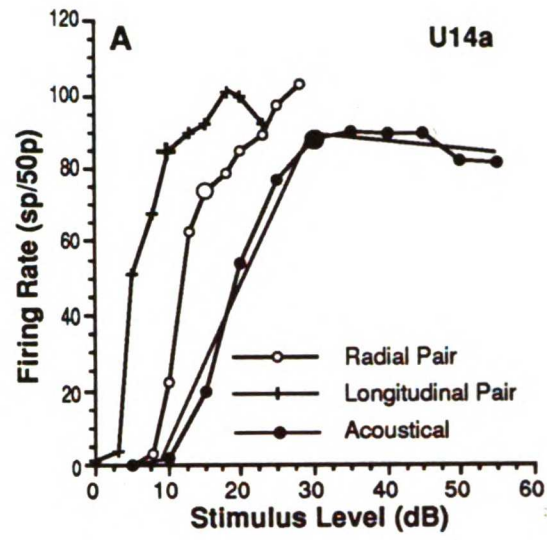


Figure 6. Comparative rate/level functions for stimulation using a radial electrode pair (1,2), a longitudinal electrode pair (1,8), and an acoustic click stimulus. Firing rate is measured in spikes/50 pulses for three single units (A,B,C). Enlarged symbols represent the slope transition point for these functions. In part A, two straight lines indicate how the rate of change in firing rate (slope) for the low level segment (for levels below the transition point) and for the high level segment (for levels above the transition point) were estimated. The dB scale is relative to  $100\mu\text{A}$  for electrical stimuli and relative to  $20\mu\text{Pa}$  for the acoustic stimuli.

LIBRARY  
UNIVERSITY OF TORONTO

FIGURE 6

Rate-Level Functions



UNIVERSITY OF CALIFORNIA LIBRARY

varied across units for different conditions. To simplify the description of the rate/level functions, the dynamic behavior of the fast growing LLS and the more slowly changing HLS were estimated by linear regression analysis of the sections above and below the transition point.

The features selected to describe rate/level functions in this study each showed a range of values across neurons resulting in varying shapes and positions of function curves. An illustration of the parametric variation in position and response strength can be seen in Figure 7. In this figure, rate/level functions are plotted for four exemplary single units for each of the three stimulating conditions, i.e. radial electrode pair, longitudinal electrode pair, and acoustic stimulation. For ease of comparison, each of the four rate/level functions for each condition have been normalized by aligning the transition point levels and placing them at zero dB and aligning the transition point firing rates and placing them at 100%. It is clear from the resulting collection of curves for each condition that there are differences in threshold, growth behavior, and dynamic range across units and across conditions. The shaded areas reflect 68% of the values or one standard deviation from the mean of the values for these rate/level function curves. It can be observed that the scatter for the radial pair is markedly greater than for either the longitudinal pair or acoustic stimulation. Globally, however, the shape of the rate/level functions for the three conditions was quite similar.

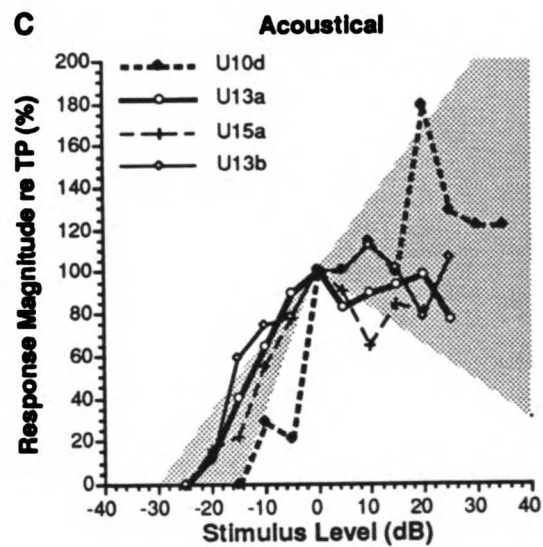
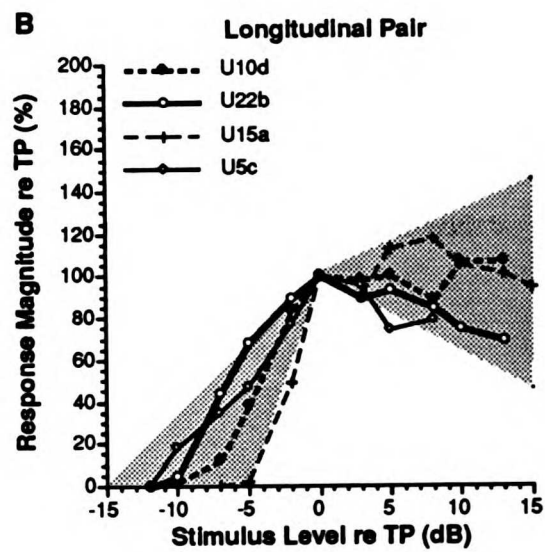
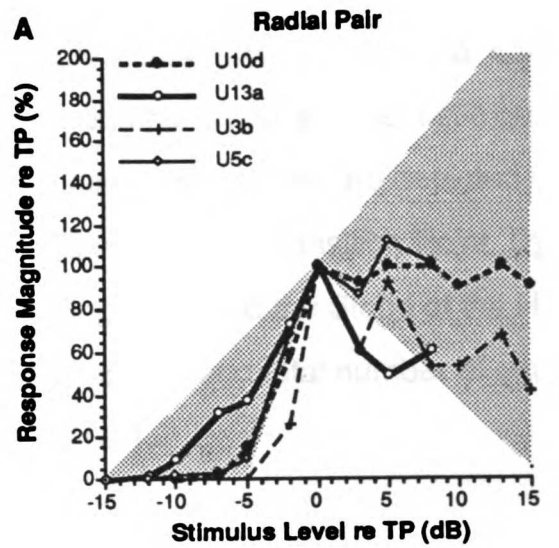
The distributions for each parameter of the rate/level functions are shown in Figure 8, and means and standard deviations are given in Table 1 for each condition. A comparison of the distributions of these parameters for the three conditions revealed some statistically significant differences between them, as shown in Table 1 (pair-wise t-test,  $p < 0.05$ ).

1000 LIBRARY

**Figure 7. Normalized rate/level functions for four exemplary single units using a radial electrode pair (1,2), a longitudinal pair (1,8), and an acoustic click stimulus. Rate/level functions are aligned along the intensity axis with slope transition points for each function placed at 0dB. Response magnitude alignment was achieved by placing the slope transition points (TPs) at 100%. Shadings represent the range of one standard deviation for the slope of the low and high level segments of the rate/level functions.**

100% LIBRARY

# Normalized Rate-Level Functions



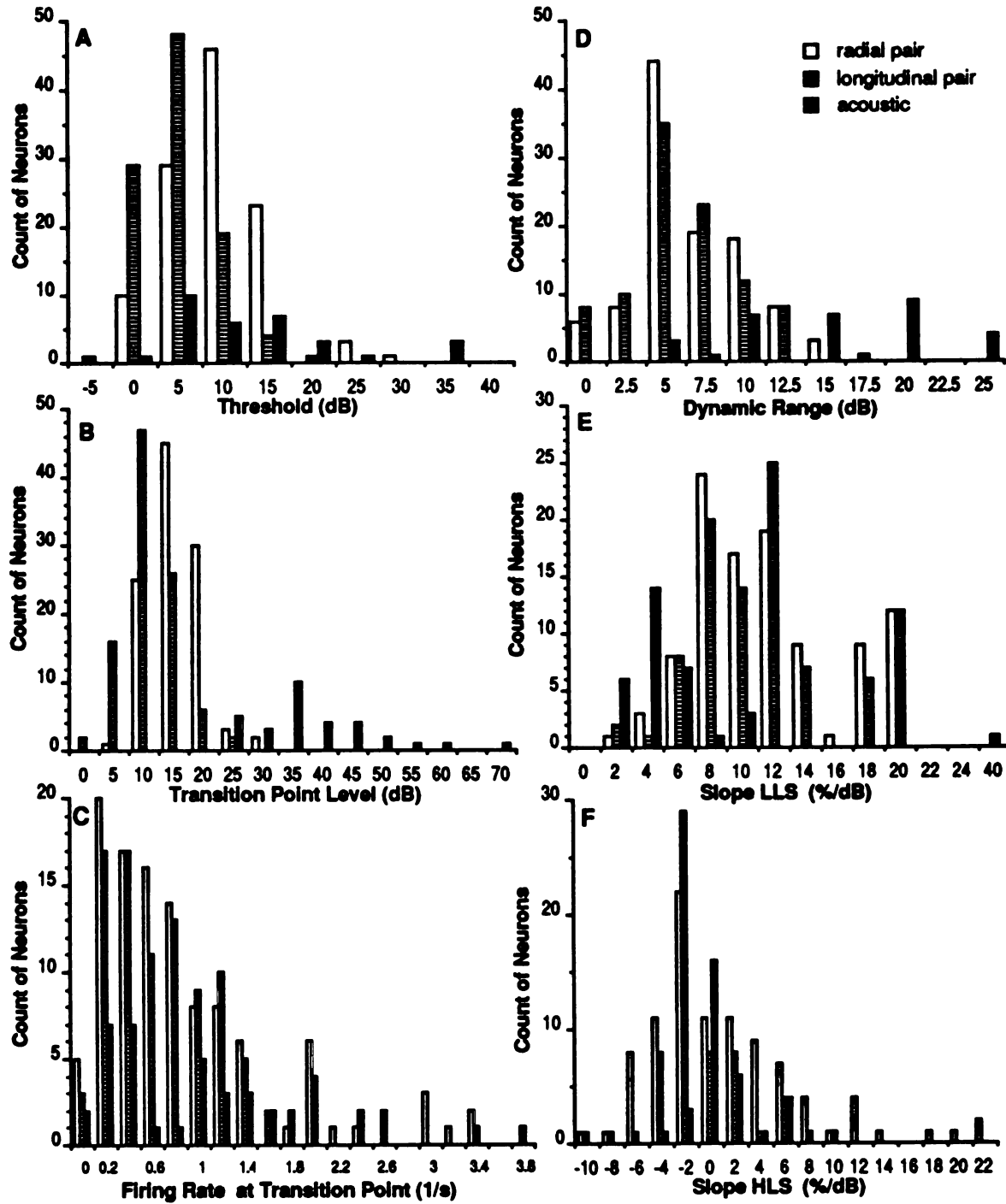
UNIVERSITY OF CALIFORNIA  
 LIBRARY

**Figure 8. Comparative parameter distributions for a radial electrode pair (1,2), a longitudinal electrode pair (1,8), and acoustic click stimulation. Parametric rate/level function distributions are depicted for Threshold, Transition Point Level, Firing Rate at Transition Point, Dynamic Range, Slope of the Low Level Segment, and the Slope of the High Level Segment (A-F). Mean, standard deviation, and total number of neurons for each condition are given in Table 1.**

1001 LIBRARY

FIGURE 8

Rate-Level Functions



1997  
 1998  
 1999  
 2000  
 2001  
 2002  
 2003  
 2004  
 2005  
 2006  
 2007  
 2008  
 2009  
 2010  
 2011  
 2012  
 2013  
 2014  
 2015  
 2016  
 2017  
 2018  
 2019  
 2020  
 2021  
 2022  
 2023  
 2024  
 2025  
 2026  
 2027  
 2028  
 2029  
 2030



Conditions where differences in the distributions were confirmed also for the population means by an analysis of variance (Fisher PLSD  $p < 0.05$ ) are marked by an asterisk. As can be seen in Table 1, thresholds for the radial pair were approximately 5dB higher than those of the longitudinal pair, i.e. radial pair mean threshold was 350 $\mu$ A and longitudinal pair mean threshold was 200 $\mu$ A. Transition point levels for the radial pair also were approximately 5dB higher than were those of the longitudinal pair. There were no differences in transition point firing rate for the two electrical conditions, however, the transition point firing rate did differ between the acoustic and the two electrical conditions. Pair-wise comparisons reveal differences in the firing rates between the electrical and acoustic transition point firing rate whereas the population means for the three conditions show no difference.

The mean dynamic range and slope of the low level segment indicated a physiological profile of a rapid increase in firing rate with small increases in intensity for both electrical conditions. The mean dynamic range for the acoustic condition is at least 8dB larger than for the two electrical conditions while concomitantly, the low level segment is at least 6.45%/dB smaller, indicating a relatively slow growth in firing rate with small increases in intensity. The pair-wise t-test showed no significant difference in the dynamic range, low level segment, or high level segment value distributions between the two electrical conditions. Again, it should be noted that dynamic range, transition point level, and slopes of LLS and HLS for the electrical and acoustic value distributions were not directly comparable due to the different stimulating modes, i.e. sound pressure versus current.

On the average, the high level segment for all three conditions shows a

relatively shallow, saturating rate/level growth function. Table 1 reveals a small difference between the radial pair mean and that of the longitudinal pair, but this difference is not statistically significant. The sign of the slope for the high level segment indicates monotonic or non-monotonic growth behavior. The mode for the electrical conditions is below zero, indicating a larger proportion of non-monotonic rate-level functions for these conditions than for the acoustic cases. If rate/level functions that have high level segment slopes of less than  $-1\%/dB$  are classified as non-monotonic (Schreiner et al. 1992), proportions of neurons with non-monotonic rate/level functions are 45%, 40%, and 13% for the radial, longitudinal, and the acoustic conditions, respectively (see Figure 8).

#### 3.1.4 Correlations of Rate/Level Function Parameters

Linear regression analysis revealed significant correlations for various rate/level function parameters for all three conditions (see Table 2 for all values and Figure 9 for four example scatter plots). For all conditions, there were significant positive correlations between threshold and transition point (Figure 9A). As might be expected, the higher or lower the threshold, the higher or lower the transition point. Figure 9C also reveals relatively high correlations between  $1/\text{dynamic range}$  and the slope of the low level segment for all conditions. This close relationship is to be expected since both measures quantify the same feature, namely, the rapid growth phase of the rate/level function. There was also a smaller but significant positive correlation for all conditions between dynamic range and transition point (Figure 9B): the higher the transition point level, the larger the dynamic range. Other, smaller but significant negative correlations can be observed including threshold and dynamic

1000  
LIBRARY

**Figure 9. Linear regression analyses of intensity parameters for a radial pair (1,2; diamonds), a longitudinal electrode pair (1,8; crosses), and acoustic click stimulation (filled squares). The correlation between threshold and transition point level is depicted in (A); transition point level and dynamic range in (B); slope of the low level segment and 1/dynamic range in (C); and transition points for rate/level and latency.level functions in (D). Solid lines represent the linear regression for both electrical conditions combined since the differences between these conditions were small. The dashed line represents the regression line for the acoustic condition. Correlation coefficients and significance levels are given in Table 2.**

1991 LIBRARY

Figure 9

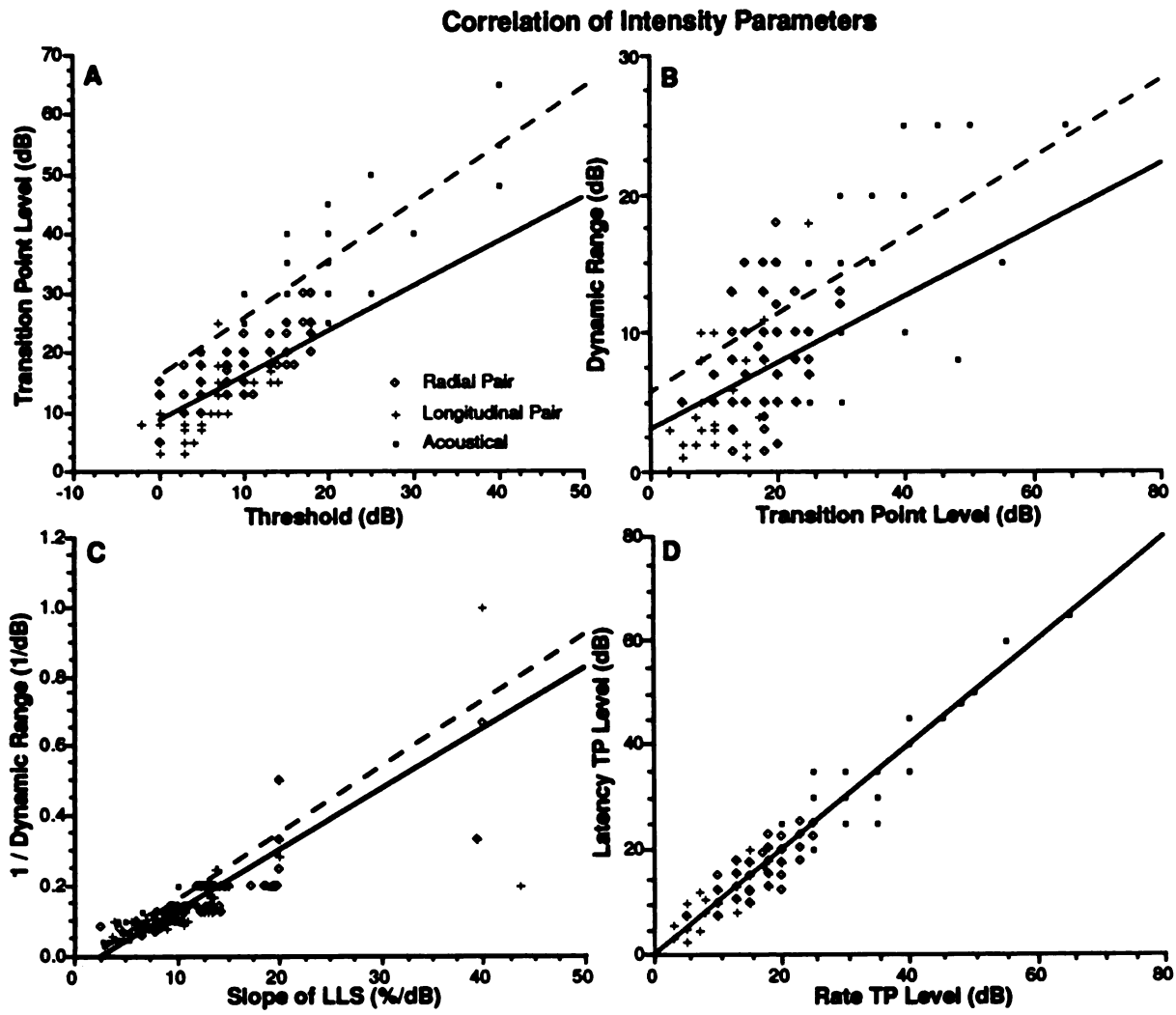


**Table 2. RATE CORRELATIONS**  
**RATE CORRELATIONS-RADIAL**

	<u>THR</u>	<u>TP</u>	<u>TP rate</u>	<u>DR</u>	<u>LLS</u>
Threshold (THR)					
Transition Point (TP)	0.73***				
Transition Point Rate	-0.33**	-0.35**			
Dynamic Range (DR)	-0.47***	0.27*			
Low Level Segment (LLS)	0.32**	-0.18		-0.66***	
High Level Segment					-0.21

**RATE CORRELATIONS-LONGITUDINAL**

	<u>THR</u>	<u>TP</u>	<u>TP rate</u>	<u>DR</u>	<u>LLS</u>
Threshold					
Transition Point	0.73***				
Transition Point Rate	-0.38				
Dynamic Range	-0.28*	0.45***			
Low Level Segment		-0.38***	-0.21	-0.70***	
High Level Segment					

**RATE CORRELATIONS-ACOUSTIC**

	<u>THR</u>	<u>TP</u>	<u>TP rate</u>	<u>DR</u>	<u>LLS</u>
Threshold					
Transition Point	0.82***				
Transition Point Rate					
Dynamic Range		0.50*			
Low Level Segment		-0.4		-0.86***	
High Level Segment					

**RATE CORRELATIONS-CONDITIONS**

	<u>R v L</u>	<u>R v AC</u>	<u>L v AC</u>
Threshold	0.60***		-0.41
Transition Point	0.50***		0.43
Transition Point Rate	0.83***		
Dynamic Range	0.34**		
Low Level Segment			
High Level Segment			

Intercorrelation of rate/level function parameters for three stimulus conditions and parametric differences between stimulus conditions. The correlation coefficient is given if level of significance was better than 0.05.

\*\*\*p=<0.0001

\*\*p=<0.001

\*p=<0.01

p=<0.05

1001 LIBRARY

range for both electrical conditions, and slope of the lower level segment and transition point for the longitudinal pair and acoustic stimulation.

The bottom of Table 2 shows the results of a correlation analysis of the six features of rate/level functions for the three stimulating conditions. Response characteristics for the radial and longitudinal pair conditions were relatively highly correlated for response threshold, and transition point level and rate. Only a small correlation was seen between the radial and longitudinal conditions for the dynamic range and no correlation was observed for either the high or low level segment slopes. For the radial pair versus acoustic conditions, no correlations were seen for any of the examined features. For the longitudinal pair versus acoustic conditions, small correlations were seen for the response threshold and the transition point level, but not for dynamic range or the slopes of the high and low level segments. The differences between the parameter distributions (see Table 1) and the lack of correlation between the radial pair and the acoustic condition (see Table 2) indicate that details of the rate/level function for the electrical and acoustic conditions were quite different for each location, despite the general similarity of their shape.

### 3.1.5 Latency/Level Functions: Properties

The response latency characteristics of neurons in auditory cortex are affected by stimulus intensity changes. Traditionally, much less attention has been given to the temporal characteristics of responses compared to the firing rate. Therefore, a number of new descriptors are introduced in order to arrive at a more thorough characterization of this aspect of the neuronal response. The latency characteristics of neurons have been determined from PSTHs, and latency/level functions have been derived for

the radial pair, the longitudinal pair, and acoustic stimulation. Figure 10 shows exemplary latency/level functions for all three stimulating conditions for three single units. As is the case for rate/level functions, the latency/level functions also share common features such as a generally precipitously sloping low level segment and a relatively shallow slope for the high level segment with a transition point at the juncture of these two slopes. Also from these functions, other latency features can be measured including minimum latency, latency at transition point, average latency of the high level segment, and the standard deviation of latency values for the high level segment.

Figure 11 shows a data presentation for latency/level functions similar to that of rate/level functions seen in Figure 7. The latency/level functions of four exemplary single units were plotted for each stimulating condition. Again, the transition point was used as an anchoring point for comparison purposes. The transition point latency and level were aligned by placing the transition point latency at the stimulating mode mean for all neurons (12ms for electrical stimulation and 14.1ms for acoustic stimulation), and the transition point level to zero. It is evident that there is a considerable difference in minimum latency, peak latency, and high and low level segment slope across units and stimulating conditions. The shaded areas reflect 68% of the values or one standard deviation from the mean of the values for the slopes of the low and high level segments of all latency/level functions. The scatter for the low level segment of the longitudinal pair is greater than that seen for the radial pair or for acoustic stimulation while the scatter for the high level segment for the longitudinal pair is smaller than for the other two conditions. However, taken as a whole, the latency/level functions of all three conditions were quite similar.

1001 LIBRARY

**Figure 10. Comparative latency/level functions for stimulation using a radial electrode pair (1,2), a longitudinal electrode pair (1,8), and an acoustic click stimulus. Latency is measured in milliseconds for three single units (A,B,C). Enlarged symbols represent the slope transition point for these functions.**

LIBRARY  
UNIVERSITY OF CALIFORNIA  
SAN DIEGO

FIGURE 10

Latency-Level Functions

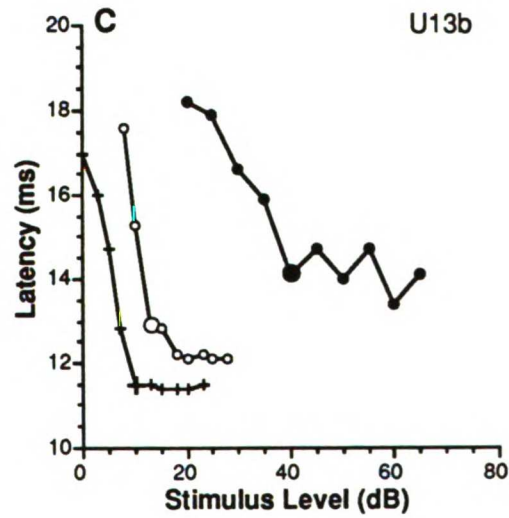
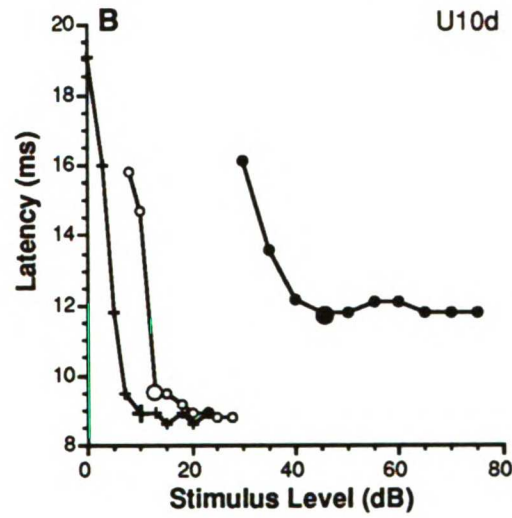
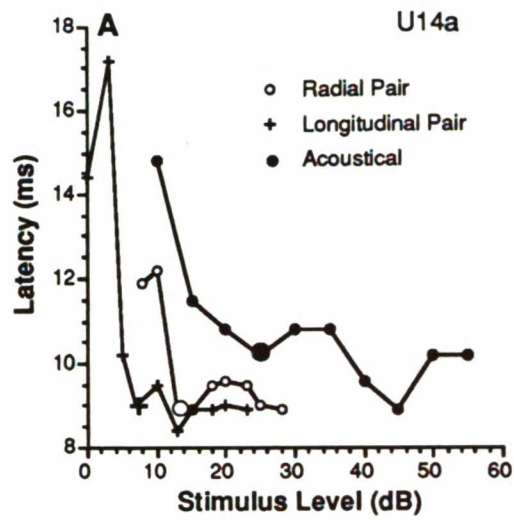
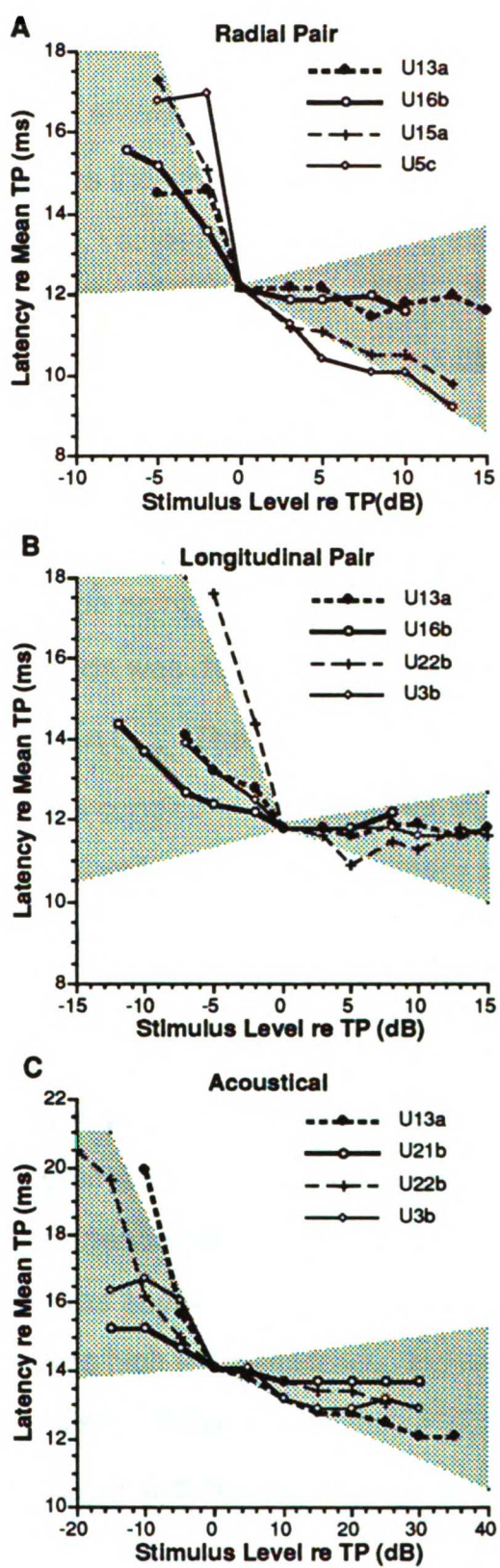


**Figure 11. Normalized latency/level functions for four exemplary single units using a radial electrode pair (1,2), a longitudinal electrode pair (1,8), and an acoustic click stimulus. Latency/level functions are aligned along the intensity axis with slope transition points for each function placed at 0dB. Response magnitude alignment was achieved by placing the slope transition points at the mean transition point for each stimulus condition (see Table 3). Shadings represent the range of one standard deviation for the slope of the low and high level segments of the latency/level functions.**

100% LIBRARY

FIGURE 11

Normalized Latency-Level Functions



UIC LIBRARY

The distributions for several latency parameters are shown in Figure 12. Figure 13 shows the distributions for parameters of the latency/level functions. Means and standard deviations are given in Table 3 for the three stimulating conditions. The minimum latency ( $L_{\min}$ ), a widely used measure of latency, shows that the mean  $L_{\min}$  differs between stimulating conditions. Whereas the latency difference is small between the two electrical conditions, i.e. less than 0.5ms, the acoustic latency shows a more substantial difference of approximately 1.7ms from the two electrical conditions. The difference between acoustically- and electrically-evoked responses holds for the population difference as well as for the pair-wise comparison for each neuron.

Since the transition point serves as an anchor point for the analysis, the latency at this position was determined ( $L_{TP}$ ). For all conditions,  $L_{TP}$  was 1 to 1.5 ms longer than  $L_{\min}$ . The mean  $L_{TP}$  difference was less than 0.5ms for the two electrical conditions, while that for the acoustic condition differed from both electrical conditions by more than 2ms. Again, these latter differences held for the population difference and for the pair-wise comparison.

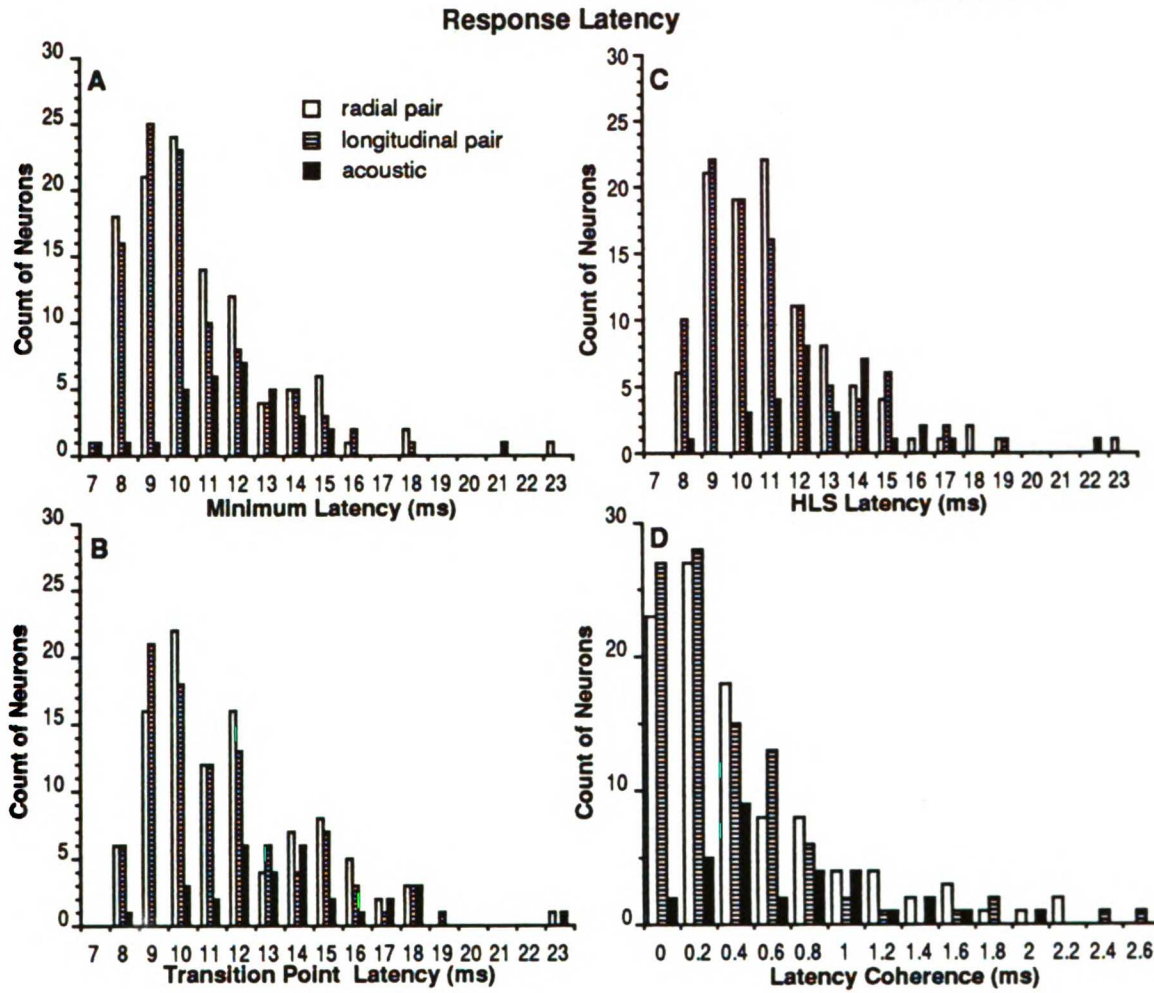
Similar to the analysis of rate/level functions, the slopes of the low and high level segment of the latency/level function were determined. In general, latency decreased with increases in stimulus level. The change in latency with level was about 6 to 13 times larger for the low level segment than for the high level segment. Since the slope of the high level segment was quite shallow for all conditions (-0.03 to -0.07 ms/dB), the average latency ( $L_{HLS}$ ) and the standard deviation for the latencies of this segment or latency coherence ( $LC_{HLS}$ ) which is a measure of the scatter of

1000 LIBRARY

**Figure 12. Comparative parameter distributions for a radial electrode pair (1,2), a longitudinal electrode pair (1,8), and acoustic click stimulation. Parametric distributions for several aspects of latency measurement distributions are depicted: minimum latency (A), latency at transition point (B), average latency of the high level segment(HLS) (C), and the latency coherence (standard deviation of high level segment latency) (D).**

100% LIBRARY

FIGURE 12



ICSF LIBRARY  
 UNIVERSITY OF CALIFORNIA  
 SAN DIEGO

**Figure 13. Comparative parameter distributions for a radial electrode pair (1,2), a longitudinal electrode pair (1,8), and acoustic click stimulation. Parametric distributions for several aspects of latency measurement distributions are depicted: slope of the low level segment (A), slope of the high level segment (B), the transition point level (C), and the difference between the transition points for rate/level and latency/level functions (D).**

1950 LIBRARY





latency values for the high level segment, was determined in order to obtain a statistically more sound estimate of the general latency behavior of each neuron. Both,  $L_{\min}$  and  $L_{TP}$ , are obtained from a single PSTH whereas  $L_{HLS}$  is based on four or more PSTHs. In addition,  $LC_{HLS}$  provided an estimate of the precision of the spike occurrence.

As expected,  $L_{HLS}$  values were between the values obtained for  $L_{\min}$  and  $L_{TP}$ .  $L_{HLS}$  shows a small difference (0.29 ms,  $p < 0.05$ , paired t-test) between the two electrical conditions, with a difference of more than 2ms between the acoustic and each electrical condition, the latter difference being significant for the population and pair-wise comparison.  $LC_{HLS}$  is the smallest for the longitudinal pair suggestive of temporally highly coherent inputs for this stimulating condition, i.e. a limited scatter of latency values. Statistically significant differences between each condition for this feature were observed. The difference between the longitudinal pair and acoustic stimulation distributions was confirmed for the population mean. The slope of the low level segment shows a small, but significant difference for the population and the pair-wise comparison between the two electrical stimulating conditions. The slope of the high level segment shows a statistically significant difference for the radial and longitudinal electrical conditions as well.

Both rate/level and latency/level functions exhibited a transition point separating regions of different dynamic characteristics. The transition point of the rate/level function showed characteristics and relationships between the stimulating conditions similar to those seen for the transition point of latency/level functions. Comparisons of the locations of the transition point for rate- and the latency-level functions indicates

that, for the population mean as well as for mean pair-wise differences, the two transition points were within 1dB. This suggests that the characteristic changes in firing rate and timing as a function of intensity are closely related and result from the same underlying mechanisms.

### 3.1.6 Correlations of Latency/Level Function Parameters

Table 4 depicts correlation analyses for latency/level parameters that indicates a consistent, high positive correlation between  $L_{\min}$  and  $L_{TP}$  and between  $L_{\min}$  and  $L_{HLS}$  for all conditions. As might be expected,  $L_{TP}$  is also highly correlated with the  $L_{HLS}$  for all conditions since all three measures simply reflect different aspects of the high level segment. A lower, but still significant correlation is also seen between the latency coherence ( $LC_{HLS}$ ) and  $L_{TP}$  as well as  $L_{HLS}$  for all stimulating conditions. Therefore, the longer the latency, the wider the distribution of latencies for the relatively shallow high level segment. However, since the high level segment shows a slight decline in latency with level, a small but significant negative correlation was seen between  $LC_{HLS}$  and the slope of the high level segment for all conditions. The slope of the low level segment did not show any consistent correlation with any of the other latency parameters. For all three conditions, the slope of the high level segment was negatively correlated with  $L_{TP}$ , that is, the longer the latency at the transition point, the greater the rate of change in the high level segment latency. This relationship may be related to the notion that by virtue of a minimum cortical latency floor of approximately 8ms, inadvertently, shorter latencies at the transition point must result in shallower slopes for the entire high level segment. Finally, Fig. 13D depicts the close relationship between the transition point levels

**Table 4. LATENCY/LEVEL CORRELATIONS**

**LATENCY CORRELATIONS-RADIAL**

	<u>Min Lat</u>	<u>Lat. at TP</u>	<u>AvLatHLS</u>	<u>LatCoh</u>	<u>LLS</u>	<u>HLS</u>
Minimum Latency						
Latency at Transition Point	0.86***					
Average Latency (HLS)	0.94***	0.93***				
Latency Coherence(HLS)		0.43***	0.31**			
Latency-Low Level Segment				-0.24		
Latency-High Level Segment		-0.25		-0.21		
TP Level (Lat)	0.35***	0.32*	0.34***			0.21

**LATENCY CORRELATIONS-LONGITUDINAL**

	<u>Min Lat</u>	<u>Lat. at TP</u>	<u>AvLatHLS</u>	<u>LatCoh</u>	<u>LLS</u>	<u>HLS</u>
Minimum Latency						
Latency at Transition Point	0.81***					
Average Latency (HLS)	0.96***	0.88***				
Latency Coherence (HLS)		0.42***	0.28*			
Latency-Low Level Segment						
Latency-High Level Segment		-0.41***	-0.22	-0.48***		
TP Level (Lat)	0.58***	0.43**	0.55***			

**LATENCY CORRELATIONS-ACOUSTIC**

	<u>Min Lat</u>	<u>Lat. at TP</u>	<u>AvLatHLS</u>	<u>LatCoh</u>	<u>LLS</u>	<u>HLS</u>
Minimum Latency						
Latency at Transition Point	0.91***					
Average Latency (HLS)	0.97***	0.96***				
Latency Coherence(HLS)	0.36	0.66***	0.52*			
Latency-Low Level Segment				-0.38		
Latency-High Level Segment	-0.42	-0.57**	-0.4	-0.42		
TP Level (Lat)						

**LATENCY CORRELATIONS-CONDITIONS**

	<u>RvL</u>	<u>RvAC</u>	<u>LvAC</u>
Minimum Latency	0.89***	0.73***	0.77***
Latency at Transition Point	0.74***	0.55***	0.65***
Average Latency (HLS)	0.87***	0.72***	0.75***
Latency Coherence (HLS)	0.35***		
Latency-Low Level Segment			0.56*
Latency-High Level Segment	0.25		0.42
TP Level (Lat)	0.41**		0.52*

Intercorrelations of latency/level parameters for three stimulus conditions and parametric differences between stimulus conditions

\*\*\*p<0.0001 \*\*p<0.001 \*P<0.01 p<0.05

UNIVERSITY OF CALIFORNIA  
 LIBRARY  
 1001  
 1001

1  
2  
3  
4  
5  
6  
7  
8  
9  
10  
11  
12  
13  
14  
15  
16  
17  
18  
19  
20  
21  
22  
23  
24  
25  
26  
27  
28  
29  
30  
31  
32  
33  
34  
35  
36  
37  
38  
39  
40  
41  
42  
43  
44  
45  
46  
47  
48  
49  
50  
51  
52  
53  
54  
55  
56  
57  
58  
59  
60  
61  
62  
63  
64  
65  
66  
67  
68  
69  
70  
71  
72  
73  
74  
75  
76  
77  
78  
79  
80  
81  
82  
83  
84  
85  
86  
87  
88  
89  
90  
91  
92  
93  
94  
95  
96  
97  
98  
99  
100

determined from rate/level and latency/level functions.

The bottom of Table 4 shows the results of correlation analyses of the six features of latency/level functions for the three stimulating conditions. The three latency measures,  $L_{min}$ ,  $L_{TP}$  and  $L_{HLS}$  were highly correlated for all three conditions. Therefore, the characteristic latency behavior for each neuron is very similar for acoustic and electrical stimulation. The other three parameters showed a less consistent correlation pattern across the three conditions. The temporal precision of spike occurrence for the high level segment, estimated by  $LC_{HLS}$ , was correlated for the two electrical conditions, but not for the electrical and acoustic conditions. Only for the longitudinal pair versus acoustic condition was a correlation seen for the slope of the low and high level segments. The slope of the high level segment showed a small correlation for the two electrical conditions.

### 3.1.7 Temporal Repetition Coding: Modulation Transfer Functions

An important characteristic of neuronal behavior is the capacity to follow repetitive stimuli. It is known that cortical neurons have a fairly poor capacity to follow repetitive acoustic signals relative to more peripherally located neurons (e.g. Schreiner and Langner, 1988). In addition, some stimulus coding strategies in cochlear implants propose modulated pulse trains as the main information carrier. Therefore, the temporal repetition coding for electrical cochlear stimulation is an important aspect of the physiological response evaluation of cortical neurons. Responses of single units and multiple units using bipolar pulses for a range of stimulus repetition rates were recorded in the primary auditory cortex of six animals. As in the case of rate/level and

LIBRARY  
UNIVERSITY OF TORONTO

1  
2  
3  
4  
5  
6  
7  
8  
9  
10  
11  
12  
13  
14  
15  
16  
17  
18  
19  
20  
21  
22  
23  
24  
25  
26  
27  
28  
29  
30  
31  
32  
33  
34  
35  
36  
37  
38  
39  
40  
41  
42  
43  
44  
45  
46  
47  
48  
49  
50  
51  
52  
53  
54  
55  
56  
57  
58  
59  
60  
61  
62  
63  
64  
65  
66  
67  
68  
69  
70  
71  
72  
73  
74  
75  
76  
77  
78  
79  
80  
81  
82  
83  
84  
85  
86  
87  
88  
89  
90  
91  
92  
93  
94  
95  
96  
97  
98  
99  
100

latency/level functions, a fairly large number of temporal repetition coding features have been evaluated in an attempt to determine those that provide useful information about physiological behavior of neurons in response to electrical stimulation.

Period histograms, generated by both electrical and acoustic stimulation of the same neuron, have provided the basis for a comparative analysis of a number of aspects of temporal coding. Temporal modulation transfer functions (tMTF) reflect the number of phase-locked spikes for the entire, one second train of impulses (each train was presented 30 times) for various repetition rates. A tMTF for repetition frequencies of 2Hz to 38Hz, in 2 Hz steps was used in most cases as long as frequency following was maintained, to some extent, at higher repetition rates. Best modulation frequency (BMF), a standard measure of temporal repetition and amplitude modulation coding, marks the highest point in the firing rate distribution. The firing rates at 6dB below maximum rate, or half the firing rate at the BMF, are also standard measurements of the width of tMTFs and correspond to the low and high cutoff frequencies. Maximum rate provides information regarding the relative strength of response at BMF.

Representative examples of PSTHs for the three stimulating conditions are shown for one neuron in Figure 14. For all three conditions, frequency following responses are observed that display varying degrees of response strength and temporal precision. From the PSTHs, period histograms were derived (Figure 15) that excluded the first 20ms of the response, which effectively eliminated onset response effects. From the period histograms, the event-locked, short-latency activity was measured in the 30 ms following the event and tMTFs were constructed.

AMMATT 1801



**Figure 14. Post-stimulus time histograms reconstructed for a single unit (U16b) in primary auditory cortex for five stimulus repetition rates. Each train of stimuli was one second long and was repeated 30 times.**

**Histograms were reconstructed for responses evoked by a radial electrode pair, a longitudinal electrode pair, and for acoustic click stimulation.**

**Binwidth of the display is 2.4 ms. Total number of spikes (N) is given for each histogram.**

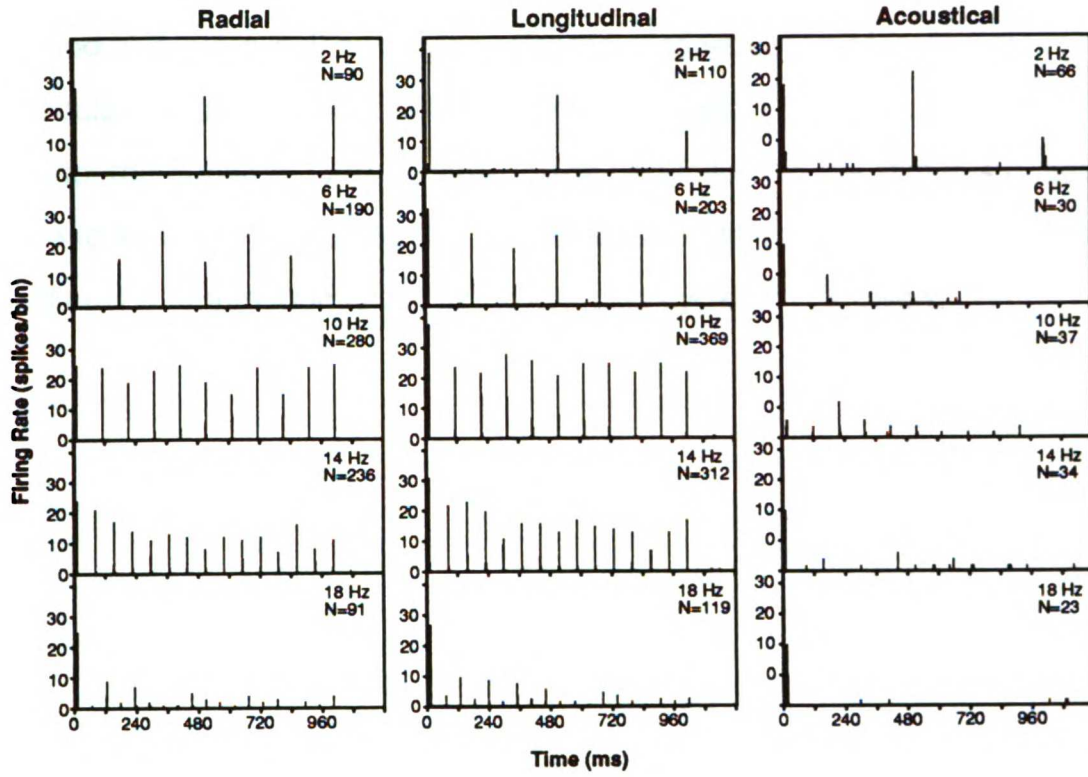
U16b  
U16b

1  
2  
3  
4  
5  
6  
7  
8  
9  
10  
11  
12  
13  
14  
15  
16  
17  
18  
19  
20  
21  
22  
23  
24  
25  
26  
27  
28  
29  
30  
31  
32  
33  
34  
35  
36  
37  
38  
39  
40  
41  
42  
43  
44  
45  
46  
47  
48  
49  
50  
51  
52  
53  
54  
55  
56  
57  
58  
59  
60  
61  
62  
63  
64  
65  
66  
67  
68  
69  
70  
71  
72  
73  
74  
75  
76  
77  
78  
79  
80  
81  
82  
83  
84  
85  
86  
87  
88  
89  
90  
91  
92  
93  
94  
95  
96  
97  
98  
99  
100

CONFIDENTIAL

FIGURE 14

Repetition Rate Post-Stimulus Time Histogram



INSTITUTIONAL LIBRARY

1  
2  
3  
4  
5  
6  
7  
8  
9  
10  
11  
12  
13  
14  
15  
16  
17  
18  
19  
20  
21  
22  
23  
24  
25  
26  
27  
28  
29  
30  
31  
32  
33  
34  
35  
36  
37  
38  
39  
40  
41  
42  
43  
44  
45  
46  
47  
48  
49  
50  
51  
52  
53  
54  
55  
56  
57  
58  
59  
60  
61  
62  
63  
64  
65  
66  
67  
68  
69  
70  
71  
72  
73  
74  
75  
76  
77  
78  
79  
80  
81  
82  
83  
84  
85  
86  
87  
88  
89  
90  
91  
92  
93  
94  
95  
96  
97  
98  
99  
100

1  
2  
3  
4  
5  
6  
7  
8  
9  
10  
11  
12  
13  
14  
15  
16  
17  
18  
19  
20  
21  
22  
23  
24  
25  
26  
27  
28  
29  
30  
31  
32  
33  
34  
35  
36  
37  
38  
39  
40  
41  
42  
43  
44  
45  
46  
47  
48  
49  
50  
51  
52  
53  
54  
55  
56  
57  
58  
59  
60  
61  
62  
63  
64  
65  
66  
67  
68  
69  
70  
71  
72  
73  
74  
75  
76  
77  
78  
79  
80  
81  
82  
83  
84  
85  
86  
87  
88  
89  
90  
91  
92  
93  
94  
95  
96  
97  
98  
99  
100

**Figure 15. Period histogram for a stimulus repetition rate of 8Hz for single neuron U16b reconstructed for a radial electrode pair (1,2), a longitudinal electrode pair (1,8), and acoustic click stimulation. Each period histogram is shown twice. For the reconstruction of temporal modulation transfer functions (see Figures 16 and 17), responses were measured during a 30ms window (black bar) following the stimulus onset. The total number of spikes (N), the vector strength (VS), and the phase (in radians) of the response within the stimulus cycle (Ph) is given.**

AMMHI 15011

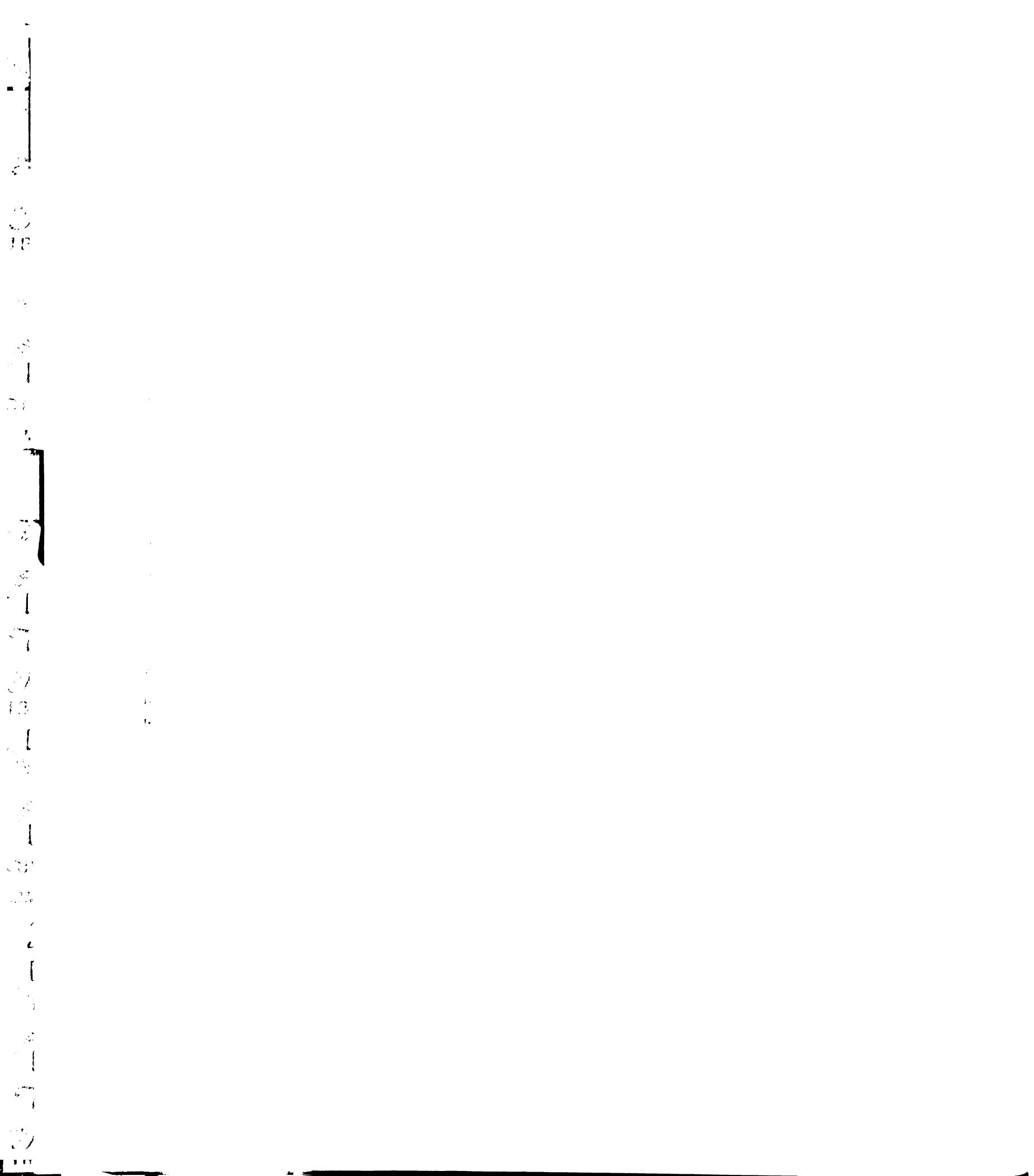
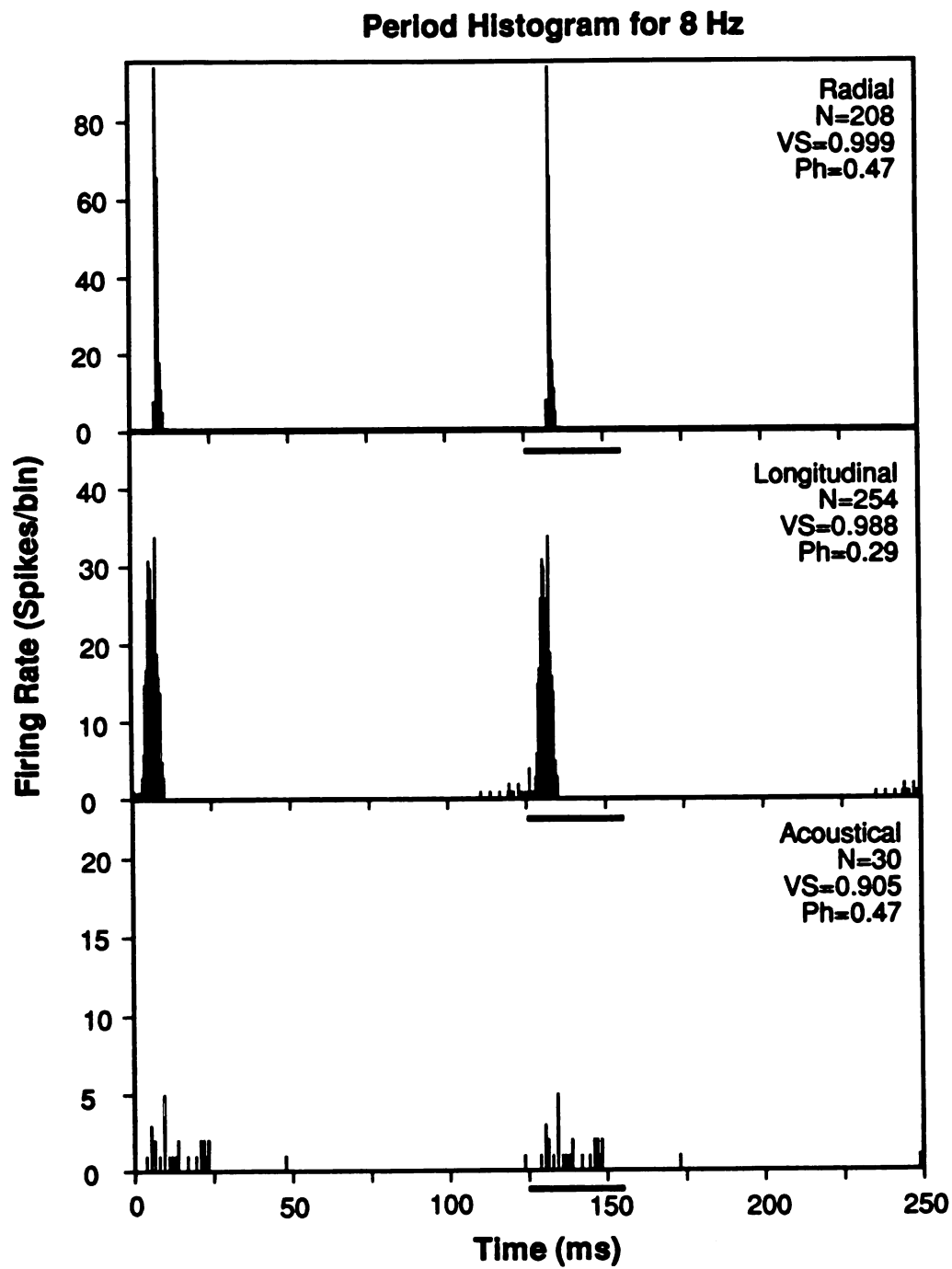


FIGURE 15



AMERICAN SOCIETY OF NEUROSCIENCE



Figure 16 shows tMTFs for four exemplary single units using all three stimulating conditions. For some neurons, the distribution of firing rate as a function of stimulus repetition rate resulted in a bell-shaped or bandpass curve with a distinct maximum, the best modulation frequency (BMF). For the radial pair, longitudinal pair, and acoustic stimulation, 57%, 62%, and 42% of neurons, respectively, showed bandpass configurations. That is, the firing rate dropped below 50% of maximum firing rate on the high and the low frequency side of the BMF. For other neurons, this distribution resulted in a lowpass configuration in which all lower frequencies produced nearly the same firing rate, or showed only a small reduction in firing rate as the stimulus frequencies reached the lower end of the repetition range. Since frequencies below 2Hz were not used as stimuli, any decrement at those points is unknown. Therefore, the determination of a low frequency cut-off frequency could not be achieved in those cases.

Figure 17 shows tMTFs for five single units that have been normalized to the firing rate at BMF for each stimulating condition. While the majority of the examples for all stimulating conditions have a bandpass configuration centered around a BMF of approximately 8-10Hz, others have a more low-pass function (e.g. Unit 12 in A,B, and C).

The distributions for several parameters of the tMTF are shown in Figure 18, and means and standard deviations are given in Table 5 for each condition. The mean BMF was very similar across all conditions, ranging from 6.47Hz (acoustic condition) to 7.81Hz (longitudinal pair), with only a small, statistically significant difference between the longitudinal pair and acoustic stimulation. The high cut-off frequency at -6dB from maximum showed greater variability across the three stimulating

1  
2  
3  
4  
5  
6  
7  
8  
9  
10  
11  
12  
13  
14  
15  
16  
17  
18  
19  
20  
21  
22  
23  
24  
25  
26  
27  
28  
29  
30  
31  
32  
33  
34  
35  
36  
37  
38  
39  
40  
41  
42  
43  
44  
45  
46  
47  
48  
49  
50  
51  
52  
53  
54  
55  
56  
57  
58  
59  
60  
61  
62  
63  
64  
65  
66  
67  
68  
69  
70  
71  
72  
73  
74  
75  
76  
77  
78  
79  
80  
81  
82  
83  
84  
85  
86  
87  
88  
89  
90  
91  
92  
93  
94  
95  
96  
97  
98  
99  
100

1  
2  
3  
4  
5  
6  
7  
8  
9  
10  
11  
12  
13  
14  
15  
16  
17  
18  
19  
20  
21  
22  
23  
24  
25  
26  
27  
28  
29  
30  
31  
32  
33  
34  
35  
36  
37  
38  
39  
40  
41  
42  
43  
44  
45  
46  
47  
48  
49  
50  
51  
52  
53  
54  
55  
56  
57  
58  
59  
60  
61  
62  
63  
64  
65  
66  
67  
68  
69  
70  
71  
72  
73  
74  
75  
76  
77  
78  
79  
80  
81  
82  
83  
84  
85  
86  
87  
88  
89  
90  
91  
92  
93  
94  
95  
96  
97  
98  
99  
100

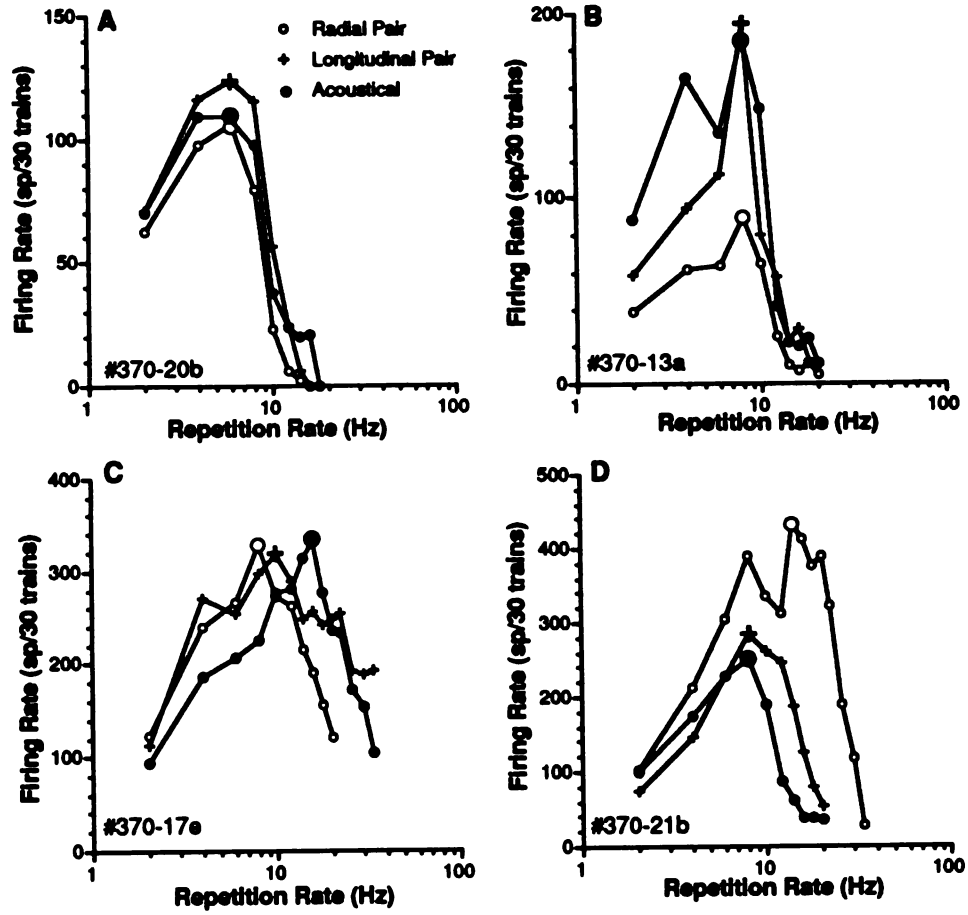
**Figure 16. Temporal modulation transfer functions for four single units (A,B,C,D) using a radial electrode pair (1,2), one longitudinal electrode pair (1,8), and acoustic click stimulation. Firing rate was determined from the period histograms, excluding the onset of the first pulse or click in each train. Firing rate is expressed in spikes/30 trains. Repetition frequencies were 2-38Hz.**

AMERICAN SCIENCE

1  
2  
3  
4  
5  
6  
7  
8  
9  
10  
11  
12  
13  
14  
15  
16  
17  
18  
19  
20  
21  
22  
23  
24  
25  
26  
27  
28  
29  
30  
31  
32  
33  
34  
35  
36  
37  
38  
39  
40  
41  
42  
43  
44  
45  
46  
47  
48  
49  
50  
51  
52  
53  
54  
55  
56  
57  
58  
59  
60  
61  
62  
63  
64  
65  
66  
67  
68  
69  
70  
71  
72  
73  
74  
75  
76  
77  
78  
79  
80  
81  
82  
83  
84  
85  
86  
87  
88  
89  
90  
91  
92  
93  
94  
95  
96  
97  
98  
99  
100

FIGURE 16

Temporal Modulation Transfer Functions



Accepted for publication  
 11/11/2011

1  
2  
3  
4  
5  
6  
7  
8  
9  
10  
11  
12  
13  
14  
15  
16  
17  
18  
19  
20  
21  
22  
23  
24  
25  
26  
27  
28  
29  
30  
31  
32  
33  
34  
35  
36  
37  
38  
39  
40  
41  
42  
43  
44  
45  
46  
47  
48  
49  
50  
51  
52  
53  
54  
55  
56  
57  
58  
59  
60  
61  
62  
63  
64  
65  
66  
67  
68  
69  
70  
71  
72  
73  
74  
75  
76  
77  
78  
79  
80  
81  
82  
83  
84  
85  
86  
87  
88  
89  
90  
91  
92  
93  
94  
95  
96  
97  
98  
99  
100

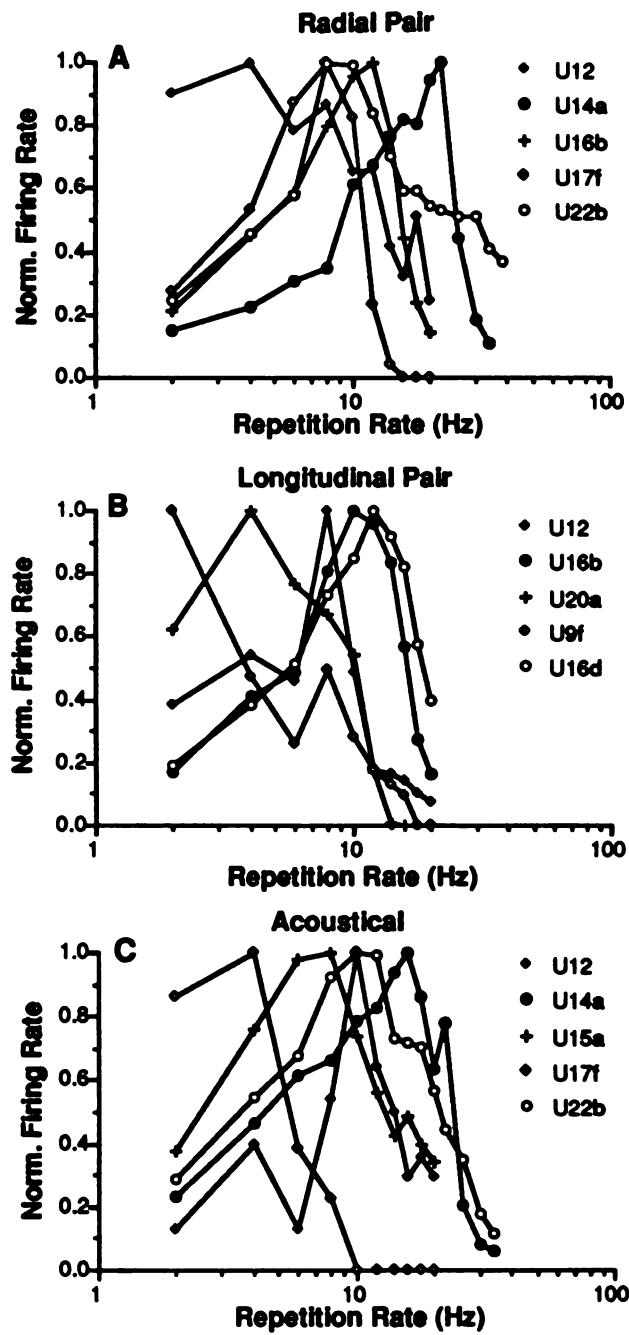
**Figure 17. Temporal modulation transfer functions for five single units using one radial electrode pair (1,2), one longitudinal electrode pair (1,8), and acoustic click stimulation. Each curve is normalized to the firing rate at the best modulation frequency (BMF). Repetition frequencies were 2-38Hz.**

APR 11 1981

1  
2  
3  
4  
5  
6  
7  
8  
9  
10  
11  
12  
13  
14  
15  
16  
17  
18  
19  
20  
21  
22  
23  
24  
25  
26  
27  
28  
29  
30  
31  
32  
33  
34  
35  
36  
37  
38  
39  
40  
41  
42  
43  
44  
45  
46  
47  
48  
49  
50  
51  
52  
53  
54  
55  
56  
57  
58  
59  
60  
61  
62  
63  
64  
65  
66  
67  
68  
69  
70  
71  
72  
73  
74  
75  
76  
77  
78  
79  
80  
81  
82  
83  
84  
85  
86  
87  
88  
89  
90  
91  
92  
93  
94  
95  
96  
97  
98  
99  
100

FIGURE 17

Normalized Temporal Modulation Transfer Functions



APR 11 1971

1  
2  
3  
4  
5  
6  
7  
8  
9  
10  
11  
12  
13  
14  
15  
16  
17  
18  
19  
20  
21  
22  
23  
24  
25  
26  
27  
28  
29  
30  
31  
32  
33  
34  
35  
36  
37  
38  
39  
40  
41  
42  
43  
44  
45  
46  
47  
48  
49  
50  
51  
52  
53  
54  
55  
56  
57  
58  
59  
60  
61  
62  
63  
64  
65  
66  
67  
68  
69  
70  
71  
72  
73  
74  
75  
76  
77  
78  
79  
80  
81  
82  
83  
84  
85  
86  
87  
88  
89  
90  
91  
92  
93  
94  
95  
96  
97  
98  
99  
100

**Figure 18. Comparative parameter distributions for a radial electrode pair (1,2), a longitudinal electrode pair (1,8), and acoustic click stimulation. Parametric distributions for several aspects of temporal repetition coding measurements are depicted: BMF for rate (A), high frequency cut-off frequency at -6dB (B), low frequency cut-off frequency at -6 dB (C), BMF for vector strength (D), and the maximum firing rate (E). Means, standard deviations, and number of neurons per condition are given in Table 5.**

ADMITTED COPY

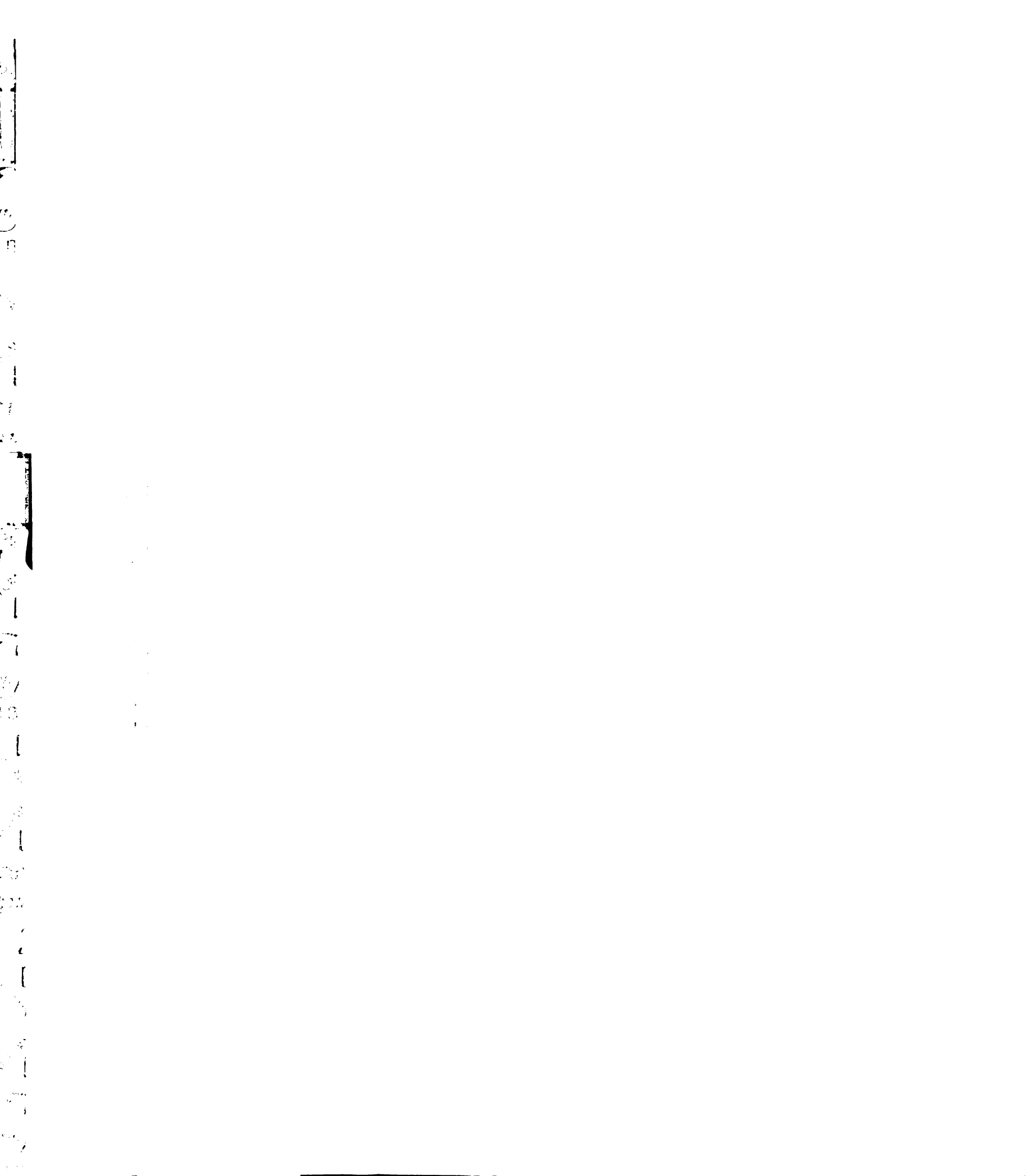
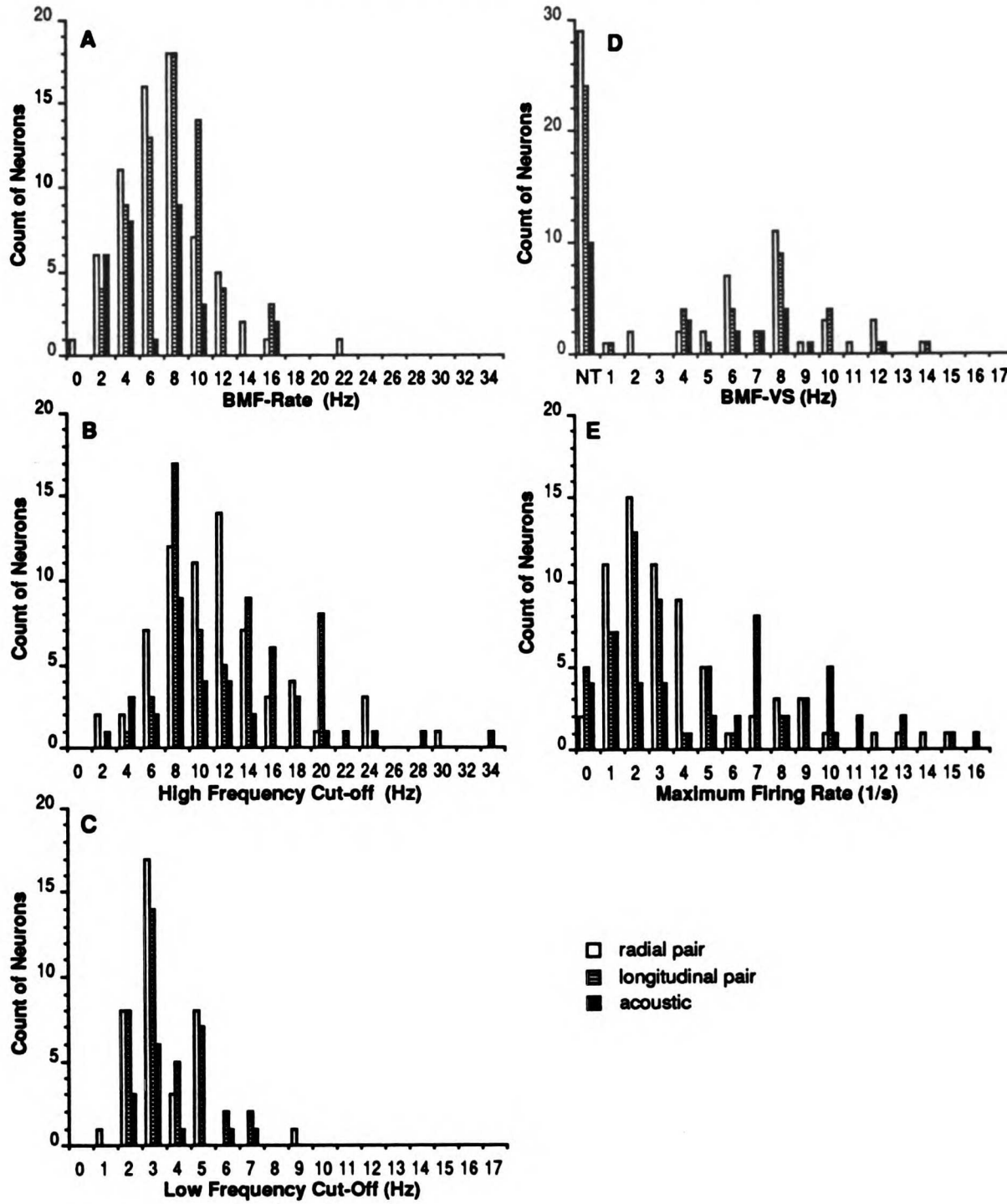


FIGURE 18

Temporal Modulation Transfer Functions



10

11

12

13

14

15

16

17

**Table 5. TEMPORAL REPETITION CODING**

	<u>RADIAL PAIR(N)</u> <u>mean ± SD</u>	<u>LONG. PAIR(N)</u> <u>mean ± SD</u>	<u>ACOUSTIC(N)</u> <u>mean ± SD</u>
Best Modulation Frequency	7.32 ± 3.63(68)	7.81 ± 3.17(65)	6.47 ± 3.81(29)
Rate -6dB (L)	3.54 ± 1.37(38)	3.87 ± 1.41(38)	3.71 ± 1.67(12)
Rate -6dB (H)	12.3 ± 5.18(67)	13.6 ± 5.32(61)	11.0 ± 5.57(28)
Maximum Rate	135.8 ± 101.9(67)	158.1 ± 119.2(63)	117.7 ± 98.6(29)
Max. Entrainment Frequency	2.83 ± 1.55(67)	2.93 ± 1.81(63)	2.76 ± 1.88(29)
Entrainment -6dB (H)	7.99 ± 3.78(66)	8.17 ± 3.65(63)	7.59 ± 3.4(28)
Entrainment 0.25spp	10.7 ± 6.21(68)	11.7 ± 6.17(61)	9.96 ± 6.42(27)
Maximum Entrainment(spp)	1.06 ± 0.58(67)	1.08 ± 0.57(63)	0.99 ± 0.65(29)

	<u>R/L DIFF</u>	<u>R/AC DIFF</u>	<u>L/AC DIFF</u>
Best Modulation Frequency			1.11
Rate -6dB (L)		1.06	
Rate -6dB (H)	1.06	2.64	2.21*
Maximum Rate		39.9	76.5
Max. Entrainment Frequency			
Entrainment -6dB (H)			
Entrainment 0.25spp		2.81	3.35
Maximum Entrainment(spp)		0.22	0.27

Means and standard deviations for temporal repetition coding parameters for three stimulus conditions and the mean pair-wise differences between stimulus conditions ( $p < 0.05$ ). Star (\*) indicates significant difference between population means (ANOVA Fisher PLSD  $p < 0.05$ ).

APPROVED FOR RELEASE  
 APR 1964  
 BY 10400  
 10400

1  
2  
3  
4  
5  
6  
7  
8  
9  
10  
11  
12  
13  
14  
15  
16  
17  
18  
19  
20  
21  
22  
23  
24  
25  
26  
27  
28  
29  
30  
31  
32  
33  
34  
35  
36  
37  
38  
39  
40  
41  
42  
43  
44  
45  
46  
47  
48  
49  
50  
51  
52  
53  
54  
55  
56  
57  
58  
59  
60  
61  
62  
63  
64  
65  
66  
67  
68  
69  
70  
71  
72  
73  
74  
75  
76  
77  
78  
79  
80  
81  
82  
83  
84  
85  
86  
87  
88  
89  
90  
91  
92  
93  
94  
95  
96  
97  
98  
99  
100

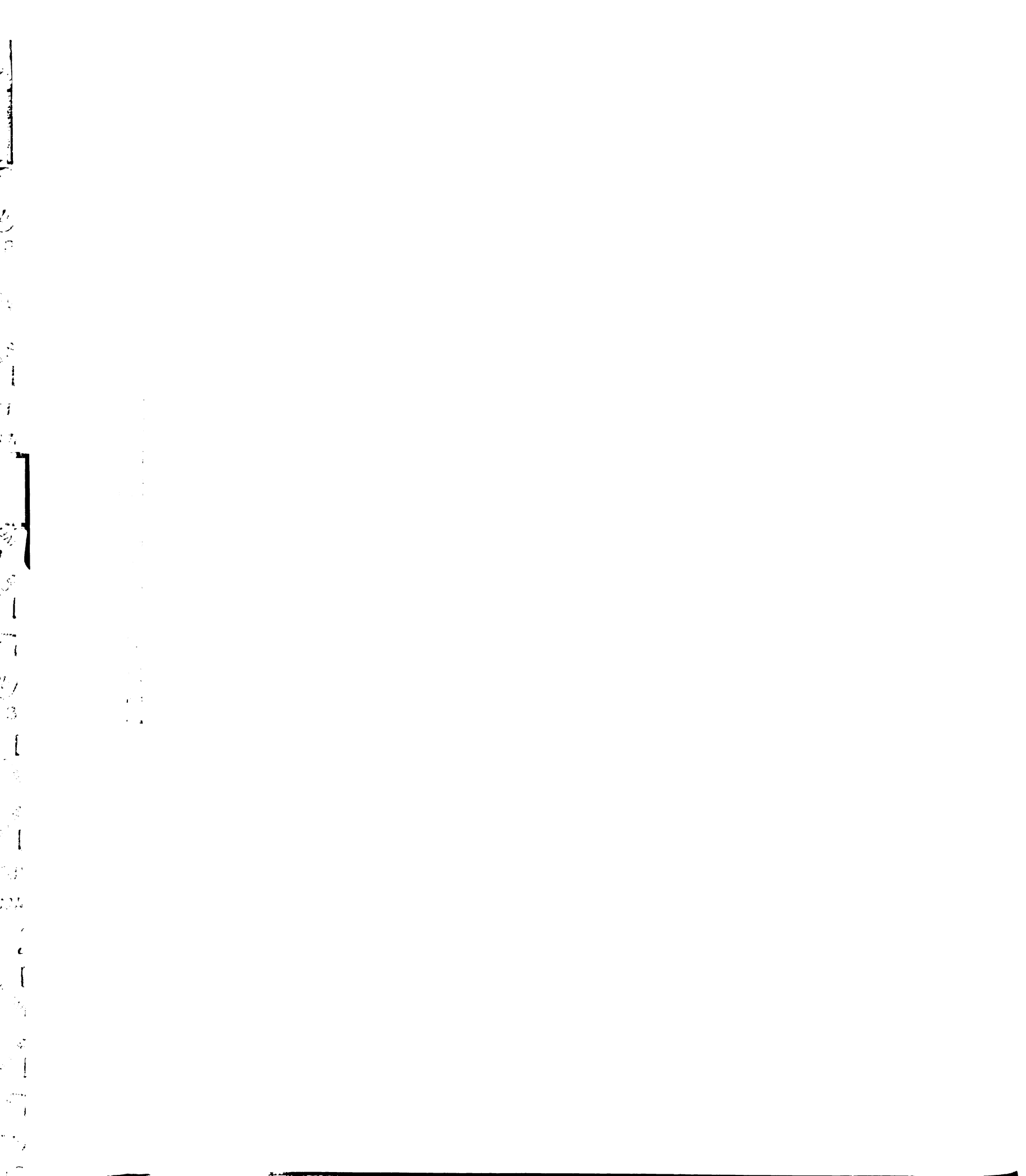
1  
2  
3  
4  
5  
6  
7  
8  
9  
10  
11  
12  
13  
14  
15  
16  
17  
18  
19  
20  
21  
22  
23  
24  
25  
26  
27  
28  
29  
30  
31  
32  
33  
34  
35  
36  
37  
38  
39  
40  
41  
42  
43  
44  
45  
46  
47  
48  
49  
50  
51  
52  
53  
54  
55  
56  
57  
58  
59  
60  
61  
62  
63  
64  
65  
66  
67  
68  
69  
70  
71  
72  
73  
74  
75  
76  
77  
78  
79  
80  
81  
82  
83  
84  
85  
86  
87  
88  
89  
90  
91  
92  
93  
94  
95  
96  
97  
98  
99  
100

conditions with the longitudinal pair having the highest value. The pair-wise t-test showed statistically significant differences between all conditions. However, only the distribution difference between the longitudinal pair and acoustic stimulation was confirmed for the population means (ANOVA Fisher PLSD,  $p < 0.05$ ). The mean low cut-off frequency at -6dB from maximum was based on fewer values than for the high cut-off frequency due to the limitations posed by low-pass distributions and stimulus constraints. There appeared to be no differences between conditions for this measure for the population means. However, the pair-wise t-test reveals a significant difference between the radial pair and acoustic conditions indicating slightly lower values for the electrical condition.

The mean maximum firing rate at BMF was similar for both electrical conditions and appreciably lower for the acoustic condition. A pair-wise t-test demonstrated a statistically significant difference between both electrical conditions and the acoustic stimulating mode for each neuron.

### 3.1.8 Temporal Repetition Coding: Entrainment

An additional aspect of temporal repetition coding used in this study is a measure known in acoustic studies as "entrainment" that measures the amount of evoked activity per event (click, impulse) rather than the global activity of an entire train. Quantitative differences in entrainment for different spectral stimuli reveal a maximum entrainment frequency. From that measurement, additional features of entrainment can be evaluated including maximum entrainment (spikes/pulse), the entrainment value at -6dB or one-half of the maximum entrainment for the positive side of the entrainment distribution, and the high-frequency cut-off at an entrainment



value of 0.25 spikes per pulses.

Figure 19 shows entrainment profiles for four exemplary single units for all three stimulating conditions. From this figure, it can be seen that the highest entrainment values always occurred at lower repetition rates, with a similar, precipitous slope to low entrainment values at higher repetitions rates for all neurons and all stimulating conditions. However, it can also be seen that the highest entrainment value differed between stimulating conditions for all neurons, although no clear mode-specific entrainment pattern emerged. Figure 20 shows entrainment profiles for five single units for each stimulating condition. Again, units varied in their highest entrainment values between units and across conditions with acoustic stimulation having the greatest spread across units. These profile collections again show that the highest entrainment occurs at lower repetition rates, and that there are no substantial differences between stimulating conditions.

The distributions for several parameters of entrainment are shown in Figure 21, and means and standard deviations are given in Table 5 for each condition. Maximum entrainment is the maximum number of spikes that occur as a result of one stimulus pulse, and corresponds to the maximum rate aspect of the tMTF. For all conditions, the mean maximum entrainment values reveal that, on the average, about one spike occurred per stimulus impulse. However, a small difference between both electrical conditions and the acoustic condition was detected using the pair-wise t-test, but did not apply for the population means. The frequency at which the maximum entrainment occurred corresponded to the BMF, although the mean maximum entrainment frequency is considerably lower than the mean BMF for all conditions, i.e. approximately 2.8Hz. There was no statistically

11  
12  
13  
14  
15  
16  
17  
18  
19  
20  
21  
22  
23  
24  
25  
26  
27  
28  
29  
30  
31  
32  
33  
34  
35  
36  
37  
38  
39  
40  
41  
42  
43  
44  
45  
46  
47  
48  
49  
50  
51  
52  
53  
54  
55  
56  
57  
58  
59  
60  
61  
62  
63  
64  
65  
66  
67  
68  
69  
70  
71  
72  
73  
74  
75  
76  
77  
78  
79  
80  
81  
82  
83  
84  
85  
86  
87  
88  
89  
90  
91  
92  
93  
94  
95  
96  
97  
98  
99  
100

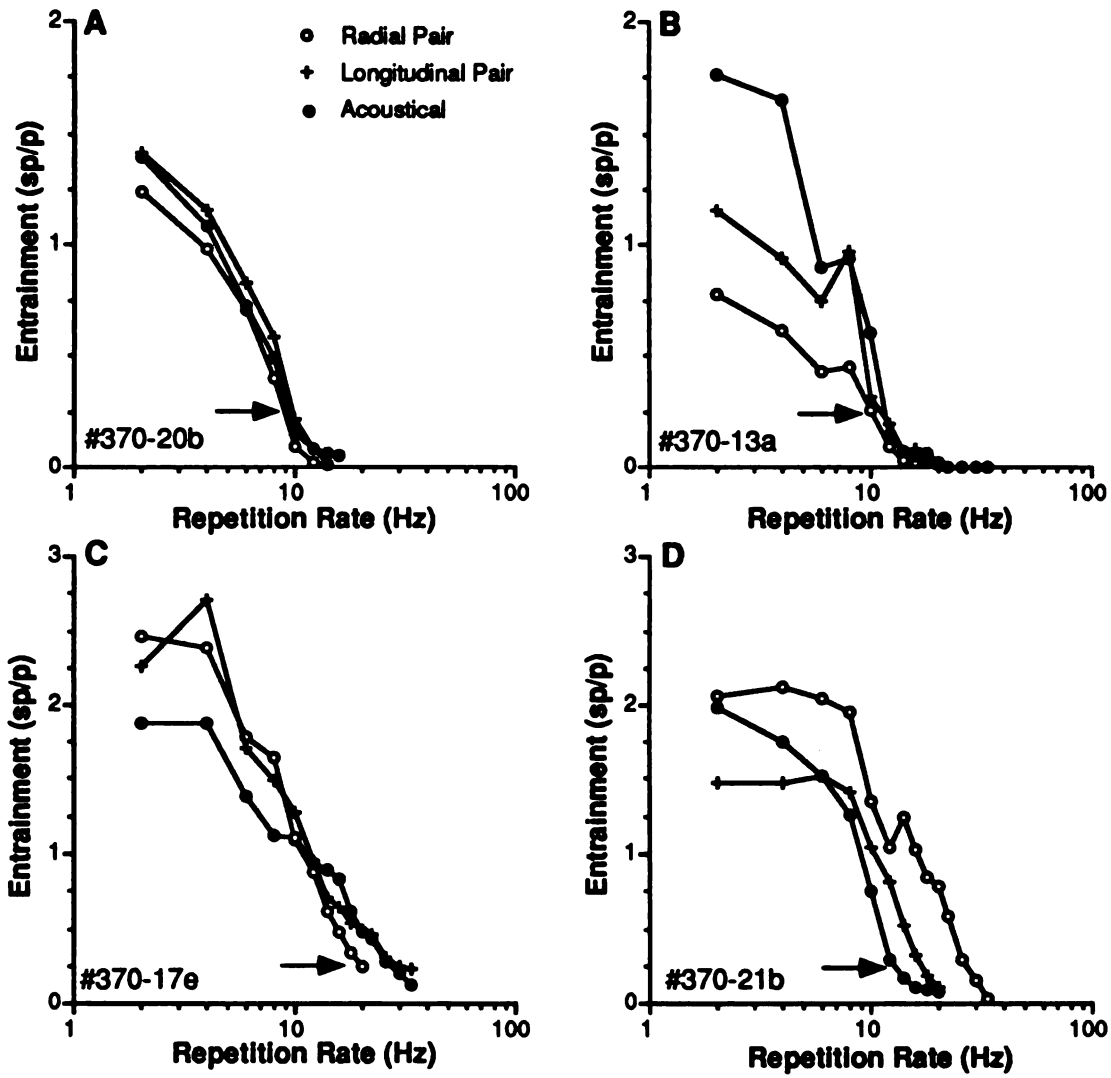
Figure 19. Repetition rate/entrainment functions for four single units (A,B,C,D) using a radial electrode pair (1,2), a longitudinal electrode pair (1,8), and acoustic click stimulation. Entrainment is measured in spikes/pulse. Repetition frequencies were 2-38Hz. The arrows point to the upper cut-off frequencies for a criterion of 0.25 spikes per pulse. The functions shown are from the same neurons as the tMTFs depicted in Fig. 14.

APR 11 1961

1  
2  
3  
4  
5  
6  
7  
8  
9  
10  
11  
12  
13  
14  
15  
16  
17  
18  
19  
20  
21  
22  
23  
24  
25  
26  
27  
28  
29  
30  
31  
32  
33  
34  
35  
36  
37  
38  
39  
40  
41  
42  
43  
44  
45  
46  
47  
48  
49  
50  
51  
52  
53  
54  
55  
56  
57  
58  
59  
60  
61  
62  
63  
64  
65  
66  
67  
68  
69  
70  
71  
72  
73  
74  
75  
76  
77  
78  
79  
80  
81  
82  
83  
84  
85  
86  
87  
88  
89  
90  
91  
92  
93  
94  
95  
96  
97  
98  
99  
100

FIGURE 19

Entrainment Functions



Acoustical

1  
2  
3  
4  
5  
6  
7  
8  
9  
10  
11  
12  
13  
14  
15  
16  
17  
18  
19  
20  
21  
22  
23  
24  
25  
26  
27  
28  
29  
30  
31  
32  
33  
34  
35  
36  
37  
38  
39  
40  
41  
42  
43  
44  
45  
46  
47  
48  
49  
50  
51  
52  
53  
54  
55  
56  
57  
58  
59  
60  
61  
62  
63  
64  
65  
66  
67  
68  
69  
70  
71  
72  
73  
74  
75  
76  
77  
78  
79  
80  
81  
82  
83  
84  
85  
86  
87  
88  
89  
90  
91  
92  
93  
94  
95  
96  
97  
98  
99  
100

1  
2  
3  
4  
5  
6  
7  
8  
9  
10  
11  
12  
13  
14  
15  
16  
17  
18  
19  
20  
21  
22  
23  
24  
25  
26  
27  
28  
29  
30  
31  
32  
33  
34  
35  
36  
37  
38  
39  
40  
41  
42  
43  
44  
45  
46  
47  
48  
49  
50  
51  
52  
53  
54  
55  
56  
57  
58  
59  
60  
61  
62  
63  
64  
65  
66  
67  
68  
69  
70  
71  
72  
73  
74  
75  
76  
77  
78  
79  
80  
81  
82  
83  
84  
85  
86  
87  
88  
89  
90  
91  
92  
93  
94  
95  
96  
97  
98  
99  
100

**Figure 20. Comparative repetition rate/entrainment functions of five single units using one radial electrode pair (1,2), one longitudinal electrode pair (1,8), and acoustic click stimulation. Entrainment is measured in spikes/pulse. Repetition frequencies were 2-38Hz.**

AMERICAN UNIVERSITY

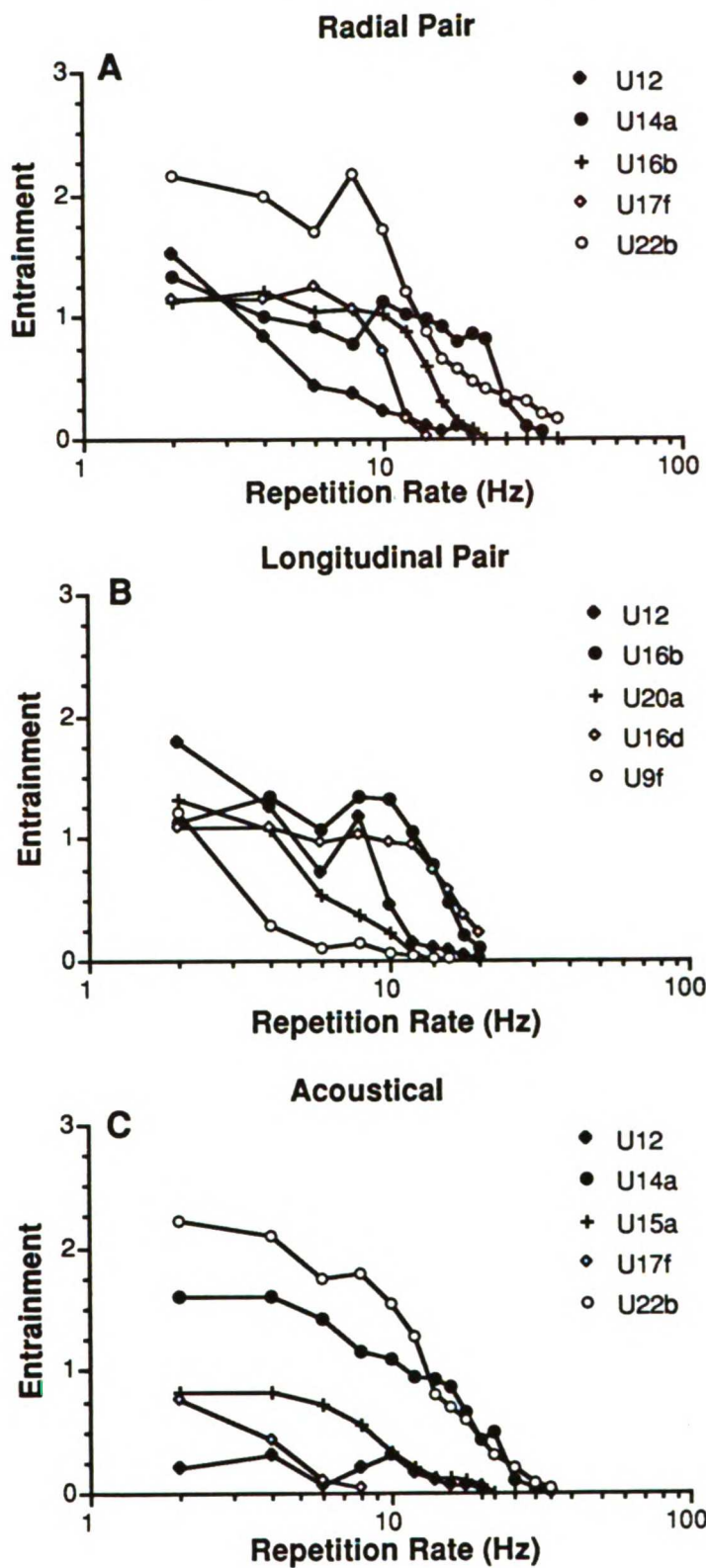
11  
12  
13  
14  
15  
16  
17  
18  
19  
20  
21  
22  
23  
24  
25  
26  
27  
28  
29  
30  
31  
32  
33  
34  
35  
36  
37  
38  
39  
40  
41  
42  
43  
44  
45  
46  
47  
48  
49  
50  
51  
52  
53  
54  
55  
56  
57  
58  
59  
60  
61  
62  
63  
64  
65  
66  
67  
68  
69  
70  
71  
72  
73  
74  
75  
76  
77  
78  
79  
80  
81  
82  
83  
84  
85  
86  
87  
88  
89  
90  
91  
92  
93  
94  
95  
96  
97  
98  
99  
100

11  
12  
13  
14  
15  
16  
17  
18  
19  
20  
21  
22  
23  
24  
25  
26  
27  
28  
29  
30  
31  
32  
33  
34  
35  
36  
37  
38  
39  
40  
41  
42  
43  
44  
45  
46  
47  
48  
49  
50  
51  
52  
53  
54  
55  
56  
57  
58  
59  
60  
61  
62  
63  
64  
65  
66  
67  
68  
69  
70  
71  
72  
73  
74  
75  
76  
77  
78  
79  
80  
81  
82  
83  
84  
85  
86  
87  
88  
89  
90  
91  
92  
93  
94  
95  
96  
97  
98  
99  
100

11  
12  
13  
14  
15  
16  
17  
18  
19  
20  
21  
22  
23  
24  
25  
26  
27  
28  
29  
30  
31  
32  
33  
34  
35  
36  
37  
38  
39  
40  
41  
42  
43  
44  
45  
46  
47  
48  
49  
50  
51  
52  
53  
54  
55  
56  
57  
58  
59  
60  
61  
62  
63  
64  
65  
66  
67  
68  
69  
70  
71  
72  
73  
74  
75  
76  
77  
78  
79  
80  
81  
82  
83  
84  
85  
86  
87  
88  
89  
90  
91  
92  
93  
94  
95  
96  
97  
98  
99  
100

FIGURE 20

Entrainment Functions



11  
12  
13  
14  
15  
16  
17  
18  
19  
20  
21  
22  
23  
24  
25  
26  
27  
28  
29  
30  
31  
32  
33  
34  
35  
36  
37  
38  
39  
40  
41  
42  
43  
44  
45  
46  
47  
48  
49  
50  
51  
52  
53  
54  
55  
56  
57  
58  
59  
60  
61  
62  
63  
64  
65  
66  
67  
68  
69  
70  
71  
72  
73  
74  
75  
76  
77  
78  
79  
80  
81  
82  
83  
84  
85  
86  
87  
88  
89  
90  
91  
92  
93  
94  
95  
96  
97  
98  
99  
100

11  
12  
13  
14  
15  
16  
17  
18  
19  
20  
21  
22  
23  
24  
25  
26  
27  
28  
29  
30  
31  
32  
33  
34  
35  
36  
37  
38  
39  
40  
41  
42  
43  
44  
45  
46  
47  
48  
49  
50  
51  
52  
53  
54  
55  
56  
57  
58  
59  
60  
61  
62  
63  
64  
65  
66  
67  
68  
69  
70  
71  
72  
73  
74  
75  
76  
77  
78  
79  
80  
81  
82  
83  
84  
85  
86  
87  
88  
89  
90  
91  
92  
93  
94  
95  
96  
97  
98  
99  
100

11  
12  
13  
14  
15  
16  
17  
18  
19  
20  
21  
22  
23  
24  
25  
26  
27  
28  
29  
30  
31  
32  
33  
34  
35  
36  
37  
38  
39  
40  
41  
42  
43  
44  
45  
46  
47  
48  
49  
50  
51  
52  
53  
54  
55  
56  
57  
58  
59  
60  
61  
62  
63  
64  
65  
66  
67  
68  
69  
70  
71  
72  
73  
74  
75  
76  
77  
78  
79  
80  
81  
82  
83  
84  
85  
86  
87  
88  
89  
90  
91  
92  
93  
94  
95  
96  
97  
98  
99  
100

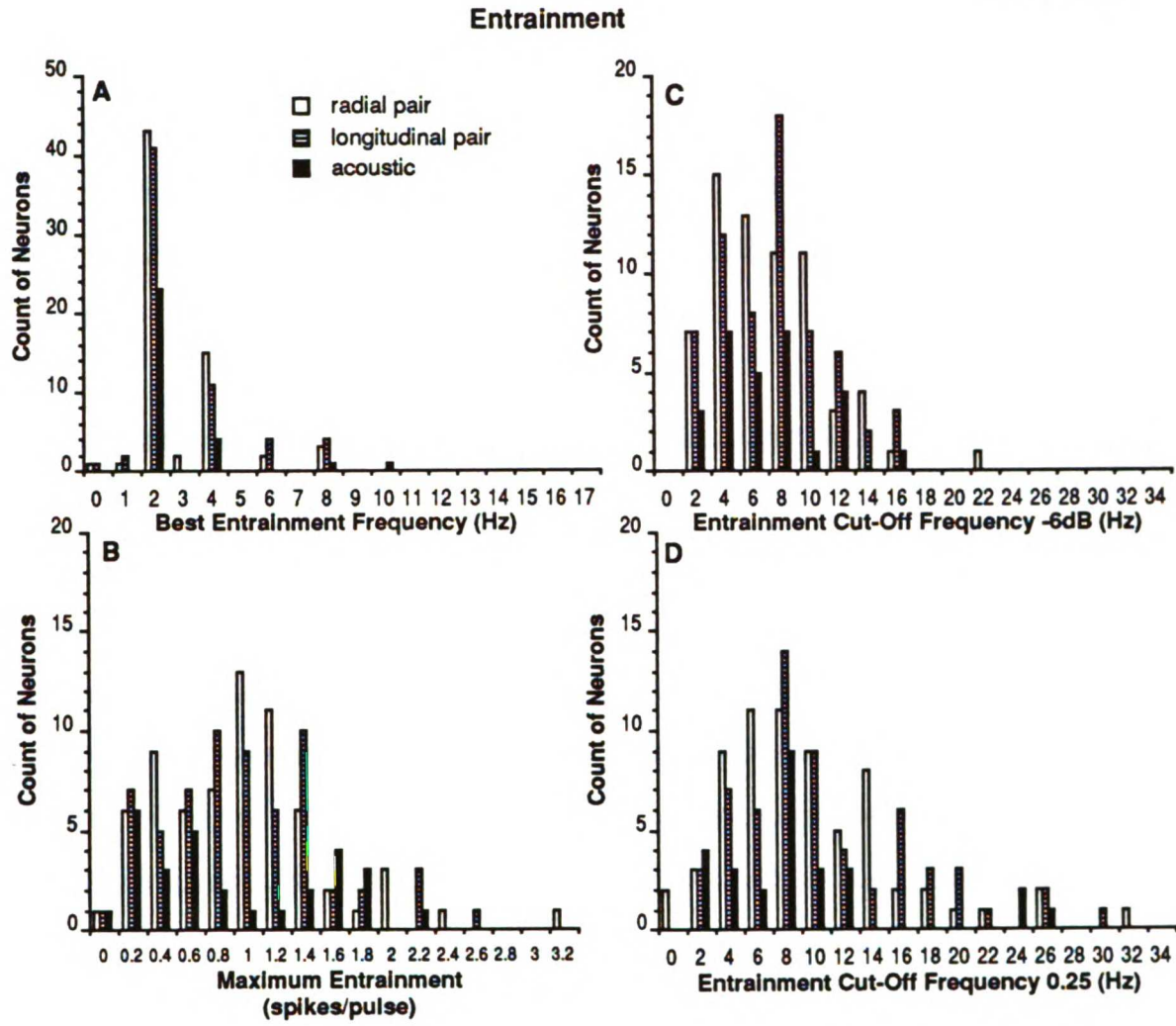
11  
12  
13  
14  
15  
16  
17  
18  
19  
20  
21  
22  
23  
24  
25  
26  
27  
28  
29  
30  
31  
32  
33  
34  
35  
36  
37  
38  
39  
40  
41  
42  
43  
44  
45  
46  
47  
48  
49  
50  
51  
52  
53  
54  
55  
56  
57  
58  
59  
60  
61  
62  
63  
64  
65  
66  
67  
68  
69  
70  
71  
72  
73  
74  
75  
76  
77  
78  
79  
80  
81  
82  
83  
84  
85  
86  
87  
88  
89  
90  
91  
92  
93  
94  
95  
96  
97  
98  
99  
100

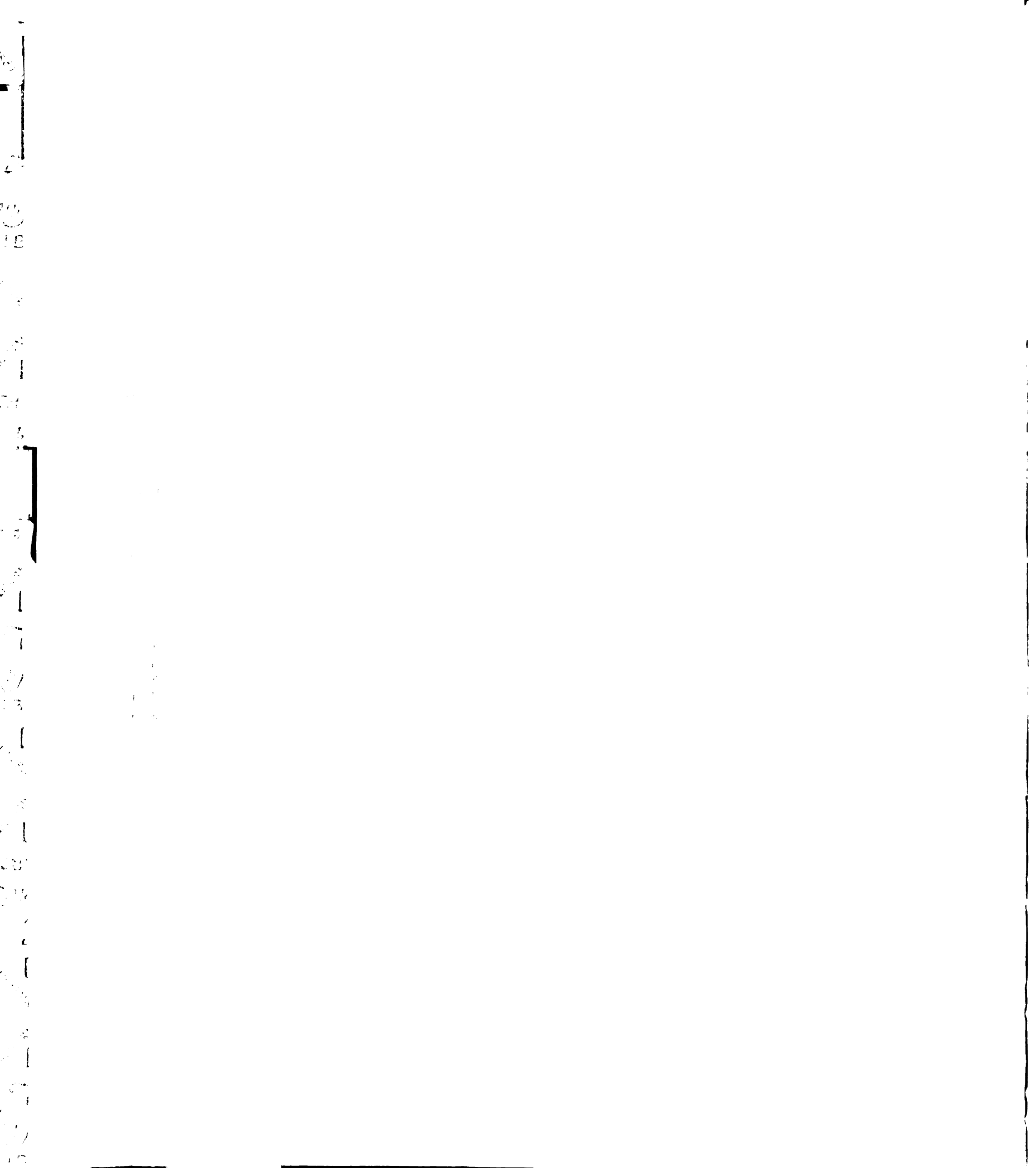
**Figure 21. Comparative parameter distributions for aspects of entrainment using a radial electrode pair (1,2), a longitudinal electrode pair (1,8), and acoustic click stimulation. Parametric distributions for entrainment measurements are depicted: maximum entrainment frequency (A), maximum entrainment (B), entrainment cut-off frequency at -6dB, and cut-off frequency for 0.25 entrainment (D). Means, standard deviations, and number of neurons per condition are given in Table 5.**

ADDITIONAL EQUIP!

7  
18  
19  
20  
21  
22  
23  
24  
25  
26  
27  
28  
29  
30  
31  
32  
33  
34  
35  
36  
37  
38  
39  
40  
41  
42  
43  
44  
45  
46  
47  
48  
49  
50  
51  
52  
53  
54  
55  
56  
57  
58  
59  
60  
61  
62  
63  
64  
65  
66  
67  
68  
69  
70  
71  
72  
73  
74  
75  
76  
77  
78  
79  
80  
81  
82  
83  
84  
85  
86  
87  
88  
89  
90  
91  
92  
93  
94  
95  
96  
97  
98  
99  
100

FIGURE 21

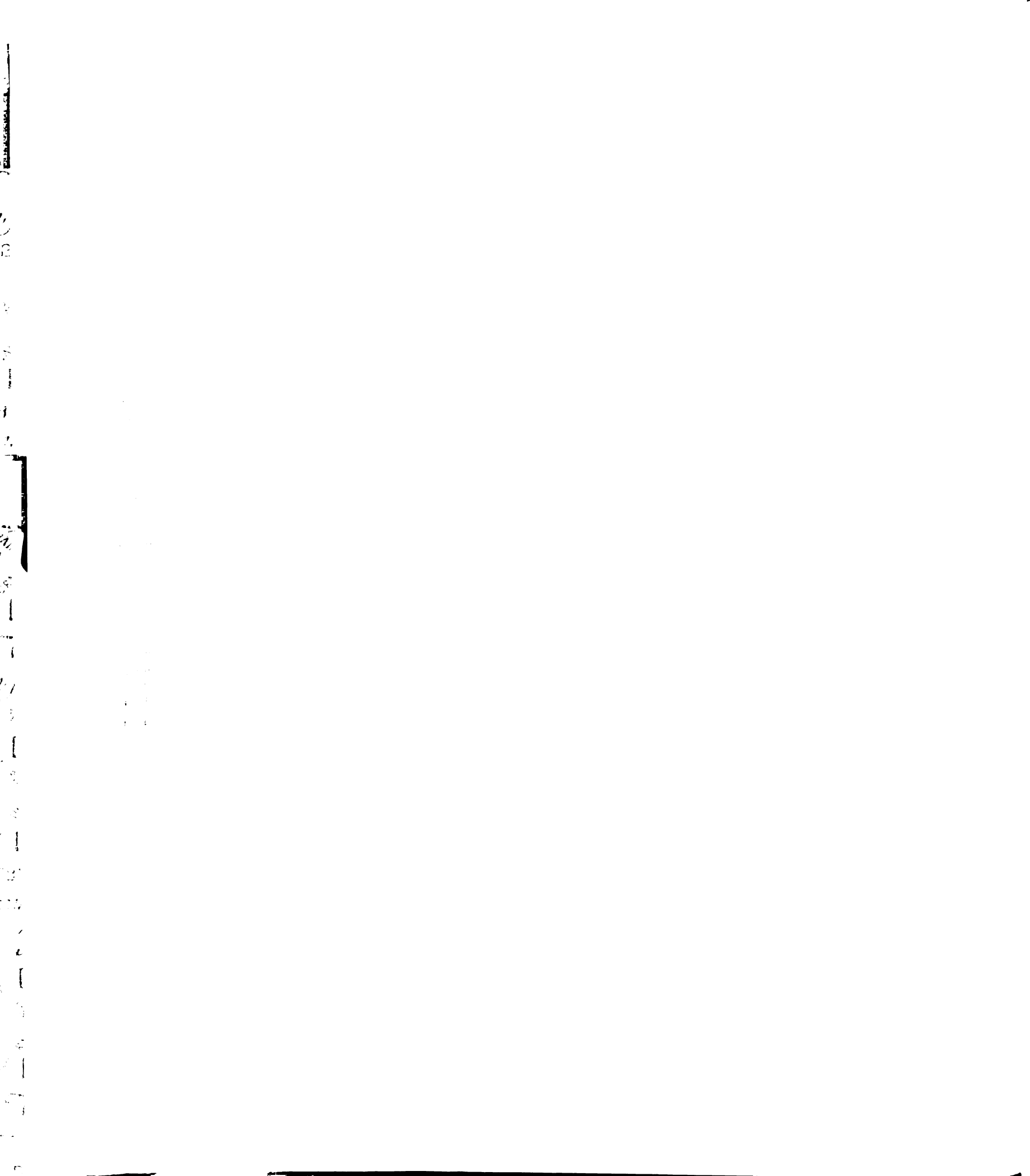




significant difference between any of the stimulating conditions for this measure.

The high-frequency cut-off of entrainment functions was determined at 6dB below maximum entrainment, consistent with the measure used for the tMTF. Similar to the tMTFs, the longitudinal pair yielded the highest cut-off frequency. However, the entrainment cut-off frequencies were only 60% to 69% of the corresponding tMTF values. No statistically significant difference was found between the -6dB entrainment cut-off for the three conditions.

An alternative measure to the high frequency cut-off at -6dB of maximum is the high frequency cut-off at an entrainment of 0.25 spikes per pulse (spp). In terms of entrainment, the necessity of an alternative measure for this aspect of entrainment responses is that it is possible for a given stimulus pulse to result in two or more spikes, thereby making the half of maximum or -6dB of maximum value an entrainment of one (or more). This entrainment value at the 'cut-off frequency' would mean that each stimulus pulse results in at least one spike which is an unrealistic criterion for a cut-off or limiting frequency considering the mean maximum entrainment values seen in Table 5. Therefore, the relative -6dB criteria is less appropriate than simply looking at an absolute entrainment value. Since the average entrainment at the -6dB cut-off frequency for the tMTF was found to be 0.25spp, this criterion was used to determine a cut-off frequency for the entrainment function, thereby providing a closer agreement between these two measures. Again, the cut-off frequency for the 0.25 spp criterion was the highest for the longitudinal pair. The acoustic value was slightly, but significantly, below the values for the electrical conditions. The 0.25spp cut-off frequencies were 86% to 90% of



the tMTF cut-off frequencies. Since entrainment functions were always low-pass, no low cut-off frequency was determined.

### 3.1.9 Correlations of Temporal Coding Parameters

Figure 22 shows the linear regression analyses for several aspects of temporal coding, while Table 6 shows the correlation analyses between the tMTF parameters discussed above for all conditions. The BMF shows a relatively high positive correlation with the low and high cut-off frequencies for all conditions with the exception of the low frequency cut-off for the acoustic condition. This correlation appears to be a straightforward relationship in which the higher the BMF, the inherently higher will be the low and high distribution cut-off frequencies at -6dB from the maximum or BMF. The BMF is also positively correlated with the maximum firing rate for all conditions. This is simply a reflection of a larger number of impulses per train at the higher BMFs. For the radial pair condition only, the high cut-off frequency is also significantly positively correlated with the low cut-off frequency, although the number of low cut-off frequency values reflect only those from bandpass neurons. There is also a positive correlation between the high cut-off frequency and the maximum firing rate for all conditions again indicative of the larger number of impulses per train for the higher cut-off frequencies. For the longitudinal pair, there is a significantly positive correlation between the maximum rate and the low-frequency cut-off.

Linear regression analysis revealed significant correlations for various temporal repetition coding parameters for all three conditions (see Table 6 for all values and Figure 22 for four example scatter plots). Table 6 shows that for all three conditions, the entrainment at -6dB of maximum or the

1  
2  
3  
4  
5  
6  
7  
8  
9  
10  
11  
12  
13  
14  
15  
16  
17  
18  
19  
20  
21  
22  
23  
24  
25  
26  
27  
28  
29  
30  
31  
32  
33  
34  
35  
36  
37  
38  
39  
40  
41  
42  
43  
44  
45  
46  
47  
48  
49  
50  
51  
52  
53  
54  
55  
56  
57  
58  
59  
60  
61  
62  
63  
64  
65  
66  
67  
68  
69  
70  
71  
72  
73  
74  
75  
76  
77  
78  
79  
80  
81  
82  
83  
84  
85  
86  
87  
88  
89  
90  
91  
92  
93  
94  
95  
96  
97  
98  
99  
100

1  
2  
3  
4  
5  
6  
7  
8  
9  
10  
11  
12  
13  
14  
15  
16  
17  
18  
19  
20  
21  
22  
23  
24  
25  
26  
27  
28  
29  
30  
31  
32  
33  
34  
35  
36  
37  
38  
39  
40  
41  
42  
43  
44  
45  
46  
47  
48  
49  
50  
51  
52  
53  
54  
55  
56  
57  
58  
59  
60  
61  
62  
63  
64  
65  
66  
67  
68  
69  
70  
71  
72  
73  
74  
75  
76  
77  
78  
79  
80  
81  
82  
83  
84  
85  
86  
87  
88  
89  
90  
91  
92  
93  
94  
95  
96  
97  
98  
99  
100

1  
2  
3  
4  
5  
6  
7  
8  
9  
10  
11  
12  
13  
14  
15  
16  
17  
18  
19  
20  
21  
22  
23  
24  
25  
26  
27  
28  
29  
30  
31  
32  
33  
34  
35  
36  
37  
38  
39  
40  
41  
42  
43  
44  
45  
46  
47  
48  
49  
50  
51  
52  
53  
54  
55  
56  
57  
58  
59  
60  
61  
62  
63  
64  
65  
66  
67  
68  
69  
70  
71  
72  
73  
74  
75  
76  
77  
78  
79  
80  
81  
82  
83  
84  
85  
86  
87  
88  
89  
90  
91  
92  
93  
94  
95  
96  
97  
98  
99  
100

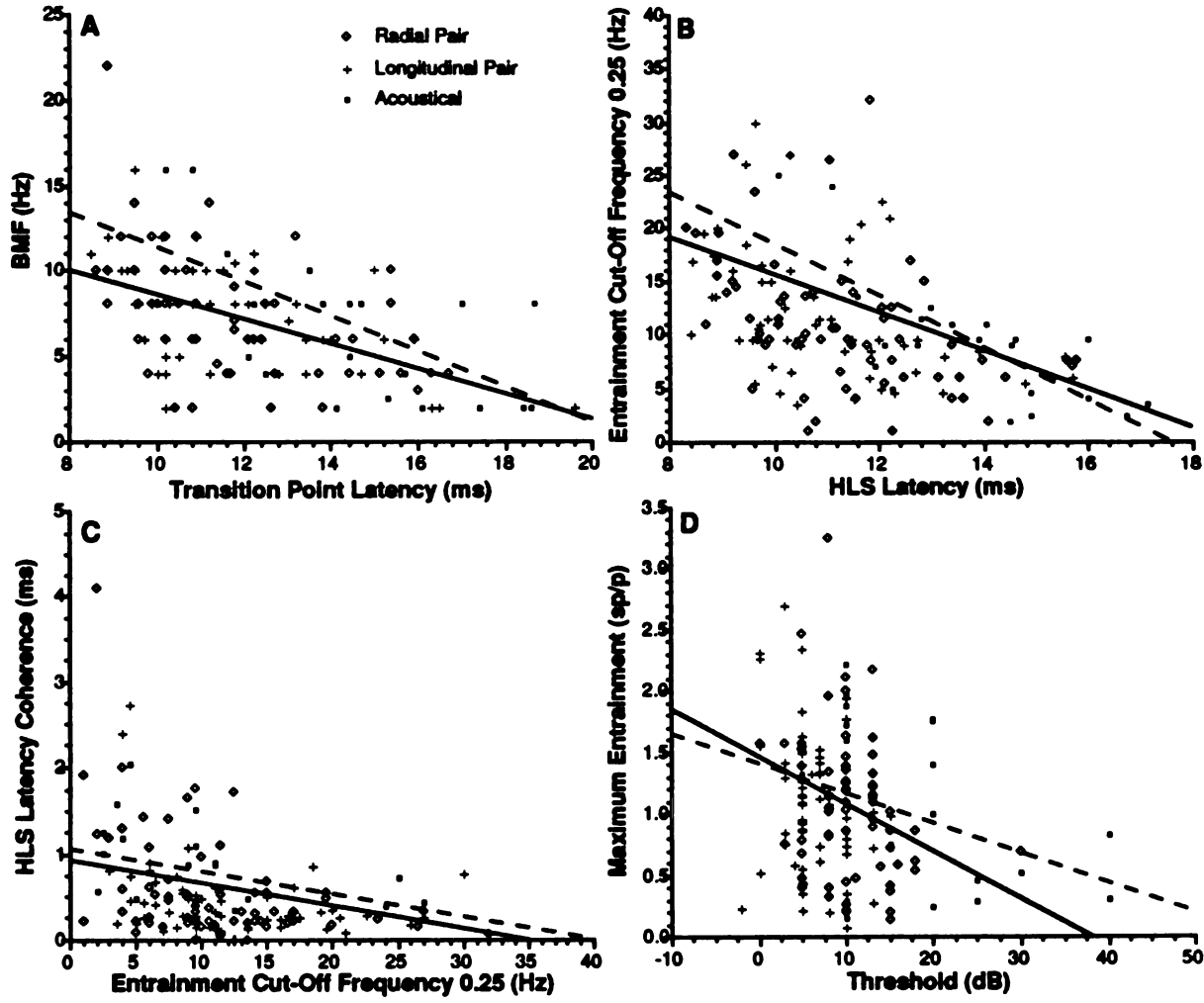
Figure 22. Linear regression analyses of temporal parameters for a radial pair (1,2), a longitudinal electrode pair (1,8), and acoustic click stimulation. The correlative relationships between transition point latency and BMF (A), latency of the high level segment and the cut-off frequency at an entrainment of 0.25spp (B), cut-off frequency at 0.25spp and high level segment latency coherence (C), and threshold and maximum entrainment (D) can be seen. Solid lines represent the linear regression for both electrical conditions combined since the differences between these conditions were small. The dashed line represents the regression line for the acoustic condition. Correlation coefficients and significance levels are given in Table 6.

ADDITIONAL COPY

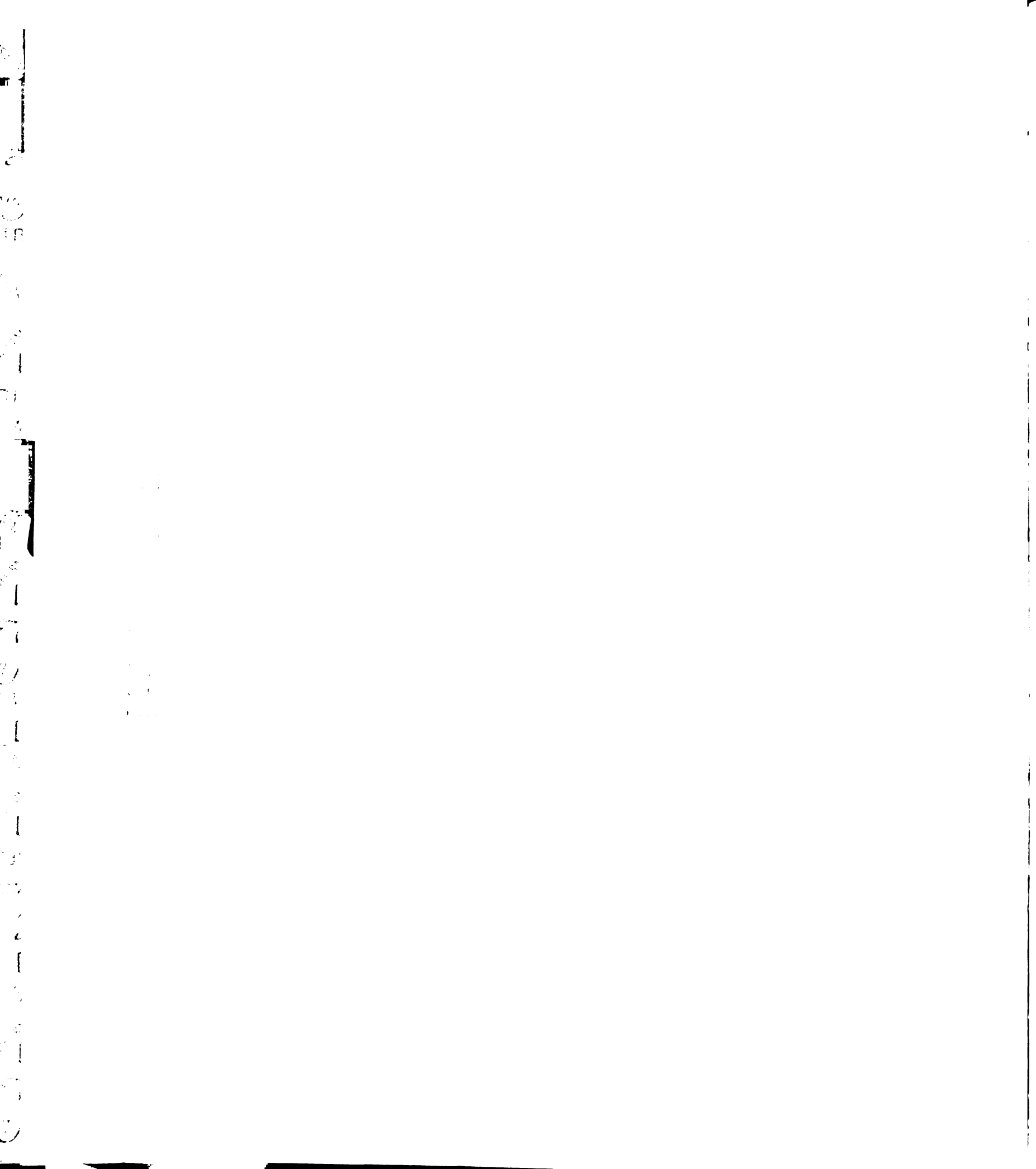
1  
2  
3  
4  
5  
6  
7  
8  
9  
10  
11  
12  
13  
14  
15  
16  
17  
18  
19  
20  
21  
22  
23  
24  
25  
26  
27  
28  
29  
30  
31  
32  
33  
34  
35  
36  
37  
38  
39  
40  
41  
42  
43  
44  
45  
46  
47  
48  
49  
50  
51  
52  
53  
54  
55  
56  
57  
58  
59  
60  
61  
62  
63  
64  
65  
66  
67  
68  
69  
70  
71  
72  
73  
74  
75  
76  
77  
78  
79  
80  
81  
82  
83  
84  
85  
86  
87  
88  
89  
90  
91  
92  
93  
94  
95  
96  
97  
98  
99  
100

FIGURE 22

Correlation of Temporal Parameters



ADDITIONAL COPY



**Table 6. TEMPORAL REPETITION CODING  
TEMPORAL CORRELATIONS-RADIAL**

	<u>BMF</u>	<u>Rt6dB(L)</u>	<u>Rt6dB(H)</u>	<u>Mx Rate</u>	<u>MxEntFr</u>	<u>Ent6dB(H)</u>	<u>Ent0.25</u>	<u>Max Ent</u>
Best Mod Freq								
Rate -6dB(L)	0.65***							
Rate -6dB(H)	0.71***	0.45**						
Max Rate	0.58***		0.45**					
Max Ent Freq			0.37*					
Ent -6dB (H)	0.77***	0.79***	0.72***	0.65***	0.40**			
Ent 0.25spp	0.62***	0.43*	0.83***	0.70***	0.3	0.74***		
Max Ent(spp)			0.3	0.65***			0.61***	

**TEMPORAL CORRELATIONS-LONGITUDINAL**

	<u>BMF</u>	<u>Rt6dB(L)</u>	<u>Rt6dB(H)</u>	<u>Mx Rate</u>	<u>MxEntFr</u>	<u>Ent6dB(H)</u>	<u>Ent0.25</u>	<u>Max Ent</u>
Best Mod Freq								
Rate -6dB (L)	0.63***							
Rate -6dB(H)	0.65***							
Max Rate	0.45**	0.46*	0.40*					
Max Ent Freq		0.36	0.25	0.58***				
Ent -6dB (H)	0.47***	0.46*	0.45**	0.72***	0.60***			
Ent 0.25spp	0.53***		0.71***	.079***	0.51***	0.81***		
Max Ent(spp)			0.35*	0.70***	0.36*		0.72***	

**TEMPORAL CORRELATIONS-ACOUSTIC**

	<u>BMF</u>	<u>Rt6dB(L)</u>	<u>Rt6dB(H)</u>	<u>Mx Rate</u>	<u>MxEntFr</u>	<u>Ent6dB(H)</u>	<u>Ent0.25</u>	<u>Max Ent</u>
Best Mod Freq								
Rate -6dB (L)								
Rate -6dB(H)	0.82***							
Max Rate	0.58**		0.58**					
Max Ent Freq		0.93***						
Ent -6dB (H)	0.90***		0.74***	0.55*	0.51*			
Ent 0.25spp	0.87***		0.92***	0.65**		0.82***		
Max Ent(spp)	0.39		0.50*	0.62**			0.69***	

**TEMPORAL CORRELATIONS-CONDITIONS**

	<u>RvL</u>	<u>RvAC</u>	<u>LvAC</u>
Best Mod Freq	0.55***	0.55*	0.73***
Rate -6dB (L)	0.47*	0.93**	
Rate -6dB (H)	0.63***	0.68***	0.82***
Max Rate	0.69***	0.70***	0.70***
Max Ent Freq	0.49***		
Ent -6dB (H)	0.64***	0.58*	
Ent 0.25spp	0.75***	0.76***	0.75**
Max Ent(spp)	0.67***	0.55*	0.67**

Intercorrelations of temporal repetition coding parameters for three stimulus conditions and parametric differences between stimulus conditions

\*\*\*p<0.0001 \*\*p<0.001 \*p<0.01 p<0.05

ACQUISITION

1  
2  
3  
4  
5  
6  
7  
8  
9  
10  
11  
12  
13  
14  
15  
16  
17  
18  
19  
20  
21  
22  
23  
24  
25  
26  
27  
28  
29  
30  
31  
32  
33  
34  
35  
36  
37  
38  
39  
40  
41  
42  
43  
44  
45  
46  
47  
48  
49  
50  
51  
52  
53  
54  
55  
56  
57  
58  
59  
60  
61  
62  
63  
64  
65  
66  
67  
68  
69  
70  
71  
72  
73  
74  
75  
76  
77  
78  
79  
80  
81  
82  
83  
84  
85  
86  
87  
88  
89  
90  
91  
92  
93  
94  
95  
96  
97  
98  
99  
100

entrainment at one-half maximum entrainment is highly positively correlated with entrainment at 0.25spp despite the differences in the definition of these two cut-off frequencies. The entrainment cut-off frequency at -6dB is also significantly correlated with the frequency of maximum entrainment. In addition, for all three conditions, maximum entrainment is relatively highly correlated with the entrainment cut-off frequency at the 0.25spp criterion. Finally, relatively small positive correlations were seen between the frequency of maximum entrainment and cut-off frequency at 0.25spp.

The tMTF high frequency cut-off at -6dB of maximum for all three conditions was positively correlated with the -6dB frequency cut-off for entrainment as well as with maximum entrainment. For all conditions, a very high, positive correlation was seen between the high frequency cut-off at -6dB of maximum for the tMTF and the entrainment cut-off frequency at 0.25spp. The close relationship of these two criteria measurements indicates that they measure the same aspect of a neuron's capacity to follow repeated stimuli. The 0.25spp criterion is actually a superior measure because of its absolute nature and its reliance on single events rather than global train responsiveness utilized for the tMTF measure.

Entrainment at -6dB of maximum, entrainment of 0.25spp, and maximum entrainment were all significantly positively correlated with the maximum firing rate for all three conditions. The correspondence between maximum firing rate and maximum entrainment was not surprising since both are measures of response strength. For all conditions, BMF was highly correlated with entrainment at -6dB of maximum as well as with entrainment of 0.25spp, reflecting the same relationship as with BMF and

ADDITIONAL COPY!

ADDITIONAL COPY!



the tMTF cut-off frequency. Some small, but significant correlations were seen for frequency of maximum entrainment and the low and high frequency cut-off frequencies for the different stimulating conditions. For the longitudinal pair, maximum rate is moderately correlated with frequency of maximum entrainment. The absence of a significant correlation between the BMF and the maximum entrainment frequency for all conditions should also be noted.

The bottom of Table 6 shows the results of a correlation analysis of the eight aspects of temporal repetition coding functions for the three stimulating conditions. All eight aspects were significantly correlated between both electrical conditions, and between the radial pair and the acoustic condition with the exception of frequency of maximum entrainment for the radial vs acoustic comparison. For the longitudinal and acoustic comparison, BMF, high frequency cut-off at -6dB of maximum of the tMTF, maximum rate, frequency cut-off at 0.25spp, and maximum entrainment are all relatively highly correlated. Since both longitudinal and acoustic stimulation can be thought of as essentially broadband stimulus modes, it is not surprising that BMF for both conditions is relatively highly correlated. It follows that the high frequency cut-off at -6dB would also be highly correlated for these two stimulating conditions. The maximum entrainment frequency for the acoustic condition appears not to be correlated with that of the electrical conditions.

### 3.1.10 Intercorrelations of Rate, Latency, and Temporal Repetition Parameters

Three main aspects of cortical responses to electrical and acoustic stimulation were investigated: firing rate, response latency, and repetition

ADDITIONAL COPY

1  
2  
3  
4  
5  
6  
7  
8  
9  
10  
11  
12  
13  
14  
15  
16  
17  
18  
19  
20  
21  
22  
23  
24  
25  
26  
27  
28  
29  
30  
31  
32  
33  
34  
35  
36  
37  
38  
39  
40  
41  
42  
43  
44  
45  
46  
47  
48  
49  
50  
51  
52  
53  
54  
55  
56  
57  
58  
59  
60  
61  
62  
63  
64  
65  
66  
67  
68  
69  
70  
71  
72  
73  
74  
75  
76  
77  
78  
79  
80  
81  
82  
83  
84  
85  
86  
87  
88  
89  
90  
91  
92  
93  
94  
95  
96  
97  
98  
99  
100

1  
2  
3  
4  
5  
6  
7  
8  
9  
10  
11  
12  
13  
14  
15  
16  
17  
18  
19  
20  
21  
22  
23  
24  
25  
26  
27  
28  
29  
30  
31  
32  
33  
34  
35  
36  
37  
38  
39  
40  
41  
42  
43  
44  
45  
46  
47  
48  
49  
50  
51  
52  
53  
54  
55  
56  
57  
58  
59  
60  
61  
62  
63  
64  
65  
66  
67  
68  
69  
70  
71  
72  
73  
74  
75  
76  
77  
78  
79  
80  
81  
82  
83  
84  
85  
86  
87  
88  
89  
90  
91  
92  
93  
94  
95  
96  
97  
98  
99  
100

coding. The following analysis attempts to establish relationships between these different response characteristics. Intercorrelation values for rate versus latency and temporal parameters for all three stimulating conditions are shown in Table 7. Only a few consistent correlations were seen between rate/level function parameters and latency/level function parameters for any stimulating conditions. Specifically, high correlations were seen only between the response threshold and the transition point level of the rate/level function with the transition point level obtained from the latency/level function for all three conditions. The lowest correlations for these parameters were found for the longitudinal pair. This may be due to the fairly shallow latency/level functions found for this condition, which results in a less distinct transition between the high and low level segments leading to a less accurate estimate of the transition point.

There was no consistent pattern of intercorrelations of temporal repetition parameters with rate parameters across the three stimulating conditions. A small negative correlation was found between response threshold and maximum entrainment for both electrical conditions. For the acoustic condition, relatively small positive correlations were seen between dynamic range and the temporal parameters BMF and the high cut-off frequencies. Therefore, the larger the dynamic range, the higher the BMF and cut-off frequencies of tMTF and entrainment. As might be expected, the slope of the low level segment also showed the same pattern of correlation with temporal factors.

Table 8 shows the intercorrelations of latency and temporal parameters. One important relationship among these intercorrelations was that between the onset latency and measures of temporal following

1  
2  
3  
4  
5  
6  
7  
8  
9  
10  
11  
12  
13  
14  
15  
16  
17  
18  
19  
20  
21  
22  
23  
24  
25  
26  
27  
28  
29  
30  
31  
32  
33  
34  
35  
36  
37  
38  
39  
40  
41  
42  
43  
44  
45  
46  
47  
48  
49  
50  
51  
52  
53  
54  
55  
56  
57  
58  
59  
60  
61  
62  
63  
64  
65  
66  
67  
68  
69  
70  
71  
72  
73  
74  
75  
76  
77  
78  
79  
80  
81  
82  
83  
84  
85  
86  
87  
88  
89  
90  
91  
92  
93  
94  
95  
96  
97  
98  
99  
100

1  
2  
3  
4  
5  
6  
7  
8  
9  
10  
11  
12  
13  
14  
15  
16  
17  
18  
19  
20  
21  
22  
23  
24  
25  
26  
27  
28  
29  
30  
31  
32  
33  
34  
35  
36  
37  
38  
39  
40  
41  
42  
43  
44  
45  
46  
47  
48  
49  
50  
51  
52  
53  
54  
55  
56  
57  
58  
59  
60  
61  
62  
63  
64  
65  
66  
67  
68  
69  
70  
71  
72  
73  
74  
75  
76  
77  
78  
79  
80  
81  
82  
83  
84  
85  
86  
87  
88  
89  
90  
91  
92  
93  
94  
95  
96  
97  
98  
99  
100

**Table 7. CORRELATION OF RATE/LEVEL PARAMETERS WITH LATENCY AND TEMPORAL PARAMETERS**

**RATE VS. LATENCY & TEMPORAL-RADIAL**

	<u>Thr</u>	<u>TP(rate)</u>	<u>TP.FR</u>	<u>DR</u>	<u>LLS-rate</u>	<u>HLS-rate</u>
Minimum Latency	0.40***	0.38***	-0.28*			
Latency at TP	0.24		-0.33*			
Average Latency	0.30*	0.28*	-0.31*			
Latency Coherence						0.22
LLS(lat)					-0.21	
HLS (lat)						-0.20
TP(lat)	0.80***	0.80***	0.33*			
Best Modulation Freq.						
Freq. at -6dB(L)						
Freq. at -6dB(H)			0.39*			
Maximum FR		0.31	0.66***			
Max.Ent. Frequency						
Entrainment at -6dB			0.49***			
			0.63***			
Entrainment 0.25spp						
Max. Entrainment	-0.27	0.28				

**RATE VS. LATENCY & TEMPORAL-LONGITUDINAL**

	<u>Thr</u>	<u>TP(rate)</u>	<u>TP.FR</u>	<u>DR</u>	<u>LLS-rate</u>	<u>HLS-rate</u>
Minimum Latency	0.53***	0.41***	-0.29*			
Latency at TP	0.40***	0.28*	-0.29*			
Average Latency	0.48***	0.39***	-0.29*			
Latency Coherence					0.33**	
LLS(lat)						
HLS(lat)						-0.21
TP (lat)	0.61***	0.58***	0.25			
Best Modulation Freq.	-0.25					
Freq. at -6dB(L)				0.33		
Freq. at -6dB(H)	-0.3		0.32			
Maximum FR	-0.27		0.49***	0.29		
Max.Ent. Frequency			0.26			
Entrainment at -6dB			0.36*			
Entrainment 0.25spp	-0.26		0.55***			
Max. Entrainment	-0.26		0.58***			

Accepted for publication



**RATE VS. LATENCY & TEMPORAL-ACOUSTIC**

	<u>Ihr</u>	<u>IP(rate)</u>	<u>TP.FR</u>	<u>DR</u>	<u>LLS(rate)</u>	<u>HLS(rate)</u>
Minimum Latency			-0.49*			0.36
Latency at TP			-0.49*			
Average Latency			-0.52*			
Latency Coherence						
LLS(lat)						
HLS(lat)						
TP (lat)	0.88***	0.92***				
Best Modulation Freq.			0.46	0.45	-0.41	
Freq. at -6dB(L)						-0.69
Freq. at -6dB(H)			0.66**	0.5	-0.42	
Maximum FR			0.65**			
Max.Ent. Frequency		0.54*		0.48		-0.41
Entrainment at -6dB			0.50	0.51	-0.43	
Entrainment 0.25spp			0.59*	0.44	-0.41	
Max. Entrainment			0.51			

Intercorrelations of rate/level parameters with latency and temporal repetition parameters

\*\*\*p<0.0001  
 \*\*p<0.001  
 \*p<0.01  
 p<0.05

ACCEPTED FOR PUBLICATION

1  
2  
3  
4  
5  
6  
7  
8  
9  
10  
11  
12  
13  
14  
15  
16  
17  
18  
19  
20  
21  
22  
23  
24  
25  
26  
27  
28  
29  
30  
31  
32  
33  
34  
35  
36  
37  
38  
39  
40  
41  
42  
43  
44  
45  
46  
47  
48  
49  
50  
51  
52  
53  
54  
55  
56  
57  
58  
59  
60  
61  
62  
63  
64  
65  
66  
67  
68  
69  
70  
71  
72  
73  
74  
75  
76  
77  
78  
79  
80  
81  
82  
83  
84  
85  
86  
87  
88  
89  
90  
91  
92  
93  
94  
95  
96  
97  
98  
99  
100

1  
2  
3  
4  
5  
6  
7  
8  
9  
10  
11  
12  
13  
14  
15  
16  
17  
18  
19  
20  
21  
22  
23  
24  
25  
26  
27  
28  
29  
30  
31  
32  
33  
34  
35  
36  
37  
38  
39  
40  
41  
42  
43  
44  
45  
46  
47  
48  
49  
50  
51  
52  
53  
54  
55  
56  
57  
58  
59  
60  
61  
62  
63  
64  
65  
66  
67  
68  
69  
70  
71  
72  
73  
74  
75  
76  
77  
78  
79  
80  
81  
82  
83  
84  
85  
86  
87  
88  
89  
90  
91  
92  
93  
94  
95  
96  
97  
98  
99  
100

**Table 8. CORRELATION OF LATENCY AND TEMPORAL PARAMETERS**

**LATENCY v. TEMPORAL-RADIAL**

	<b>BME</b>	<b>Rt6dB(L)</b>	<b>Rt6dB(H)</b>	<b>MaxRate</b>	<b>MxEntFr</b>	<b>Ent-6dB</b>	<b>Ent.25</b>	<b>MaxEnt</b>
Min Lat			-0.28	-0.35*		-0.40**	-0.37*	-0.27
Lat at TP	-0.31*	0.32	-0.32	-0.39*		-0.47***	-0.50***	-0.25
AverLat	-0.24		-0.3	-0.40**		-0.44**	-0.45***	-0.28
Lat Coh			-0.25			-0.27	-0.40**	
LLS(Lat)								
HLS(Lat)	0.25	0.33			0.28	0.29	0.31	
TP(Lat)								

**LATENCY v. TEMPORAL-LONGITUDINAL**

	<b>BME</b>	<b>Rt6dB(L)</b>	<b>Rt6dB(H)</b>	<b>MaxRate</b>	<b>MaxEntFr</b>	<b>Ent-6dB</b>	<b>Ent.25</b>	<b>MaxEnt</b>
Min Lat			-0.38*	-0.30		-0.34*	-0.38*	
Lat at TP	-0.32*		-0.34*	-0.38*		-0.47**	-0.49***	-0.26
Aver Lat			-0.33*	-0.35*		-0.40*	-0.44**	-0.27
Lat Coh						-0.31	-0.29	
LLS(Lat)			-0.32	-0.33	-0.25	-0.35*	-0.45**	-0.37*
HLS(Lat)								
TP(Lat)								

**LATENCY v. TEMPORAL-ACOUSTIC**

	<b>BME</b>	<b>Rt6dB(L)</b>	<b>Rt6dB(H)</b>	<b>MaxRate</b>	<b>MaxEntFr</b>	<b>Ent-6dB</b>	<b>Ent.25</b>	<b>MaxEnt</b>
Min Lat	-0.68**		-0.71***	-0.60**		-0.74***	-0.77***	-0.39
Lat at TP	-0.61*		-0.53*	-0.53*		-0.67**	-0.66**	
Aver Lat	-0.64**		-0.63**	-0.60*		-0.69**	-0.72**	-0.44
Lat Coh	-0.39					-0.46	-0.39	
LLS(Lat)								
HLS(Lat)		0.82*			0.58*	0.43		
TP(Lat)					0.45			

Intercorrelations of latency parameters and temporal repetition coding parameters

\*\*\*p=<0.0001

\*\*p=<0.001

\*p=<0.01

p=<0.05

ACCEPTED FOR PUBLICATION



capacity. For all three cases, the latency at the transition point was negatively correlated with BMF, high frequency cut-off for tMTF, and both high frequency cut-offs for entrainment. That is, the shorter the onset latency, the higher the ability of the neuron to follow rapidly repeated signals. In addition, latency at the transition point was also negatively correlated with the maximum rate of the tMTF, reflecting the finding that higher BMFs resulted in higher firing rates due to the higher number of events per train to which the neuron can respond. A clear correlation pattern can be seen for minimal latency and high level segment latency. The only exceptions to this pattern were the lack of correlation of  $L_{\min}$  and  $L_{\text{HLS}}$  with the BMF for the longitudinal pair, and no correlation for BMF and  $L_{\min}$  for the radial pair. Latency values were also negatively correlated with maximum entrainment particularly for the two electrical conditions. It should be noted that latency values were not correlated with frequency at maximum entrainment and the low cut-off frequency of bandpass tMTFs. The temporal coherence measure of the high level segment ( $LC_{\text{HLS}}$ ) was correlated with the entrainment cut-off frequencies in the sense that the higher the coherence, the higher the cut-off frequency.

Only for the longitudinal pair condition, the slope of the low level segment of latency/level functions showed a correlation with the high-frequency cut-off frequencies, maximum rate, maximum entrainment, and frequency of maximum entrainment. The slope of the high level segment showed some correlation with temporal parameters for the radial and acoustic conditions, most notably with the low-frequency cut-off frequency of the tMTF, the frequency of maximum entrainment, and the high frequency cut-off frequency 6dB below maximum entrainment.

APR 11 1971

1  
2  
3  
4  
5  
6  
7  
8  
9  
10  
11  
12  
13  
14  
15  
16  
17  
18  
19  
20  
21  
22  
23  
24  
25  
26  
27  
28  
29  
30  
31  
32  
33  
34  
35  
36  
37  
38  
39  
40  
41  
42  
43  
44  
45  
46  
47  
48  
49  
50  
51  
52  
53  
54  
55  
56  
57  
58  
59  
60  
61  
62  
63  
64  
65  
66  
67  
68  
69  
70  
71  
72  
73  
74  
75  
76  
77  
78  
79  
80  
81  
82  
83  
84  
85  
86  
87  
88  
89  
90  
91  
92  
93  
94  
95  
96  
97  
98  
99  
100

1  
2  
3  
4  
5  
6  
7  
8  
9  
10  
11  
12  
13  
14  
15  
16  
17  
18  
19  
20  
21  
22  
23  
24  
25  
26  
27  
28  
29  
30  
31  
32  
33  
34  
35  
36  
37  
38  
39  
40  
41  
42  
43  
44  
45  
46  
47  
48  
49  
50  
51  
52  
53  
54  
55  
56  
57  
58  
59  
60  
61  
62  
63  
64  
65  
66  
67  
68  
69  
70  
71  
72  
73  
74  
75  
76  
77  
78  
79  
80  
81  
82  
83  
84  
85  
86  
87  
88  
89  
90  
91  
92  
93  
94  
95  
96  
97  
98  
99  
100

### **3.2 Experimental Series Two: Spatial Distribution of Electrical Response Threshold**

Of interest in these experimental series is not only the physiological behavior and functional relationships of primary auditory cortical neurons when stimulated electrically, but also the distribution of these electrically-elicited responses in the rostral-caudal and dorsal-ventral domains of AI. Underlying an analysis of these distributions relative to acoustic parametric distributions could be significant information regarding the success or failure of human cochlear implant recipients in terms of open speech understanding.

Due to the necessary length of some experimental protocols, electrical threshold was deemed the first and most important spatial response distribution to obtain in the time available. In six experimental cases, multiple penetration maps were obtained in which stimulus thresholds were determined for all four radial electrode pairs and one longitudinal electrode pair. The orientation of recording electrode placement was provided by initial, contralateral, pre-implant acoustic frequency stimulation mapping.

#### **3.2.1 Rostral-Caudal Distributions: Cochlear Place Domain**

For six cases, thresholds were recorded for all electrode configurations at all penetration sites. Pair 1,2 was located most apically and Pair 7,8 was located most basally. Pair 1,7 or 1,8 represent longitudinal stimulation since each electrode contact making up the pair was located at the opposite ends of the electrode carrier. The approximate locations of all recording sites were marked on a schematic representation of the

AMERICAN

1  
2  
3  
4  
5  
6  
7  
8  
9  
10  
11  
12  
13  
14  
15  
16  
17  
18  
19  
20  
21  
22  
23  
24  
25  
26  
27  
28  
29  
30  
31  
32  
33  
34  
35  
36  
37  
38  
39  
40  
41  
42  
43  
44  
45  
46  
47  
48  
49  
50  
51  
52  
53  
54  
55  
56  
57  
58  
59  
60  
61  
62  
63  
64  
65  
66  
67  
68  
69  
70  
71  
72  
73  
74  
75  
76  
77  
78  
79  
80  
81  
82  
83  
84  
85  
86  
87  
88  
89  
90  
91  
92  
93  
94  
95  
96  
97  
98  
99  
100

1  
2  
3  
4  
5  
6  
7  
8  
9  
10  
11  
12  
13  
14  
15  
16  
17  
18  
19  
20  
21  
22  
23  
24  
25  
26  
27  
28  
29  
30  
31  
32  
33  
34  
35  
36  
37  
38  
39  
40  
41  
42  
43  
44  
45  
46  
47  
48  
49  
50  
51  
52  
53  
54  
55  
56  
57  
58  
59  
60  
61  
62  
63  
64  
65  
66  
67  
68  
69  
70  
71  
72  
73  
74  
75  
76  
77  
78  
79  
80  
81  
82  
83  
84  
85  
86  
87  
88  
89  
90  
91  
92  
93  
94  
95  
96  
97  
98  
99  
100

IB

L

11/1/19

12/1/19

1/1/20

2/1/20

3/1/20

4/1/20

ectosylvian gyrus for the six cases (see Figure 23). The number of recording locations ranged from 48 to 104.

Figure 24 depicts the method used for reconstruction of the spatial distributions of response thresholds for an electrical stimulating mode. Figure 24A shows the locations of the recording sites for an exemplary case. Figure 24B shows the threshold values obtained at each location for stimulation with the most apical electrode pair. The contour lines superimposed on this figure provide the basis for the three-dimensional depiction of threshold seen in Figure 24D. Contour lines connect points of equal threshold. Since some of these contours fall between points of actually measured threshold values, an interpolation algorithm was used to derive a complete value distribution across the mapped area. The ten nearest neighboring points were weighted according to an inverse distance law to calculate the interpolated values necessary for a complete description of the mapped area. The same interpolated contour lines seen in Figure 24B are replotted in Figure 24C. The areas enclosed by the contour lines, i.e. regions with thresholds below the contour line value, are marked by graduated shadings. Finally, to further enhance the visual depiction of the parameter distributions, areas of equivalent shading or of the same contour value are assigned different elevations in a pseudo-three dimensional depiction of the threshold distribution. In this plot, two axes correspond to the two spatial dimensions of the cortical surface and the third axis, elevation, is proportional to the threshold value at each location.

Figure 25 depicts the threshold distribution for four radial electrode pairs and one longitudinal electrode pair (case C163). In these plots, the highest elevation corresponds to the greatest sensitivity to electrical

LIB

FOR

MEM

OF

THE

UNIVERSITY

OF

CHICAGO

ILLINOIS

19

19

19

19

19

19

19

19

19

19

19

19

19

19

19

19

19

19

19

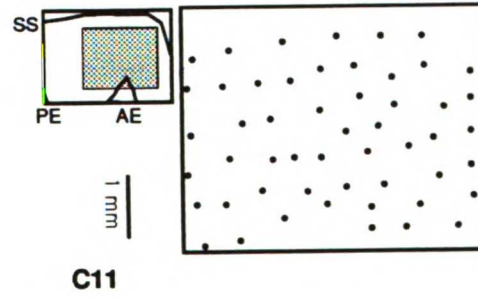
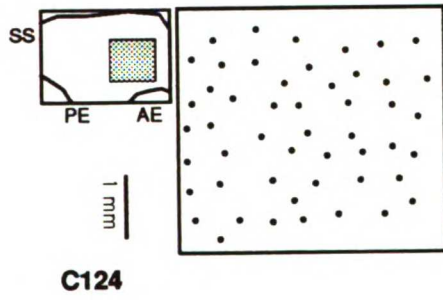
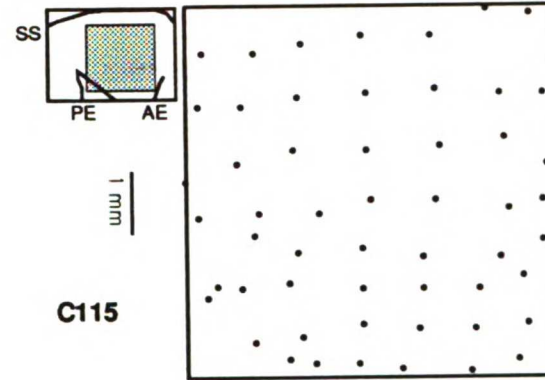
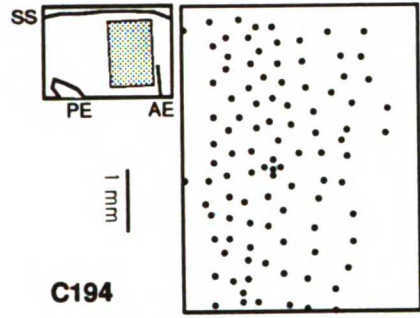
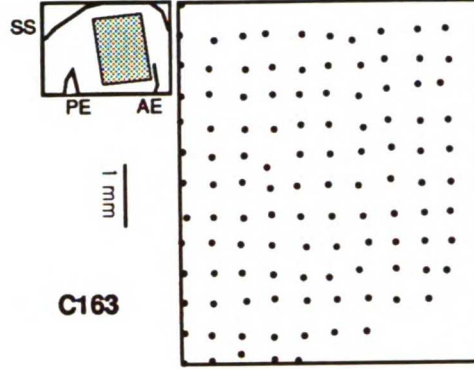
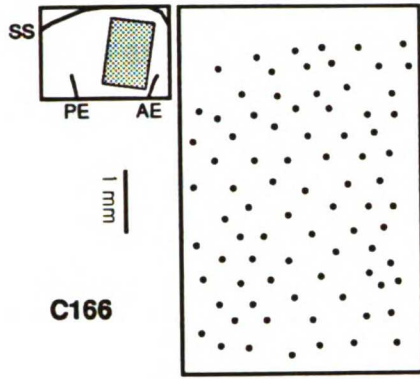
**Figure 23. Recording locations (maps) on the right ectosylvian gyrus in primary auditory cortex (AI) for six animals. The scale of all maps is identical. The shaded areas in the schematic drawings reflects the approximate site of the mapped areas. (SS= supra sylvia sulcus; PE = posterior ectosylvian sulcus; AE = anterior ectosylvian sulcus)**

AMNH 1001



FIGURE 23

Recording Locations in AI



ACI/NCJ 110011



**Figure 24. Sequential depiction of exemplary data reconstruction and representation: (A) locations of recording sites in primary auditory cortex (case C163); (B) electrical thresholds (in dB re 100 $\mu$ A) and isothreshold contours at 15, 25, and 35dB; (C) isothreshold contours shaded according to their threshold constituents re levels in B; (D) stacked contours or resulting three-dimensional reconstruction of data point values.**

ADDITIONAL

1  
2  
3  
4  
5  
6  
7  
8  
9  
10  
11  
12  
13  
14  
15  
16  
17  
18  
19  
20  
21  
22  
23  
24  
25  
26  
27  
28  
29  
30  
31  
32  
33  
34  
35  
36  
37  
38  
39  
40  
41  
42  
43  
44  
45  
46  
47  
48  
49  
50  
51  
52  
53  
54  
55  
56  
57  
58  
59  
60  
61  
62  
63  
64  
65  
66  
67  
68  
69  
70  
71  
72  
73  
74  
75  
76  
77  
78  
79  
80  
81  
82  
83  
84  
85  
86  
87  
88  
89  
90  
91  
92  
93  
94  
95  
96  
97  
98  
99  
100

FIGURE 24

Three-Dimensional Reconstruction of Spatial Distribution of Electrical Threshold in AI

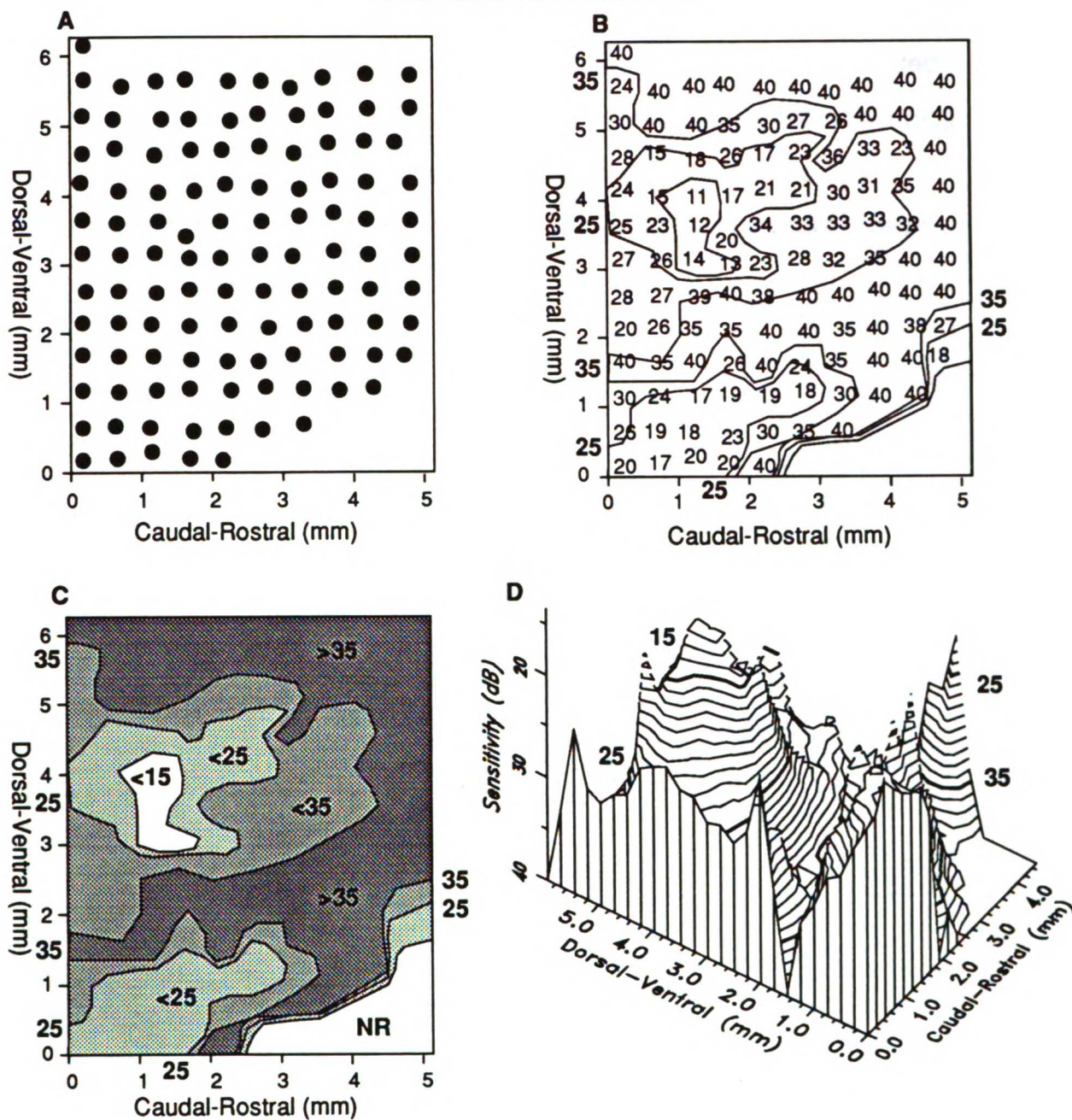




**Figure 25. Three-dimensional reconstructions of electrical threshold distributions in primary auditory cortex for individual electrode pairs (case C163). Schematic drawings of the basilar membrane and electrode carrier are below each plot. Darkened carrier contacts represent the stimulated electrode pair that results in the threshold distribution plotted above each drawing. Higher elevations reflect lower response thresholds. The highest thresholds (40dB) are at the bottom of the plot surface. Contour intervals are 1 dB. (See Figures 22 and 28 for additional views of these distributions.)**

ADDITIONAL COPY

RESEARCH CENTER FOR HUMAN DEVELOPMENT AND DISABILITIES

1  
2  
3  
4  
5  
6  
7  
8  
9  
10  
11  
12  
13  
14  
15  
16  
17  
18  
19  
20  
21  
22  
23  
24  
25  
26  
27  
28  
29  
30  
31  
32  
33  
34  
35  
36  
37  
38  
39  
40  
41  
42  
43  
44  
45  
46  
47  
48  
49  
50  
51  
52  
53  
54  
55  
56  
57  
58  
59  
60  
61  
62  
63  
64  
65  
66  
67  
68  
69  
70  
71  
72  
73  
74  
75  
76  
77  
78  
79  
80  
81  
82  
83  
84  
85  
86  
87  
88  
89  
90  
91  
92  
93  
94  
95  
96  
97  
98  
99  
100



1  
2  
3  
4  
5  
6  
7  
8  
9  
10  
11  
12  
13  
14  
15  
16  
17  
18  
19  
20  
21  
22  
23  
24  
25  
26  
27  
28  
29  
30  
31  
32  
33  
34  
35  
36  
37  
38  
39  
40  
41  
42  
43  
44  
45  
46  
47  
48  
49  
50  
51  
52  
53  
54  
55  
56  
57  
58  
59  
60  
61  
62  
63  
64  
65  
66  
67  
68  
69  
70  
71  
72  
73  
74  
75  
76  
77  
78  
79  
80  
81  
82  
83  
84  
85  
86  
87  
88  
89  
90  
91  
92  
93  
94  
95  
96  
97  
98  
99  
100

stimulation. To optimize the visual depictions of response distributions, the primary feature of interest is displayed as a maximum in these three dimensional plots. Therefore, sensitivity is plotted rather than threshold. Each successive contour line depicted in this figure corresponds to a 2dB change in sensitivity. These three-dimensional depictions suggest the close alignment between cochlear place of stimulation and electrical threshold distribution for the four radial electrode configurations, such that cochleotopic, electrode-specific low threshold 'ridges' can be seen in this Figure 25 to shift in a caudal to rostral direction as the stimulating electrode pair designation shifted from an apical to a basal peripheral stimulus location (note the schematic drawing of the basilar membrane and the corresponding stimulation electrodes below each plot). This electrical 'frequency tuning' was not surprising, considering the early work of Woolsey and Walzl (1944) and Walzl (1947), a systematic electrical stimulation of small groups of nerve fibers along the edge of the exposed osseous spiral lamina resulted in preferential, tonotopically- appropriate areas of response in auditory cortex. The resulting threshold distribution has been termed a "spatial tuning curve" (Snyder, et al., 1990). Note that the threshold distribution for the longitudinal pair (Pair 1,8), by contrast, was flat revealing nearly equal sensitivity across any caudal-rostral trajectory. This reflects the consequence of nearly simultaneous stimulation across a large sector of the spiral ganglion that is spatially equivalent to that of a broadband acoustic signal.

For each mapped case, electrode-specific preferential spatial tuning curves were obtained. However, not every case and not every electrode pair showed a clear spatially restricted representation as other cases or other pairs. Figures 26 and 27 are additional examples of three-dimensional depictions of spatial tuning for all electrode pairs. As

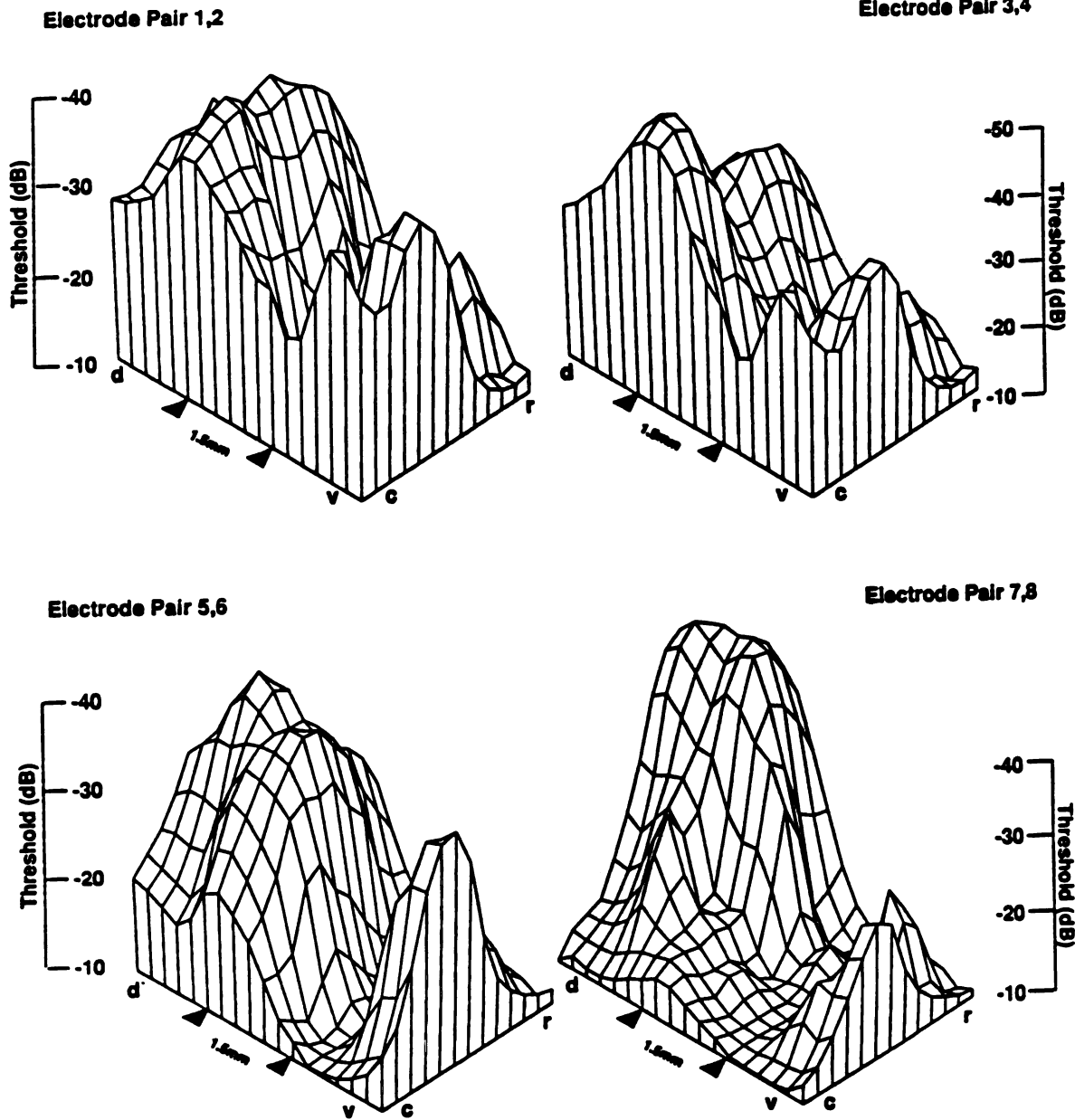


**Figure 26. Three-dimensional reconstructions of electrical threshold distributions in primary auditory cortex for individual electrode pairs (case C166). Elevation of the surface is proportional to the threshold values at each cortical location. Higher elevations reflect lower response thresholds. The highest thresholds (-10dB re 100mA) are at the bottom of the plot surface. Reconstruction is based on 68 points (see Figure 21).**

1  
2  
3  
4  
5  
6  
7  
8  
9  
10  
11  
12  
13  
14  
15  
16  
17  
18  
19  
20  
21  
22  
23  
24  
25  
26  
27  
28  
29  
30  
31  
32  
33  
34  
35  
36  
37  
38  
39  
40  
41  
42  
43  
44  
45  
46  
47  
48  
49  
50  
51  
52  
53  
54  
55  
56  
57  
58  
59  
60  
61  
62  
63  
64  
65  
66  
67  
68  
69  
70  
71  
72  
73  
74  
75  
76  
77  
78  
79  
80  
81  
82  
83  
84  
85  
86  
87  
88  
89  
90  
91  
92  
93  
94  
95  
96  
97  
98  
99  
100

1  
2  
3  
4  
5  
6  
7  
8  
9  
10  
11  
12  
13  
14  
15  
16  
17  
18  
19  
20  
21  
22  
23  
24  
25  
26  
27  
28  
29  
30  
31  
32  
33  
34  
35  
36  
37  
38  
39  
40  
41  
42  
43  
44  
45  
46  
47  
48  
49  
50  
51  
52  
53  
54  
55  
56  
57  
58  
59  
60  
61  
62  
63  
64  
65  
66  
67  
68  
69  
70  
71  
72  
73  
74  
75  
76  
77  
78  
79  
80  
81  
82  
83  
84  
85  
86  
87  
88  
89  
90  
91  
92  
93  
94  
95  
96  
97  
98  
99  
100

Threshold Distribution in AI for Electrical Stimulation of the Cochlea



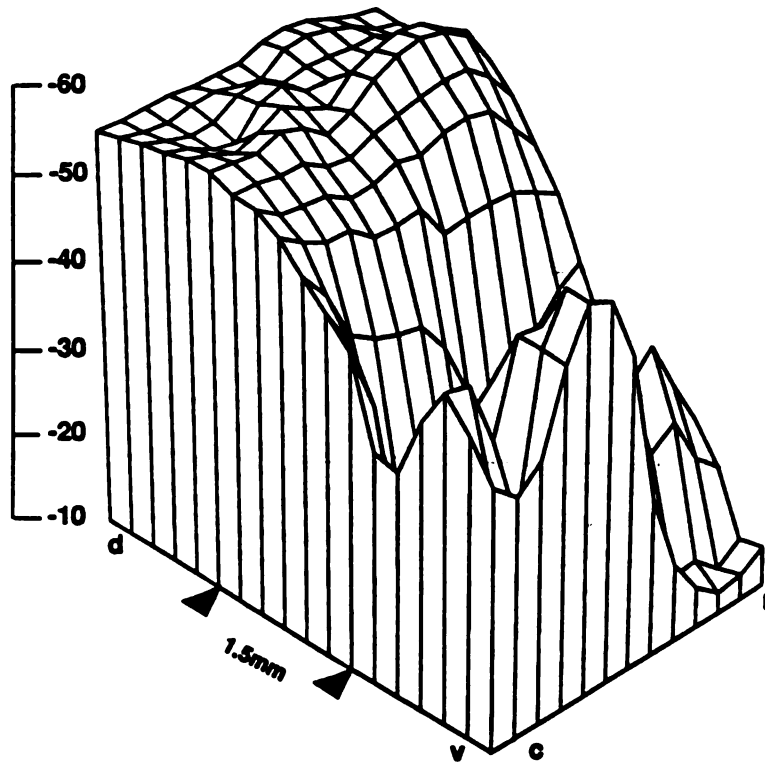
Ch-166

1  
2  
3  
4  
5  
6  
7  
8  
9  
10  
11  
12  
13  
14  
15  
16  
17  
18  
19  
20  
21  
22  
23  
24  
25  
26  
27  
28  
29  
30  
31  
32  
33  
34  
35  
36  
37  
38  
39  
40  
41  
42  
43  
44  
45  
46  
47  
48  
49  
50  
51  
52  
53  
54  
55  
56  
57  
58  
59  
60  
61  
62  
63  
64  
65  
66  
67  
68  
69  
70  
71  
72  
73  
74  
75  
76  
77  
78  
79  
80  
81  
82  
83  
84  
85  
86  
87  
88  
89  
90  
91  
92  
93  
94  
95  
96  
97  
98  
99  
100

1  
2  
3  
4  
5  
6  
7  
8  
9  
10  
11  
12  
13  
14  
15  
16  
17  
18  
19  
20  
21  
22  
23  
24  
25  
26  
27  
28  
29  
30  
31  
32  
33  
34  
35  
36  
37  
38  
39  
40  
41  
42  
43  
44  
45  
46  
47  
48  
49  
50  
51  
52  
53  
54  
55  
56  
57  
58  
59  
60  
61  
62  
63  
64  
65  
66  
67  
68  
69  
70  
71  
72  
73  
74  
75  
76  
77  
78  
79  
80  
81  
82  
83  
84  
85  
86  
87  
88  
89  
90  
91  
92  
93  
94  
95  
96  
97  
98  
99  
100

**FIGURE 26 (Cont)**  
**Threshold Distribution in AI for Electrical Stimulation of the Cochlea**

**Electrode Pair 1,8**



Ch-166



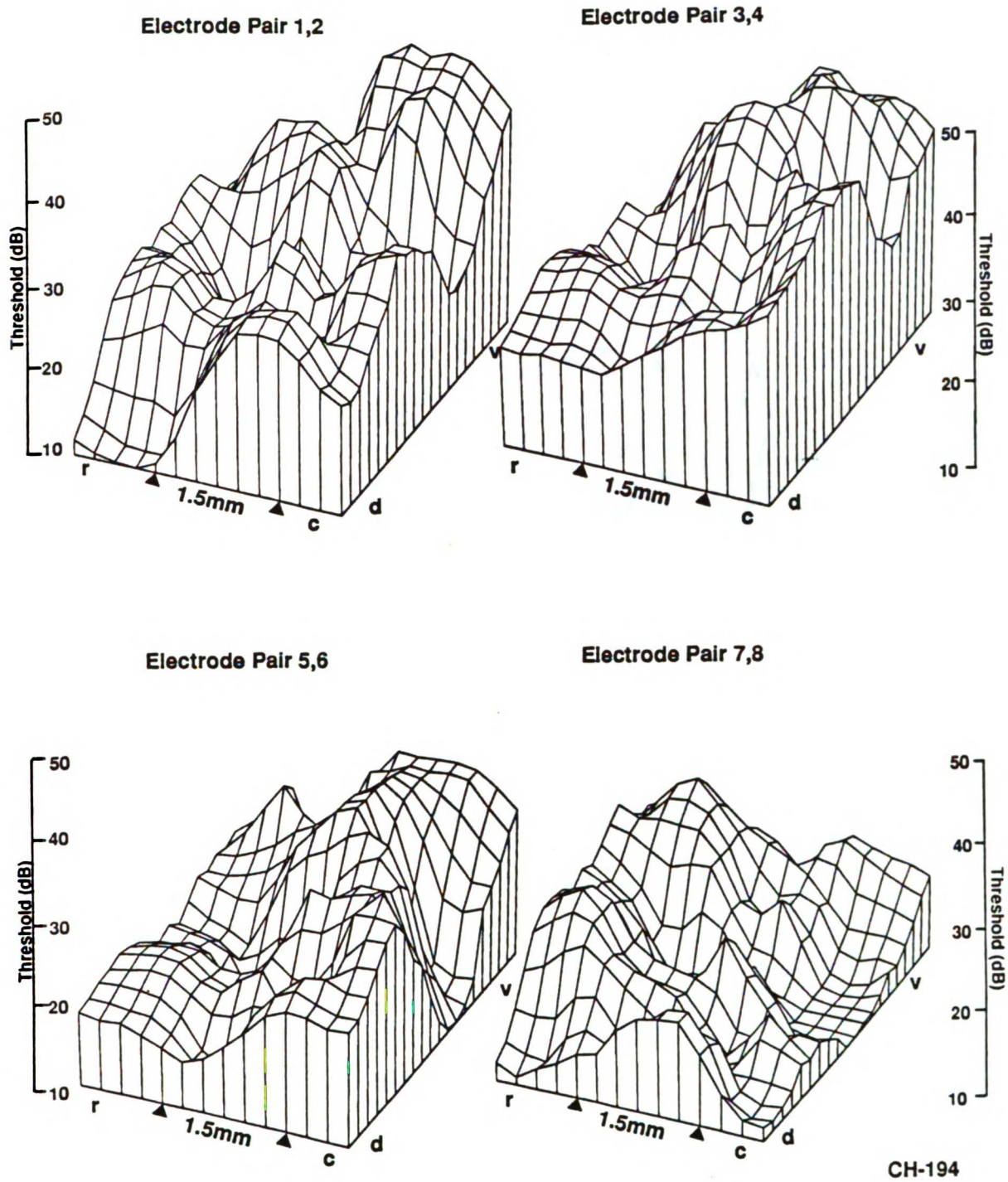
**Figure 27. Three-dimensional reconstructions of electrical threshold distributions in primary auditory cortex for individual electrode pairs (case C194). See Figure 24 for details.**

APR 11 1991

18  
19  
20  
21  
22  
23  
24  
25  
26  
27  
28  
29  
30  
31  
32  
33  
34  
35  
36  
37  
38  
39  
40  
41  
42  
43  
44  
45  
46  
47  
48  
49  
50  
51  
52  
53  
54  
55  
56  
57  
58  
59  
60  
61  
62  
63  
64  
65  
66  
67  
68  
69  
70  
71  
72  
73  
74  
75  
76  
77  
78  
79  
80  
81  
82  
83  
84  
85  
86  
87  
88  
89  
90  
91  
92  
93  
94  
95  
96  
97  
98  
99  
100

[Illegible text]

Threshold Distribution in AI for Electrical Stimulation of the Cochlea



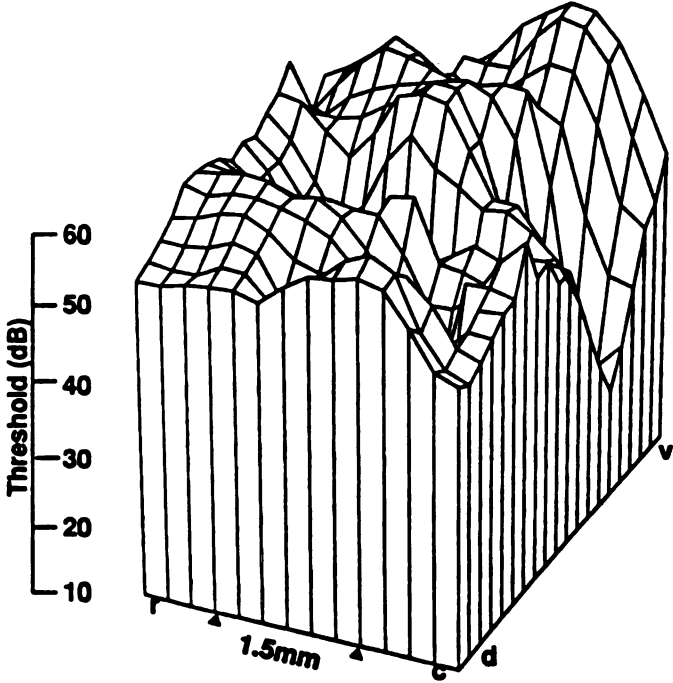
UNIVERSITY OF CALIFORNIA LIBRARY

CH-194

1  
2  
3  
4  
5  
6  
7  
8  
9  
10  
11  
12  
13  
14  
15  
16  
17  
18  
19  
20  
21  
22  
23  
24  
25  
26  
27  
28  
29  
30  
31  
32  
33  
34  
35  
36  
37  
38  
39  
40  
41  
42  
43  
44  
45  
46  
47  
48  
49  
50  
51  
52  
53  
54  
55  
56  
57  
58  
59  
60  
61  
62  
63  
64  
65  
66  
67  
68  
69  
70  
71  
72  
73  
74  
75  
76  
77  
78  
79  
80  
81  
82  
83  
84  
85  
86  
87  
88  
89  
90  
91  
92  
93  
94  
95  
96  
97  
98  
99  
100

Threshold Distribution in AI for Electrical Stimulation of the Cochlea

Electrode Pair 1,7



ADDITIONAL COPY

CH-194

18  
19  
20  
21  
22  
23  
24  
25  
26  
27  
28  
29  
30  
31  
32  
33  
34  
35  
36  
37  
38  
39  
40  
41  
42  
43  
44  
45  
46  
47  
48  
49  
50  
51  
52  
53  
54  
55  
56  
57  
58  
59  
60  
61  
62  
63  
64  
65  
66  
67  
68  
69  
70  
71  
72  
73  
74  
75  
76  
77  
78  
79  
80  
81  
82  
83  
84  
85  
86  
87  
88  
89  
90  
91  
92  
93  
94  
95  
96  
97  
98  
99  
100

in the previous example, a 'ridge' of higher sensitivity can be seen to shift from caudal to rostral as the stimulated electrode pairs moved from apical (Pair 1,2) to basal (Pair 7,8). In these cases, as in others to follow, the elevation of sensitivity to electrical stimuli is depicted not by contour lines, but by an equivalent visual display using a grid format. The underlying calculations and interpolations are identical to those used for the contour plots. In Figure 27, it should be noted that the three-dimensional plots have been rotated 55 degrees for ease of visualization of tuning relative to those seen in Figures 25 and 26.

It is obvious from the above electrical threshold 'tuning' data that the farther away penetration sites were from the preferential location of a given electrode pair, the higher their thresholds. To compare the relative threshold values between electrode pairs as well as across cases, an analysis method was required that would allow for the measurement of threshold within a parcellated area of like-threshold values that contained enough data points to provide for adequate statistical analysis. Therefore, means and standard deviations for electrical thresholds for each pair were determined for penetration sites that were divided into four, narrow dorso-ventral "slices". Using this parcellation method, parameter distributions along the ventral-dorsal domain could be analyzed and compared without contamination from global trends in the rostral-caudal domain. The spatial dimensions and neuronal constituency for each slice was determined case by case using four criteria: each slice should 1) cover about a quarter of the mapped area; 2) contain approximately a quarter of the recording sites, 3) represent a narrow CF range, and 4) contain enough points for an adequate data analysis. On the average, each slice covered approximately 0.6 octaves of the mapped frequency range. Examples of slices are given in Figures 42, 43, 44 and 45.

1  
2  
3  
4  
5  
6  
7  
8  
9  
10  
11  
12  
13  
14  
15  
16  
17  
18  
19  
20  
21  
22  
23  
24  
25  
26  
27  
28  
29  
30  
31  
32  
33  
34  
35  
36  
37  
38  
39  
40  
41  
42  
43  
44  
45  
46  
47  
48  
49  
50  
51  
52  
53  
54  
55  
56  
57  
58  
59  
60  
61  
62  
63  
64  
65  
66  
67  
68  
69  
70  
71  
72  
73  
74  
75  
76  
77  
78  
79  
80  
81  
82  
83  
84  
85  
86  
87  
88  
89  
90  
91  
92  
93  
94  
95  
96  
97  
98  
99  
100

1  
2  
3  
4  
5  
6  
7  
8  
9  
10  
11  
12  
13  
14  
15  
16  
17  
18  
19  
20  
21  
22  
23  
24  
25  
26  
27  
28  
29  
30  
31  
32  
33  
34  
35  
36  
37  
38  
39  
40  
41  
42  
43  
44  
45  
46  
47  
48  
49  
50  
51  
52  
53  
54  
55  
56  
57  
58  
59  
60  
61  
62  
63  
64  
65  
66  
67  
68  
69  
70  
71  
72  
73  
74  
75  
76  
77  
78  
79  
80  
81  
82  
83  
84  
85  
86  
87  
88  
89  
90  
91  
92  
93  
94  
95  
96  
97  
98  
99  
100

Table 9 shows the results of this data analysis which includes the means and standard deviations for each of the five electrode pair configurations for six cases. For some cases, particular electrode pairs were not used due to electrode faults discovered during initial stimulation trials. As can be seen, the radial pair thresholds were similar across cases and across pairs. However, the longitudinal pair thresholds, while similar across cases, were consistently lower than were those of the radial pairs for all cases and nearly all slices.

It is also apparent that the mean electrical threshold is typically lower for the slice or slices in which a given pair might be most appropriately represented. While this is not always the case, the trend for the 'primary' or 'primary and secondary' slices to have the lowest threshold at the cochleotopically appropriate cortical sector was observed. Figure 28D shows histograms of the distributions of the two slices with the lowest response thresholds for a given electrode pair with slice 1 being the most caudal slice and slice 4 the most rostral slice. It is apparent that the maximum in the distribution moves from the most caudal slice for the most apical pair 1,2 to the most rostral slice for the most basal pair 7,8. The mean values of the slice with the lowest threshold are 2.1 (pair 1,2), 2.6 (pair 3,4), 2.7 (pair 5,6) and 3.5 (pair 7,8). This increase in rank order with changing of the cochlear stimulation location from apical to basal is consistent with a cochleotopic organization of AI reflected in the electrically evoked activity profile. That is, low frequencies are represented more caudally while high frequencies are represented more rostrally.

A more detailed analysis of the location and widths of spatial tuning curves was performed by determining the position of the lowest threshold



Table 9.

**ELECTRICAL THRESHOLDS: MEANS AND STANDARD DEVIATIONS  
FOR EACH ELECTRODE PAIR BY SLICE**

<u>Case</u>	<u>Sl</u>	<u>N</u>	<u>Pair 1,2</u>	<u>Pair 3,4</u>	<u>Pair 5,6</u>	<u>Pair 7,8</u>	<u>Pair 1,7-8</u>
C11	1	13	24.1±6.3	22.7±7.9	35.4±1.9	35.4±1.9	13.8±12.2
	2	9	25.8±8.2	19.2±3.3	35.0±1.8	34.3±1.9	8.4±3.0
	3	15	32.7±4.5	18.9±2.3	32.0±2.9	32.5±2.0	9.9±1.7
	4	11	35.1±1.4	17.4±1.4	31.4±1.9	30.2±0.8	9.3±1.4
	All	48	29.6±7.0	19.6±4.9	33.4±2.8	33.1±2.6	10.5±6.7
	(range)		(16-36)	(15-36)	(27-36)	(29-36)	(5-36)
C115	1	13	34.5±1.7	29.9±3.6		27.7±3.5	12.5±5.0
	2	12	32.2±3.5	27.0±5.9		25.3±4.3	10.3±7.5
	3	13	28.4±4.4	21.6±7.7		21.8±2.8	4.8±5.3
	4	13	24.6±3.9	15.4±6.5		20.5±4.5	4.3±4.7
	All	51	29.8±5.2	23.3±8.2		23.7±4.8	7.9±6.6
	(range)		(21-36)	(10-36)	(15-36)	(0-22)	
C163	1	24	25.7±6.2	27.7±7.1	30.1±5.6	34.7±2.9	17.0±9.3
	2	25	25.2±9.4	23.0±10.9	26.3±8.0	32.9±4.9	16.5±10.5
	3	23	29.2±7.0	16.4±13.7	16.5±11.9	28.8±7.9	14.9±10.4
	4	29	34.2±2.9	29.1±6.1	22.1±7.7	19.1±11.3	14.2±10.9
	All	101	28.8±7.6	24.0±10.9	23.8±9.7	28.5±9.8	15.6±10.2
	(range)		(11-36)	(3-36)	(2-36)	(2-36)	(-6-36)
C166	1	20	30.8±5.9	25.7±11.3	31.9±4.8	35.7±1.3	21.4±11.7
	2	15	31.3±5.4	30.3±6.7	27.3±6.9	35.9±5.2	18.4±12.1
	3	16	31.0±4.8	29.8±7.0	30.3±6.2	32.2±3.9	17.1±11.8
	4	17	33.3±3.8	33.2±5.5	34.9±3.2	32.0±4.7	20.4±13.0
	All	68	31.5±5.1	29.5±8.4	31.3±5.9	33.9±3.5	19.4±12.0
	(range)		(18-36)	(5-36)	(17-36)	(25-36)	(3-36)
C124	1	13	30.6±7.4		27.4±10.5	35.8±6.0	21.5±10.5
	2	11	31.7±7.1		14.7±11.5	32.5±6.9	16.3±7.9
	3	13	34.7±3.1		22.8±10.5	31.5±3.8	15.2±4.2
	4	12	31.0±7.8		30.3±9.7	25.8±8.6	16.3±7.9
	All	49	32.0±6.6		24.0±11.7	31.5±6.6	17.4±8.1
	(range)		(14-36)	(5-36)	(11-36)	(5-36)	
C194	1	11	24.9±8.4	19.2±7.9	28.8±4.7	35.9±0.4	10.8±7.4
	2	25	28.6±5.4	21.5±6.3	28.7±4.5	35.4±2.1	10.1±7.3
	3	37	31.2±5.2	26.9±6.5	34.6±13.2	36.0±0	12.6±7.3
	4	33	30.7±4.7	26.6±5.1	34.8±4.7	33.6±2.9	9.4±8.1
	All	104	29.1±6.4	23.8±7.2	31.8±4.9	35.3±1.9	10.8±7.5
	(range)		(12-36)	(11-36)	(17-36)	(25-36)	(1-36)

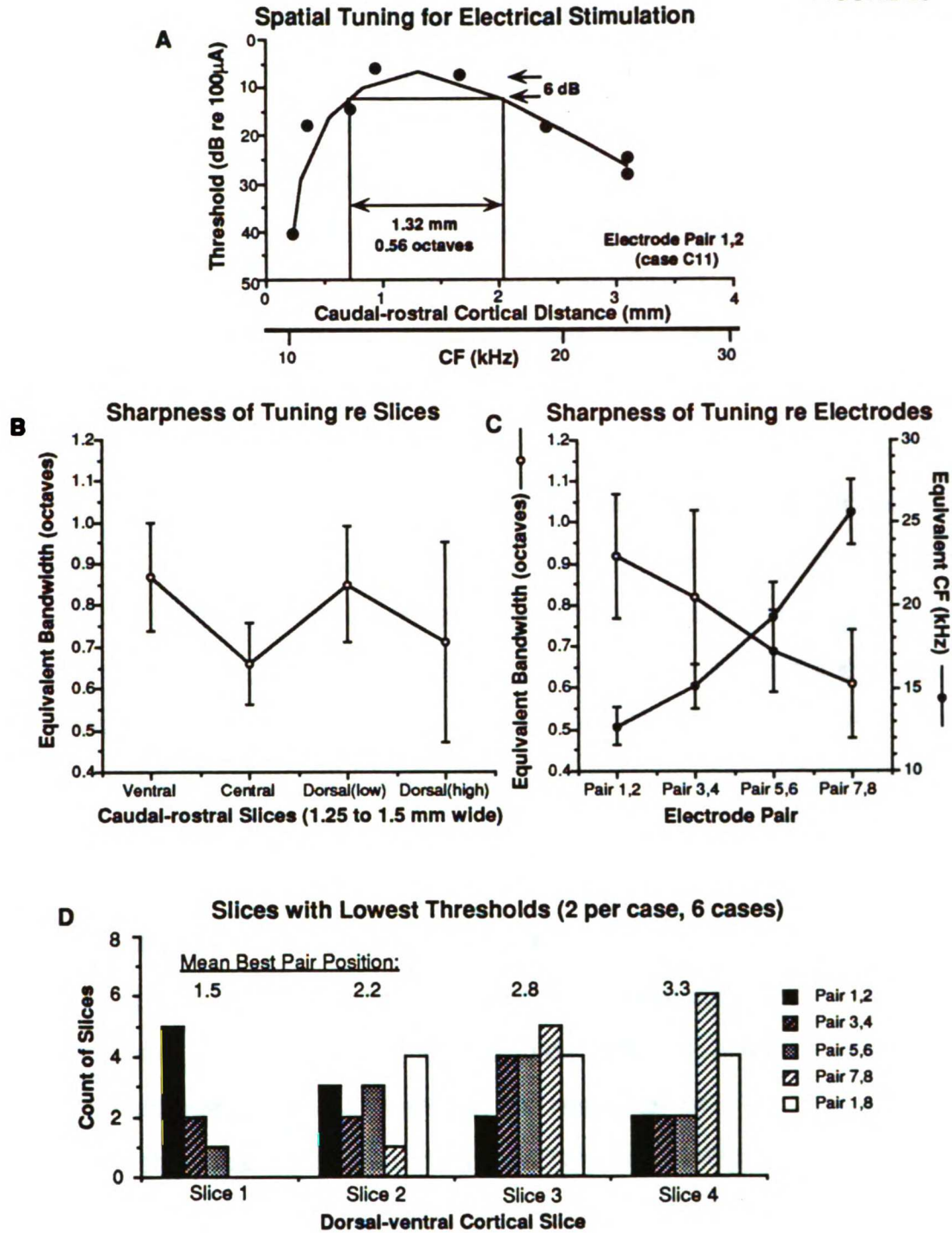
Means and standard deviations are expressed in dB re 100µA.



**Figure 28. Spatial tuning for electrical stimulation. A) Exemplary spatial tuning curve in AI for a radial electrode pair. Threshold is plotted on the ordinate and caudal-rostral distance as well as the corresponding CF distribution are plotted on the abscissa. B) The mean value (and standard error bars) for sharpness of tuning for four caudal-rostral slices for all experimental cases is shown. C) Mean characteristic frequency and the equivalent bandwidth in octaves for each of four radial electrode pairs for all cases are shown. D) Cumulative distribution of lowest electrical threshold in dorso-ventral slices across AI for six animals. Each map was divided into four dorso-ventral slices. The two slices that showed the lowest threshold for any given electrode configuration was selected resulting in a total of 12 slices per configuration. For two animals, only four electrode configurations were obtained resulting in a total of 56 slices. The numbers above each slice column represent the 'mean best pair', i.e. which electrode position, on the average, resulted in the lowest thresholds for each slice (D).**



FIGURE 28





(or highest sensitivity) for electrical stimulation along caudal-rostral slices of the mapped cortical area. Each slice was 1.25 or 1.5mm wide in the dorsal-ventral domain. For four of the six cases, four slices were reconstructed. The dorsal-ventral extent of the remaining cases were covered by two (case C124) or three slices (case C11). The position of threshold minimum and the width of each spatial tuning curve was expressed relative to the underlying frequency organization which was determined from frequency response areas measured prior to the electrical stimulation mapping (see below). Figure 28A shows an example of a spatial tuning curve. Two abscissae are shown, the caudal-rostral cortical distance as well as the corresponding frequency gradient. Figure 28C shows the average frequency position of spatial tuning curves for the four radial electrode configurations. A clear increase of the corresponding 'characteristic frequency' for progressively more basal electrode positions is shown providing strong evidence for a cochleotopic cortical organization of electrical stimulation. The width of the spatial tuning curves was assessed 6dB below maximum sensitivity and expressed as bandwidth in octaves. In some cases, especially for electrode pairs 1,2 and 7,8, the descending slope of one side of the spatial tuning curve did not reach the 6dB point due to the boundaries of the mapped area. These slices were excluded from consideration of bandwidth. The resulting bandwidth estimates of the spatial tuning appear to decrease for progressively more basal electrode positions. However, this result can only be considered to reflect a statistical trend in the data (ANOVA  $p < 0.1$ ). The average bandwidth for all radial electrode configurations was 0.76 octaves (N=63 slices). Finally, the bandwidth of spatial tuning curves was assessed separately for each of the 2 to 4 dorsal-ventral slice positions. In Figure 28B, the average bandwidth with standard error is shown for the four slice positions. The central slice exhibited the narrowest spatial tuning,



however, this result reflects only a statistical trend (ANOVA  $p < 0.1$ ).

### 3.2.2 Dorsal-Ventral Distributions: Isofrequency Domain

In addition to the six cases listed above, four cases of threshold distribution maps along an approximation of an isofrequency strip were also obtained. From these ten cases, a clear non-uniform and non-random pattern of threshold distribution along the dorsal-ventral or isofrequency domain can be observed, regardless of whether the field involves a relatively large portion of AI or a narrow 'isofrequency' strip. Figure 29 shows the distribution of response thresholds for largely multiple units along the dorso-ventral extent of AI for stimulation of electrode pair 1,2 in two animals. In the approximate center of the mapped dorso-ventral strips, a number of recording locations showed higher response thresholds, or no response thresholds were encountered before reaching the highest applied stimulation current (3 mA). Further cases confirmed that, regardless of which electrode was stimulated, a characteristic threshold pattern emerges in which thresholds vary systematically along the dorso-ventral axis, such that relatively poor thresholds were found in a band running essentially orthogonal to the isofrequency axis while lower thresholds were found in the more ventral and dorsal portions of AI. Figure 30 shows the threshold values and a three-dimensional reconstruction of this typical distribution pattern for a cortex mapped at 90 locations. In this case, response *sensitivity* is plotted, i.e., the lowest threshold values are plotted as having the highest elevation and the highest threshold values correspond to the lowest points in the map. The resulting sensitivity distribution to electrical cochlear stimulation demonstrate a low sensitivity (high threshold) region (a 'valley') in the central area of the ectosylvian gyrus running caudorostrally with high sensitivity (low



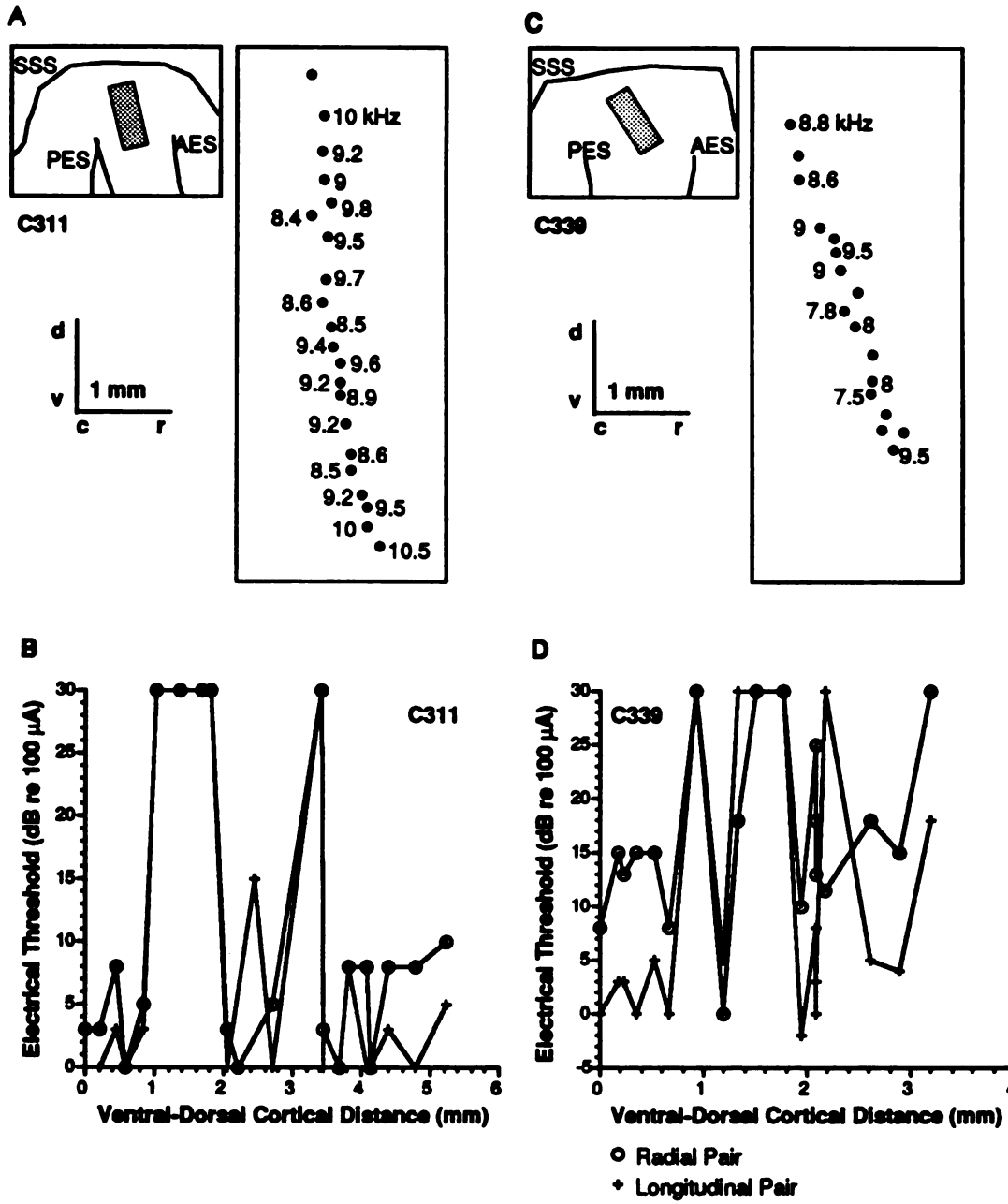
**Figure 29. Electrical threshold distribution along approximated isofrequency contours for a radial pair (1,2) and a longitudinal pair (1,8) for two cases. Corresponding maps of recording sites in primary auditory cortex are included. CF designations (in kHz) obtained with ipsilateral stimulation are adjacent to the recording sites. The majority of the responses are from multiple unit recordings.**

100-10000



FIGURE 29

Multiple Neuron Thresholds Across Ventral-Dorsal Extent of AI



1  
2  
3  
4  
5  
6  
7  
8  
9  
10  
11  
12  
13  
14  
15  
16  
17  
18  
19  
20  
21  
22  
23  
24  
25  
26  
27  
28  
29  
30  
31  
32  
33  
34  
35  
36  
37  
38  
39  
40  
41  
42  
43  
44  
45  
46  
47  
48  
49  
50  
51  
52  
53  
54  
55  
56  
57  
58  
59  
60  
61  
62  
63  
64  
65  
66  
67  
68  
69  
70  
71  
72  
73  
74  
75  
76  
77  
78  
79  
80  
81  
82  
83  
84  
85  
86  
87  
88  
89  
90  
91  
92  
93  
94  
95  
96  
97  
98  
99  
100

1  
2  
3  
4  
5  
6  
7  
8  
9  
10  
11  
12  
13  
14  
15  
16  
17  
18  
19  
20  
21  
22  
23  
24  
25  
26  
27  
28  
29  
30  
31  
32  
33  
34  
35  
36  
37  
38  
39  
40  
41  
42  
43  
44  
45  
46  
47  
48  
49  
50  
51  
52  
53  
54  
55  
56  
57  
58  
59  
60  
61  
62  
63  
64  
65  
66  
67  
68  
69  
70  
71  
72  
73  
74  
75  
76  
77  
78  
79  
80  
81  
82  
83  
84  
85  
86  
87  
88  
89  
90  
91  
92  
93  
94  
95  
96  
97  
98  
99  
100

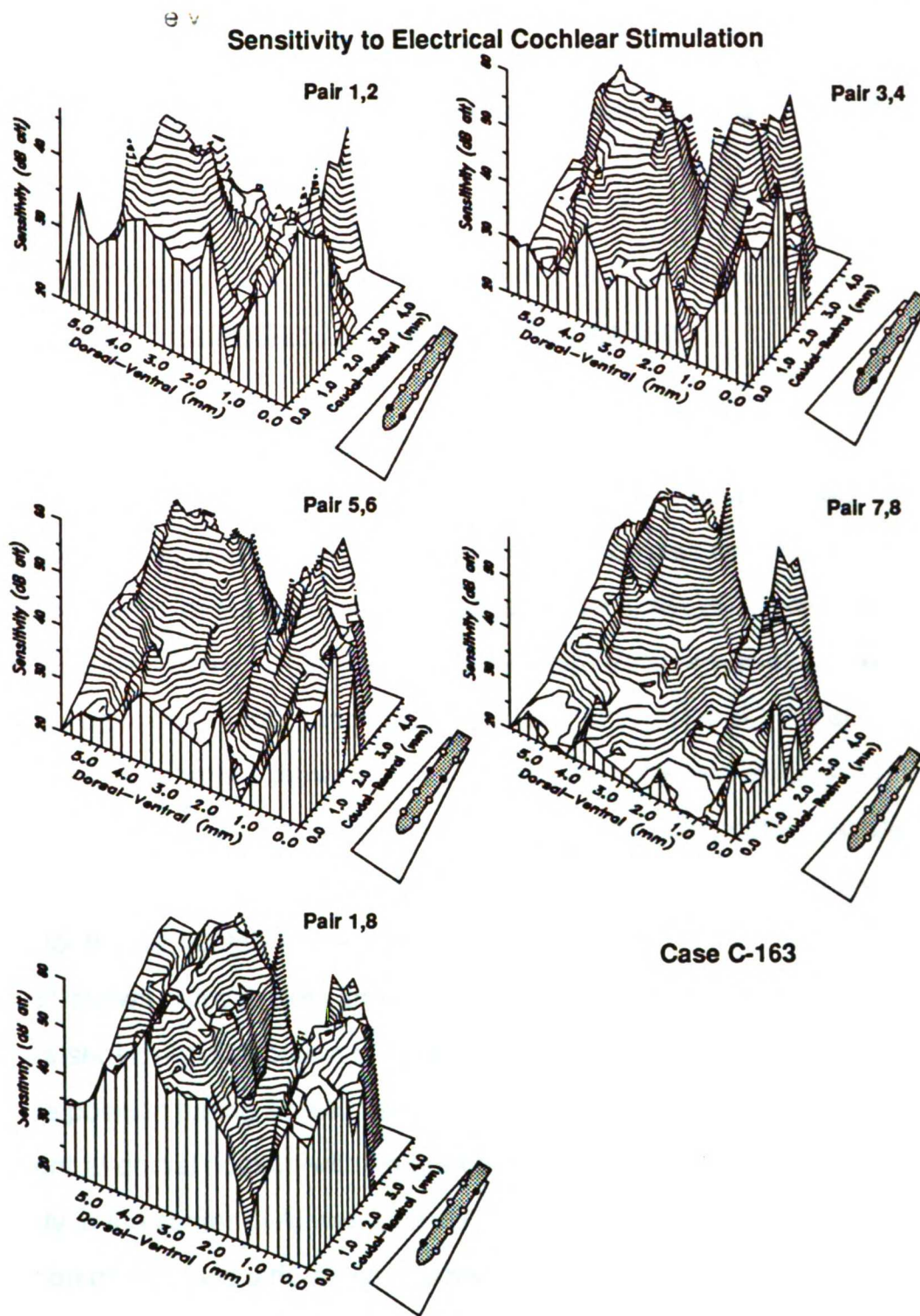
**Figure 30. Three-dimensional electrical threshold distributions in primary auditory cortex for four radial electrode pairs and one longitudinal electrode pair (case C163). Threshold distributions are identical to those shown in Fig. 23, however, turned 65 degrees. For details see Figure 23.**

1981

1981



Figure 30





threshold) regions ('peaks') present at the ventral and dorsal portions of the distribution map. It should be noted that the main valley makes an obvious break in the dorso-ventral tuning 'ridge' of each electrode pair (see Figures 25). Figures 26 and 27 show the same non-uniform ventral-dorsal threshold distribution including the break in the maxima of the spatial tuning. Similar distributions were observed in all tested animals.

### 3.2.3 Control Animals

#### 3.2.3.1 Control: Implantation Two Weeks Prior to Mapping

Additional control cases were undertaken to examine electrical threshold distributions in AI. In one case, an animal was implanted two weeks prior to electrical threshold mapping in order to evaluate whether acute implantation of the cochlear electrodes results in different, possibly higher threshold values. Other studies had indicated that thresholds may drop a few days after implantation (Snyder et al. 1990). The results of this mapping experiment showed minimum thresholds for two radial pairs of 11dB (mean 19.6dB) and 10dB (mean 27.9dB), and one longitudinal pair of 10dB (mean 21.4dB). In comparing these mean thresholds with those in Table 9 for the six acutely implanted animals, little difference was seen. Figure 31 shows contour plots and three-dimensional depictions of the response sensitivity distribution for this case. As in the other cases, electrode position tuning as well as a non-uniform threshold distribution in the ventral-dorsal domain with an area of relatively lower electrical sensitivity in the center of AI was seen. However, the spatial threshold distribution of this case differed somewhat from other cases by clearly showing a narrow low-threshold 'bridge' across the typical high threshold central region, thereby connecting the dorsal and the ventral low-threshold



**Figure 31. Contour plots with recording locations and corresponding three-dimensional representations of two electrical threshold distributions in primary auditory cortex for an animal implanted two weeks prior to mapping (case C325; radial Pairs 1 and 3). Contour line separation is 3 dB.**

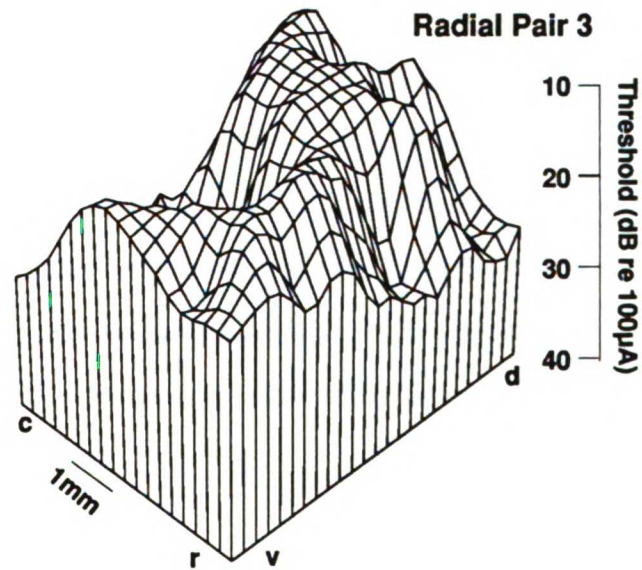
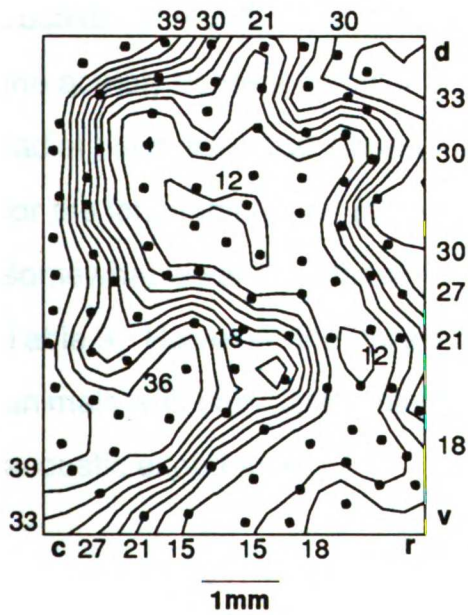
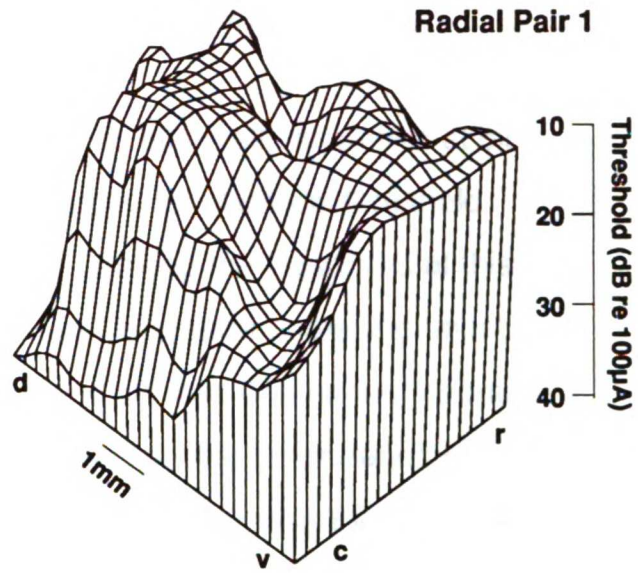
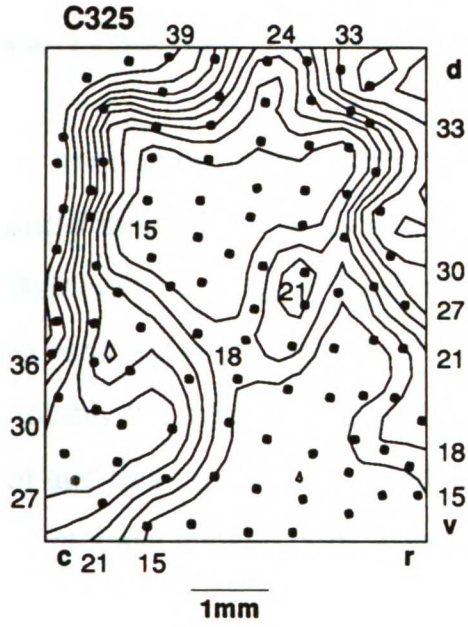
1000 Hz

1  
2  
3  
4  
5  
6  
7  
8  
9  
10  
11  
12  
13  
14  
15  
16  
17  
18  
19  
20  
21  
22  
23  
24  
25  
26  
27  
28  
29  
30  
31  
32  
33  
34  
35  
36  
37  
38  
39  
40  
41  
42  
43  
44  
45  
46  
47  
48  
49  
50  
51  
52  
53  
54  
55  
56  
57  
58  
59  
60  
61  
62  
63  
64  
65  
66  
67  
68  
69  
70  
71  
72  
73  
74  
75  
76  
77  
78  
79  
80  
81  
82  
83  
84  
85  
86  
87  
88  
89  
90  
91  
92  
93  
94  
95  
96  
97  
98  
99  
100

1  
2  
3  
4  
5  
6  
7  
8  
9  
10  
11  
12  
13  
14  
15  
16  
17  
18  
19  
20  
21  
22  
23  
24  
25  
26  
27  
28  
29  
30  
31  
32  
33  
34  
35  
36  
37  
38  
39  
40  
41  
42  
43  
44  
45  
46  
47  
48  
49  
50  
51  
52  
53  
54  
55  
56  
57  
58  
59  
60  
61  
62  
63  
64  
65  
66  
67  
68  
69  
70  
71  
72  
73  
74  
75  
76  
77  
78  
79  
80  
81  
82  
83  
84  
85  
86  
87  
88  
89  
90  
91  
92  
93  
94  
95  
96  
97  
98  
99  
100

FIGURE 31

Electrical Threshold Distribution in AI:  
Two Weeks Post-Implantation



1  
2  
3  
4  
5  
6  
7  
8  
9  
10  
11  
12  
13  
14  
15  
16  
17  
18  
19  
20  
21  
22  
23  
24  
25  
26  
27  
28  
29  
30  
31  
32  
33  
34  
35  
36  
37  
38  
39  
40  
41  
42  
43  
44  
45  
46  
47  
48  
49  
50  
51  
52  
53  
54  
55  
56  
57  
58  
59  
60  
61  
62  
63  
64  
65  
66  
67  
68  
69  
70  
71  
72  
73  
74  
75  
76  
77  
78  
79  
80  
81  
82  
83  
84  
85  
86  
87  
88  
89  
90  
91  
92  
93  
94  
95  
96  
97  
98  
99  
100

1  
2  
3  
4  
5  
6  
7  
8  
9  
10  
11  
12  
13  
14  
15  
16  
17  
18  
19  
20  
21  
22  
23  
24  
25  
26  
27  
28  
29  
30  
31  
32  
33  
34  
35  
36  
37  
38  
39  
40  
41  
42  
43  
44  
45  
46  
47  
48  
49  
50  
51  
52  
53  
54  
55  
56  
57  
58  
59  
60  
61  
62  
63  
64  
65  
66  
67  
68  
69  
70  
71  
72  
73  
74  
75  
76  
77  
78  
79  
80  
81  
82  
83  
84  
85  
86  
87  
88  
89  
90  
91  
92  
93  
94  
95  
96  
97  
98  
99  
100

regions. The position of the 'bridge' shifted with changes in the stimulating electrode pair as was particularly notable in the contour plots, and was in accordance with a cochleotopic organization. Although the acute cases occasionally showed similar 'bridges' for certain electrode configuration, none of those cases showed such a consistent pattern as seen in case 325 (Fig. 31).

### 3.2.3.2 Control: Deafened Three Years. Unstimulated

In another single control case, an animal bilaterally deafened at birth and implanted three years later was mapped for electrical threshold distribution one week after implantation. Among the objectives of this experiment was to assess the influence of long-term deafening, most notably the lack of prior auditory input and the loss of a large proportion of auditory nerve fibers, on the efficacy and spatial organization of the electrically evoked cortical threshold response. This experiment revealed that the character of the threshold responses in AI evoked by electrical cochlear stimulation were essentially indistinguishable from those seen in the acutely deafened/implanted animals. The lowest thresholds for two radial pairs were 3dB (mean 10.02dB), and -3dB (mean 7.26dB), and 0dB for the longitudinal pair (mean 4.26dB). These mean thresholds were somewhat lower than those for the acutely implanted animals listed in Table 9. However, the lowest thresholds were comparable to those seen in animals with completely intact auditory nerves and extensive prior acoustic experience.

Figure 32 shows a three-dimensional depiction of the threshold distribution in this case for an apical electrode pair. As in the acute implant cases, a clear non-uniform threshold distribution is seen with a



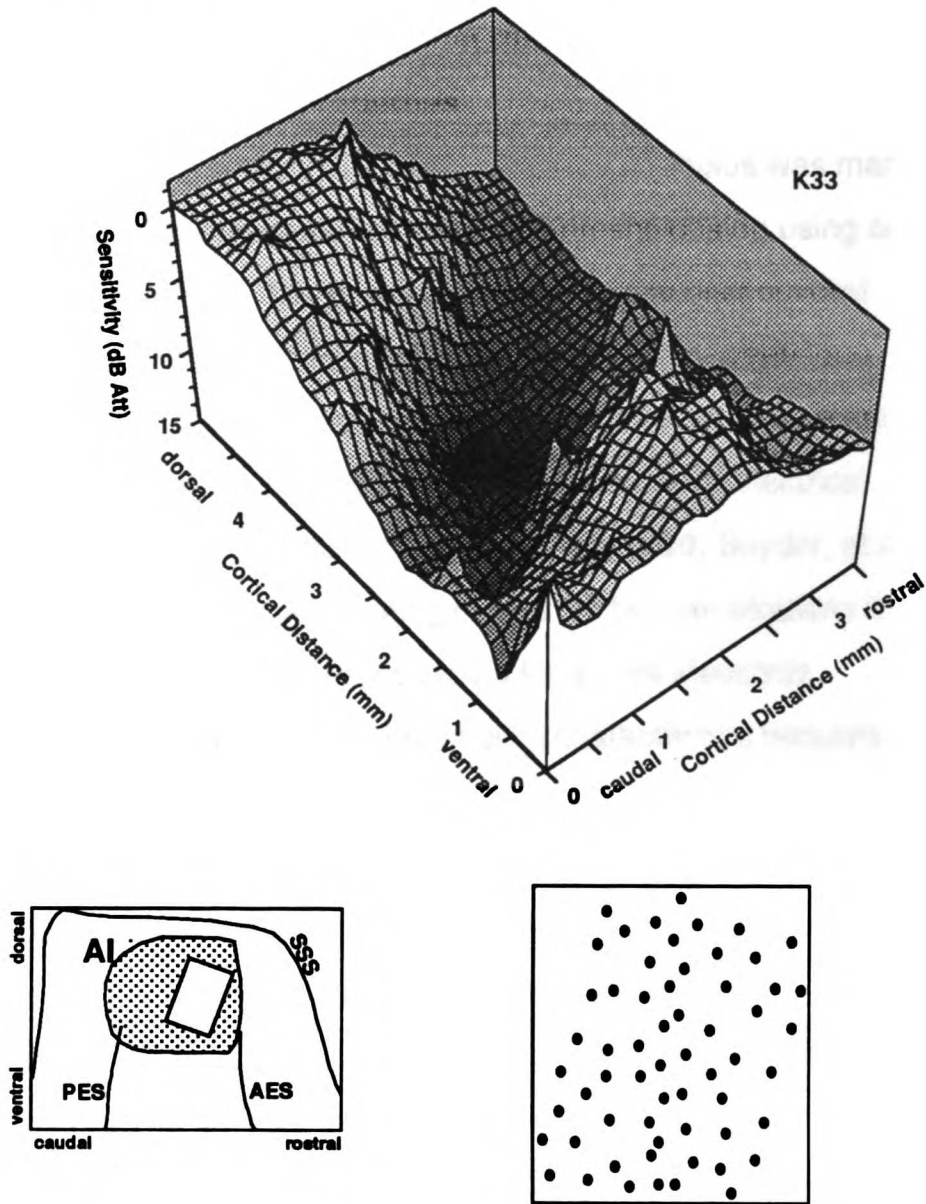


1  
2  
3  
4  
5  
6  
7  
8  
9  
10  
11  
12  
13  
14  
15  
16  
17  
18  
19  
20  
21  
22  
23  
24  
25  
26  
27  
28  
29  
30  
31  
32  
33  
34  
35  
36  
37  
38  
39  
40  
41  
42  
43  
44  
45  
46  
47  
48  
49  
50  
51  
52  
53  
54  
55  
56  
57  
58  
59  
60  
61  
62  
63  
64  
65  
66  
67  
68  
69  
70  
71  
72  
73  
74  
75  
76  
77  
78  
79  
80  
81  
82  
83  
84  
85  
86  
87  
88  
89  
90  
91  
92  
93  
94  
95  
96  
97  
98  
99  
100

1  
2  
3  
4  
5  
6  
7  
8  
9  
10  
11  
12  
13  
14  
15  
16  
17  
18  
19  
20  
21  
22  
23  
24  
25  
26  
27  
28  
29  
30  
31  
32  
33  
34  
35  
36  
37  
38  
39  
40  
41  
42  
43  
44  
45  
46  
47  
48  
49  
50  
51  
52  
53  
54  
55  
56  
57  
58  
59  
60  
61  
62  
63  
64  
65  
66  
67  
68  
69  
70  
71  
72  
73  
74  
75  
76  
77  
78  
79  
80  
81  
82  
83  
84  
85  
86  
87  
88  
89  
90  
91  
92  
93  
94  
95  
96  
97  
98  
99  
100

FIGURE 32

**Cortical Response Distribution (Sensitivity) to Electrical Cochlear Stimulation 3-year old cat, deafened at birth**





centralized area of AI having relatively lower electrical sensitivity. Some spatial tuning is also noted, most clearly in the caudal-ventral region of the map, that appears to be relatively broad.

### 3.2.3.3 Control: Inferior Colliculus

In a third control case, the contralateral inferior colliculus was mapped in an animal that had previously undergone cortical mapping using acoustic and electrical stimulation. The goal was to directly compare cortical threshold values with those in the inferior colliculus, to assess contributions from central (thalamic/cortical) mechanisms and to enable a comparison with previous studies of the representation of electrical stimulation in the inferior colliculus (Snyder, et al., 1990; Snyder, et al., 1991). Figure 33 shows spatial tuning curves for two penetrations through the central nucleus of the inferior colliculus for all five electrode configurations. The lower right panel depicts characteristic frequency versus depth. The two penetrations were laterally separated by about 500  $\mu\text{m}$  and showed congruent spatial tuning. The sharpest tuning was seen for the most basal pair, while the longitudinal pair (Pair 1,8) showed a nearly flat threshold distribution. The minima of the spatial tuning curves shifted toward high frequencies with increasingly more basal electrode pair stimulation. The lowest thresholds were 17 and 15dB (Pair 1,2), 1 and 8dB (Pair 3,4), 13 and 9dB (Pair 5,6), 8 and 11dB (Pair 7,8), 9 and 10dB (Pair 1,8). The lowest threshold for the first penetration was 1dB while that of the second penetration was 9dB. The smallest difference in minimum threshold between inferior colliculus and cortex (IC minus cortex) was 4dB (pair 1,2), -2dB (Pair 3,4), 7dB (Pair 5,6), 7dB (Pair 7,8), and 15dB (Pair 1,8). That is, overall, the minimum thresholds found for inferior colliculus neurons were similar to the lowest cortical thresholds

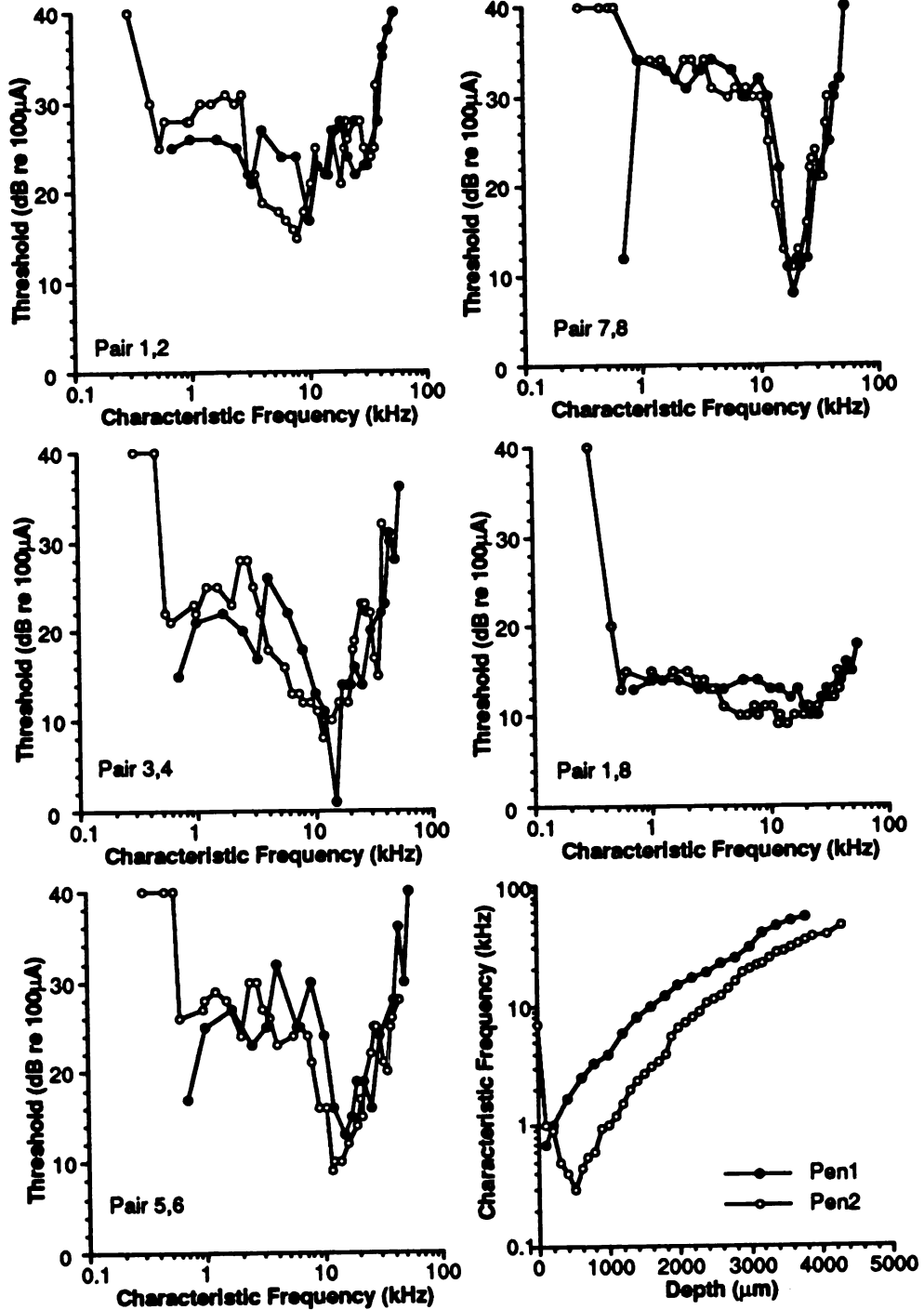


**Figure 33. Two electrical spatial tuning curves in the central nucleus of the inferior colliculus for each of four radial electrode pairs and one longitudinal electrode pair (case C163). The bottom right panel shows a plot of characteristic frequency versus penetration depth determined for ipsilateral acoustic stimulation.**



FIGURE 33

Spatial Tuning Curves in the Inferior Colliculus



1947-1948  
1949-1950  
1951-1952  
1953-1954  
1955-1956  
1957-1958  
1959-1960  
1961-1962  
1963-1964  
1965-1966  
1967-1968  
1969-1970  
1971-1972  
1973-1974  
1975-1976  
1977-1978  
1979-1980  
1981-1982  
1983-1984  
1985-1986  
1987-1988  
1989-1990  
1991-1992  
1993-1994  
1995-1996  
1997-1998  
1999-2000  
2001-2002  
2003-2004  
2005-2006  
2007-2008  
2009-2010  
2011-2012  
2013-2014  
2015-2016  
2017-2018  
2019-2020  
2021-2022  
2023-2024  
2025-2026  
2027-2028  
2029-2030  
2031-2032  
2033-2034  
2035-2036  
2037-2038  
2039-2040  
2041-2042  
2043-2044  
2045-2046  
2047-2048  
2049-2050  
2051-2052  
2053-2054  
2055-2056  
2057-2058  
2059-2060  
2061-2062  
2063-2064  
2065-2066  
2067-2068  
2069-2070  
2071-2072  
2073-2074  
2075-2076  
2077-2078  
2079-2080  
2081-2082  
2083-2084  
2085-2086  
2087-2088  
2089-2090  
2091-2092  
2093-2094  
2095-2096  
2097-2098  
2099-2100

1947-1948  
1949-1950  
1951-1952  
1953-1954  
1955-1956  
1957-1958  
1959-1960  
1961-1962  
1963-1964  
1965-1966  
1967-1968  
1969-1970  
1971-1972  
1973-1974  
1975-1976  
1977-1978  
1979-1980  
1981-1982  
1983-1984  
1985-1986  
1987-1988  
1989-1990  
1991-1992  
1993-1994  
1995-1996  
1997-1998  
1999-2000  
2001-2002  
2003-2004  
2005-2006  
2007-2008  
2009-2010  
2011-2012  
2013-2014  
2015-2016  
2017-2018  
2019-2020  
2021-2022  
2023-2024  
2025-2026  
2027-2028  
2029-2030  
2031-2032  
2033-2034  
2035-2036  
2037-2038  
2039-2040  
2041-2042  
2043-2044  
2045-2046  
2047-2048  
2049-2050  
2051-2052  
2053-2054  
2055-2056  
2057-2058  
2059-2060  
2061-2062  
2063-2064  
2065-2066  
2067-2068  
2069-2070  
2071-2072  
2073-2074  
2075-2076  
2077-2078  
2079-2080  
2081-2082  
2083-2084  
2085-2086  
2087-2088  
2089-2090  
2091-2092  
2093-2094  
2095-2096  
2097-2098  
2099-2100

for this animal and revealed no systematic and consistent differences across all stimulation conditions. Inferior colliculus neuronal response thresholds determined by Snyder and colleagues (1990) ranged from -10 to 17dB which overlaps with the range of thresholds in the current ICC experiment. However, the mean value for the ICC range in the current experiment is higher than the mean value found by Snyder and colleagues.

### **3.2.4 Summary**

In summary, threshold distributions in AI for electrical cochlear stimulation revealed two distinct patterns. First, electrode position spatial tuning across the cochleotopic domain of AI was recorded, such that apical pairs had their lowest thresholds in the most caudal (low-frequency) sector of mapped AI, while more basal electrode pairs had their lowest thresholds in the rostral (high-frequency) sector. These areas of lowest thresholds were fairly circumscribed. Second, there was a systematic threshold distribution in the dorsal-ventral domain, such that an area running roughly orthogonal to the isofrequency domain contained neurons with high response thresholds that were flanked by lower threshold areas on the ventral and dorsal sides of this low sensitivity 'valley'. These threshold distributions were also seen in control animals that were either implanted two weeks prior to stimulation or implanted three years after postnatal deafening. Inferior colliculus neurons revealed similar thresholds to those of cortical neurons.

As expected, stimulation of the longitudinal electrode pair resulted in a broad spatial pattern, i.e. lack of cochleotopic tuning, along the caudo-rostral axis but showed the same dorso-ventral pattern as seen with the radial pairs. In terms of relative threshold values, stimulation of

1948  
1949  
1950  
1951  
1952  
1953  
1954  
1955  
1956  
1957  
1958  
1959  
1960  
1961  
1962  
1963  
1964  
1965  
1966  
1967  
1968  
1969  
1970  
1971  
1972  
1973  
1974  
1975  
1976  
1977  
1978  
1979  
1980  
1981  
1982  
1983  
1984  
1985  
1986  
1987  
1988  
1989  
1990  
1991  
1992  
1993  
1994  
1995  
1996  
1997  
1998  
1999  
2000  
2001  
2002  
2003  
2004  
2005  
2006  
2007  
2008  
2009  
2010  
2011  
2012  
2013  
2014  
2015  
2016  
2017  
2018  
2019  
2020  
2021  
2022  
2023  
2024  
2025

1948  
1949  
1950  
1951  
1952  
1953  
1954  
1955  
1956  
1957  
1958  
1959  
1960  
1961  
1962  
1963  
1964  
1965  
1966  
1967  
1968  
1969  
1970  
1971  
1972  
1973  
1974  
1975  
1976  
1977  
1978  
1979  
1980  
1981  
1982  
1983  
1984  
1985  
1986  
1987  
1988  
1989  
1990  
1991  
1992  
1993  
1994  
1995  
1996  
1997  
1998  
1999  
2000  
2001  
2002  
2003  
2004  
2005  
2006  
2007  
2008  
2009  
2010  
2011  
2012  
2013  
2014  
2015  
2016  
2017  
2018  
2019  
2020  
2021  
2022  
2023  
2024  
2025

the longitudinal pair routinely resulted in lower thresholds than those for radial electrode pairs with little variation in absolute threshold for a given longitudinal pair across cases.

### **3.3 Experimental Series Two: Spatial Distribution of Acoustic Response Properties**

While the detailed distribution of electrical threshold is only now being investigated in primary auditory cortex, several spatial distributions of response characteristics using acoustic stimulation have been long known. For example, Merzenich and colleagues (1975) as well as Reale and Imig (1980) described a low to high CF gradient across the caudal-rostral extent of AI reflecting peripheral tonotopicity. In addition to the distribution of frequency and binaural interaction classes (see Imig and Adrian, 1977; Middlebrooks, et al., 1980), other parametric distributions have been documented in AI. Specifically, Schreiner and colleagues (1990, 1991, 1992) have defined a number of systematic physiological response distributions including minimum threshold, sharpness of tuning, latency, strongest response, and monotonicity of rate/level functions.

One goal of the present study was to determine these acoustic parametric response distributions in AI, to enable a comparative analysis with neuronal response distributions revealed by peripheral electrical stimulation at or near the same cortical locations in the same animals.

Frequency response areas and binaural interaction types were determined at 50 to 90 locations in the primary auditory cortex of the right hemisphere of six adult cats. From frequency response areas obtained for multiple unit and single unit responses, several descriptive parameters



were extracted including characteristic frequency, minimum threshold, best level (level at which strongest responses were recorded), response bandwidths 10 and 40 dB above threshold (Q10dB, Q40dB), latency, and monotonicity. The means and standard deviations for these seven acoustic physiological response parameters for the same slice domain noted for electrical threshold data analysis are shown in Table 10. As previously noted, analyzing the data was best served by the use of 'slice' data. All comparative slice data for both stimulating modes were taken from the same or nearly the same recording sites. The strategy behind these divisions was based on the criteria that the chosen ventral-dorsal sector width (usually 500 to 1000 $\mu$ m) would allow for a large enough number of points as required for statistical purposes, while still restricting the width such that influences of CF/cochlear stimulation location on response thresholds would be minimized within each sector. Therefore, the magnitude of variations in electrical or acoustic thresholds that were simply the result of place of basilar membrane stimulation or electrode position would be reduced or largely eliminated. The need for this parcellation technique arose when it became clear that the results of correlation analyses using the entire data set were always very poor due to the significant variations in response behavior across both the ventral-dorsal and caudal-rostral extents of AI.

### 3.3.1 Characteristic Frequency (CF)

As shown in Table 10, CF varied from case to case, due to the variation in craniotomy site that invariably occurred. As can be seen, CFs ranged over approximately 20kHz for all cases, with the mean CF per slice increasing with each subsequent slice. Across all cases, the mean characteristic frequency per slice ranged from 2.34kHz to 39.4kHz with an

1  
2  
3  
4  
5  
6  
7  
8  
9  
10  
11  
12  
13  
14  
15  
16  
17  
18  
19  
20  
21  
22  
23  
24  
25  
26  
27  
28  
29  
30  
31  
32  
33  
34  
35  
36  
37  
38  
39  
40  
41  
42  
43  
44  
45  
46  
47  
48  
49  
50  
51  
52  
53  
54  
55  
56  
57  
58  
59  
60  
61  
62  
63  
64  
65  
66  
67  
68  
69  
70  
71  
72  
73  
74  
75  
76  
77  
78  
79  
80  
81  
82  
83  
84  
85  
86  
87  
88  
89  
90  
91  
92  
93  
94  
95  
96  
97  
98  
99  
100

1  
2  
3  
4  
5  
6  
7  
8  
9  
10  
11  
12  
13  
14  
15  
16  
17  
18  
19  
20  
21  
22  
23  
24  
25  
26  
27  
28  
29  
30  
31  
32  
33  
34  
35  
36  
37  
38  
39  
40  
41  
42  
43  
44  
45  
46  
47  
48  
49  
50  
51  
52  
53  
54  
55  
56  
57  
58  
59  
60  
61  
62  
63  
64  
65  
66  
67  
68  
69  
70  
71  
72  
73  
74  
75  
76  
77  
78  
79  
80  
81  
82  
83  
84  
85  
86  
87  
88  
89  
90  
91  
92  
93  
94  
95  
96  
97  
98  
99  
100

TABLE 10. ACOUSTIC PARAMETERS: MEANS AND STANDARD DEVIATIONS

CASE	SI	N	Char.Frq.	Threshold	Best Level	Q10	Q40	Latency	HLS Slope	Binaural		
										EI	EE	EO
C11	1	13	12.6±2.12	-3.8±11.5	25.8±20.5	5.1±3.8	1.5±0.9	10.3±0.6	-0.42±0.59	6	7	0
	2	9	18.5±0.98	-3.0±10.0	22.0±10.6	4.0±2.2	1.6±0.9	10.1±0.8	-0.83±0.95	4	5	0
	3	15	25.6±2.23	0.3±7.0	32.2±16.2	4.4±3.3	1.1±0.2	10.1±0.9	-0.34±0.66	8	7	0
	4	12	39.4±4.90	8.3±8.3	41.0±16.8	3.7±1.3	1.4±0.4	10.3±0.8	-0.29±0.89	0	8	3
C115	1	12	2.34±0.72	5.3±12.1	38.3±20.9	2.4±1.7	0.9±0.5	12.4±1.5	0.06±1.38			
	2	12	5.06±1.09	-5.1±9.4	23.7±19.9	2.2±1.1	1.0±0.7	12.6±2.5	-0.21±0.99			
	3	13	9.04±1.74	-4.5±8.0	30.8±14.9	3.1±2.2	1.2±0.7	11.9±1.3	-0.52±1.10			
	4	14	17.5±3.65	-3.0±13.3	39.5±14.9	3.1±2.8	1.2±0.7	11.4±2.5	0.04±1.50			
C163	1	24	5.13±1.68	10.1±10.5	36.6±22.7	4.1±3.1	1.6±1.1	12.6±1.5	-1.43±1.25	8	15	1
	2	25	7.73±1.08	9.6±10.0	42.0±19.9	5.7±4.4	1.6±0.8	12.0±1.5	-1.73±1.61	10	12	3
	3	23	11.8±1.24	12.7±12.0	41.3±18.7	3.9±1.5	1.5±0.9	11.9±1.9	-2.20±1.75	12	9	2
	4	27	18.5±3.21	4.2±12.7	38.1±17.0	7.0±3.5	2.6±2.1	11.7±1.7	-1.39±1.26	10	14	3
C166	1	20	11.9±1.56	-5.0±8.5	20.0±14.0	4.1±4.4	1.5±1.2	10.7±1.2	-0.85±0.41	7	10	3
	2	15	16.0±2.78	-4.3±6.4	28.0±18.3	3.4±1.8	1.2±0.7	9.9±0.9	-0.88±0.63	5	5	5
	3	16	19.5±3.21	-3.0±6.8	32.0±16.9	3.4±2.3	1.3±0.7	10.4±1.3	-0.63±0.45	1	11	4
	4	17	29.1±3.01	-0.6±8.8	40.5±13.9	3.5±2.4	1.3±0.6	10.4±1.0	-0.72±0.99	2	5	10
C124	1	12	12.3±1.27	-4.4±8.1	27.9±22.5	4.4±2.2	1.8±1.2	12.0±3.7	-0.92±1.8	5	6	1
	2	11	18.1±1.79	-0.3±8.7	30.2±17.1	3.7±1.9	1.7±0.7	9.8±1.1	-0.29±0.94	7	4	0
	3	12	24.4±2.56	11.6±10.3	49.9±18.1	3.8±2.5	1.6±0.9	9.8±1.9	0.03±1.36	7	7	0
	4	11	35.1±6.68	18.1±11.9	52.0±21.6	4.3±2.3	1.5±0.7	9.9±0.3	-0.13±0.81	1	8	2
C194	1	24	14.6±1.06	5.3±10.2	26.0±14.9	4.9±3.1	1.7±1.7	12.2±1.3	-0.87±0.72	11	10	3
	2	25	18.6±0.87	2.0±10.3	28.2±15.5	6.0±3.8	1.7±1.0	11.6±1.2	-0.34±0.80	11	8	6
	3	35	23.3±2.41	9.6±14.8	42.1±18.0	4.0±2.6	1.4±0.5	11.2±0.7	-0.34±1.20	14	19	2
	4	29	34.5±4.79	17.6±13.3	49.2±13.5	3.2±2.0	1.2±0.3	11.1±0.9	0.09±1.20	0	16	0
Total	24	426		4.1±12.5	35.4±19.0	4.3±3.0	1.5±1.1	11.2±1.7	-0.68±1.22	129	186	48

1  
2  
3  
4  
5  
6  
7  
8  
9  
10  
11  
12  
13  
14  
15  
16  
17  
18  
19  
20  
21  
22  
23  
24  
25  
26  
27  
28  
29  
30  
31  
32  
33  
34  
35  
36  
37  
38  
39  
40  
41  
42  
43  
44  
45  
46  
47  
48  
49  
50  
51  
52  
53  
54  
55  
56  
57  
58  
59  
60  
61  
62  
63  
64  
65  
66  
67  
68  
69  
70  
71  
72  
73  
74  
75  
76  
77  
78  
79  
80  
81  
82  
83  
84  
85  
86  
87  
88  
89  
90  
91  
92  
93  
94  
95  
96  
97  
98  
99  
100

1  
2  
3  
4  
5  
6  
7  
8  
9  
10  
11  
12  
13  
14  
15  
16  
17  
18  
19  
20  
21  
22  
23  
24  
25  
26  
27  
28  
29  
30  
31  
32  
33  
34  
35  
36  
37  
38  
39  
40  
41  
42  
43  
44  
45  
46  
47  
48  
49  
50  
51  
52  
53  
54  
55  
56  
57  
58  
59  
60  
61  
62  
63  
64  
65  
66  
67  
68  
69  
70  
71  
72  
73  
74  
75  
76  
77  
78  
79  
80  
81  
82  
83  
84  
85  
86  
87  
88  
89  
90  
91  
92  
93  
94  
95  
96  
97  
98  
99  
100

average increase in mean CF from slice to slice of approximately half an octave. The CF distribution covered by each slice had, on the average, a standard deviation of 15% of the mean CF. In all animals, an analysis of Frequency Response Areas (FRAs) with regard to characteristic frequency revealed a low to high CF gradient across the caudal-rostral extent of AI clearly reflecting the known cochleotopic organization (Merzenich, et al., 1975; Reale and Imig, 1980) (see Figure 34). Reversals or disruptions in frequency gradient were observed at the margins of some maps probably indicating the transition to auditory fields surrounding AI, e.g. Anterior Auditory Field (AAF) or the secondary auditory field (AII).

### 3.3.2 Intensity Parameters

#### 3.3.2.1 Acoustic Threshold

The mean acoustic threshold across all cases and all slices was 4.1dBSPL with a range extending from -5.1dBSPL to 18.1dBSPL. As can be observed in Table 10, the mean acoustic threshold varies from slice to slice in every case. Across all cases, the mean of the largest difference between slices was 10.8dB, and exceeded 13dBSPL in only two cases. It should also be noted that as the CF increased, thresholds also increased due to the increased hearing threshold of the animal at higher frequencies as well as a consequence of the transfer function of the speakers, namely its 10dB/octave roll-off above 14kHz. Three-dimensional distributions of acoustic thresholds for two exemplary cases are shown in Figure 35. As can be seen, a band of relatively low thresholds, running rostrocaudally, can be found in an area located essentially in the dorso-ventral center of AI. Areas of higher thresholds are identified ventral and dorsal to this central, low threshold, region.

1  
2  
3  
4  
5  
6  
7  
8  
9  
10  
11  
12  
13  
14  
15  
16  
17  
18  
19  
20  
21  
22  
23  
24  
25  
26  
27  
28  
29  
30  
31  
32  
33  
34  
35  
36  
37  
38  
39  
40  
41  
42  
43  
44  
45  
46  
47  
48  
49  
50  
51  
52  
53  
54  
55  
56  
57  
58  
59  
60  
61  
62  
63  
64  
65  
66  
67  
68  
69  
70  
71  
72  
73  
74  
75  
76  
77  
78  
79  
80  
81  
82  
83  
84  
85  
86  
87  
88  
89  
90  
91  
92  
93  
94  
95  
96  
97  
98  
99  
100

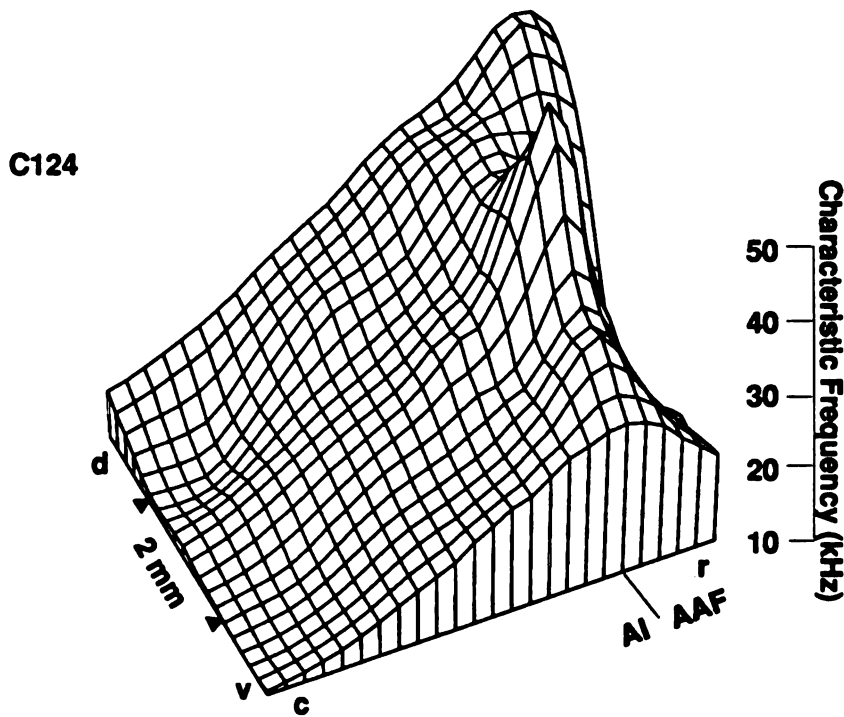
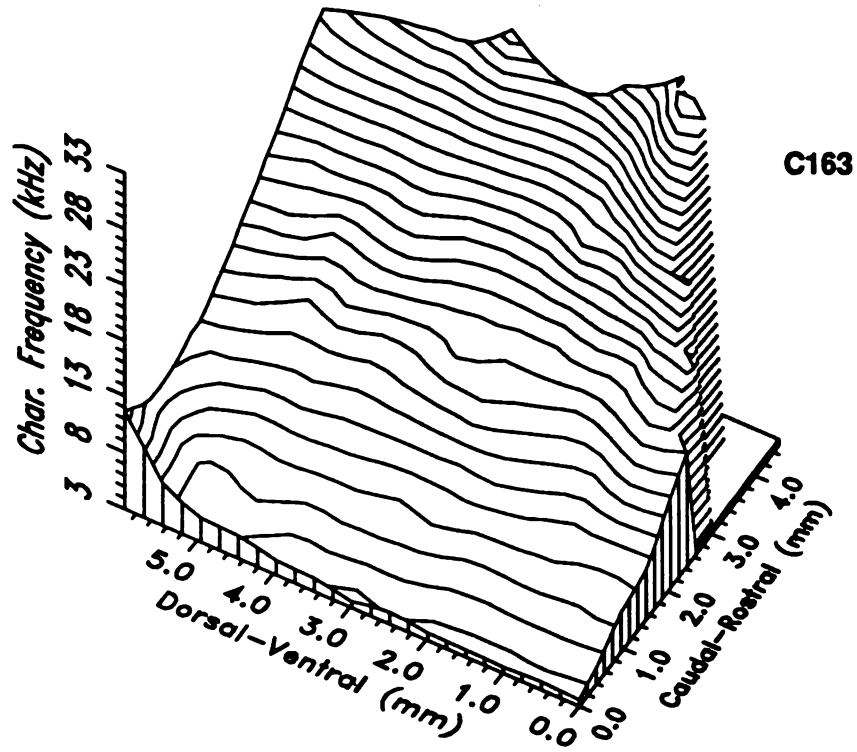
1  
2  
3  
4  
5  
6  
7  
8  
9  
10  
11  
12  
13  
14  
15  
16  
17  
18  
19  
20  
21  
22  
23  
24  
25  
26  
27  
28  
29  
30  
31  
32  
33  
34  
35  
36  
37  
38  
39  
40  
41  
42  
43  
44  
45  
46  
47  
48  
49  
50  
51  
52  
53  
54  
55  
56  
57  
58  
59  
60  
61  
62  
63  
64  
65  
66  
67  
68  
69  
70  
71  
72  
73  
74  
75  
76  
77  
78  
79  
80  
81  
82  
83  
84  
85  
86  
87  
88  
89  
90  
91  
92  
93  
94  
95  
96  
97  
98  
99  
100

**Figure 34. Two exemplary three-dimensional representations of characteristic frequency (CF) across primary auditory cortex (AI). Contour lines are separated by 1kHz for case C163. In the second case (C124), a reversal of the frequency gradient can be seen reflecting the transition into the Anterior Auditory Field (AAF).**

1  
2  
3  
4  
5  
6  
7  
8  
9  
10  
11  
12  
13  
14  
15  
16  
17  
18  
19  
20  
21  
22  
23  
24  
25  
26  
27  
28  
29  
30  
31  
32  
33  
34  
35  
36  
37  
38  
39  
40  
41  
42  
43  
44  
45  
46  
47  
48  
49  
50  
51  
52  
53  
54  
55  
56  
57  
58  
59  
60  
61  
62  
63  
64  
65  
66  
67  
68  
69  
70  
71  
72  
73  
74  
75  
76  
77  
78  
79  
80  
81  
82  
83  
84  
85  
86  
87  
88  
89  
90  
91  
92  
93  
94  
95  
96  
97  
98  
99  
100

1  
2  
3  
4  
5  
6  
7  
8  
9  
10  
11  
12  
13  
14  
15  
16  
17  
18  
19  
20  
21  
22  
23  
24  
25  
26  
27  
28  
29  
30  
31  
32  
33  
34  
35  
36  
37  
38  
39  
40  
41  
42  
43  
44  
45  
46  
47  
48  
49  
50  
51  
52  
53  
54  
55  
56  
57  
58  
59  
60  
61  
62  
63  
64  
65  
66  
67  
68  
69  
70  
71  
72  
73  
74  
75  
76  
77  
78  
79  
80  
81  
82  
83  
84  
85  
86  
87  
88  
89  
90  
91  
92  
93  
94  
95  
96  
97  
98  
99  
100

Characteristic Frequency Distribution in AI



1  
2  
3  
4  
5  
6  
7  
8  
9  
10  
11  
12  
13  
14  
15  
16  
17  
18  
19  
20  
21  
22  
23  
24  
25  
26  
27  
28  
29  
30  
31  
32  
33  
34  
35  
36  
37  
38  
39  
40  
41  
42  
43  
44  
45  
46  
47  
48  
49  
50  
51  
52  
53  
54  
55  
56  
57  
58  
59  
60  
61  
62  
63  
64  
65  
66  
67  
68  
69  
70  
71  
72  
73  
74  
75  
76  
77  
78  
79  
80  
81  
82  
83  
84  
85  
86  
87  
88  
89  
90  
91  
92  
93  
94  
95  
96  
97  
98  
99  
100

1  
2  
3  
4  
5  
6  
7  
8  
9  
10  
11  
12  
13  
14  
15  
16  
17  
18  
19  
20  
21  
22  
23  
24  
25  
26  
27  
28  
29  
30  
31  
32  
33  
34  
35  
36  
37  
38  
39  
40  
41  
42  
43  
44  
45  
46  
47  
48  
49  
50  
51  
52  
53  
54  
55  
56  
57  
58  
59  
60  
61  
62  
63  
64  
65  
66  
67  
68  
69  
70  
71  
72  
73  
74  
75  
76  
77  
78  
79  
80  
81  
82  
83  
84  
85  
86  
87  
88  
89  
90  
91  
92  
93  
94  
95  
96  
97  
98  
99  
100

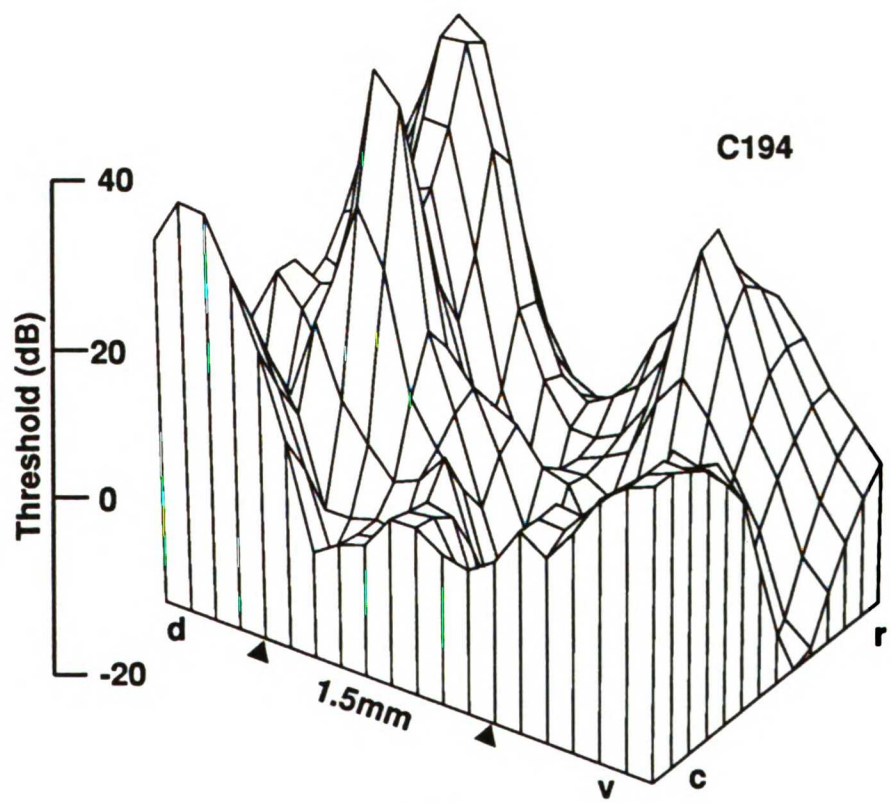
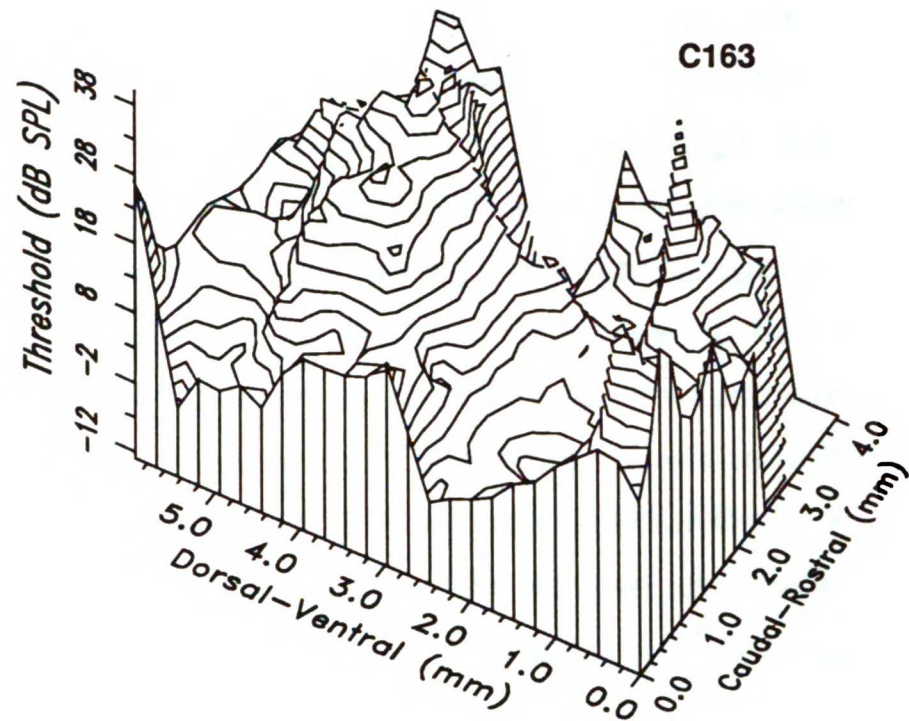
**Figure 35. Two exemplary three-dimensional representations of acoustic (tone) threshold distributions across primary auditory cortex (AI) using acoustic tone burst stimulation. Contour lines for case C163 are separated by 2dB.**

1  
2  
3  
4  
5  
6  
7  
8  
9  
10  
11  
12  
13  
14  
15  
16  
17  
18  
19  
20  
21  
22  
23  
24  
25  
26  
27  
28  
29  
30  
31  
32  
33  
34  
35  
36  
37  
38  
39  
40  
41  
42  
43  
44  
45  
46  
47  
48  
49  
50  
51  
52  
53  
54  
55  
56  
57  
58  
59  
60  
61  
62  
63  
64  
65  
66  
67  
68  
69  
70  
71  
72  
73  
74  
75  
76  
77  
78  
79  
80  
81  
82  
83  
84  
85  
86  
87  
88  
89  
90  
91  
92  
93  
94  
95  
96  
97  
98  
99  
100

1  
2  
3  
4  
5  
6  
7  
8  
9  
10  
11  
12  
13  
14  
15  
16  
17  
18  
19  
20  
21  
22  
23  
24  
25  
26  
27  
28  
29  
30  
31  
32  
33  
34  
35  
36  
37  
38  
39  
40  
41  
42  
43  
44  
45  
46  
47  
48  
49  
50  
51  
52  
53  
54  
55  
56  
57  
58  
59  
60  
61  
62  
63  
64  
65  
66  
67  
68  
69  
70  
71  
72  
73  
74  
75  
76  
77  
78  
79  
80  
81  
82  
83  
84  
85  
86  
87  
88  
89  
90  
91  
92  
93  
94  
95  
96  
97  
98  
99  
100

FIGURE 35

Tone Threshold Distribution in AI



1  
2  
3  
4  
5  
6  
7  
8  
9  
10  
11  
12  
13  
14  
15  
16  
17  
18  
19  
20  
21  
22  
23  
24  
25  
26  
27  
28  
29  
30  
31  
32  
33  
34  
35  
36  
37  
38  
39  
40  
41  
42  
43  
44  
45  
46  
47  
48  
49  
50  
51  
52  
53  
54  
55  
56  
57  
58  
59  
60  
61  
62  
63  
64  
65  
66  
67  
68  
69  
70  
71  
72  
73  
74  
75  
76  
77  
78  
79  
80  
81  
82  
83  
84  
85  
86  
87  
88  
89  
90  
91  
92  
93  
94  
95  
96  
97  
98  
99  
100

1  
2  
3  
4  
5  
6  
7  
8  
9  
10  
11  
12  
13  
14  
15  
16  
17  
18  
19  
20  
21  
22  
23  
24  
25  
26  
27  
28  
29  
30  
31  
32  
33  
34  
35  
36  
37  
38  
39  
40  
41  
42  
43  
44  
45  
46  
47  
48  
49  
50  
51  
52  
53  
54  
55  
56  
57  
58  
59  
60  
61  
62  
63  
64  
65  
66  
67  
68  
69  
70  
71  
72  
73  
74  
75  
76  
77  
78  
79  
80  
81  
82  
83  
84  
85  
86  
87  
88  
89  
90  
91  
92  
93  
94  
95  
96  
97  
98  
99  
100

### **3.3.2.2 Best Level/Strongest Response Level**

An additional acoustic parametric measurement is best level or strongest response level. For this parameter, the intensity level that results in the highest firing rate is measured for each penetration. The notion is that neurons that respond with their highest firing rate at low stimulation levels reflect the invocation of inhibitory influences that occur with increases in stimulus intensity. The mean strongest response level across all cases is 35.4dB SPL, as noted in Table 10. As in the case of acoustic threshold distribution, the strongest response level distribution varies across slices in each case. It also differs across slices within a single case by as much as 24dB SPL and as little as 5.4dB SPL. Figure 36 shows a three-dimensional depiction of the strongest response level distribution for two exemplary cases. Once again, much as in the case of acoustic threshold distribution, the central region of AI contains a valley of low best level response neurons with areas of high best level on the ventral and dorsal sides of central AI.

### **3.3.2.3 Monotonicity of Rate/Level Functions**

An additional parameter investigated in this mapping study was the monotonicity or the slope of the high level segment of rate/level functions (see section 3.1.3). The growth rate of neuronal response with increasing stimulus level was an important measure that reflects, among other characteristics, the degree of involvement of inhibitory mechanisms in the processing at a given cortical location. Monotonicity is measured in percent change in growth/dB above the transition point. As can be seen in Table 10, the vast majority of mean values across all cases and all slices were negative values including the total mean value of -0.68%/dB. These

1947-1948

1947-1948

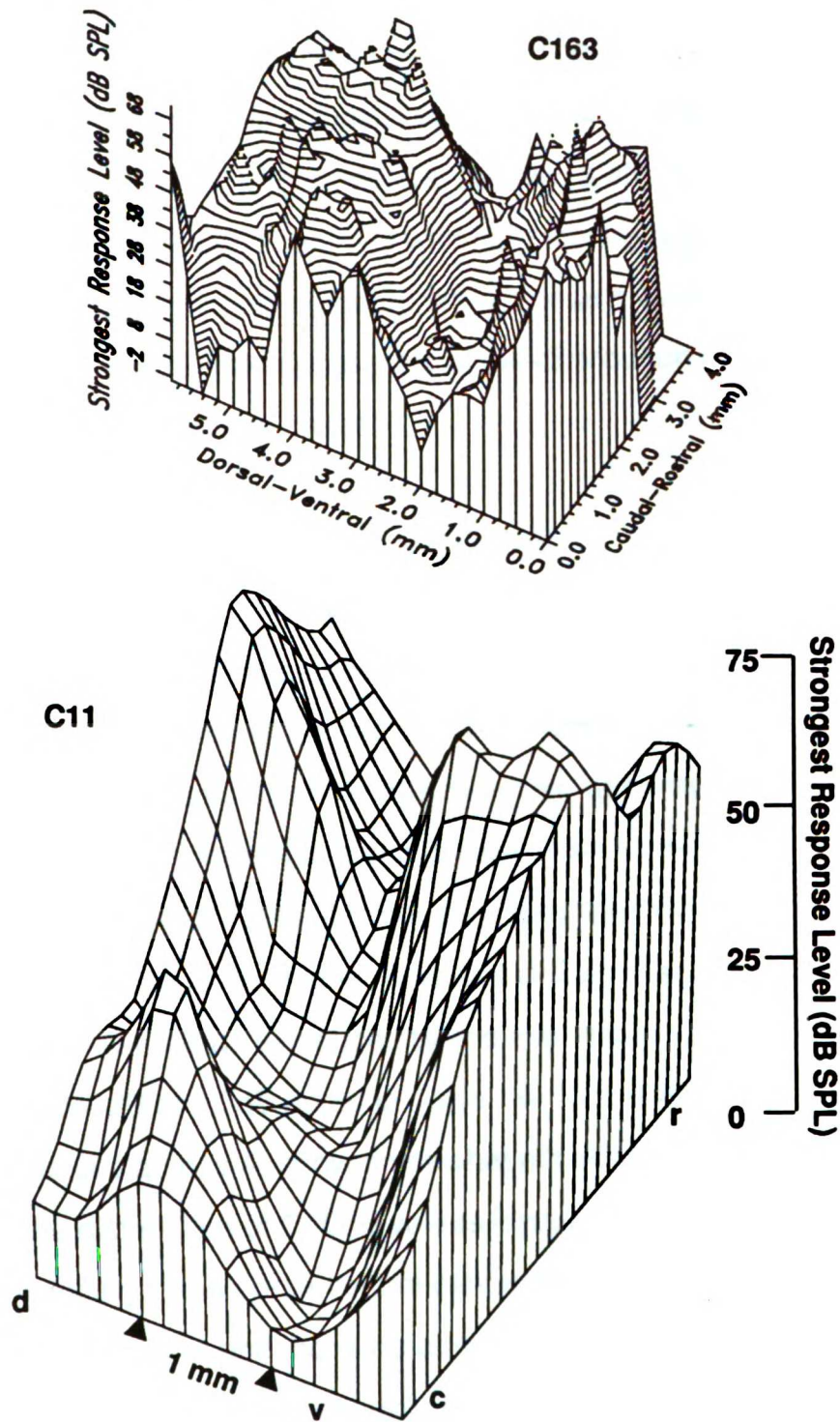
**Figure 36. Two exemplary three-dimensional representations of strongest response level or best level distributions across primary auditory cortex (AI) using acoustic tone burst stimulation. Contour lines in case C163 are separated by 1.5 dB.**

1947-1948  
1949-1950  
1951-1952  
1953-1954  
1955-1956  
1957-1958  
1959-1960  
1961-1962  
1963-1964  
1965-1966  
1967-1968  
1969-1970  
1971-1972  
1973-1974  
1975-1976  
1977-1978  
1979-1980  
1981-1982  
1983-1984  
1985-1986  
1987-1988  
1989-1990  
1991-1992  
1993-1994  
1995-1996  
1997-1998  
1999-2000  
2001-2002  
2003-2004  
2005-2006  
2007-2008  
2009-2010  
2011-2012  
2013-2014  
2015-2016  
2017-2018  
2019-2020  
2021-2022  
2023-2024  
2025-2026  
2027-2028  
2029-2030  
2031-2032  
2033-2034  
2035-2036  
2037-2038  
2039-2040  
2041-2042  
2043-2044  
2045-2046  
2047-2048  
2049-2050  
2051-2052  
2053-2054  
2055-2056  
2057-2058  
2059-2060  
2061-2062  
2063-2064  
2065-2066  
2067-2068  
2069-2070  
2071-2072  
2073-2074  
2075-2076  
2077-2078  
2079-2080  
2081-2082  
2083-2084  
2085-2086  
2087-2088  
2089-2090  
2091-2092  
2093-2094  
2095-2096  
2097-2098  
2099-2100

1947-1948  
1949-1950  
1951-1952  
1953-1954  
1955-1956  
1957-1958  
1959-1960  
1961-1962  
1963-1964  
1965-1966  
1967-1968  
1969-1970  
1971-1972  
1973-1974  
1975-1976  
1977-1978  
1979-1980  
1981-1982  
1983-1984  
1985-1986  
1987-1988  
1989-1990  
1991-1992  
1993-1994  
1995-1996  
1997-1998  
1999-2000  
2001-2002  
2003-2004  
2005-2006  
2007-2008  
2009-2010  
2011-2012  
2013-2014  
2015-2016  
2017-2018  
2019-2020  
2021-2022  
2023-2024  
2025-2026  
2027-2028  
2029-2030  
2031-2032  
2033-2034  
2035-2036  
2037-2038  
2039-2040  
2041-2042  
2043-2044  
2045-2046  
2047-2048  
2049-2050  
2051-2052  
2053-2054  
2055-2056  
2057-2058  
2059-2060  
2061-2062  
2063-2064  
2065-2066  
2067-2068  
2069-2070  
2071-2072  
2073-2074  
2075-2076  
2077-2078  
2079-2080  
2081-2082  
2083-2084  
2085-2086  
2087-2088  
2089-2090  
2091-2092  
2093-2094  
2095-2096  
2097-2098  
2099-2100

FIGURE 36

Strongest Response Level Distribution in AI



1  
2  
3  
4  
5  
6  
7  
8  
9  
10  
11  
12  
13  
14  
15  
16  
17  
18  
19  
20  
21  
22  
23  
24  
25  
26  
27  
28  
29  
30  
31  
32  
33  
34  
35  
36  
37  
38  
39  
40  
41  
42  
43  
44  
45  
46  
47  
48  
49  
50  
51  
52  
53  
54  
55  
56  
57  
58  
59  
60  
61  
62  
63  
64  
65  
66  
67  
68  
69  
70  
71  
72  
73  
74  
75  
76  
77  
78  
79  
80  
81  
82  
83  
84  
85  
86  
87  
88  
89  
90  
91  
92  
93  
94  
95  
96  
97  
98  
99  
100

1  
2  
3  
4  
5  
6  
7  
8  
9  
10  
11  
12  
13  
14  
15  
16  
17  
18  
19  
20  
21  
22  
23  
24  
25  
26  
27  
28  
29  
30  
31  
32  
33  
34  
35  
36  
37  
38  
39  
40  
41  
42  
43  
44  
45  
46  
47  
48  
49  
50  
51  
52  
53  
54  
55  
56  
57  
58  
59  
60  
61  
62  
63  
64  
65  
66  
67  
68  
69  
70  
71  
72  
73  
74  
75  
76  
77  
78  
79  
80  
81  
82  
83  
84  
85  
86  
87  
88  
89  
90  
91  
92  
93  
94  
95  
96  
97  
98  
99  
100

negative values reflect the fact that the slopes of firing rate vs. level functions are typically negative, reflecting a non-monotonic growth behavior of the majority of the rate/level functions. The differences in these values across cases appears to be small. The distribution of monotonic and non-monotonic values across AI, in some cases, reflect the same pattern as seen in other parameters, namely, a strongly non-monotonic region located centrally with neighboring regions ventrally and dorsally with more monotonic neuronal response growth. Figure 37 shows exemplary three-dimensional plots of the distribution of monotonicity across AI for two cases.

### 3.3.3 Bandwidth Parameters: Q10dB and Q40dB

Q10dB and Q40dB are measures of excitatory bandwidth of frequency response areas at two intensity levels above minimum threshold. Both sharpness of tuning estimates show little mean variation from one case to the next, or between slices within a single case (see Table 10). Considering the shape of FRAs, it is not surprising that the Q10dB values across all cases demonstrate higher Q values or narrower tuning bandwidths than Q40dB as evidenced by the total mean Q10dB of 4.3dB and a total mean Q40dB of 1.5dB noted in Table 10. The distribution of Q10dB and Q40dB values across AI show somewhat different patterns. Figure 38 shows that the distribution of Q10dB values indicate a tendency toward the sharpest tuning in the dorso-ventral center of AI. However, the pattern is generally less uniform and more variable from case to case than those seen for Q40dB or response threshold. In at least several cases, Q40dB shares more clearly the same overall characteristic pattern as seen in acoustic threshold and best level. That is, the area of sharpest tuning is generally found in the central region of AI with surrounding ventral and

1  
2  
3  
4  
5  
6  
7  
8  
9  
10  
11  
12  
13  
14  
15  
16  
17  
18  
19  
20  
21  
22  
23  
24  
25  
26  
27  
28  
29  
30  
31  
32  
33  
34  
35  
36  
37  
38  
39  
40  
41  
42  
43  
44  
45  
46  
47  
48  
49  
50  
51  
52  
53  
54  
55  
56  
57  
58  
59  
60  
61  
62  
63  
64  
65  
66  
67  
68  
69  
70  
71  
72  
73  
74  
75  
76  
77  
78  
79  
80  
81  
82  
83  
84  
85  
86  
87  
88  
89  
90  
91  
92  
93  
94  
95  
96  
97  
98  
99  
100

1  
2  
3  
4  
5  
6  
7  
8  
9  
10  
11  
12  
13  
14  
15  
16  
17  
18  
19  
20  
21  
22  
23  
24  
25  
26  
27  
28  
29  
30  
31  
32  
33  
34  
35  
36  
37  
38  
39  
40  
41  
42  
43  
44  
45  
46  
47  
48  
49  
50  
51  
52  
53  
54  
55  
56  
57  
58  
59  
60  
61  
62  
63  
64  
65  
66  
67  
68  
69  
70  
71  
72  
73  
74  
75  
76  
77  
78  
79  
80  
81  
82  
83  
84  
85  
86  
87  
88  
89  
90  
91  
92  
93  
94  
95  
96  
97  
98  
99  
100

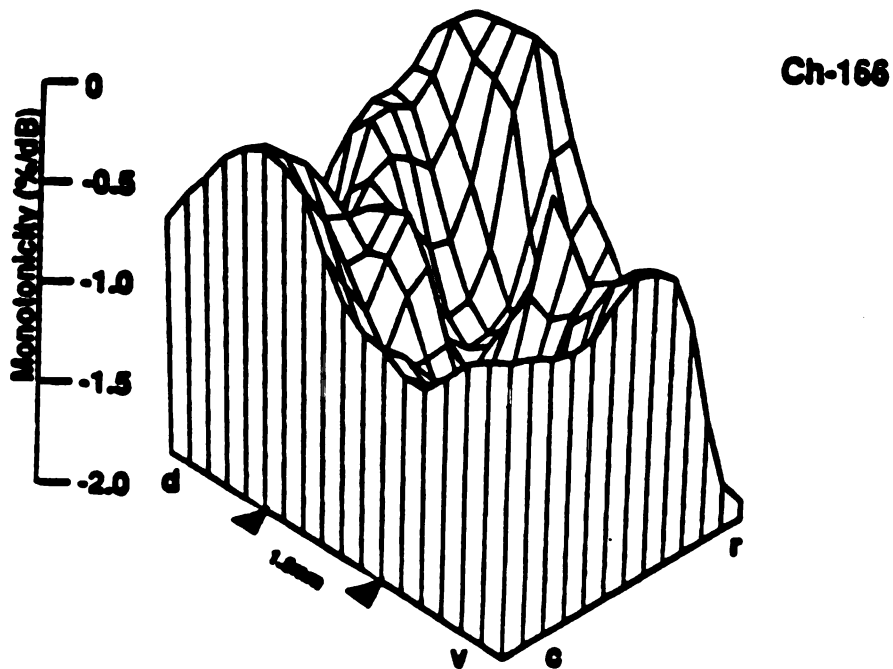
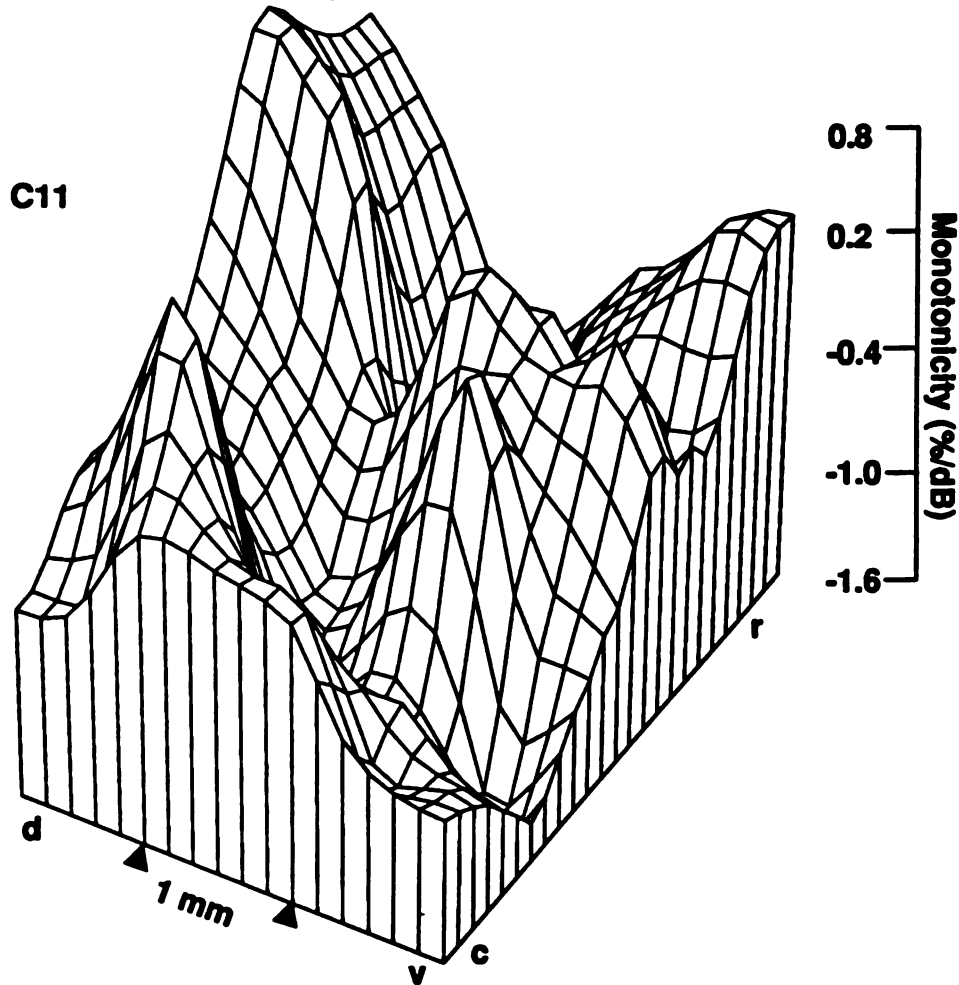
**Figure 37. Two exemplary three-dimensional representations of monotonicity (slope of the high level segment) distributions across primary auditory cortex (AI) using acoustic tone burst stimulation.**

SECRET  
IB  
SECRET

SECRET

FIGURE 37

Monotonicity (Slope of HLS) Distribution in Al



1950-1951

1950-1951

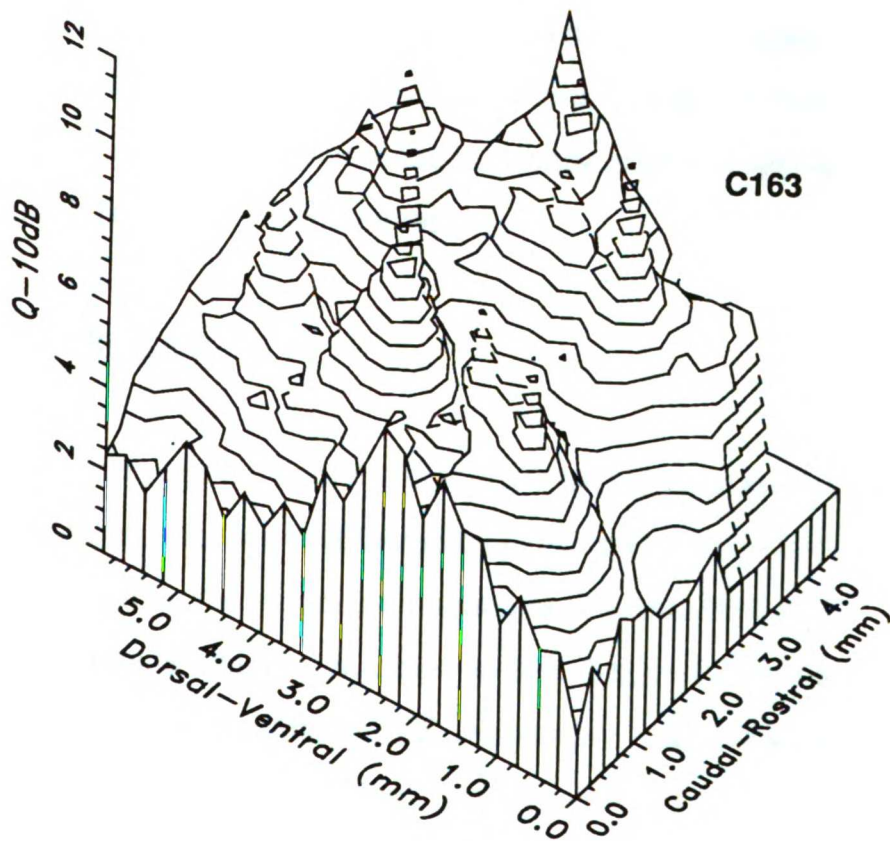
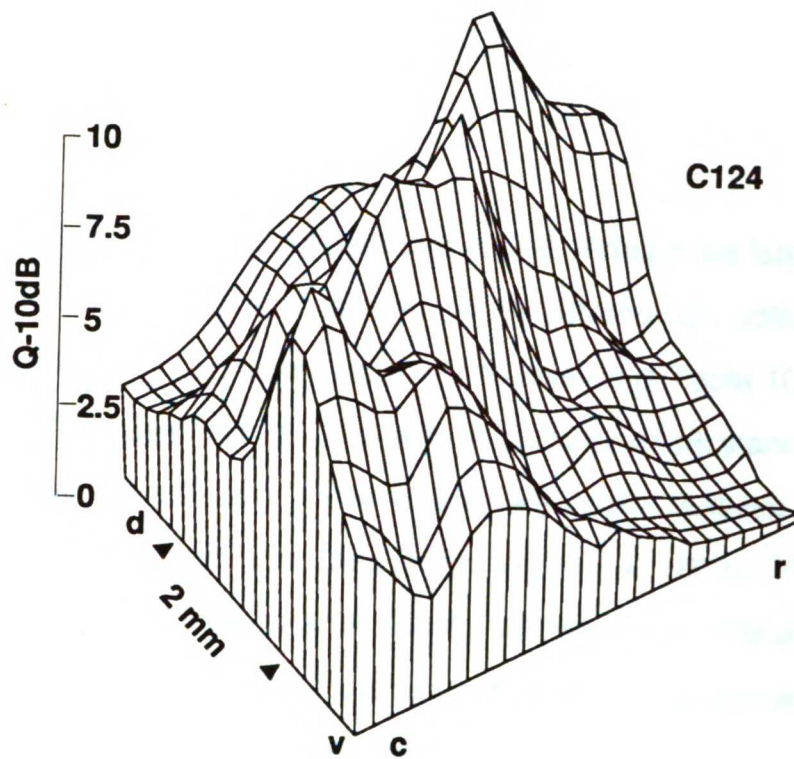
**Figure 38. Two exemplary three-dimensional representations of tuning bandwidth distribution at 10dB above threshold across primary auditory cortex (AI) using acoustic tone burst stimulation. Contour lines for case C163 are separated by approximately 0.5.**

1  
2  
3  
4  
5  
6  
7  
8  
9  
10  
11  
12  
13  
14  
15  
16  
17  
18  
19  
20  
21  
22  
23  
24  
25  
26  
27  
28  
29  
30  
31  
32  
33  
34  
35  
36  
37  
38  
39  
40  
41  
42  
43  
44  
45  
46  
47  
48  
49  
50  
51  
52  
53  
54  
55  
56  
57  
58  
59  
60  
61  
62  
63  
64  
65  
66  
67  
68  
69  
70  
71  
72  
73  
74  
75  
76  
77  
78  
79  
80  
81  
82  
83  
84  
85  
86  
87  
88  
89  
90  
91  
92  
93  
94  
95  
96  
97  
98  
99  
100

1  
2  
3  
4  
5  
6  
7  
8  
9  
10  
11  
12  
13  
14  
15  
16  
17  
18  
19  
20  
21  
22  
23  
24  
25  
26  
27  
28  
29  
30  
31  
32  
33  
34  
35  
36  
37  
38  
39  
40  
41  
42  
43  
44  
45  
46  
47  
48  
49  
50  
51  
52  
53  
54  
55  
56  
57  
58  
59  
60  
61  
62  
63  
64  
65  
66  
67  
68  
69  
70  
71  
72  
73  
74  
75  
76  
77  
78  
79  
80  
81  
82  
83  
84  
85  
86  
87  
88  
89  
90  
91  
92  
93  
94  
95  
96  
97  
98  
99  
100

# Q-10dB Distribution in AI

FIGURE 38



1  
2  
3  
4  
5  
6  
7  
8  
9  
10  
11  
12  
13  
14  
15  
16  
17  
18  
19  
20  
21  
22  
23  
24  
25  
26  
27  
28  
29  
30  
31  
32  
33  
34  
35  
36  
37  
38  
39  
40  
41  
42  
43  
44  
45  
46  
47  
48  
49  
50  
51  
52  
53  
54  
55  
56  
57  
58  
59  
60  
61  
62  
63  
64  
65  
66  
67  
68  
69  
70  
71  
72  
73  
74  
75  
76  
77  
78  
79  
80  
81  
82  
83  
84  
85  
86  
87  
88  
89  
90  
91  
92  
93  
94  
95  
96  
97  
98  
99  
100

1  
2  
3  
4  
5  
6  
7  
8  
9  
10  
11  
12  
13  
14  
15  
16  
17  
18  
19  
20  
21  
22  
23  
24  
25  
26  
27  
28  
29  
30  
31  
32  
33  
34  
35  
36  
37  
38  
39  
40  
41  
42  
43  
44  
45  
46  
47  
48  
49  
50  
51  
52  
53  
54  
55  
56  
57  
58  
59  
60  
61  
62  
63  
64  
65  
66  
67  
68  
69  
70  
71  
72  
73  
74  
75  
76  
77  
78  
79  
80  
81  
82  
83  
84  
85  
86  
87  
88  
89  
90  
91  
92  
93  
94  
95  
96  
97  
98  
99  
100

dorsal neuronal response regions with wider excitatory bandwidths (see Figures 39).

#### 3.3.4 Temporal Parameters: Latency

Another standard physiological measure is that of response latency. As in the case of Q10dB and Q40dB, latency values differed very little across cases or between slices in a single case. As illustrated in Table 10, the mean latency for all cases was 11.2ms with a relatively small standard deviation. The latency values in Table 10 are very similar to those seen in other acoustic cortical mapping studies (Mendelson et al. 1993). The distribution of latency values characteristically follows that for the other acoustic parameters listed above in the sense that shorter latencies are generally found for neurons in the central region of AI while neurons with longer latencies tend to be found in the dorsal and ventral regions. Figure 40 shows two three-dimensional representations of latency distribution which depict this systematic difference in latency response along the dorsal-ventral dimension for two cases.

#### 3.3.5 Binaural Interaction

In five animals, estimates of the binaural interaction type at each mapped cortical location were obtained by judging the influence of an ipsilateral stimulus on the response magnitude of a near threshold contralateral stimulus (usually for a tone at CF). Locations with binaural summation (excitatory-excitatory or EE interaction), binaural suppression (excitatory-inhibitory or EI interaction), and only monaural responses (E0) were distinguished. Across all cases, the majority of locations exhibited binaural summation (EE: 51.2%) with 35.5% showing binaural suppression

1  
2  
3  
4  
5  
6  
7  
8  
9  
10  
11  
12  
13  
14  
15  
16  
17  
18  
19  
20  
21  
22  
23  
24  
25  
26  
27  
28  
29  
30  
31  
32  
33  
34  
35  
36  
37  
38  
39  
40  
41  
42  
43  
44  
45  
46  
47  
48  
49  
50  
51  
52  
53  
54  
55  
56  
57  
58  
59  
60  
61  
62  
63  
64  
65  
66  
67  
68  
69  
70  
71  
72  
73  
74  
75  
76  
77  
78  
79  
80  
81  
82  
83  
84  
85  
86  
87  
88  
89  
90  
91  
92  
93  
94  
95  
96  
97  
98  
99  
100

1  
2  
3  
4  
5  
6  
7  
8  
9  
10  
11  
12  
13  
14  
15  
16  
17  
18  
19  
20  
21  
22  
23  
24  
25  
26  
27  
28  
29  
30  
31  
32  
33  
34  
35  
36  
37  
38  
39  
40  
41  
42  
43  
44  
45  
46  
47  
48  
49  
50  
51  
52  
53  
54  
55  
56  
57  
58  
59  
60  
61  
62  
63  
64  
65  
66  
67  
68  
69  
70  
71  
72  
73  
74  
75  
76  
77  
78  
79  
80  
81  
82  
83  
84  
85  
86  
87  
88  
89  
90  
91  
92  
93  
94  
95  
96  
97  
98  
99  
100

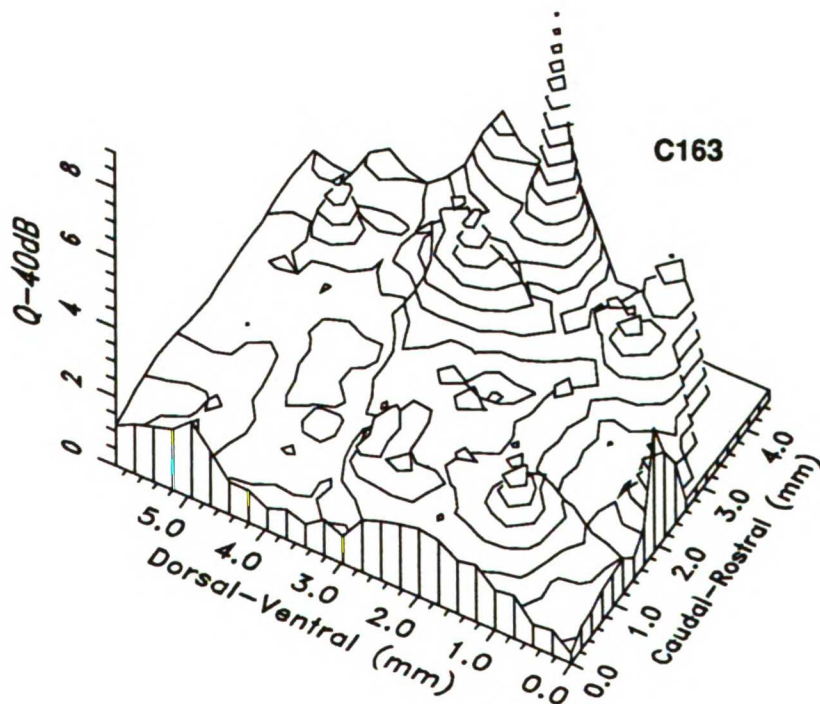
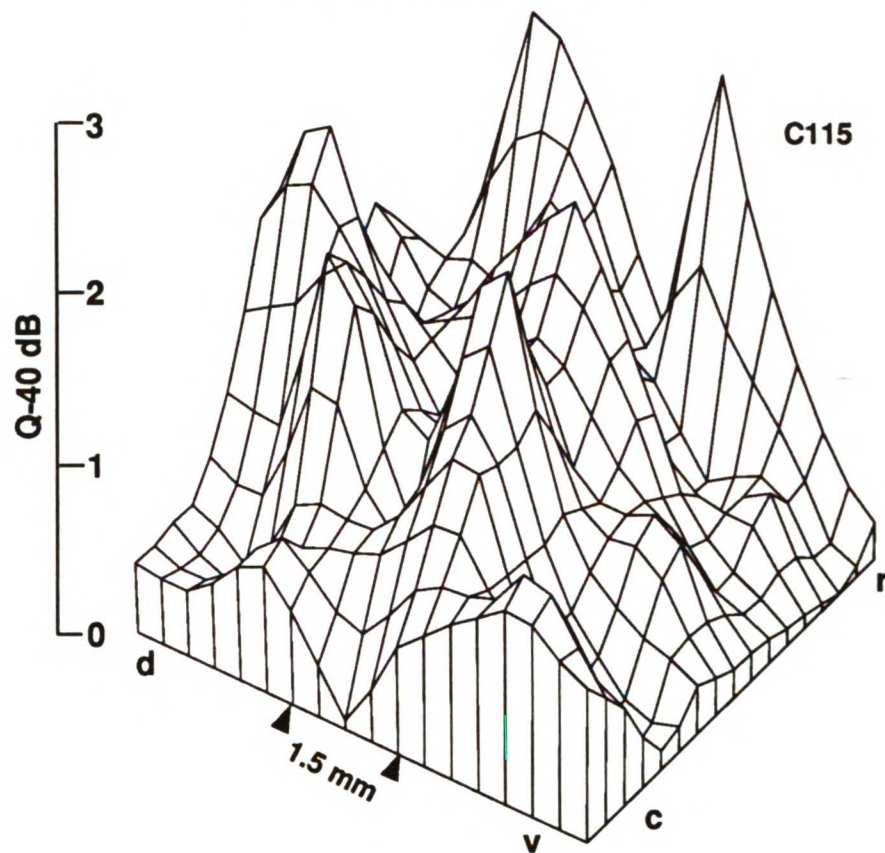
**Figure 39. Two exemplary three-dimensional representations of tuning bandwidth distribution at 40dB above threshold across primary auditory cortex (AI) using acoustic tone burst stimulation. Contour lines are separated by 0.5.**

1  
2  
3  
4  
5  
6  
7  
8  
9  
10  
11  
12  
13  
14  
15  
16  
17  
18  
19  
20  
21  
22  
23  
24  
25  
26  
27  
28  
29  
30  
31  
32  
33  
34  
35  
36  
37  
38  
39  
40  
41  
42  
43  
44  
45  
46  
47  
48  
49  
50  
51  
52  
53  
54  
55  
56  
57  
58  
59  
60  
61  
62  
63  
64  
65  
66  
67  
68  
69  
70  
71  
72  
73  
74  
75  
76  
77  
78  
79  
80  
81  
82  
83  
84  
85  
86  
87  
88  
89  
90  
91  
92  
93  
94  
95  
96  
97  
98  
99  
100

1  
2  
3  
4  
5  
6  
7  
8  
9  
10  
11  
12  
13  
14  
15  
16  
17  
18  
19  
20  
21  
22  
23  
24  
25  
26  
27  
28  
29  
30  
31  
32  
33  
34  
35  
36  
37  
38  
39  
40  
41  
42  
43  
44  
45  
46  
47  
48  
49  
50  
51  
52  
53  
54  
55  
56  
57  
58  
59  
60  
61  
62  
63  
64  
65  
66  
67  
68  
69  
70  
71  
72  
73  
74  
75  
76  
77  
78  
79  
80  
81  
82  
83  
84  
85  
86  
87  
88  
89  
90  
91  
92  
93  
94  
95  
96  
97  
98  
99  
100

Q-40dB Distribution in AI

FIGURE 39



1  
2  
3  
4  
5  
6  
7  
8  
9  
10  
11  
12  
13  
14  
15  
16  
17  
18  
19  
20  
21  
22  
23  
24  
25  
26  
27  
28  
29  
30  
31  
32  
33  
34  
35  
36  
37  
38  
39  
40  
41  
42  
43  
44  
45  
46  
47  
48  
49  
50  
51  
52  
53  
54  
55  
56  
57  
58  
59  
60  
61  
62  
63  
64  
65  
66  
67  
68  
69  
70  
71  
72  
73  
74  
75  
76  
77  
78  
79  
80  
81  
82  
83  
84  
85  
86  
87  
88  
89  
90  
91  
92  
93  
94  
95  
96  
97  
98  
99  
100

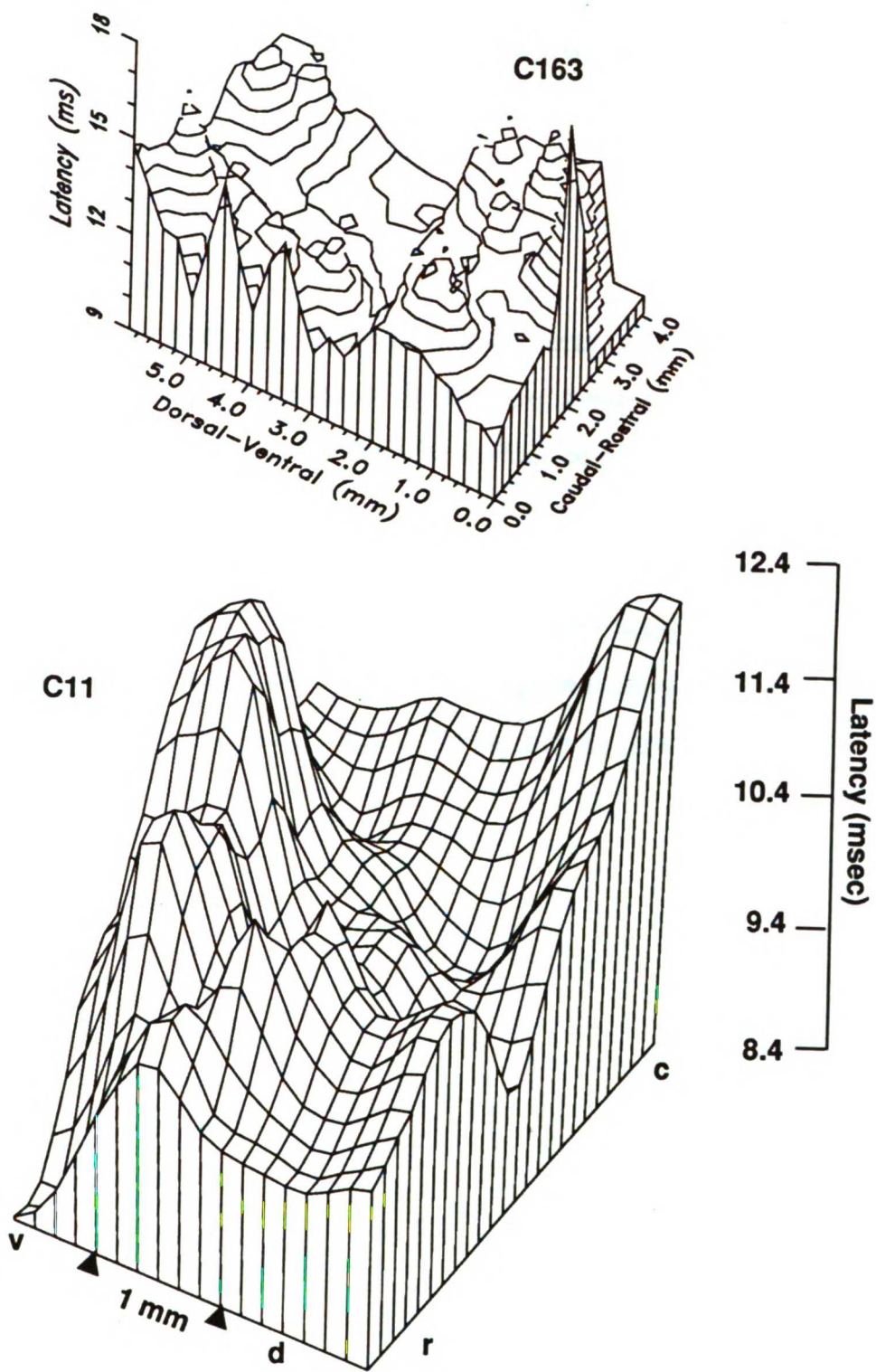
1  
2  
3  
4  
5  
6  
7  
8  
9  
10  
11  
12  
13  
14  
15  
16  
17  
18  
19  
20  
21  
22  
23  
24  
25  
26  
27  
28  
29  
30  
31  
32  
33  
34  
35  
36  
37  
38  
39  
40  
41  
42  
43  
44  
45  
46  
47  
48  
49  
50  
51  
52  
53  
54  
55  
56  
57  
58  
59  
60  
61  
62  
63  
64  
65  
66  
67  
68  
69  
70  
71  
72  
73  
74  
75  
76  
77  
78  
79  
80  
81  
82  
83  
84  
85  
86  
87  
88  
89  
90  
91  
92  
93  
94  
95  
96  
97  
98  
99  
100

**Figure 40. Two exemplary three-dimensional representations of onset latency distribution across primary auditory cortex (AI) using acoustic tone burst stimulation. Contour lines for case C163 are separated by 1 ms.**



FIGURE 40

### Onset Latency Distribution in AI



1. The first part of the document is a list of names and addresses.

1. The first part of the document is a list of names and addresses.

(EI) and 13.2% of the locations with no apparent binaural component (EO). Slices with CFs higher than approximately 30 kHz appeared to have the lowest proportion of EI neurons. In every case, spatial clusters of similar binaural interaction types were observed as illustrated for two cases in Figure 41.

### 3.3.6 Summary

This study confirms the clear, systematic constructs of physiological responses in AI to acoustic stimulation. In addition, these organizational principles of functional distributions show a confluence of responses that is uniform across the the rostral-caudal and ventral-dorsal domains such that the center of AI becomes the focal point of this confluence. To greater and lesser extents, organizational constructs for acoustic threshold, best level, monotonicity, width of tuning, and latency across AI all reveal a non-uniform distribution that is similar across parameters.

1  
2  
3  
4  
5  
6  
7  
8  
9  
10  
11  
12  
13  
14  
15  
16  
17  
18  
19  
20  
21  
22  
23  
24  
25  
26  
27  
28  
29  
30  
31  
32  
33  
34  
35  
36  
37  
38  
39  
40  
41  
42  
43  
44  
45  
46  
47  
48  
49  
50  
51  
52  
53  
54  
55  
56  
57  
58  
59  
60  
61  
62  
63  
64  
65  
66  
67  
68  
69  
70  
71  
72  
73  
74  
75  
76  
77  
78  
79  
80  
81  
82  
83  
84  
85  
86  
87  
88  
89  
90  
91  
92  
93  
94  
95  
96  
97  
98  
99  
100

1  
2  
3  
4  
5  
6  
7  
8  
9  
10  
11  
12  
13  
14  
15  
16  
17  
18  
19  
20  
21  
22  
23  
24  
25  
26  
27  
28  
29  
30  
31  
32  
33  
34  
35  
36  
37  
38  
39  
40  
41  
42  
43  
44  
45  
46  
47  
48  
49  
50  
51  
52  
53  
54  
55  
56  
57  
58  
59  
60  
61  
62  
63  
64  
65  
66  
67  
68  
69  
70  
71  
72  
73  
74  
75  
76  
77  
78  
79  
80  
81  
82  
83  
84  
85  
86  
87  
88  
89  
90  
91  
92  
93  
94  
95  
96  
97  
98  
99  
100

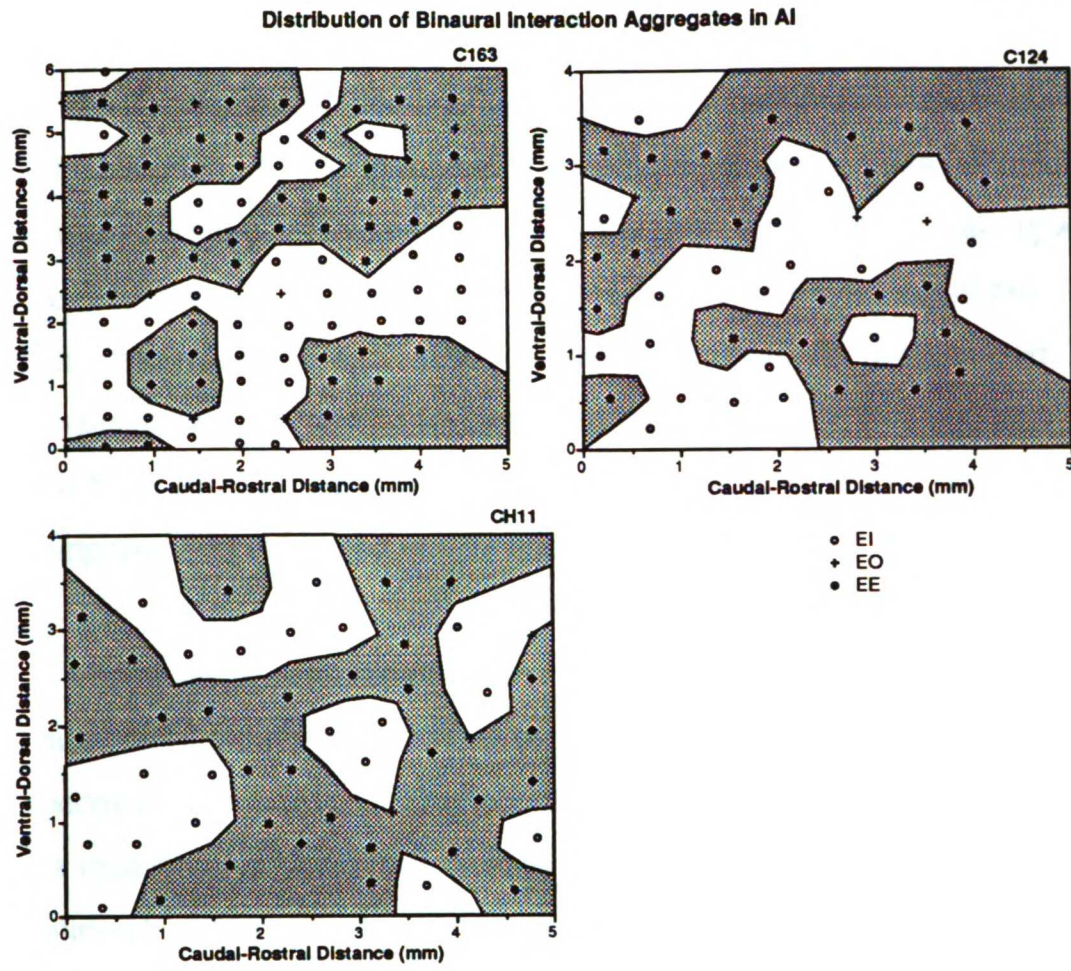
1  
2  
3  
4  
5  
6  
7  
8  
9  
10  
11  
12  
13  
14  
15  
16  
17  
18  
19  
20  
21  
22  
23  
24  
25  
26  
27  
28  
29  
30  
31  
32  
33  
34  
35  
36  
37  
38  
39  
40  
41  
42  
43  
44  
45  
46  
47  
48  
49  
50  
51  
52  
53  
54  
55  
56  
57  
58  
59  
60  
61  
62  
63  
64  
65  
66  
67  
68  
69  
70  
71  
72  
73  
74  
75  
76  
77  
78  
79  
80  
81  
82  
83  
84  
85  
86  
87  
88  
89  
90  
91  
92  
93  
94  
95  
96  
97  
98  
99  
100

**Figure 41. Distribution of binaural interaction aggregates across primary auditory cortex (AI) for three exemplary cases. Shaded areas represent the distributions of EE neurons (dots) and unshaded areas represent the distributions of EI neurons (circles). Locations that showed only monaural responses (EO) are marked by a cross.**

1  
2  
3  
4  
5  
6  
7  
8  
9  
10  
11  
12  
13  
14  
15  
16  
17  
18  
19  
20  
21  
22  
23  
24  
25  
26  
27  
28  
29  
30  
31  
32  
33  
34  
35  
36  
37  
38  
39  
40  
41  
42  
43  
44  
45  
46  
47  
48  
49  
50  
51  
52  
53  
54  
55  
56  
57  
58  
59  
60  
61  
62  
63  
64  
65  
66  
67  
68  
69  
70  
71  
72  
73  
74  
75  
76  
77  
78  
79  
80  
81  
82  
83  
84  
85  
86  
87  
88  
89  
90  
91  
92  
93  
94  
95  
96  
97  
98  
99  
100

1  
2  
3  
4  
5  
6  
7  
8  
9  
10  
11  
12  
13  
14  
15  
16  
17  
18  
19  
20  
21  
22  
23  
24  
25  
26  
27  
28  
29  
30  
31  
32  
33  
34  
35  
36  
37  
38  
39  
40  
41  
42  
43  
44  
45  
46  
47  
48  
49  
50  
51  
52  
53  
54  
55  
56  
57  
58  
59  
60  
61  
62  
63  
64  
65  
66  
67  
68  
69  
70  
71  
72  
73  
74  
75  
76  
77  
78  
79  
80  
81  
82  
83  
84  
85  
86  
87  
88  
89  
90  
91  
92  
93  
94  
95  
96  
97  
98  
99  
100

FIGURE 41



1  
2  
3  
4  
5  
6  
7  
8  
9  
10  
11  
12  
13  
14  
15  
16  
17  
18  
19  
20  
21  
22  
23  
24  
25  
26  
27  
28  
29  
30  
31  
32  
33  
34  
35  
36  
37  
38  
39  
40  
41  
42  
43  
44  
45  
46  
47  
48  
49  
50  
51  
52  
53  
54  
55  
56  
57  
58  
59  
60  
61  
62  
63  
64  
65  
66  
67  
68  
69  
70  
71  
72  
73  
74  
75  
76  
77  
78  
79  
80  
81  
82  
83  
84  
85  
86  
87  
88  
89  
90  
91  
92  
93  
94  
95  
96  
97  
98  
99  
100

1  
2  
3  
4  
5  
6  
7  
8  
9  
10  
11  
12  
13  
14  
15  
16  
17  
18  
19  
20  
21  
22  
23  
24  
25  
26  
27  
28  
29  
30  
31  
32  
33  
34  
35  
36  
37  
38  
39  
40  
41  
42  
43  
44  
45  
46  
47  
48  
49  
50  
51  
52  
53  
54  
55  
56  
57  
58  
59  
60  
61  
62  
63  
64  
65  
66  
67  
68  
69  
70  
71  
72  
73  
74  
75  
76  
77  
78  
79  
80  
81  
82  
83  
84  
85  
86  
87  
88  
89  
90  
91  
92  
93  
94  
95  
96  
97  
98  
99  
100

### **3.4 Experimental Series Two: Comparison of Acoustic and Electrical Response Properties and Distributions**

While the above findings for acoustic and electrical stimulation provide valuable information with regard to the physiological response behavior of primary auditory cortical neurons, they take on even greater meaning when the response behaviors and distributions for each stimulus mode are evaluated relative to each other. That is, using these known acoustic physiological response behaviors and distributions in AI as a template, the response behaviors and distributions for electrical stimulation can be compared and evaluated in a functionally more meaningful context.

The ability to determine the absolute location of primary auditory cortex among the many auditory cortical fields is fundamental to successful comparisons. Confounding this task, however, is the fact that the location of AI varies significantly from one animal to another as defined by anatomical landmarks, e.g. sulcal patterns (Merzenich, et al., 1975). Therefore, in order to more accurately define AI topographically using any stimulus mode, it is of primary importance that known cortical acoustic response boundaries and spatial distributions for the physiological parameters previously discussed first be established. These spatial distributions can then be used to provide topographic benchmarks for mapping the spatial distributions of electrically-evoked response patterns across AI in terms of their constituency and relative location in AI. Physiological comparisons may then be made between these two stimulus modes.

As discussed, there are a number of systematic physiological response property distributions in AI that have been established including

1  
2  
3  
4  
5  
6  
7  
8  
9  
10  
11  
12  
13  
14  
15  
16  
17  
18  
19  
20  
21  
22  
23  
24  
25  
26  
27  
28  
29  
30  
31  
32  
33  
34  
35  
36  
37  
38  
39  
40  
41  
42  
43  
44  
45  
46  
47  
48  
49  
50  
51  
52  
53  
54  
55  
56  
57  
58  
59  
60  
61  
62  
63  
64  
65  
66  
67  
68  
69  
70  
71  
72  
73  
74  
75  
76  
77  
78  
79  
80  
81  
82  
83  
84  
85  
86  
87  
88  
89  
90  
91  
92  
93  
94  
95  
96  
97  
98  
99  
100

1  
2  
3  
4  
5  
6  
7  
8  
9  
10  
11  
12  
13  
14  
15  
16  
17  
18  
19  
20  
21  
22  
23  
24  
25  
26  
27  
28  
29  
30  
31  
32  
33  
34  
35  
36  
37  
38  
39  
40  
41  
42  
43  
44  
45  
46  
47  
48  
49  
50  
51  
52  
53  
54  
55  
56  
57  
58  
59  
60  
61  
62  
63  
64  
65  
66  
67  
68  
69  
70  
71  
72  
73  
74  
75  
76  
77  
78  
79  
80  
81  
82  
83  
84  
85  
86  
87  
88  
89  
90  
91  
92  
93  
94  
95  
96  
97  
98  
99  
100

characteristic frequency, threshold, tuning bandwidth, monotonicity of rate/level functions, binaural interaction, strongest response/best level, and onset latency. The values and spatial distributions of these physiological parameters for primary auditory cortical neurons to acoustic stimulation were evaluated and compared to the cortical response thresholds for cochlear electrical stimulation in six animals.

To compare neuronal response properties to acoustic stimulation with those of electrical stimulation, two successive maps of the primary auditory cortex were obtained using multiple and single unit recordings. Each map consisted of 50 to 90 recording locations spaced 150 to 300 $\mu$ m apart covering 4-5mm caudo-rostrally and 3.5-5mm dorso-ventrally. The recording locations were marked on a video-picture of the brain surface. In the initial map, several acoustic response properties were obtained. The animal was then implanted with a cochlear prosthesis introduced into the scala tympani of the contralateral cochlea. The recording locations for the second, electrical threshold map were placed as close as possible to the original acoustic mapping locations. The positioning of the recording electrode for the second mapping deviated from the original recording locations by as much as 100 $\mu$ m, although most locations were judged to be within 50 $\mu$ m of initial sample sites.

In an effort to estimate the extent of potential disparities in acoustic properties or electrical thresholds between initial penetrations and subsequent repenetrations at the same or nearly the same cortical location, additional penetrations (8-10) were made, in a box fashion, at points within 50 $\mu$ m around given, initial penetration sites. Acoustic or electrical responses were then measured. In an exemplary acoustic penetration, the CF of the initial site was 24.4kHz while the mean CF of



the surrounding box penetrations was 23.8kHz, a difference of 0.6kHz. For the box penetrations, a standard deviation of  $\pm 1.5$ kHz was obtained. Correspondingly, the mean thresholds and standard deviations for each electrode pair for a given penetration site and its surrounding 9 control penetrations was as follows: Pair 1,2:  $31.3 \pm 1$ dB; Pair 3,4:  $28.2 \pm 1.6$ dB; Pair 5,6:  $20.1 \pm 1.7$ dB; Pair 7,8:  $45 \pm 1.1$ dB. These comparisons would suggest that there are small, but measurable differences in physiological neuronal behavior acoustically and electrically within  $50\mu\text{m}$  of the initial recording site which would not compromise the reliability of a map/remap strategy or would do so only to a limited extent.

#### 3.4.1 Equalization of Acoustic and Electrical Stimulus Domains

A normalizing procedure was used to compensate for variations in mean acoustic parameter values as well as mean electrical threshold values due to response differences between animals as well as variations due to influences of stimulation position in the cochlea. That is, the response value or threshold at each recording location was adjusted so that the mean of each slice coincided with the mean of all slices. Prior to normalizing the electrical threshold values, an arbitrary cut off threshold of 30dB ( $3000\mu\text{A}$ ) was applied for each location since higher currents were consistently avoided in all animals to prevent cochlear damage due to high currents.

#### 3.4.2 Correlation Analysis

Table 11 reveals the results of a linear regression analyses for acoustic parameters and electrical thresholds for each electrode pair by case, and by slice. As can be seen, the parcellation of values into spatial

1  
2  
3  
4  
5  
6  
7  
8  
9  
10  
11  
12  
13  
14  
15  
16  
17  
18  
19  
20  
21  
22  
23  
24  
25  
26  
27  
28  
29  
30  
31  
32  
33  
34  
35  
36  
37  
38  
39  
40  
41  
42  
43  
44  
45  
46  
47  
48  
49  
50  
51  
52  
53  
54  
55  
56  
57  
58  
59  
60  
61  
62  
63  
64  
65  
66  
67  
68  
69  
70  
71  
72  
73  
74  
75  
76  
77  
78  
79  
80  
81  
82  
83  
84  
85  
86  
87  
88  
89  
90  
91  
92  
93  
94  
95  
96  
97  
98  
99  
100

1  
2  
3  
4  
5  
6  
7  
8  
9  
10  
11  
12  
13  
14  
15  
16  
17  
18  
19  
20  
21  
22  
23  
24  
25  
26  
27  
28  
29  
30  
31  
32  
33  
34  
35  
36  
37  
38  
39  
40  
41  
42  
43  
44  
45  
46  
47  
48  
49  
50  
51  
52  
53  
54  
55  
56  
57  
58  
59  
60  
61  
62  
63  
64  
65  
66  
67  
68  
69  
70  
71  
72  
73  
74  
75  
76  
77  
78  
79  
80  
81  
82  
83  
84  
85  
86  
87  
88  
89  
90  
91  
92  
93  
94  
95  
96  
97  
98  
99  
100

**Table 11.****CORRELATIONS OF ACOUSTIC PARAMETRIC VALUES AND ELECTRICAL THRESHOLDS BY CASE AND BY SLICE****Case: C11**

Pair	CF	Threshold	Q10	Q40	Latency	Best Level	Monotonicity	Binaural
------	----	-----------	-----	-----	---------	------------	--------------	----------

## Slice 1

1,2		-0.57				-0.57		-0.67*
3,4		-0.66*				-0.73*		-0.71*
5,6	0.63	-0.54				-0.68*		
7,8	0.62	-0.62				-0.72*		
1,8		-0.63*				-0.62		-0.65

## Slice 2

1,2								
3,4								
5,6		-0.76			0.72			-0.85*
7,8		-0.78*	0.73	0.81*	0.77			-0.76
1,8				0.82*				-0.69

Slice 3 - No significant correlations

## Slice 4

1,2								
3,4								
5,6	0.59		0.62					

**Case: C115**

Pair	CF	Threshold	Q10	Q40	Latency	Best Level	Monotonicity	Binaural
------	----	-----------	-----	-----	---------	------------	--------------	----------

Slice 1 - No significant correlations

## Slice 2

1,2			0.82**	0.83**				
3,4		-0.60	0.80*	0.70*				
7,8			0.90**		0.71*			
1,7			0.72*					

## Slice 3

1,2		-0.70						
3,4								
7,8								
1,7								

## Slice 4

1,2								
3,4				0.60				
7,8								
1,7								

IB

WASH.

1

2

3

4

5

6

7

8

9

10

11

12

13

14

15

16

17

18

19

20

21

22

23

1  
2  
3  
4  
5  
6  
7  
8  
9  
10  
11  
12  
13  
14  
15  
16  
17  
18  
19  
20  
21  
22  
23

**Case: C163**

Pair	CF	Threshold	Q10	Q40	Latency	Best Level	Monotonicity	Binaural
<b>Slice 1</b>								
1,2						-0.42		
3,4		-0.44				-0.62*		
5,6						-0.52*		
7,8						-0.52*	-0.47	
1,8						-0.43		
<b>Slice 2</b>								
1,2		-0.41				-0.60*		
3,4		-0.58*			0.44	-0.64**		
5,6		-0.42			0.44	-0.50*		0.47
7,8								0.47
1,8					0.50*	-0.54*		
<b>Slice 3</b>								
1,2		-0.67**				-0.47		
3,4		-0.49						
5,6		-0.65**				-0.58*		
7,8		-0.78***				-0.65**		
1,8		-0.45						
<b>Slice 4</b>								
1,2		-0.47*				-0.38		
3,4						-0.40		
5,6					0.38			
7,8					0.42			
1,8					0.45			

**Case: C194**

Pair	CF	Threshold	Q10	Q40	Latency	Best Level	Monotonicity	Binaural
<b>Slice 1</b>								
1,2						-0.70		
3,4								
5,6								
7,8								
1,8								
<b>Slice 2</b>								
1,2								
3,4								
5,6		-0.42			0.56*			
7,8								
1,7		-0.42			0.54*			
<b>Slice 3</b>								
1,2								
3,4								
5,6	0.60**		0.50*	0.40				
7,8								
1,7								
<b>Slice 4</b>								
1,2							0.54	
3,4							0.63*	
5,6								
7,8								
1,7							0.60	

1  
2  
3  
4  
5  
6  
7  
8  
9  
10  
11  
12  
13  
14  
15  
16  
17  
18  
19  
20  
21  
22  
23  
24  
25  
26  
27  
28  
29  
30  
31  
32  
33  
34  
35  
36  
37  
38  
39  
40  
41  
42  
43  
44  
45  
46  
47  
48  
49  
50  
51  
52  
53  
54  
55  
56  
57  
58  
59  
60  
61  
62  
63  
64  
65  
66  
67  
68  
69  
70  
71  
72  
73  
74  
75  
76  
77  
78  
79  
80  
81  
82  
83  
84  
85  
86  
87  
88  
89  
90  
91  
92  
93  
94  
95  
96  
97  
98  
99  
100

1  
2  
3  
4  
5  
6  
7  
8  
9  
10  
11  
12  
13  
14  
15  
16  
17  
18  
19  
20  
21  
22  
23  
24  
25  
26  
27  
28  
29  
30  
31  
32  
33  
34  
35  
36  
37  
38  
39  
40  
41  
42  
43  
44  
45  
46  
47  
48  
49  
50  
51  
52  
53  
54  
55  
56  
57  
58  
59  
60  
61  
62  
63  
64  
65  
66  
67  
68  
69  
70  
71  
72  
73  
74  
75  
76  
77  
78  
79  
80  
81  
82  
83  
84  
85  
86  
87  
88  
89  
90  
91  
92  
93  
94  
95  
96  
97  
98  
99  
100

**Case: C166**

Pair	CF	Threshold	Q10	Q40	Latency	Best Level	Monotonicity	Binaural
<b>Slice 1</b>								
1,2		-0.47				-0.58*	-0.48	
3,4		-0.57*				-0.49	-0.54*	
5,6	0.45					-0.69**		
7,8								
1,8		-0.60*				-0.81***	-0.61*	
<b>Slice 2</b>								
1,2		-0.57				-0.79**		
3,4						-0.70*		
5,6								
7,8								
1,8			-0.60			-0.62		
<b>Slice 3</b>								
1,2						-0.60*		
3,4						-0.60	-0.50	
5,6								
7,8						-0.52		
1,8						-0.50		
<b>Slice 4</b>								
1,2		-0.73**						
3,4								
5,6		-0.60						
7,8	0.64*				-0.49			-0.53
1,8	0.53				-0.49			

**Case: C124**

Pair	CF	Threshold	Q10	Q40	Latency	Best Level	Monotonicity	Binaural
<b>Slice 1</b>								
1,2		-0.70*						
5,6								
7,8								
1,7								
<b>Slice 2</b>								
1,2								
5,6								
7,8								
1,7					0.60			
<b>Slice 3</b>								
1,2								
5,6								
7,8	0.53	-0.60						-0.60
1,7								
<b>Slice 4</b>								
1,2	0.63							
5,6								
7,8								
1,7					0.83*		-0.70	

\*\*\* p=<0.0001

\*\* p=<0.001

\* p=<0.01

p=<0.05

1  
2  
3  
4  
5  
6  
7  
8  
9  
10  
11  
12  
13  
14  
15  
16  
17  
18  
19  
20  
21  
22  
23  
24  
25  
26  
27  
28  
29  
30  
31  
32  
33  
34  
35  
36  
37  
38  
39  
40  
41  
42  
43  
44  
45  
46  
47  
48  
49  
50  
51  
52  
53  
54  
55  
56  
57  
58  
59  
60  
61  
62  
63  
64  
65  
66  
67  
68  
69  
70  
71  
72  
73  
74  
75  
76  
77  
78  
79  
80  
81  
82  
83  
84  
85  
86  
87  
88  
89  
90  
91  
92  
93  
94  
95  
96  
97  
98  
99  
100

1  
2  
3  
4  
5  
6  
7  
8  
9  
10  
11  
12  
13  
14  
15  
16  
17  
18  
19  
20  
21  
22  
23  
24  
25  
26  
27  
28  
29  
30  
31  
32  
33  
34  
35  
36  
37  
38  
39  
40  
41  
42  
43  
44  
45  
46  
47  
48  
49  
50  
51  
52  
53  
54  
55  
56  
57  
58  
59  
60  
61  
62  
63  
64  
65  
66  
67  
68  
69  
70  
71  
72  
73  
74  
75  
76  
77  
78  
79  
80  
81  
82  
83  
84  
85  
86  
87  
88  
89  
90  
91  
92  
93  
94  
95  
96  
97  
98  
99  
100

slice domains resulted in significant correlations within some slices but not within others for the same animal. It is also clear that in some cases, there were very few or only very occasional correlations (e.g. C124). In several cases, a similar pattern of correlations between acoustic and electrical parameters emerge (e.g. C163, C166, C11) across cases. One of the more consistent patterns was that electrical thresholds were highly negatively correlated with acoustic threshold and best level: locations that had high electrical thresholds had low acoustic thresholds and low best levels. These significant negative correlation coefficients ranged from -0.41 to -0.78 for acoustic threshold, and -0.38 to -0.85 for best level. Other less prominent but still apparent relationships existed between electrical threshold and sharpness of tuning (cases C115, C11; the higher the electrical threshold, the sharper the acoustic tuning), and between electrical threshold and monotonicity (cases C194, C166; the higher the electrical threshold, the more nonmonotonic the acoustic rate/level function). Some of these individual correlations had coefficients as high as 0.90. Although seen only in a few cases, relatively high positive correlations were occasionally observed between electrical thresholds and response latencies with correlations ranging from 0.38 to 0.83. Positive correlations were also seen for electrical thresholds and binaural interaction type in a few slices in most cases.

These interrelationships of electrical and acoustic parameters were also reflected in the spatial organization of these parameters. Figure 42 shows the spatial relationship between acoustic threshold and a particular electrode pair along the ventral-dorsal slice domain. There, it can be seen that along the ventral-dorsal dimension, areas with low electrical thresholds were the same areas in which acoustic thresholds are high, and vice versa. Figure 43 shows a similar relationship for best level

1  
2  
3  
4  
5  
6  
7  
8  
9  
10  
11  
12  
13  
14  
15  
16  
17  
18  
19  
20  
21  
22  
23  
24  
25  
26  
27  
28  
29  
30  
31  
32  
33  
34  
35  
36  
37  
38  
39  
40  
41  
42  
43  
44  
45  
46  
47  
48  
49  
50  
51  
52  
53  
54  
55  
56  
57  
58  
59  
60  
61  
62  
63  
64  
65  
66  
67  
68  
69  
70  
71  
72  
73  
74  
75  
76  
77  
78  
79  
80  
81  
82  
83  
84  
85  
86  
87  
88  
89  
90  
91  
92  
93  
94  
95  
96  
97  
98  
99  
100

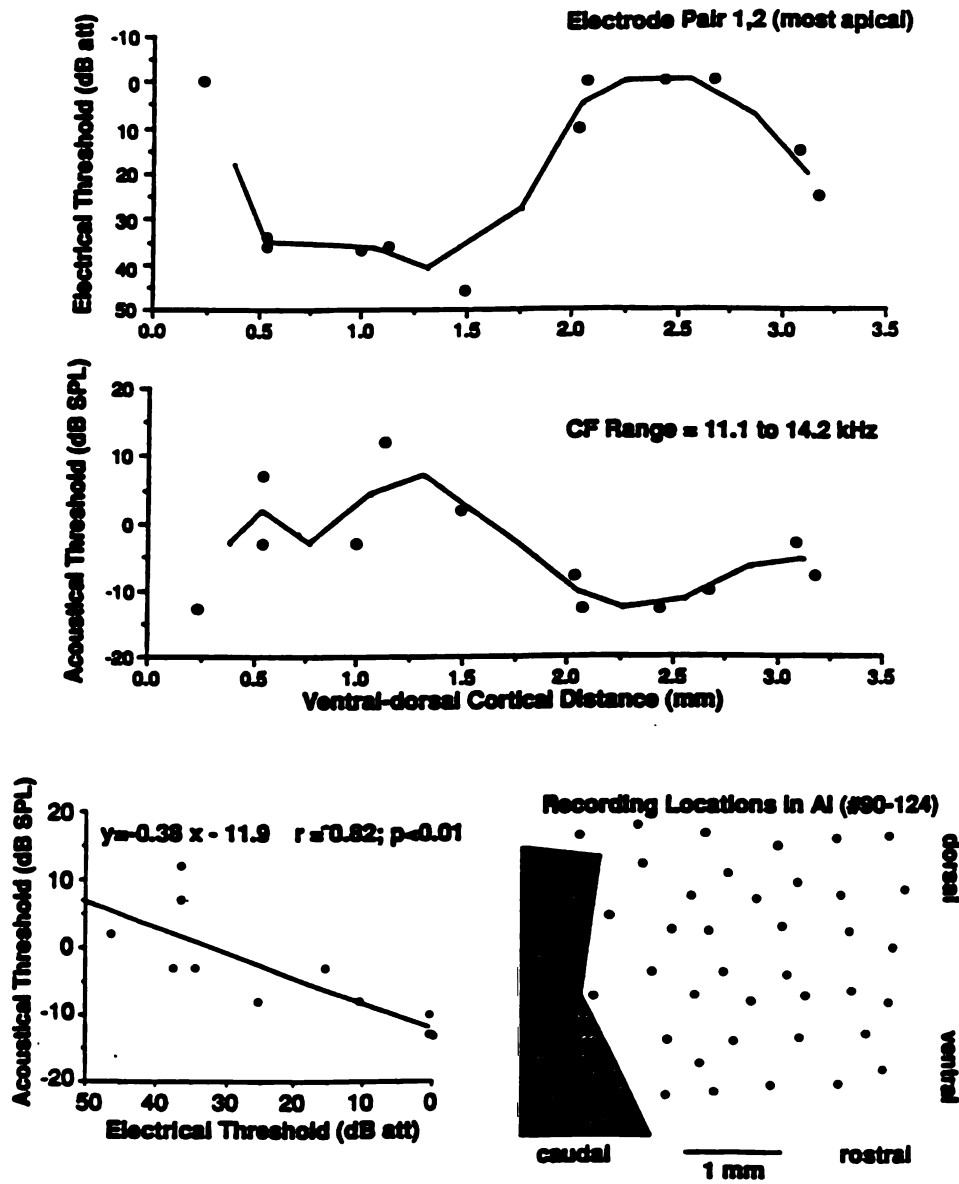
1000

**Figure 42. Spatial correlation of acoustic and electrical threshold distributions for a ventral-dorsal slice. The upper panel shows the distribution of electrical response thresholds across the dorso-ventral domain of AI. The middle panel shows the acoustic thresholds for (nearly) the same locations obtained prior to implantation. AI recording locations for this slice are depicted in the shaded area of the lower right panel. The results of a linear regression analysis are depicted in the lower left panel.**



FIGURE 42

Correlation of Electrical Threshold with Acoustical Response Threshold in Frequency Band 11.1 to 14.2 kHz





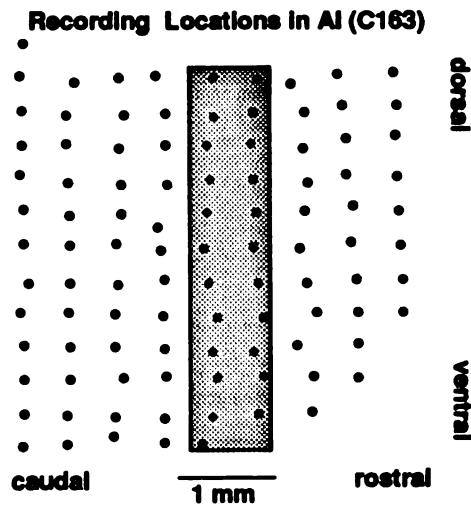
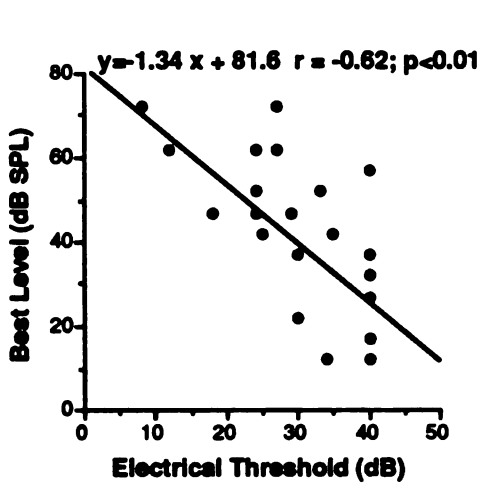
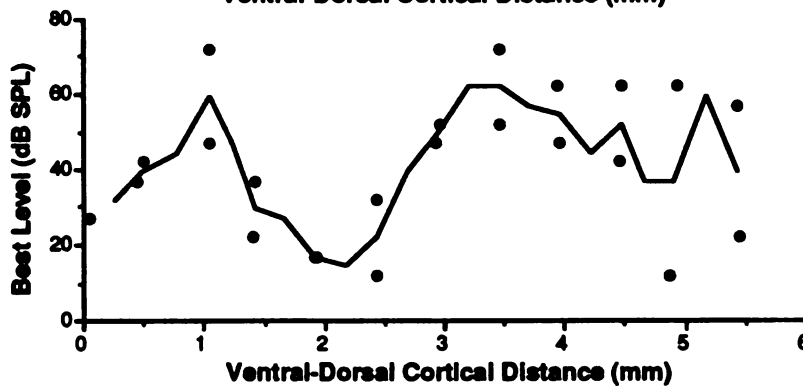
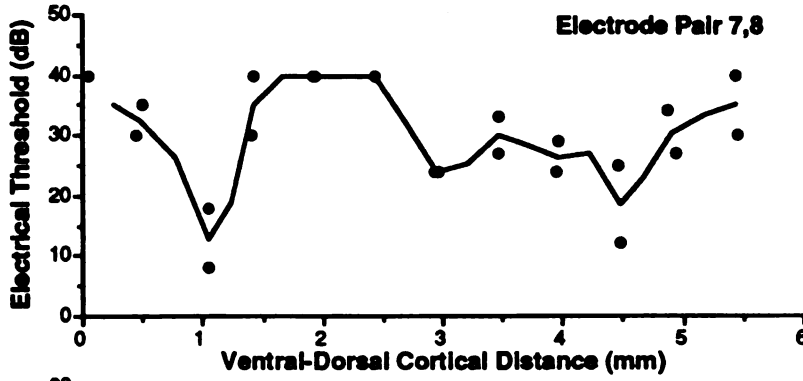
**Figure 43. Spatial correlation of best level (strongest response level) and electrical threshold distributions for a ventral-dorsal slice. The upper panel shows the distribution of electrical response thresholds across the dorso-ventral domain of AI. The middle panel shows the best level. AI recording locations for this slice are depicted in the shaded area of the lower right panel. The results of a linear regression analysis are depicted in the lower left panel.**





FIGURE 43

Correlation of Electrical Threshold with Best Level  
in Frequency Band 10.0-13.5 kHz



IB

FOR

MAN

1947

(strongest response level) versus electrical threshold along the ventral-dorsal dimension. Areas with high electrical threshold correspond to areas of low best level while areas of low electrical threshold correspond to areas of high best level. Another example demonstrates the spatial correspondence between electrical threshold and Q40 (Figure 44). A less robust demonstration of negative correlations can be seen between electrical thresholds and monotonicity (see Figure 45). Figure 46 shows the spatial correspondence between electrical threshold and binaural interaction demonstrating a negative correlation for these two parameters, i.e. preponderance of EI areas had high electrical thresholds, while areas of predominantly EE representation were marked by low electrical thresholds.

To probe statistically significant global relationships across all animals, correlations for the normalized acoustic and electrical values were analyzed using data combined from all slices (Table 12A). Relatively small but highly significant negative correlations between the thresholds for all electrode pairs and acoustic threshold were seen. A slightly higher, significant negative correlation was also seen between best level and electrical thresholds for all pairs. Small but significant positive correlations are also observed between all electrode pair thresholds and response latency. As in the single slice correlations noted in the individual cases in Table 11, the same limited but significant negative correlation were seen between monotonicity and some electrode pairs, with a few positive correlations seen between the Q values, binaural interaction, and the electrical pair thresholds.

As previously discussed, electrical spatial tuning or tonotopically preferential spatial representation of lowest threshold for a given

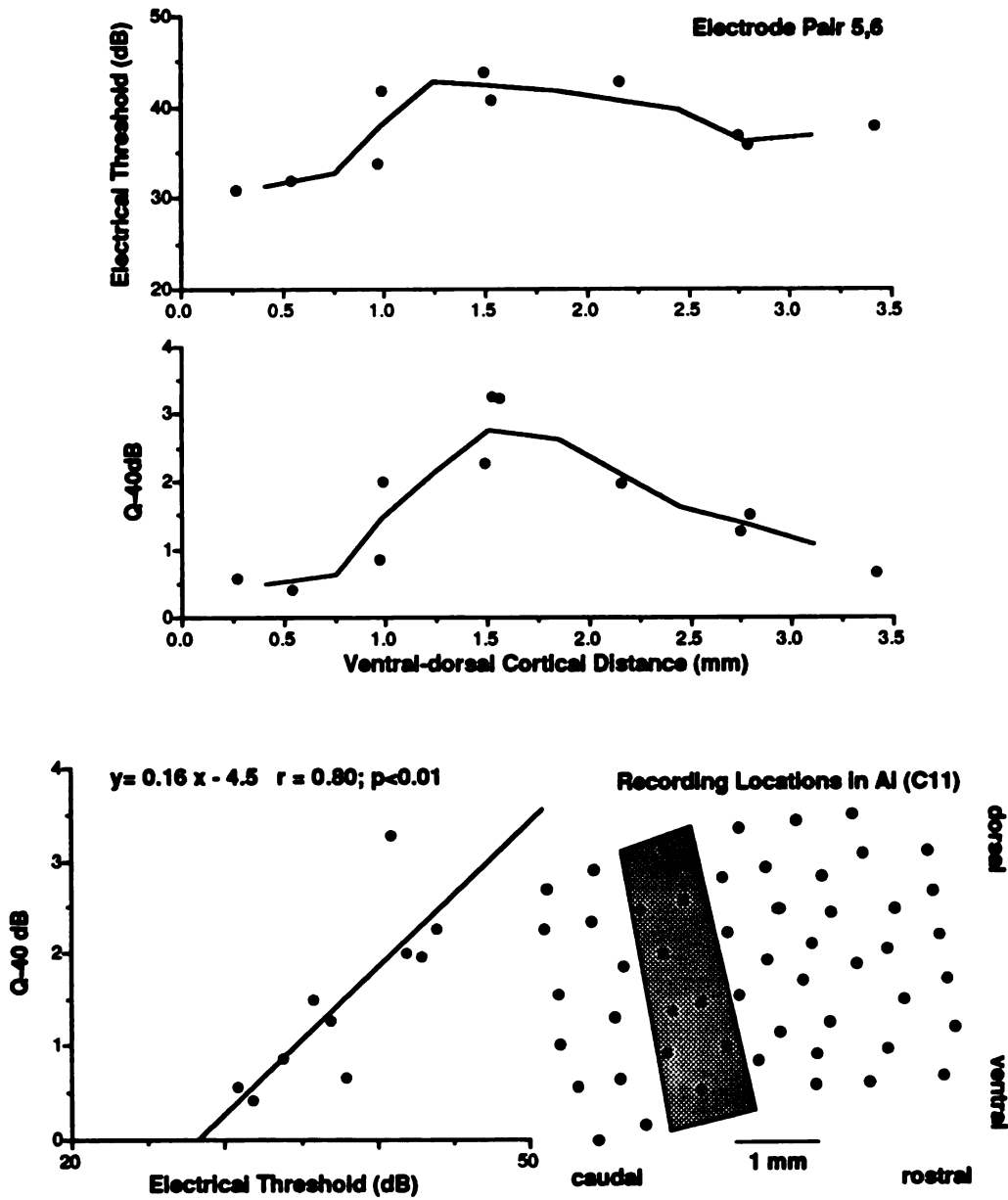


**Figure 44. Spatial correlation of Q-40dB and electrical threshold distributions for a ventral-dorsal slice. The upper panel shows the distribution of electrical response thresholds across the dorso-ventral domain of AI. The middle panel shows the Q-40dB values. AI recording locations for this slice are depicted in the shaded area of the lower right panel. The results of a linear regression analysis are depicted in the lower left panel.**



FIGURE 44

Correlation of Electrical Threshold with Q-40dB in Frequency Band 17.1-20.9 kHz



IB

100

100

R

100

100

100

100

100

100

100

100

100

100

100

100

100

100

100

**Figure 45. Spatial correlation of monotonicity (slope of HLS) and electrical threshold distributions for a ventral-dorsal slice. The upper panel shows the distribution of electrical response thresholds across the dorso-ventral domain of AI. The middle panel shows the monotonicity distribution. AI recording locations for this slice are depicted in the shaded area of the lower right panel. The results of a linear regression analysis are depicted in the lower left panel.**



FIGURE 45

Correlation of Electrical Threshold with Monotonicity of Rate-Level Functions in Frequency Band 30-51kHz

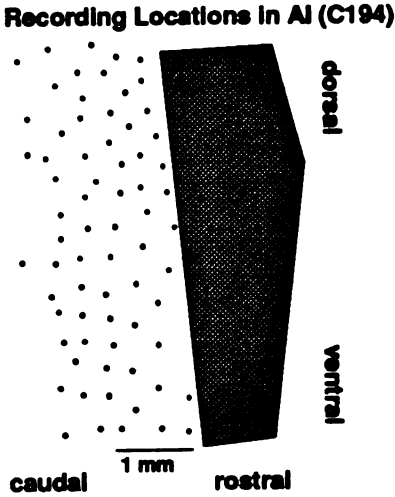
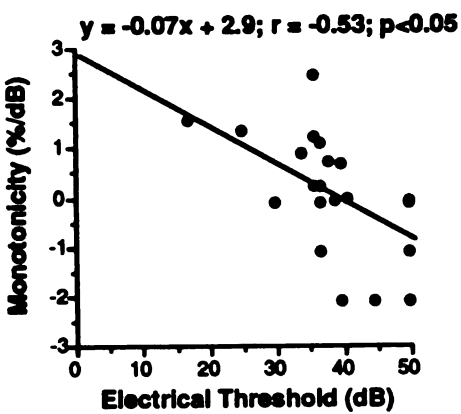
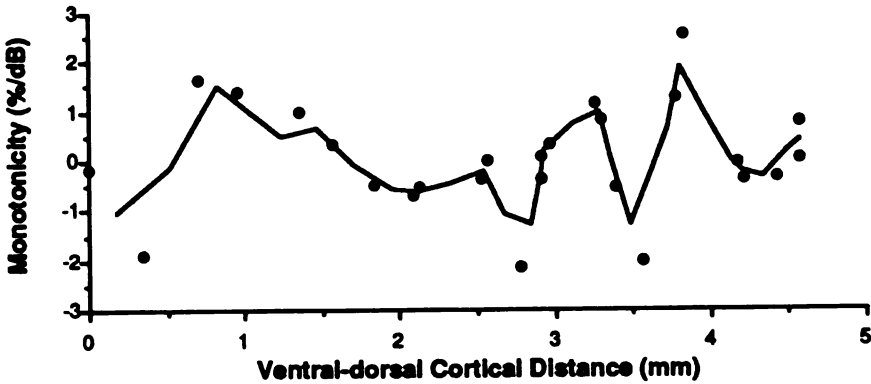
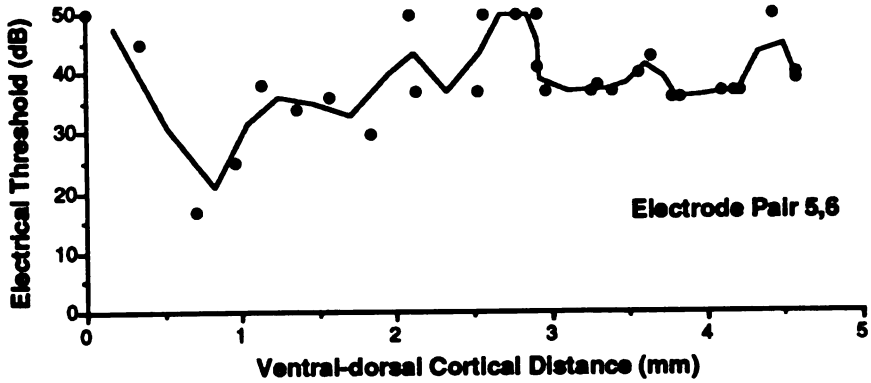


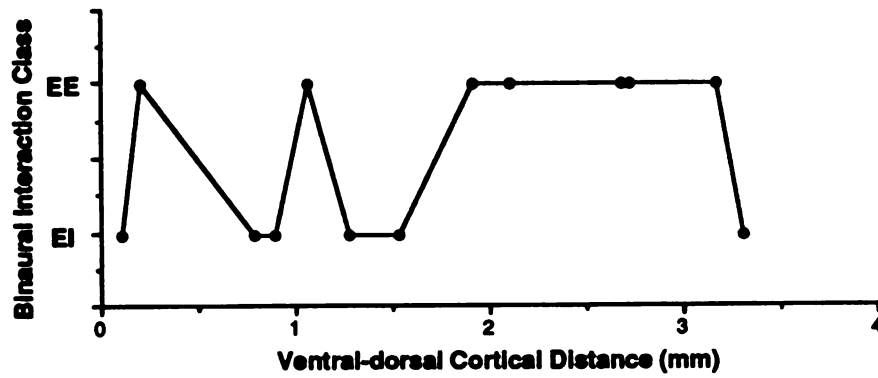
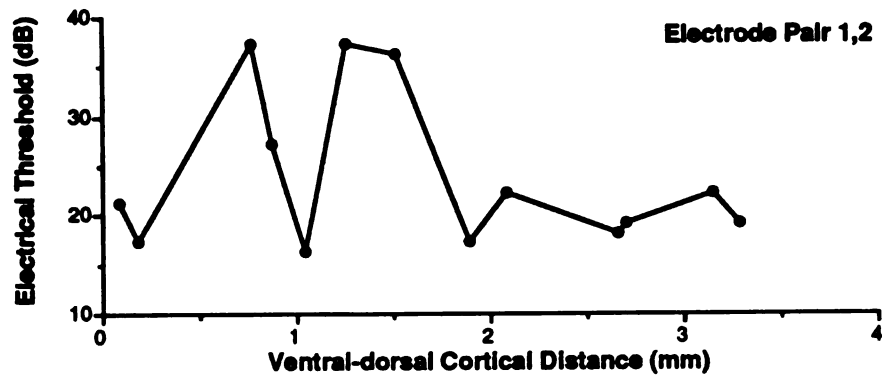


**Figure 46. Spatial correlation of binaural interaction type and electrical threshold distributions for a ventral-dorsal slice. The upper panel shows the distribution of electrical response thresholds across the dorso-ventral domain of AI. The middle panel shows the binaural interaction type. AI recording locations for this slice are depicted in the shaded area of the lower right panel. Differences in the electrical thresholds for the EE and EI neurons (lower left) were statistically significant.**



**FIGURE 46**

**Correlation of Electrical Threshold with Binaural Interaction Classes  
in Frequency Band 10.9 to 16.3 kHz**

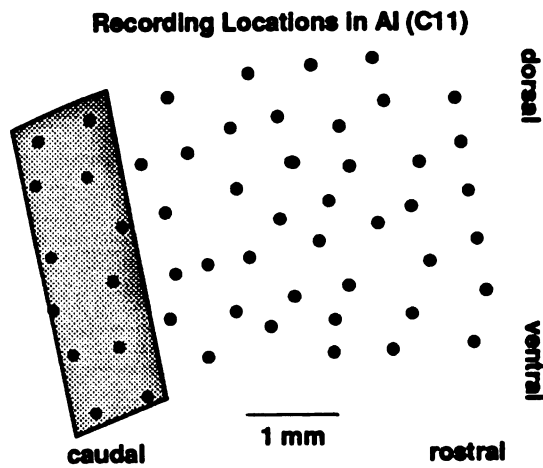


**Average Electrical Threshold (dB re 100 $\mu$ A):**

**EE =  $26.2 \pm 3.6$  dB**

**EI =  $34.4 \pm 6.1$  dB**

**(N=13; ANOVA  $p < 0.05$ )**



1  
2  
3  
4  
5  
6  
7  
8  
9  
10  
11  
12  
13  
14  
15  
16  
17  
18  
19  
20  
21  
22  
23  
24  
25  
26  
27  
28  
29  
30  
31  
32  
33  
34  
35  
36  
37  
38  
39  
40  
41  
42  
43  
44  
45  
46  
47  
48  
49  
50  
51  
52  
53  
54  
55  
56  
57  
58  
59  
60  
61  
62  
63  
64  
65  
66  
67  
68  
69  
70  
71  
72  
73  
74  
75  
76  
77  
78  
79  
80  
81  
82  
83  
84  
85  
86  
87  
88  
89  
90  
91  
92  
93  
94  
95  
96  
97  
98  
99  
100

100

100

**Table 12A.****CORRELATIONS OF NORMALIZED ACOUSTIC PARAMETER VALUES WITH NORMALIZED ELECTRICAL PAIR THRESHOLDS FOR ALL SLICES**

Pair	Threshold	Best Level	Q10	Q40	Latency	HLS Slope	Binaural
1,2	-0.22***	-0.32***		0.15*	0.12		
3,4	-0.25***	-0.36***		0.12	0.15*	-0.14*	
5,6	-0.11	-0.23***			0.15*		
7,8	-0.16**	-0.13*	0.11	0.10	0.14*		0.12
1,7-8	-0.19***	-0.30***			0.14*	-0.14*	

\*\*\*p&lt;0.0001

\*\*p&lt;0.001

\*p&lt;0.01

p&lt;0.05

**Table 12B.****CORRELATIONS OF NORMALIZED ACOUSTIC PARAMETER VALUES WITH NORMALIZED ELECTRICAL THRESHOLDS FOR TWO SLICES WITH THE BEST ELECTRICAL THRESHOLDS**

Pair	Threshold	Best Level	Q10	Q40	Latency	HLS Slope	Binaural
1,2	-0.28***	-0.41***		0.17	0.16		
3,4	-0.32***	-0.39***			0.23*		
5,6	-0.17	-0.22*			0.27**		
7,8	-0.23**				0.18*		
1,7-8	-0.14	-0.25**			0.22*		

\*\*\*p&lt;0.0001

\*\*p&lt;0.001

\*p&lt;0.01

p&lt;0.05



electrode pair was commonly observed. Therefore, additional correlation analyses were undertaken to determine the relationship between normalized acoustic parametric values and electrical thresholds for the two slices ('primary and secondary') with the best or lowest electrical thresholds. The results of these analyses are shown in Table 12B. As might be expected, the correlations between the acoustic parameters and electrical thresholds were higher than those noted for the combined slice analysis (Table 12A) with essentially the same relationships. That is, acoustic threshold and best level were both significantly negatively correlated with electrical threshold for all pairs with the exception of best level and pair 7,8. Again, latency was significantly positively correlated with all electrode pair thresholds. However, the other small correlations that had been present in the combined slice analysis have dropped out in the present analysis, possibly due to the smaller number of points included in these statistics.

### 3.4.3 Principal Component Analysis

Some of the acoustic parameters that were used in the analysis had a fairly high intercorrelation. For example Q10 and Q40 were highly correlated as were threshold and best level (see Schreiner and Mendelson 1990, Schreiner et al. 1992). A principal component or factor analysis was undertaken to determine how many independent explanatory factors might underlie the above data. Table 13A shows a factor analysis of normalized acoustic parameters. Binaural interaction types were excluded, as they were not determined for one case (but see below). From this analysis, it can be seen that there are three factors which emerge. For ease of interpretation, each factor has been provisionally named according to its principal contributing response parameters. For example, Q10 and Q40dB

1  
2  
3  
4  
5  
6  
7  
8  
9  
10  
11  
12  
13  
14  
15  
16  
17  
18  
19  
20  
21  
22  
23  
24  
25  
26  
27  
28  
29  
30  
31  
32  
33  
34  
35  
36  
37  
38  
39  
40  
41  
42  
43  
44  
45  
46  
47  
48  
49  
50  
51  
52  
53  
54  
55  
56  
57  
58  
59  
60  
61  
62  
63  
64  
65  
66  
67  
68  
69  
70  
71  
72  
73  
74  
75  
76  
77  
78  
79  
80  
81  
82  
83  
84  
85  
86  
87  
88  
89  
90  
91  
92  
93  
94  
95  
96  
97  
98  
99  
100

1  
2  
3  
4  
5  
6  
7  
8  
9  
10  
11  
12  
13  
14  
15  
16  
17  
18  
19  
20  
21  
22  
23  
24  
25  
26  
27  
28  
29  
30  
31  
32  
33  
34  
35  
36  
37  
38  
39  
40  
41  
42  
43  
44  
45  
46  
47  
48  
49  
50  
51  
52  
53  
54  
55  
56  
57  
58  
59  
60  
61  
62  
63  
64  
65  
66  
67  
68  
69  
70  
71  
72  
73  
74  
75  
76  
77  
78  
79  
80  
81  
82  
83  
84  
85  
86  
87  
88  
89  
90  
91  
92  
93  
94  
95  
96  
97  
98  
99  
100

**Table 13A.**  
**FACTOR ANALYSIS OF NORMALIZED ACOUSTIC PARAMETER VALUES**  
**EXCLUDING BINAURAL VALUES**

Factors:	F1	F2	F3
Threshold	-0.33	0.81	
Best Level		0.88	
Q10	0.86		
Q40	0.80		
Latency			0.80
Monotonicity			-0.67
(Σ=71%)			

**Table 13B.**  
**CORRELATIONS OF ACOUSTIC FACTORS WITH NORMALIZED ELECTRICAL**  
**THRESHOLDS**

Pairs:	1,2	3,4	5,6	7,8	1,7-8
F1					
F2	-0.31***	-0.33***	-0.16*		0.29***
F3	0.15*	0.20**	0.16*	0.15*	0.18**

\*\*\*p=<0.0001

\*\*p=<0.001

\*p=<0.01

p=<0.05

1950-1951

1950-1951

fall under Factor 1 which also has a small contribution from response threshold. Therefore, this factor is referred to as the "Bandwidth Factor". The second Factor is dominated by threshold and best level ("Intensity Factor"), and latency and monotonicity fall under Factor 3. One possible link between these last two parameters is the strong influence of inhibition on their behavior. Therefore, this third factor has been descriptively named the "Time/Inhibition Factor". These three factors explain 71% of the variance in the data. It would appear, then, that there are three main independent factors underlying the acoustic data set as can be seen in the graphic display in Figure 47. For each cortical location, a value can be assigned that reflects the magnitude of each Factor. Table 13B shows the correlation between these three acoustic Factor values and the normalized thresholds for each of the five electrode pairs. There were no significant correlations between Factor 1 and any electrode pair, but Factors 2 and 3 both showed small, but significant correlations with nearly all electrical pair thresholds.

Principal component analysis was also undertaken for all electrical thresholds by pair, to investigate whether several independent factors contributed to the observed variance. Table 14A shows that two factors emerged that explain 81% of the variance (Factor 1: 60%; Factor 2: 21%). Essentially, the most apical Pairs 1-2, 3-4, and the longitudinal Pair 1,7-8 provided the strongest load for Factor 1, while the most basal Pair 7,8 was in close alignment with Factor 2. Variance in the thresholds of Pair 5-6 could be contributed by both Factors. Accordingly, Factor 1 has provisionally been named "Apical Factor" and Factor 2, the "Basal Factor". Figure 48 shows a graphic display of the results of the factor analysis. It can be seen from this display that electrical thresholds by pair segregate, as noted above. A correlation analysis of these electrical factors and the



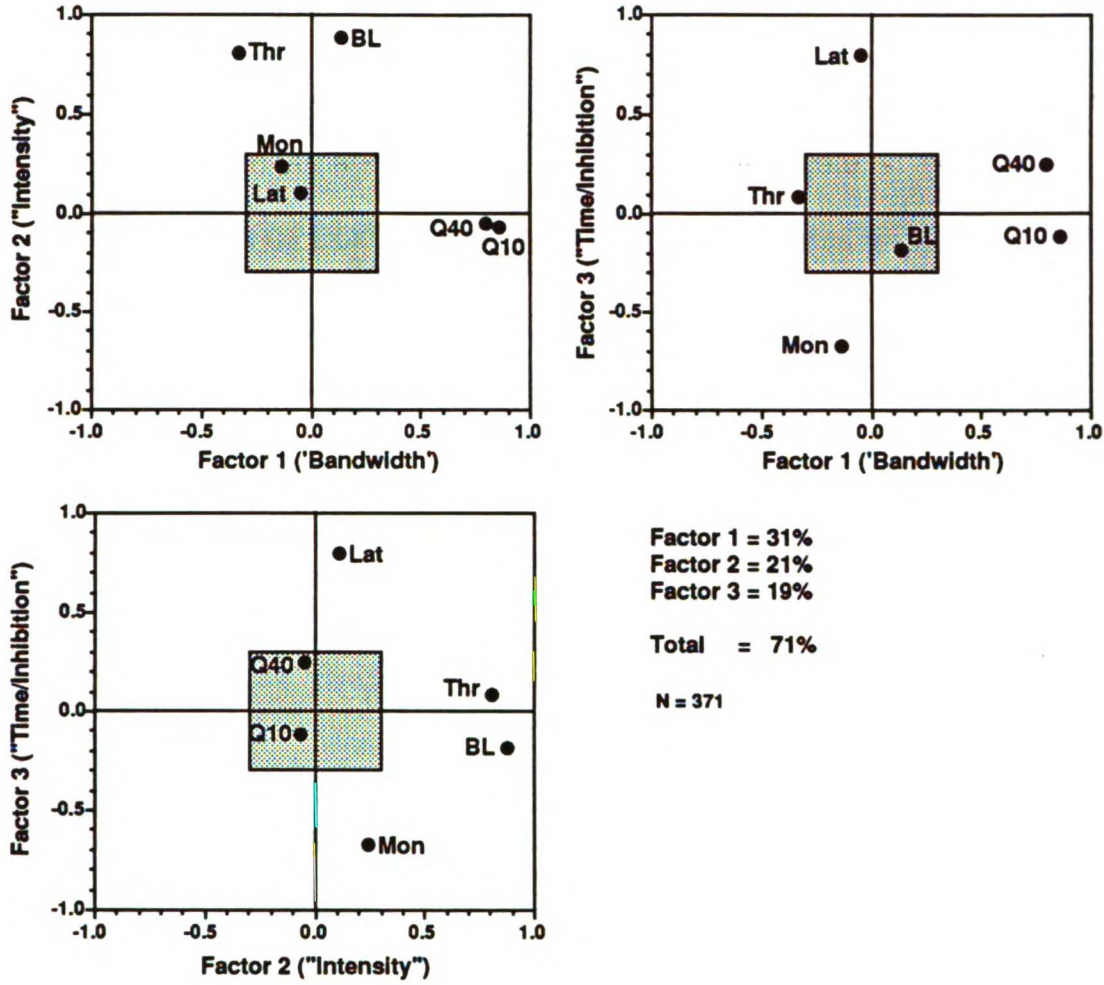
**Figure 47. Principal component analysis for acoustic parameters including threshold, best level, Q40, Q10, latency, and non-monotonicity. The contribution of each parameter to the emerging independent factors (see Table 13A) is plotted for the three main factors. The three factors explain 71% of the variance in the data. Only contributions larger than 0.3 (shaded box in center of each diagram) are given in Table 13A.**

01  
P  
1  
2  
3  
4  
5  
6  
7  
8  
9  
10  
11  
12  
13  
14  
15  
16  
17  
18  
19  
20  
21  
22  
23  
24  
25  
26  
27  
28  
29  
30  
31  
32  
33  
34  
35  
36  
37  
38  
39  
40  
41  
42  
43  
44  
45  
46  
47  
48  
49  
50  
51  
52  
53  
54  
55  
56  
57  
58  
59  
60  
61  
62  
63  
64  
65  
66  
67  
68  
69  
70  
71  
72  
73  
74  
75  
76  
77  
78  
79  
80  
81  
82  
83  
84  
85  
86  
87  
88  
89  
90  
91  
92  
93  
94  
95  
96  
97  
98  
99  
100

1  
2  
3  
4  
5  
6  
7  
8  
9  
10  
11  
12  
13  
14  
15  
16  
17  
18  
19  
20  
21  
22  
23  
24  
25  
26  
27  
28  
29  
30  
31  
32  
33  
34  
35  
36  
37  
38  
39  
40  
41  
42  
43  
44  
45  
46  
47  
48  
49  
50  
51  
52  
53  
54  
55  
56  
57  
58  
59  
60  
61  
62  
63  
64  
65  
66  
67  
68  
69  
70  
71  
72  
73  
74  
75  
76  
77  
78  
79  
80  
81  
82  
83  
84  
85  
86  
87  
88  
89  
90  
91  
92  
93  
94  
95  
96  
97  
98  
99  
100

FIGURE 47

Principal Component Analysis: Acoustic Parameters



1  
2  
3  
4  
5  
6  
7  
8  
9  
10  
11  
12  
13  
14  
15  
16  
17  
18  
19  
20  
21  
22  
23  
24  
25  
26  
27  
28  
29  
30  
31  
32  
33  
34  
35  
36  
37  
38  
39  
40  
41  
42  
43  
44  
45  
46  
47  
48  
49  
50  
51  
52  
53  
54  
55  
56  
57  
58  
59  
60  
61  
62  
63  
64  
65  
66  
67  
68  
69  
70  
71  
72  
73  
74  
75  
76  
77  
78  
79  
80  
81  
82  
83  
84  
85  
86  
87  
88  
89  
90  
91  
92  
93  
94  
95  
96  
97  
98  
99  
100

100

100

IB

**Table 14A.****FACTOR ANALYSIS OF ALL ELECTRICAL THRESHOLDS BY PAIR**

Pair	F1	F2	$\Sigma = 81\%$
1,2	0.84		N = 321
3,4	0.92		
5,6	0.74	0.41	
7,8		0.97	
1,7-8	0.80	0.30	

**Table 14B.****CORRELATION OF ELECTRICAL FACTORS AND NORMALIZED ACOUSTIC PARAMETER VALUES**

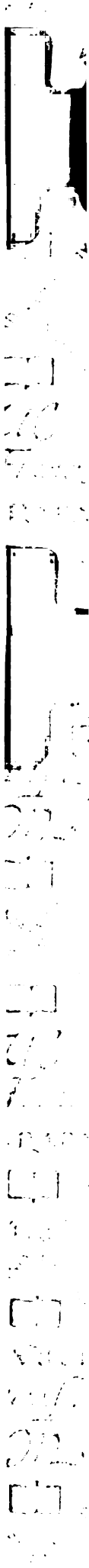
	F1(EL)	F2(EL)
Threshold	-0.25***	
Best Level	-0.41***	
Q10		
Q40		
Latency	0.12	0.16*
Monotonicity		
Binaural		0.14

**Table 14C.****FACTOR ANALYSIS OF NORMALIZED ACOUSTIC PARAMETERS AND ELECTRICAL FACTOR ONE**

	F1	F2	F3	$\Sigma = 58\%$
Threshold	0.65	-0.49		N = 321
Best Level	0.85			
Q10		0.84		
Q40		0.76		
Latency			0.76	
Monotonicity			-0.57	
Binaural	0.52			
F1Electrical	-0.59		0.41	



**Figure 48. Principal component analysis for the corrected threshold values for four radial electrode pairs and one longitudinal electrode pair. Two main factors emerge (Table 14A) that explain 81% of the variance in the electrical threshold data.**

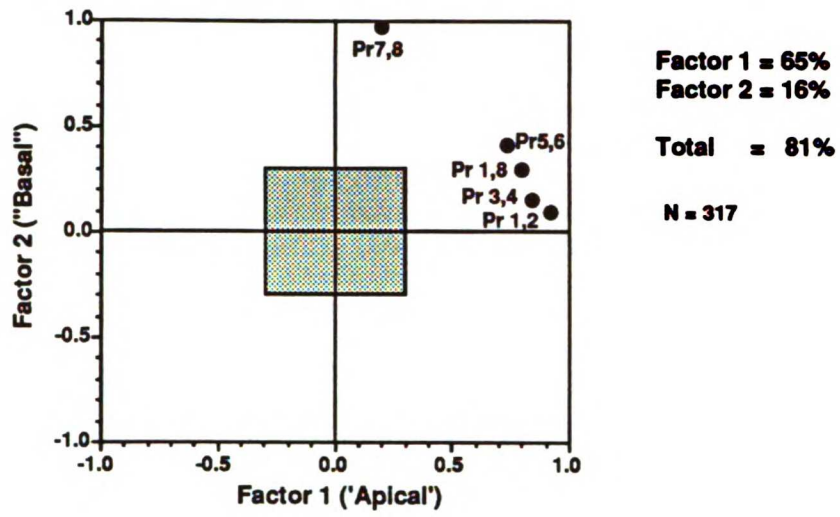


13

13

FIGURE 48

Principial Component Analysis: Electrical Parameters





normalized acoustic parameter values can be seen in Table 14B. It is apparent that threshold and best level show significant negative correlations with electrical Factor 1, and that latency and binaural interaction fall under electrical Factor 2. Latency also appears to have some small relationship with electrical Factor 1.

The main result of all of these analyses is that there is a close correspondence between acoustic intensity data and electrical threshold data obtained at (nearly) the same cortical locations. This relationship is most clearly revealed by comparing the spatial distribution of the two factors most closely aligned with these parameters in a combined plot for all animals. Figure 49 shows a color representation of the distribution of Factor 2 for acoustically-evoked responses, the 'Intensity Factor', and Factor 1 of the electrical threshold data, the 'Apical Factor', across AI and pooled for all animals. The different maps were combined by first calculating the spatial CF gradient for each case and adjusting the resulting slope to the average of all slopes. This provides proper alignment of the rostro-caudal dimensions of AI. The dorso-ventral dimension was aligned by assigning the most prominent dorso-ventral distribution feature, a central area of lowest acoustic threshold, the same constant position in all cases. As can be seen, areas of high electrical threshold (high yellow-red concentration) were found along a caudal-rostral stripe across the dorso-ventral center of AI. This area was surrounded ventrally and dorsally by areas of low electrical thresholds (blue). Conversely, to the right, a blue area of low acoustic threshold was found in the center of AI surrounded by areas of yellow-red or high acoustic threshold.

A final principal component analysis essentially summarizes the above data for five of the six cases. Here the binaural interaction data was

1  
2  
3  
4  
5  
6  
7  
8  
9  
10  
11  
12  
13  
14  
15  
16  
17  
18  
19  
20  
21  
22  
23  
24  
25  
26  
27  
28  
29  
30  
31  
32  
33  
34  
35  
36  
37  
38  
39  
40  
41  
42  
43  
44  
45  
46  
47  
48  
49  
50  
51  
52  
53  
54  
55  
56  
57  
58  
59  
60  
61  
62  
63  
64  
65  
66  
67  
68  
69  
70  
71  
72  
73  
74  
75  
76  
77  
78  
79  
80  
81  
82  
83  
84  
85  
86  
87  
88  
89  
90  
91  
92  
93  
94  
95  
96  
97  
98  
99  
100

100

100

**Figure 49. Spatial distribution of stimulus intensity factors in primary auditory cortex (AI). The spatial distribution for electrical threshold (Factor 1) is shown in the left color panel and the spatial distribution for the acoustic Intensity Factor (Factor 1) is shown in the right color panel. Contour lines of the electrical factor are superimposed on both plots to ease comparison of the two distributions. The AI area mapped is depicted in the lower left schematic drawing. A color gradient scale is shown in the lower right.**



IB

SECRET

SECRET

SECRET

SECRET

SECRET

SECRET

SECRET

IB

SECRET

SECRET

SECRET

SECRET

SECRET

SECRET

SECRET

SECRET

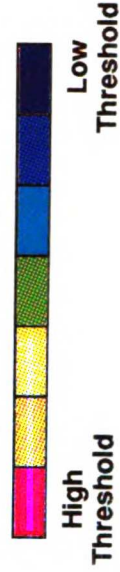
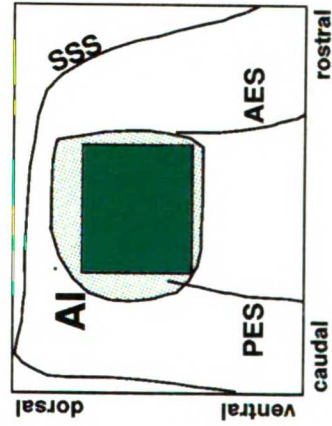
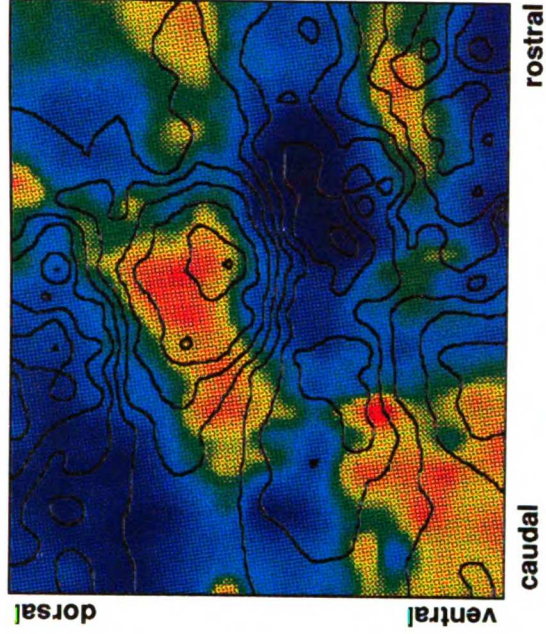
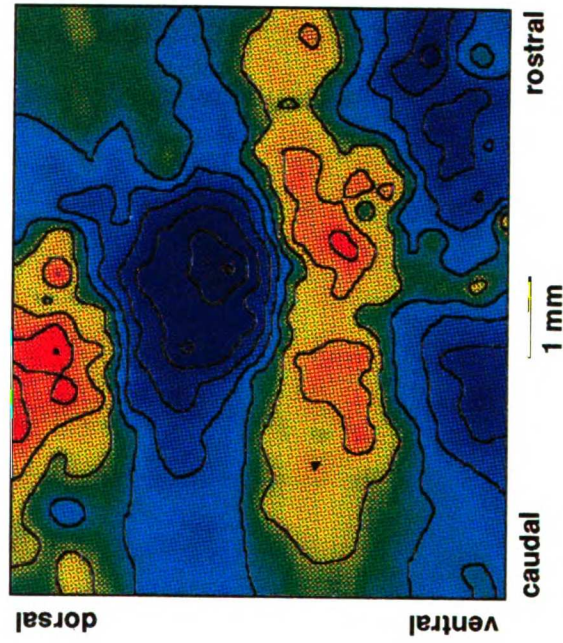
SECRET

**FIGURE 49**

**Spatial Distribution of Stimulus Intensity Factors in Primary Auditory Cortex**

Electrical Threshold (Factor 1 electr.)

Acoustical Threshold (Factor 1 acoust.)





included, thus eliminating case C115 from consideration. Most importantly, the main electrical factor (the 'Apical Factor') was also included. That is, a factor analysis involving essentially all response aspects, acoustic and electrical, was obtained. Three main global factors emerged that can account for both acoustically and electrically evoked response distributions as can be seen in Table 14C and graphically in Figure 50. These three factors account for 57% of the variance in the data, which is clearly less than for the acoustic or electrical data alone, possibly because the inclusion of binaural and electrical data increases the variance of the data considerably. Acoustic threshold, best level, binaural interaction, and Electrical Factor 1 (Apical Factor) appear under Global Factor 1. As might be expected from early data analysis, the Apical Factor has a negative relationship to this factor. Q10dB and Q40dB appear under Global Factor 2 along with a small negative relationship between this factor and acoustic threshold. Latency and monotonicity appear under Factor 3 with monotonicity having a negative relationship to this factor. The Apical Factor also shows a relatively small positive relationship to Factor 3.

#### **3.4.4 Summary**

The above data show a clearly demonstrable relationship between the behavior and distributions of responses to acoustic versus electrical cochlear stimulation. A comparison of the response distributions for these two stimulus modes reveal organizational constructs across AI that are consistent, non-uniform, and correlated. Specifically, an area in the center of AI running orthogonal to the isofrequency gradient responds with lowest acoustic thresholds, but with highest electrical thresholds. This same centralized area of high electrical threshold also shows, to greater



**Figure 50. Combined principal component analysis for acoustic parameters and electrical Factor 1. The contribution of each parameter to the emerging independent factors (see Table 14C) is plotted for the three main factors. The three factors explain 57% of the variance in the data. Only contributions larger than 0.3 (shaded box in center of each diagram) are given in Table 14C.**

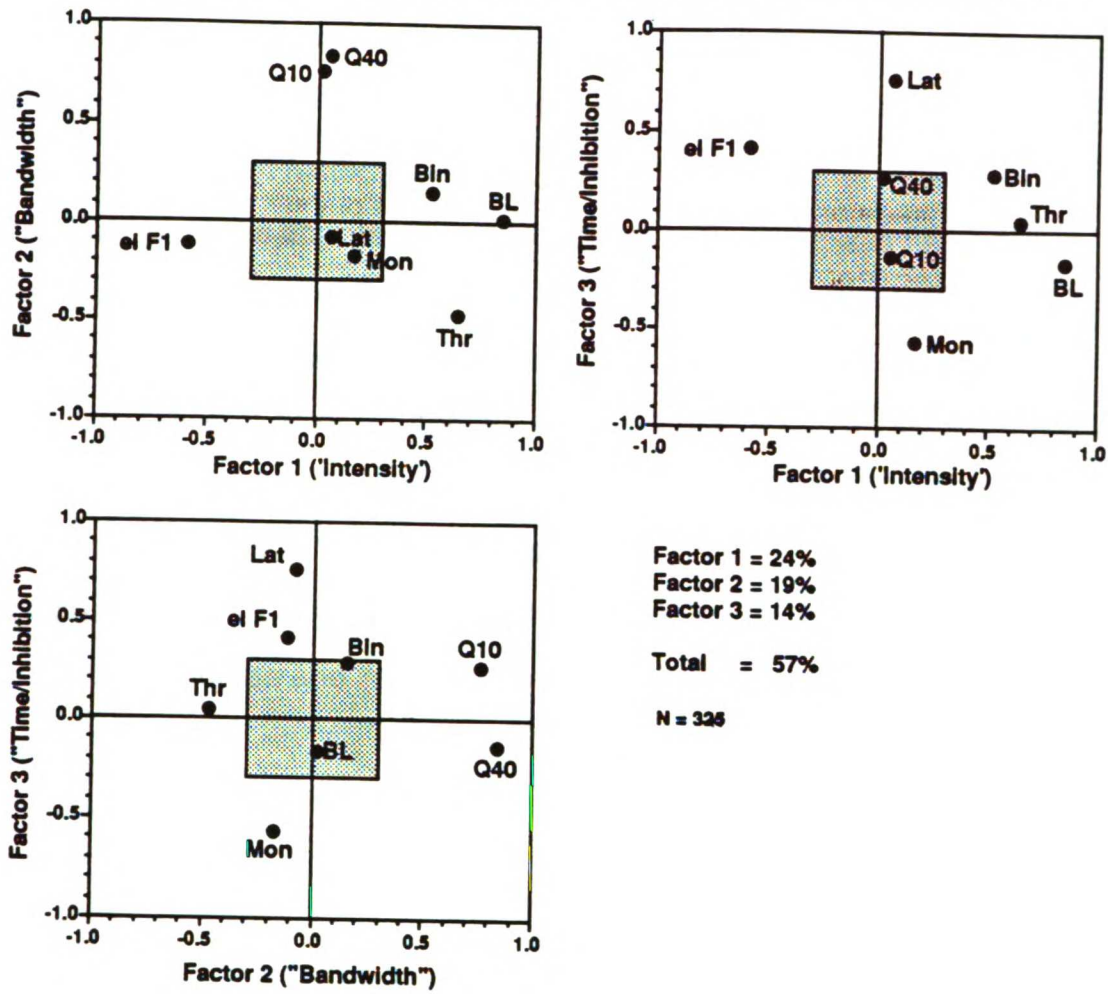
1  
2  
3  
4  
5  
6  
7  
8  
9  
10  
11  
12  
13  
14  
15  
16  
17  
18  
19  
20  
21  
22  
23  
24  
25  
26  
27  
28  
29  
30  
31  
32  
33  
34  
35  
36  
37  
38  
39  
40  
41  
42  
43  
44  
45  
46  
47  
48  
49  
50  
51  
52  
53  
54  
55  
56  
57  
58  
59  
60  
61  
62  
63  
64  
65  
66  
67  
68  
69  
70  
71  
72  
73  
74  
75  
76  
77  
78  
79  
80  
81  
82  
83  
84  
85  
86  
87  
88  
89  
90  
91  
92  
93  
94  
95  
96  
97  
98  
99  
100

100

100

FIGURE 50

Principal Component Analysis: Acoustic Parameters & Electrical Factor 1



13

1

1

1

1

1

1

UNIVERSITY OF CALIFORNIA

and lesser degrees, low best level, sharp tuning, short latencies, high non-monotonicity, and EI binaural interaction.

Principal component analyses suggest that there are three, relatively independent factors underlying the expression of the acoustic parametric data and the primary electrical factor. Of importance in this finding is that the primary electrical factor does not seem to be explained by yet a fourth independent factor, but rather, is found negatively expressed under the same factor as acoustic threshold and best level. Due to the primary elements that fall under Factor 1, i.e. threshold, best level, F1 Electrical threshold, it would seem that this factor bears some relationship to intensity coding. Factor 2's primary elements are Q10 and Q40dB, which suggest that Factor 2 is involved in tuning bandwidth properties. The elements of Factor 3, latency and monotonicity, do not appear to share obvious common physiological characteristics and may reflect additional temporal properties and inhibitory contributions.

100

100

#### **4. DISCUSSION**

With some exceptions, postlingually deafened cochlear implant patients do not understand auditorily-represented speech immediately after implantation. However, after a period of weeks, months or even years, many of these patients develop at least some open speech understanding (Schindler, et al., 1987; Schindler and Kessler, 1989; Spivak and Waltzman, 1990). The present studies represent preliminary steps in providing a physiological explanation for how the auditory central nervous system, and its capacity for plasticity, might initially represent implant-encoded speech, and how it might accomplish this conversion of initially distorted perceptions into meaningful stimuli. This goal was approached by the evaluation of the efficacy of a multi-electrode, pulsatile electrical stimulation scheme in driving primary auditory cortical neurons.

Although the representation of electrical stimuli applied to the cochlea has been studied by use of electrophysiological methods in some detail in the auditory nerve (Kiang and Moxon, 1972; Hartmann, et al., 1984, 1989; van den Honert and Stypulkowski, 1987a,b; Parkins, 1989; Javel, et al., 1987; Javel, 1989), cochlear nucleus (Glass, 1983; Clopton and Glass, 1984), and auditory midbrain (Merzenich and Reid, 1974; Merzenich and White, 1977; Snyder, et al., 1990,1991), the representations of cochlear stimulation in the auditory cortex have been studied only using methods that do not provide high spatial resolution, e.g. by positron emission tomography (Herzog, et al., 1991; LeScao, et al., 1992) or by use of evoked potentials (Woolsey and Walzl, 1942; Hari, et al., 1988; Hoke, et al., 1989). Relatively little is known about the representation of electrically evoked inputs referenced to the normal sound coding representations of the auditory cortex. Initial goals, then, were 1) to establish how cochlear



electrical stimulation is represented in the primary auditory cortex, and 2) to relate that representation of electrically-evoked inputs to that of sound inputs, i.e. to the normal auditory representations within AI. To comprehensively evaluate these central electrical/sound representational parallels and distinctions, it is necessary to investigate a large number of physiological response parameters. Given the great idiosyncratic variability in the representation of acoustic stimuli in normal adult cats, it was important that physiological responses to both electrical and acoustic stimuli be obtained in the same experimental animals, with responses sampled at the same or nearly the same recording locations. By this strategy, known representational boundaries and distributions for acoustic stimuli can be used as topographical landmarks for assessing electrically-evoked neuronal response distributions, as well as provide direct stimulus-mode comparisons.

For the following discussion of the stimulus intensity response behavior of cortical neurons, it is useful to keep in mind the characteristics of the three compared stimulation conditions applied in this study. First, for acoustic stimulation, stimuli were brief, band-limited clicks. The temporal character of this stimulus is similar to that of pulsatile electrical stimulation. The acoustic stimulus was a broad-band stimulus that excited a significant, extended, but spectrally limited zone of the Organ of Corti. Second, the longitudinal electrode pair condition resembled the acoustic broad-band characteristics in the sense that it also generated excitation from along the cochlear partition over a zone nearly a centimeter in length. In contrast, the third, radial electrode stimulation condition might be considered to generate distributed inputs more like those generated in an acoustic narrow-band condition, e.g. resembling stimulation with a pure tone.



## **4.1 Experimental Series One: Neuronal Response Properties**

### **4.1.1 Rate/Level Functions**

The recording of neuronal responses to stimuli of increasing intensity spanning an operational dynamic range is a common physiological response measurement strategy for acoustic stimulation that provides a characterization of one dimension of the 'receptive field' of a neuron (e.g. Brugge and Merzenich, 1973; Suga, 1977; Phillips and Hall, 1986; Phillips, 1988). The second main dimension of auditory receptive fields, the representation of the receptor surface or frequency axis, is more difficult to characterize in detail with electrical stimulation since the cochlear electrode allows access to only a limited number of cochlear positions. Stimulus intensity response relationships were studied in detail for peripheral electrical stimulation, using the two electrode configurations noted above. For comparative purposes, responses to acoustic stimulation were also obtained. Note that single and multiple unit data were combined in the Results section, since for most parameters there was no statistically significant difference between the two data sets. On the average, however, multiple units had lower thresholds and shorter latencies, presumably because multiple unit responses include those units at any given recording site with the lowest thresholds and the shortest latencies. Since approximately 80% of recordings were made from single units and because most response parameters did not show differences between the single and multiple unit samples, both will be discussed together.

Rate/level functions with significantly differing thresholds, growth functions, and dynamic ranges across stimulus conditions were recorded in



this AI sample. Linear regression analyses revealed that threshold and transition point, as well as 1/dynamic range and the slopes of the low level segment of intensity-response functions were highly correlated for all stimulus conditions. Another confirmed correlation was between dynamic range and transition point for all conditions, i.e. the higher the transition point, the greater the dynamic range.

An important finding was that some response characteristics for stimulation with the radial versus the longitudinal electrode pairs were highly correlated, especially a) response threshold, b) transition point levels, c) firing rates at the transition point, and d) to a weaker extent, dynamic ranges. These high correlations between presumably narrow-band (radial electrode) and broad-band (longitudinal electrode) electrical conditions are surprising because systematic differences between responses evoked with acoustic stimulation using narrow-band and broad-band stimuli for these response parameters are found (e.g. Phillips, 1988; Phillips and Hall, 1987; Schreiner and Mendelson, 1990). More in line with the distinction of the narrow-band versus broad-band character of the radial versus longitudinal stimulation was the finding that the longitudinal pair stimulation and acoustic stimulation were also correlated for threshold and transition point, while the responses from the radial pair stimulation were uncorrelated with those of acoustic stimulation.

Due to the difference in the two intensity scales for the acoustic and electrical stimulating conditions (current versus sound pressure), parametric responses involving intensity issues cannot be directly compared. A conversion factor would be useful that would align the electrical intensity scale with the acoustic intensity scale. One strategy

1950

for scale adjustment is to determine the correction factor required to align the slopes of the low level segments of rate/level functions for acoustic and electrical 'broad-band' stimulation. Comparison of the average slopes of the LLS indicates a conversion factor of approximately 2.5, i.e. the electrical level scale has to be expanded or the acoustic scale compressed by that factor to align the two intensity scales. Based on a comparison of psychophysical data for electrical and acoustic stimulation, Zeng and Shannon (1992) has proposed that psychophysical functions on a linear scale for electrical stimulation magnitude closely match acoustic data plotted on a logarithmic magnitude scale. Comparison of the overall shape of rate/level functions plotted on linear and logarithmic scales in the present data revealed only minor differences. However, numerical comparisons across linear (absolute) scales and logarithmic (relative) scales is difficult. In any event, the proposed conversion between electrical and acoustic logarithmic scales by multiplication or division by 2.5 provides a straightforward way of comparing electrophysiological and psychophysical data obtained for the two stimulation conditions.

With this tentative alignment of the two intensity scales, other response characteristics obtained for acoustic and electrical conditions can be more directly compared, including the widths of spatial tuning curves and the slopes of the high level segments of rate and latency level functions. The slope of the high level segment was typically a negative value for longitudinal electrical stimulation and typically a positive value for acoustic stimulation and radial electrical stimulation. Therefore, 'broad-band' electrical stimulation resulted in a markedly larger proportion of non-monotonic rate/level functions than did acoustic stimulation or 'narrow-band' electrical stimulation. This discrepancy in the high level behavior became even more pronounced if the conversion of



the intensity scales was taken into account. Whereas the average unconverted HLS slope for the radial pair was 0.88 %/dB, and -0.27 %/dB for the longitudinal pair, the converted HLS slope for acoustic rate/level functions was 2.1 %/dB. The clear difference in the growth behavior of the high level segment suggests that the relative contributions from excitatory and inhibitory mechanisms invoked by electrical and acoustic stimulation that determine the firing behavior of cortical neurons are different. At this stage of the argument, it can only be speculated that this difference may result from differences in spread of excitation along the basilar membrane or are due to temporal differences in the stimuli, e.g. to the stronger temporal coherence for electrical stimulation.

Although the spatial distribution of responses to electrical stimulation is discussed in detail later, it should be mentioned here that the dorso-ventral center of AI responded only poorly if at all to electrical stimulation. In the current sample of single and multiple unit responses from AI, the center of AI was strongly underrepresented because the selection criterion was based on electrical responses with a wide enough dynamic range to reconstruct complete rate/level functions, i.e. encompassing current values of a range of at least 10-15 dB. Since the center of AI had a number of physiological properties for acoustic stimulation that were distinctly different from more dorsal and ventral portions of AI (see below) the range of acoustic response properties in this sample was not representative for all of AI.

It is clear that while there are differences in some aspects of rate/level functions across stimulus conditions, the functions for both electrical and acoustic stimulation show considerable similarity. Differences observed between properties of rate/level function for the

1  
2  
3  
4  
5  
6  
7  
8  
9  
10  
11  
12  
13  
14  
15  
16  
17  
18  
19  
20  
21  
22  
23  
24  
25  
26  
27  
28  
29  
30  
31  
32  
33  
34  
35  
36  
37  
38  
39  
40  
41  
42  
43  
44  
45  
46  
47  
48  
49  
50  
51  
52  
53  
54  
55  
56  
57  
58  
59  
60  
61  
62  
63  
64  
65  
66  
67  
68  
69  
70  
71  
72  
73  
74  
75  
76  
77  
78  
79  
80  
81  
82  
83  
84  
85  
86  
87  
88  
89  
90  
91  
92  
93  
94  
95  
96  
97  
98  
99  
100

FOR LEADERS

1000  
1000

1000

three conditions did not appear to strictly follow the distinction of broad-versus narrow-band stimulation pattern. In addition, the salient measurement features that appear to comprehensively describe rate/level functions for all conditions appear to be threshold, transition point, and the slopes of the low and high level segments.

#### 4.1.2 Latency/Level Functions

Historically, assessments of the latency characteristics of primary auditory cortical neurons have been few or limited in scope (Oonishi and Katsuki, 1965; Phillips and Irvine, 1981; Phillips 1988; Sutter and Schreiner, 1991). Although changes in response latency with level or other stimulus conditions have been described (e.g. Phillips and Cynader, 1985; Phillips, 1988; Phillips, et al., 1989), most studies use only a single parameter for characterizing temporal response properties. Therefore, in order to more completely characterize response latency behavior, several descriptive parameters of latency/level functions were used and compared across stimulus conditions in the present study.

Fundamentally, as in the case of firing rate, response latency was affected by changes in stimulus intensity, i.e. latency decreased with an increase in intensity. Near response threshold, the resulting function showed a precipitous drop in latency with increasing stimulus levels (slope of the low level segment or LLS), which typically flattened out to a shallow latency function for higher stimulus levels (slope of the high level segment or HLS). Therefore, due to the tangential relationship of these two slopes, there was generally a clear transition point at their juncture. The slope of the LLS was between 7 (acoustic condition) to 13 times (longitudinal electrical condition) steeper than the slope of the HLS.

1901  
1902  
1903  
1904  
1905  
1906  
1907  
1908  
1909  
1910  
1911  
1912  
1913  
1914  
1915  
1916  
1917  
1918  
1919  
1920  
1921  
1922  
1923  
1924  
1925  
1926  
1927  
1928  
1929  
1930  
1931  
1932  
1933  
1934  
1935  
1936  
1937  
1938  
1939  
1940  
1941  
1942  
1943  
1944  
1945  
1946  
1947  
1948  
1949  
1950  
1951  
1952  
1953  
1954  
1955  
1956  
1957  
1958  
1959  
1960  
1961  
1962  
1963  
1964  
1965  
1966  
1967  
1968  
1969  
1970  
1971  
1972  
1973  
1974  
1975  
1976  
1977  
1978  
1979  
1980  
1981  
1982  
1983  
1984  
1985  
1986  
1987  
1988  
1989  
1990  
1991  
1992  
1993  
1994  
1995  
1996  
1997  
1998  
1999  
2000  
2001  
2002  
2003  
2004  
2005  
2006  
2007  
2008  
2009  
2010  
2011  
2012  
2013  
2014  
2015  
2016  
2017  
2018  
2019  
2020  
2021  
2022  
2023  
2024  
2025  
2026  
2027  
2028  
2029  
2030  
2031  
2032  
2033  
2034  
2035  
2036  
2037  
2038  
2039  
2040  
2041  
2042  
2043  
2044  
2045  
2046  
2047  
2048  
2049  
2050  
2051  
2052  
2053  
2054  
2055  
2056  
2057  
2058  
2059  
2060  
2061  
2062  
2063  
2064  
2065  
2066  
2067  
2068  
2069  
2070  
2071  
2072  
2073  
2074  
2075  
2076  
2077  
2078  
2079  
2080  
2081  
2082  
2083  
2084  
2085  
2086  
2087  
2088  
2089  
2090  
2091  
2092  
2093  
2094  
2095  
2096  
2097  
2098  
2099  
2100

Estimates of these parameters from published latency/level functions for tones with sharp onsets compare favorably, whereas tones with shallow onset slopes give rise to smaller differences between the slopes for the LLS and the HLS (Phillips, 1988).

Minimum latencies, a commonly used latency descriptor, were approximately 11ms for either electrical stimulation condition and 12.5ms for acoustic stimulation. The average latency difference of approximately 1.5ms between electrical and acoustic conditions can be accounted for by the travel time of the sound from the speaker to the oval window (0.3ms), and the travel time along the basal portion of the basilar membrane of approximately 1.3ms, delays that are circumvented by electrical stimulation. The minimum latency values for acoustic stimulation are similar or slightly shorter than those found in previous studies of AI with tone bursts (Phillips and Irvine, 1981). In a comparison of neurons with monotonic and non-monotonic rate/level functions for tone stimulation, Phillips and colleagues (1985) demonstrated mean response latencies for monotonic neurons of 14 ms and for non-monotonic neurons of 19.1 ms. Oonishi and Katsuki (1965) and Eggermont (1991) also showed a slightly larger range of onset latencies (10 to 28 ms) in AI with click stimuli. The reason for the slightly shorter mean response latencies in this study may be due to the inclusion of some multiple unit responses that showed statistically significant shorter latencies than those for single neurons (see Results).

Latency/level functions show significant parametric differences across conditions. Small but significant differences were observed between the two electrical conditions, with notably larger differences noted between the two electrical conditions versus the acoustic condition

1000

for some parameters, i.e. transition point latency, average latency of the high level segment. While minimum latency was somewhat longer for acoustic stimulation, the difference in latency between acoustic and electrical stimulation at the transition point was nearly twice that of either electrical stimulation configuration. This significantly shorter transition point latency for electrical stimulation may result from higher temporal coherence of this stimulation mode, and/or from greater inhibitory influences operating during electrical stimulation.

The average latency of the relatively flat high level segment was calculated to obtain a statistically more reliable evaluation. In contrast, minimum latency and latency at transition point were single point measurements that are more vulnerable to fluctuations of the noise floor. The average HLS latency values were between those for minimum latency and transition point latency. A significant difference was observed in the rate of change of the low level segment and the high level segment between the two electrical conditions. The slopes for longitudinal electrical stimulation were shallower than those for radial electrical stimulation. Since the temporal characteristics of the stimulus were the same for both electrical conditions, an explanation of this discrepancy has to take into account the larger population of coherently activated neuronal elements for longitudinal stimulation. If the intensity scale of the acoustic stimulus is aligned with that of the electrical stimulation (see above), the slopes of the acoustic latency/level functions can be compared. With that correction, they were quite similar to those for the radial electrode pair. This closer correspondence of 'broad-band' acoustic stimulation results with 'narrow-band' electrical stimulation results than with 'broad-band' electrical behavior is consistent with the response parallels for non-monotonicity of rate/level functions (see above).

1951

An additional finding that tied together rate and latency behavior was the corresponding location of the transition point between the two segments of rate/level functions and latency/level functions, which were, on the average, within 1 dB. That suggests that intensity-related changes in rate and latency share common, underlying mechanisms regardless of the type of stimulation. It also supports the notion that the transition point is an important anchor point for the description of the response behavior of cortical neurons as a function of stimulus intensity.

Linear regression analyses showed high correlations for all conditions between latency/level parameters, including a) minimum latency, b) latency at the transition point, and c) the average latency of the high level segment. Consequently, only one of these measures is needed to adequately describe a neuron's behavior. Traditionally, the minimum latency has been the parameter of choice. Since the latency at the transition point in conjunction with the slopes of the two adjoining segments allows a nearly complete reconstruction of the latency behavior as a function of intensity, this measure is appropriate for an abbreviated characterization of the response behavior of a cortical neuron.

Just as for rate/level functions, there are some parametric differences between the electrical and acoustic stimulating conditions, but generally, the shapes of latency/level functions are quite similar with long latencies at low stimulus levels dropping to shorter latencies for high stimulus levels. Differences observed between properties of latency/level function for the three conditions do not appear to strictly follow the distinction of broad- versus narrow-band stimulation pattern. It is concluded that the features that adequately describe latency/level functions for all stimulus conditions are latency at transition point and the slope of the high and low

1001 LINDEN

level segments which clearly reflect, by their dissimilar behavior for all conditions, differences in the relative influence of excitatory and inhibitory mechanisms.

#### 4.1.3 Temporal Repetition Coding: Modulation Transfer Functions

The capacity of cortical neurons to follow repetitive signal presentations is an important aspect of cortical responses that has consequences for the encoding of complex signals. An understanding of this temporal coding behavior in the cortex may enhance the development of optimal stimulation strategies for cochlear prostheses. Studies using different acoustic signals ranging from clicks to repeated tone bursts and sinusoidally amplitude modulated tones and noises has revealed that the ability of most primary auditory cortical neurons to respond to repeated signals is limited to repetition rates below 20 Hz (Schreiner and Urbas, 1988; Phillips, et al., 1989; Eggermont, 1991, 1992). Only one study has reported considerably higher event-locking in AI with limiting repetition rates of 100 to 200 Hz (de Ribaupierre et al., 1972), however, those results were obtained from a special group of small cells (thin-spike neurons) in layer IV in awake animals. Apparently, this group of neurons has either not been sampled in the other studies or was silenced by the use of anesthesia.

A large number of temporal repetition coding features have been evaluated both electrically and acoustically. It is in this domain that a clear departure appears to exist between the behavior of cortical neurons using electrical and acoustic stimulation. In terms of response strength, temporal precision, and frequency-following capacity, it appears that electrical stimulation results in slightly superior repetition coding

1001 EDWIN

behavior relative to acoustic stimulation (see for example Figure 14 and Table 5). A further comparative analysis between stimulus conditions shows a larger number of neurons with bandpass temporal modulation transfer functions (tMTFs) for the two electrical conditions than for the acoustic stimulus condition, which tended to produce more low pass tMTFs. These results for acoustic stimulation are supported by an AI study by Phillips and colleagues (1989) using tone pulse stimuli, in which it was observed that regardless of tone level, all response rates displayed a low pass characteristic (1-4Hz). Further, the mean maximum firing rate at BMF was considerably lower for the acoustic condition, although all conditions showed a mean best modulation frequency (BMF) of approximately 6.5-7.8 Hz. The rate at -6dB for the high-frequency side of the tMTF distribution was 1.3 to 2.6 Hz higher for the electrical stimulus modes over that of the acoustic stimulus mode. A compilation of this data supports the notion that electrical stimulation leads to stronger and more precise temporal repetition coding relative to acoustic stimulation, resulting in slightly higher following rates. This may not be surprising considering that electrical stimulation using pulsed stimuli is a more temporally and spatially coherent stimulus in comparison to the acoustically induced temporal-spatial pattern that, due to the traveling wave and local resonances, shows distinct differences in the temporal behavior along the engaged part of the basilar membrane. The range of best modulation frequencies and limiting rates at 50% of maximum of the tMTFs is in close agreement with the values obtained for click stimulation of 7.9 Hz (BMF) and 12 Hz (-6dB), respectively, (Eggermont, 1991). However, the frequency steps in that study were too large (1, 2, 4, 8, 16, 32Hz) to allow a more thorough comparison. BMF values for acoustic sinusoidal amplitude modulation showed somewhat higher values (approximately 16 Hz; Schreiner and Urbas, 1988) than seen for click stimulation in this study or

1001 LINDEN

in a similar study by Eggermont (1991). An explanation for this discrepancy may have to do with the difference in signal bandwidth, resulting in less inhibition for the AM signal (see below) sampled mostly in central AI, and a potential sampling bias for dorsal and ventral portions of AI in the click study which respond better to broad-band signals.

An additional measure of temporal repetition coding, response "entrainment", measures the number of spikes per stimulus pulse. Entrainment functions are typically lowpass for all stimulus conditions in the present study, a finding also noted in AI for tone pulse stimuli (Phillips, et al., 1989) and clicks (Eggermont, 1991). Entrainment values varied across conditions, however, the mean number of spikes that resulted from one stimulus pulse is one for all stimulus conditions. This finding is corroborated by Phillips and colleagues (1989) as well as Eggermont (1991) for low repetition rates. Since the maximum entrainment frequency and low pass characteristics are similar across conditions, it may be that cortical neurons experience relatively long accommodation periods that disallow entrainment at higher repetition rate for any stimulus mode. In spite of these stimulus mode similarities, a relatively large difference is seen between electrical and acoustic stimulation for pair-wise comparisons (Table 5, bottom) for the high frequency cut-off at an entrainment of 0.25spp. Electrical stimulation resulted in 2.8 to 3.3 Hz higher cut-off frequencies at an entrainment of 0.25spp. It may be that accommodation/inhibitory periods are relatively shorter for electrical stimulation, allowing for slightly higher cut-off frequencies. The reason for this difference, again, may be related to the balance of excitatory and inhibitory inputs, potentially influenced by the different spatial timing pattern along the cochlear partition (see below).

1937

Linear regression analyses show high positive correlations for all eight aspects of temporal repetition coding between both electrical stimulus conditions, and for nearly all aspects between the radial pair and acoustic conditions. These findings and the mean and pair-wise differences of the parameter distributions also appear to support the close relationship between 'narrow-band' electrical stimulation and acoustic stimulation seen for rate/level and latency/level functions. However, many features are also highly correlated between the electrical longitudinal pair ('broad-band') and the acoustic condition including BMF and firing rate at -6dB for the high level segment. These findings suggest that while both electrical conditions share common response properties with those for acoustic stimulation, there are significant apparent difference between some physiological aspects of rate/level, latency/level, and temporal repetition coding between acoustic stimulation and stimulation of the longitudinal electrode pair even though they may both be thought of as 'broad-band' stimulation. These differences appears to be smaller between acoustic and radial or 'narrow-band' electrical stimulation.

The parameters that most comprehensively describe temporal repetition coding appear to be BMF, firing rate at -6dB (H), maximum rate, maximum entrainment frequency, and entrainment at 0.25spp. In previous studies, the limiting rate of entrainment functions was arbitrarily set at an absolute entrainment value of 0.85spp or 85% (de Ribaupierre, et al., 1972; Phillips, et al., 1989). In this study, a new measure was introduced, a limiting rate or cut-off frequency at an entrainment value of 0.25spp or 25%. The reason for introducing this new parameter was twofold. First, the 85% entrainment value underestimated the capacity of a neuron to follow repeated signals since entrainments of 0.5spp or even 0.3spp are still clearly signaling significant amounts of event-locking in the

JOHN LEBMAN

response. Secondly, the cut-off frequencies of tMTFs (-6dB) and entrainment functions (0.85) are not directly comparable or even exchangeable. It was observed in this study that entrainment at the cut-off frequency of the tMTF was 0.25spp. Therefore, by using the 0.25spp criterion for the entrainment function, one gains a good estimate of the cut-off frequency of the tMTF as well (and vice versa).

#### 4.1.4 Intercorrelation of Rate, Latency, and Temporal Repetition Parameters

Cortical neuronal responses to acoustic and electrical stimulation can be described to a large extent by rate, latency, and temporal repetition parameters. A correlation analysis undertaken to evaluate the relationships between these parameters revealed some patterns of correlation between the parameters as well as between the stimulating conditions. Although the data do not allow a direct determination of what mechanisms are underlying these relationships, the results will be discussed with regard to indirect evidence regarding the balance of excitatory and inhibitory influences on cortical responses. This approach has been used with some success in the interpretation of response properties of auditory neurons in general (e.g. Suga, 1977,1988; Phillips, 1988; Schreiner and Mendelson, 1990; Sutter and Schreiner, 1991; Shamma et al. 1992) and, specifically, for the interpretation of the behavior of rate/level functions in cat auditory cortex (Phillips and Cynader, 1985; Phillips and Hall,1987; Phillips, 1988; Phillips, et al. 1985, 1989; Phillips and Sark, 1991; Schreiner et al. 1992). The main physiological aspects and assumptions underlying this interpretation are the following: a) the receptive fields of the vast majority of auditory cortical neurons are characterized by several components involving excitatory frequency

1001 LIBRARY

response areas and inhibitory sidebands; b) the extent, location, and strength of each of these components of the receptive field can be quite different from neuron to neuron, resulting in a wide range of possible input preferences; c) the firing rate and onset latency of a response are a result of the distribution of incoming excitation patterns across the receptive field components and shaped by the resulting proportion or balance of excitation and inhibition. The effects of the involvement of strong inhibitory influences on cortical neurons result, in general, in lower firing rates (Phillips, 1988; Schreiner and Mendelson, 1990), in non-monotonic rate/level functions (Phillips, et al., 1985; Phillips 1988), in longer onset latencies (Phillips et al., 1985), and in an earlier onset of inhibition (although usually still after some excitatory activity; Phillips and Sark, 1991); d) the strength of inhibition is usually correlated with the spread of excitation, due to the bandwidth and the intensity of the signal, which determines the degree of activation of the inhibitory sidebands. The facts and assumptions outlined above will be utilized to interpret some of the relationships between response parameters for electrical and acoustic stimulation.

For electrical stimulation conditions, response threshold and transition point level were positively correlated with all three measures of response latency ( $L_{min}$ ,  $L_{TP}$ ,  $L_{HLS}$ ), i.e. longer latencies were more often found for neurons with higher response thresholds (transition points) than for neurons with low thresholds. In addition, firing rate magnitudes appear to be negatively correlated with these latency measures as well as with response threshold. These three relationships can be interpreted as reflecting the strength of invoked inhibitory influences on the response. In particular, it appears that strong inhibitory influences invoked by electrical stimulation result in higher response thresholds, lower firing

1000 LINDEN

rates and longer latencies, while weaker inhibitory influences result in lower response thresholds, shorter latencies, and higher firing rates. The same relationships should be observable for the broad-band acoustic condition. However, the regression analysis only shows a correlation between firing rate and response latencies, but not with response threshold or transition point. Therefore, there appears to be a distinct difference in the influence of inhibition on threshold between electrical and acoustic stimulation. Whereas for electrical stimulation threshold is strongly influenced by inhibitory factors, this appears not to be the case for acoustic stimulation. While the reasons for this finding are not intuitively obvious, it bears some agreement with the observation of Schreiner and colleagues (1992), who found neurons in the center of AI responding to acoustic stimulation with non-monotonic rate/level functions that suggest strong inhibition in this portion of AI while, at the same time, expressing very low thresholds. Therefore, inhibition appears to play a lesser role in influencing acoustic threshold than electrical threshold.

Why do electrical and acoustic stimulus forms engage the central inhibitory mechanisms differently? One possible explanation lies in the timing of the inhibitory contributions in cortical response activity. It may be that the timing of the electrically induced activity plays a major role in the expression of excitation and inhibition. The virtually simultaneous excitation of a large number of peripheral neurons may contribute strongly to the central balance of excitation and inhibition. The high degree of synchrony in the peripheral excitation pattern likely results in a more effective and temporally more coherent transmission through the auditory pathways, and contributes to excitatory cortical activity with higher response rates and shorter latencies. In addition, the timing of the

1001 10011111

inhibitory components may be influenced by the higher rate/higher synchrony as well. Phillips and Sark (1991), using tone pulse stimuli in non-monotonic AI neurons, showed that increases in level resulted in differences in the timing of inhibitory influences. Effectively, increases in level were seen to produce PSTHs that showed a progressively greater reduction in firing rate. Interestingly, the reduction appeared first in the later portion of the onset response and then occurred progressively earlier in the response with progressively higher intensities. In other words, the more the inhibitory influence was invoked, the earlier the inhibition was effective. This behavior is borne out in highly non-monotonic neurons which show absolutely no response at high stimulus intensities, suggesting that inhibitory influences actually precede excitatory influences. This phenomenon appears to occur only when inhibition is most effectively engaged. For acoustic stimulation, this occurs only at high stimulus levels well above threshold, even for broad-band stimuli. Therefore, it may not influence the excitatory threshold itself. For electrical stimulation, however, it appears that only minimal levels of stimulation are needed to engage sufficiently strong inhibition that interferes early with excitatory inputs. Response thresholds are thereby directly influenced. In fact, many locations in certain sectors of AI do not respond to electrical stimulation at all, suggesting that the inhibition produced occurs early enough and with sufficient strength to override any excitatory responses. Other neurons express high thresholds, suggesting that inhibition had occurred early, but since excitatory response thresholds are achievable, it is clear that excitatory strength can exceed inhibitory strength. The majority of single neurons included in this study had relatively low thresholds for electrical stimulation, suggesting that the inhibitory components of their receptive fields were relatively weak. This is supported by the finding that the acoustic rate/level functions for

JOHN EDWARDS

these same neurons showed relatively little non-monotonic growth behavior.

Another potential effect of the earlier onset of inhibitory contributions for electrical stimulation may be the slight increase in BMF and limiting following rates for repetitive signals. It was shown that the limiting rates of tMTFs and entrainment functions were 1.3 to 2.6 Hz higher for electrical stimulation than for acoustic stimulation. An increase in secure synaptic transmission, due to the high synchrony in the response, resulted in an overall increase of entrainment and was, therefore, sufficient to explain the increase in the limiting frequency of the entrainment function when using a fixed criterion, e.g. 0.25 spp. However, this argument is not applicable to measures of limiting rate that use a relative criterion such as 50% of the firing rate. Instead, the duration and onset time of inhibition may help to explain the slightly higher following abilities that are seen even for the relative criteria (see Table 5). It has been shown that the duration of the inhibitory component is directly related to the period of the best modulation frequency of cortical neurons (Schreiner and Joris, 1986; Eggermont, 1992). Increased limiting following rates for electrical stimulation suggest that the end of the inhibitory period, often marked by a post-inhibitory rebound, occurs earlier. This earlier termination of the inhibitory period can either be accomplished by shortening the duration of the inhibition or, alternatively, by starting the inhibition slightly earlier. The latter was suggested to play a role in the correlation between response threshold and inhibitory influence for electrical stimulation (see above). Since the onset of inhibition in acoustic non-monotonic functions has been estimated to occur about 5 to 25ms past the excitatory onset (Phillips and Sark, 1991), the inhibitory period can be shifted forward in time by that amount. Consequently, the

1000 LITERS

increased following frequency for a unit with a limiting rate of 10 Hz (period: 100ms) for acoustic stimulation would be 10.5Hz ( $100 - 5 = 95\text{ms}$ ) to 13.3 Hz ( $100 - 25 = 75\text{ms}$ ) for electrical stimulation. This range corresponds very closely to the increase in following rate seen for electrical versus acoustic stimulation in this study.

Interestingly, the correlation analysis of temporal repetition parameters and latency parameters revealed a strong link between repetition following capacity and onset latency of cortical neurons. The higher the BMF or limiting rate is, the shorter the onset latency of the neuron (see Table 8). This relationship held for acoustic as well as electrical stimulation, however, it was more strongly expressed for the acoustic condition. A similar relationship between onset latency and BMF has been previously described for neurons in the central nucleus of the inferior colliculus (ICC) (Langner, et al., 1987; Langner and Schreiner, 1988; Schreiner and Langner, 1988). The significance of this relationship pertains to possible mechanisms that determine the frequency-following capacity of a central auditory neuron. Specifically, this relationship indicates that the mechanisms that are involved are based on temporal aspects, e.g. involving delay lines, as opposed to purely spectral mechanisms and are generally similar for the low following rates of cortical neurons (2-20Hz) and for the higher following rates in the ICC (20-200Hz, Rees and Møller, 1987; Langner and Schreiner, 1988). However, some differences in the underlying mechanisms must be present since the latency range seen in the inferior colliculus (5 to 20ms) is only slightly different from that seen in the auditory cortex (9 to 25ms), in contrast to the large differences in the following rates of these two processing stations.

JOHN LIBRARY

It is noteworthy that the correlation between temporal coding capacity and onset latency is considerably weaker for the electrical stimulation condition than for the acoustic condition. Two contributing aspects have to be considered in explaining this difference. It is conceivable that the highly synchronized input from electrical stimulation will disrupt or override some of the mechanisms that determine the following rate, and that are normally based on finely tuned temporal differences from different locations along the basilar membrane. In addition, the onset latency in the electrical conditions covaries with the response threshold, unlike the acoustic case. This added independent influence on the onset latency will weaken the correlation between latency and BMF in the electrical conditions.

In general, the differences between acoustic and electrical conditions can be accounted for by the hypothesized changes in the sequence of excitatory and inhibitory events and the difference in the synchronization of the inputs. Further insight into the effects of electrical stimulation on cortical activity is provided by considering differences between the two electrical stimulation conditions. Overall, the radial and presumably more 'narrow-band' electrical stimulation and the longitudinal 'broad-band' stimulation resulted in very similar response behaviors as determined with rate/level functions, latency/level functions, and temporal encoding capacities. For acoustic stimulation, broad-band stimulation (noise, clicks, tones with fast onsets) versus narrow-band stimulation (tones with slow onsets) results in a number of distinct response differences that are due to the spread of excitation, with the amount of evoked inhibition being proportional to the spread (e.g. Phillips, 1988; Schreiner and Mendelson, 1990). As a consequence, cortical locations with strong inhibitory potential show a smaller magnitude of firing rates, higher

JOHN LIBRARY

non-monotonicities, and longer latencies (Phillips, 1988; Schreiner and Mendelson, 1990). The explanation for the similarity of the two electrical stimulation conditions may reflect the possibility that the spread of excitation for the radial pair is not as restricted as might be expected for a pure tone with a slow rise time. Consequently, the response behavior for radial pair stimulation more closely resembles the response to a pure tone with a steep onset (Phillips 1988), as steep onsets result in a near-click stimulus that contains many frequencies. Model calculations of the spread of the electrical potential for radial and near-radial pairs (Finley, et al., 1989), and estimates based on the width of spatial tuning curves indicate that the spread of excitation for current levels near the lowest thresholds seen in this study are already more than one millimeter corresponding to about 1/3 of an octave. For acoustically narrowly tuned neurons that often have an excitatory bandwidth of less than 1/5 of an octave (Schreiner and Sutter, 1992), this spread of excitation would already be sufficient to invade the surrounding inhibitory sidebands and to activate those inputs. Since most radial electrode configurations in this study had a longitudinal component, i.e. the contacts for a given pair had a lateral separation of between 0.3 and 1.0 mm, the spread of excitation was even further increased by that amount. However, the spread of excitation for the radial and off-set radial electrodes is still 2 to 4 times smaller than that for the longitudinal electrode with a contact separation of 6 to 7 mm.

A few small but significant differences in the response behaviors between the two electrical stimulation conditions should be noted: a) the response threshold for the longitudinal pair was generally 5 dB lower and the response latency was about 0.3 ms shorter than for the radial pair; b) the slopes of the latency/level functions of the longitudinal pair were shallower than for the radial pair; and c) stimulation of the longitudinal

JOHN LINDVALL

pair resulted in more non-monotonic rate/level functions. These differences suggest that the greater spread of excitation and greater synchronous involvement of neural units using longitudinal stimulation result in a summing effect that lowers the overall threshold and produces shorter onset latencies. Since the spread of excitation changes for the longitudinal pair only minimally with increase in level, a lower rate of change for latency/level functions is recorded. The larger amount of non-monotonicity observed with longitudinal stimulation indicates that the larger stimulated area can still increase the amount of inhibition although, overall, the inhibition evoked by the radial pair appears to be already rather strong (see above). The threshold difference between longitudinal and the radial electrode pair could also reflect the fact that the radial pair almost certainly did not have the most optimal location in the cochlea for each neuron. Although the radial pair was the best of the available radial pairs in these cases, deviations of the actual position from the optimal electrode position for a given neuron may have been as large as 1mm.

It is concluded that electrical stimulation of the cochlea results in neuronal response characteristics that are generally similar to those induced by broad-band acoustic stimulation. However, it is hypothesized that electrical stimulation provides a strong indication of a more efficient synaptic transmission resulting in a stronger and earlier onset of both excitatory and inhibitory contributions to the cortical response.

1007 LINDEN

## **4.2 Experimental Series Two: Spatial Distributions of Acoustic and Electrical Responses**

### **4.2.1 Caudal-Rostral Domain**

An understanding of the distribution of cortical physiological responses to electrical stimulation, and a determination of their relationship to the physiological response distributions for acoustic stimulation was of primary interest in the present study. For electrical stimulation, however, time permitted only the evaluation of response threshold distributions in AI in these initial studies. An analysis of these distributions in the rostral-caudal domain revealed that electrical stimulation at a given peripheral location resulted in a tonotopically- appropriate, spatially-preferential low threshold response area in AI. As noted earlier, this preferential spatial tuning in primary auditory cortex is not surprising as the early electrical stimulus cochlear mapping studies of Woolsey and Walzl (1942) coupled with later acoustic mapping experiments (Merzenich, et al., 1975; Reale and Imig, et al., 1980) had already noted a clear relationship between restricted cochlear stimulation and tonotopically-appropriate evoked responses in AI. An approximation of the locations of these sensitive areas across the isofrequency band domain, to some extent, was predictable. By aligning the electrode contact location measurements along the carrier length with frequency representation along the cochlear partition as determined by Greenwood (1961; 1974) and Liberman (1982), a prediction of the areas of maximum electrode response sensitivity in AI could be made. The anchoring cuff-to-basalmost electrode contact and distances electrode pairs were not always uniform, although an attempt was made during electrode fabrication to make all of these distances 2mm. In reality, these

1000 LINDEN

distances could vary by as much as 1mm in either direction. In addition, the depth of insertion of the electrode array relative to the round window may have varied by as much as 1mm due to differences in the point to which the anchoring cuff was attached to the bone surrounding the round window. Finally, the length of the basilar membrane can vary by approximately 4mm (Liberman, 1982) adding further potential discrepancies to the estimates of the actual electrode location. Therefore, it was difficult to make a precise prediction of electrode contact-to-cochlear location for all cases. In one exemplary case (C163), for example, electrode contacts were estimated to be located at 7.1mm (Pair 7,8), 9mm (Pair 5,6), 10.9mm (Pair 3,4), and 12.1mm (Pair 1,2) from the extreme cochlear base, if 4mm was allotted to the hook portion of the basilar membrane. These distances, according to Greenwood (1974) would be aligned with characteristic frequencies of 14.1kHz, 9.7kHz, 6.7kHz, and 5.1kHz, respectively. An analysis of the cortical threshold distribution for this case referenced to a tone-generated AI map, revealed electrical stimulation-evoked ventral-dorsal sensitivity 'peaks' in AI that corresponded to CFs of approximately 25kHz, 13.0kHz, 10.8kHz, and 6.8kHz (see Figures 25 and 34). Taking into account insertion depth and hook length deviations of 2mm, a much closer match between physiologically determined electrode locations and predicted values of 21kHz, 14.4kHz, 9.9kHz, and 7.8kHz can be obtained.

#### 4.2.2 Ventral-Dorsal Domain

Evaluation of the spatial distributions of physiological response properties for several acoustic parameters and measured electrical thresholds revealed clearly non-uniform spatial organizations across the extent of AI. Although not all estimated parameters showed spatial

JOSE LIBRARI

congruency, there was a consonance in the spatial configurations of these parametric response distributions in that they generally involved a centralized maximum or minimum running orthogonal to the isofrequency gradient, with slopes toward the dorsal and ventral sectors.

A principal component analysis of the acoustic response parameters showed that there are three groups of fairly highly correlated parameters which indicate the existence of three largely independent relationships among the studied parameters. The correlations between acoustic parameters observed in this study confirm previously described correlations (Schreiner and Mendelson, 1990; Schreiner et al., 1992). Descriptively, the three emerging independent factors were labeled 'bandwidth', mainly consisting of Q-10dB and Q-40dB, 'intensity', consisting of threshold and best level, and 'time/inhibition', consisting of latency and (non-)monotonicity. The compatibility of the spatial alignment of most parameter gradients in central AI with the relative independence of these parameters as revealed by a principal component analysis may be explained by the notion that a global independence of the factors across all of AI exists with a locally restricted covariance in the center of AI. A more detailed analysis of the spatial distribution of the emerging acoustic response factors (Schreiner, personal communication) reveals that the length constant or spatial frequency of the gradients is different for each of the factors.

Although the spatial distributions of acoustic response parameters and electrical thresholds display very similar configurations, the relationship between electrical and acoustic parameters is rather complex, showing varying degrees of positive and negative correlations among the studied parameters. Most noteworthy is a negative correlation between electrical

JOSE LEBLANC

threshold and the parameters subsumed in the intensity factor (threshold and best level). This finding supports the hypothesis that there are distinct differences in the excitatory/inhibitory sequence and balance of neuronal responses between acoustically evoked, fairly non-synchronous activity and highly synchronous, electrical stimulation with a larger spread of excitation. Therefore, the resulting response differences between these two stimulus modes lies in the relatively greater influence of inhibition using electrical stimulation over that of acoustic stimulation.

The distributions of acoustic and electrical thresholds were negatively correlated such that a central AI area running orthogonal to the isofrequency domain revealed low acoustic thresholds and high electrical thresholds. Conversely, acoustic thresholds in the dorsal and ventral regions showed the opposite relationship, i.e. proportionally low electrical thresholds and proportionally high acoustic thresholds. These spatial relationships suggest that the balance of excitatory/inhibitory influences varies not only with stimulus mode, but also with cortical location. Electrical stimulation appears to result in a strong inhibitory influence on response thresholds in central AI that does not occur in kind for acoustic stimulation, i.e. the dorsal-ventral center of AI appears to contain relatively stronger inhibitory influences which electrical stimulation elicits earlier and more coherently. Many locations within this central, high electrical threshold zone were silent, suggesting that inhibitory influences may even precede excitatory influences. Stronger inhibitory influences in the center of AI are further supported by the findings of Prieto and Winer (1992), in the cat, which show that there are more GABAergic neurons located in central AI than in its dorsal-ventral regions. In the dorsal and ventral regions of AI, electrical thresholds were low

1007 LIBRARY

suggesting that there are relatively weaker existing inhibitory influences in these regions, again, supported by the anatomical findings of Winer (1992). An explanation of why low acoustic thresholds correlated with the presence of strong inhibition is unclear.

The spatial distribution of "best" level or the level evoking the strongest response is also related to electrical response threshold. Neurons in central AI reveal low best levels relative to more dorsal or ventral regions. These neurons respond with their highest firing rate at low stimulus levels, again reflecting a strong inhibitory influence in this region that manifests itself with increases in stimulus intensity and results in non-monotonic rate/level functions. Typically, the dorsal and ventral areas of AI show relatively high best levels, indicating that there is a relatively weaker inhibitory influence in these regions.

Spatial distributions of other physiological parameters also reflect the strong inhibitory influence in the center of AI. While effects do not appear to be as clear cut for these parameters as those of acoustic threshold and best level versus electrical thresholds, the trends are still appreciable. The spatial distribution of monotonicity of rate/level functions shows an area in the center of AI in which neurons respond most often with non-monotonic rate/level functions. Again, non-monotonicity reflects a strong inhibitory influence such that increases in stimulus intensity ultimately result in a decrease in firing rate. In ventral AI, most neurons show monotonic rate/level functions, indicating a relatively weaker inhibitory influence. In the dorsal region of AI, an area exists that also shows low non-monotonicity, however in some cases, a second region near the most dorsal extent, also shows non-monotonic responses. This may explain why the factor analysis shows that monotonicity contributes not



only to the intensity factor but also contributes to a factor that is independent (time/inhibition), i.e. non-monotonicity may be the result of two different mechanisms that are active in different parts of AI (Sutter and Schreiner, 1993).

In individual cases, the spatial distributions of excitatory bandwidth parameters Q10dB and Q40dB do not show the definitively demarcated central versus dorsal and ventral AI response areas. However, among the six cases, a fairly clear trend emerges in which neurons that exhibit the sharpest tuning are found in central AI while those with more broad tuning are found in the dorsal and ventral regions. Since sharpness of tuning is considered to reflect the action of inhibitory sidebands, the weakness in its correlation with electrical threshold is somewhat surprising. However, it has to be considered that sharpness of tuning is mostly a function of the location of inhibitory sidebands relative to the excitatory region and not so much a function of the strength of inhibition. It can be hypothesized that those neurons that are sharply tuned *and* are strongly non-monotonic reflect the strongest inhibitory components and should be found in central AI. Other neurons that are sharply tuned but are not non-monotonic should be found mostly outside central of AI. Recent studies by Schreiner and Sutter (1992) and Sutter and Schreiner (1993) have found evidence supporting this hypothesis.

Response latency for acoustic stimulation reveals a global spatial distribution across AI that finds neurons that respond with shorter latencies near the center and those with longer latencies in the more dorsal and ventral regions. Of interest is the finding that non-monotonicity is correlated with onset latency for acoustic stimulation (Phillips and Cynader, 1985), i.e. neurons that exhibit

JOSE LIBRARY

non-monotonicity also exhibit longer latencies. The present data analysis also shows a correlation between minimum latency and the slope of the high level segment of the rate/level function. This finding was borne out by the principal component analysis for acoustic parameters which found latency and non-monotonicity emerging alone under the same factor ('Time/Inhibition Factor'). It is known from earlier work by Phillips and Sark (1991) that acoustic stimulation results in a progressively earlier onset of inhibition with level increase for non-monotonic neurons. Therefore, it can be assumed that inhibitory mechanisms are in place in the central, non-monotonic region of AI. As a consequence, the spatial distribution for latency and monotonicity show their minimum in the central region of AI, but are slightly offset.

One further piece of evidence for a strong inhibitory influence in the center of AI is the spatial distributions of binaural interaction type, i.e. neurons in the central region of AI tend to exhibit binaural suppression (EI interaction) while dorsal and ventral area neurons responded more often with binaural summation (EE interaction). Once again, a greater inhibitory influence is found in the central region of AI, although in this case the inhibition was invoked by stimulation of the ipsilateral ear.

In summary, a comparison of the spatial distributions of a variety of acoustic response parameters with electrical thresholds in primary auditory cortex revealed a large number of positive and negative correlations. The congruence of these relationships demonstrates a dominant theme suggesting that central AI contains a strong inhibitory capacity that when engaged with electrical stimulation results in restricted neuronal responses relative to those for acoustic stimulation. An explanation for the enhanced engagement of the strong inhibitory

JOSEF LEHMANN

capacity in central AI by peripheral electrical stimulation lies with the notion of an early, fully-activated response of inhibitory mechanisms already present at low electrical stimulus intensities. These temporally highly coherent inputs are acoustically unfeasible at low stimulus levels. Apparently, full engagement of inhibition using acoustic stimulation only occurs at relatively higher stimulus levels. In the ventral and dorsal regions, a generally weaker inhibitory capacity appears to be in place so that an early, coherent onset of inhibition has a more limited impact on evoked neuronal responses. One caveat to the above findings is that unanesthetized preparations may reveal a somewhat altered weight of excitatory and inhibitory contributions.

### **4.3 Comparison of Electrical Stimulation Effects with Other Auditory Stations**

#### **4.3.1 Auditory Nerve**

A number of studies have explored the response of auditory nerve fibers to various modes of intracochlear electrical stimulation (e.g. Kiang and Moxon, 1972; Hartmann, et al., 1984, 1987, 1989; van den Honert and Stypulkowski, 1984, 1987a,b; Parkins, 1989; Javel, et al., 1987; Javel, 1989). However, there are few comparative studies in which the same electrode configurations, electrode polarity, and stimulus waveforms are used as in the present study. Studies using biphasic 0.2ms/phase pulses applied extracochlearly (Hartmann, et al., 1984) and intracochlearly (Javel, 1989) found auditory nerve fiber thresholds of 60 to 350  $\mu$ A in normal hearing cats. The mean cortical electrical thresholds for both electrode configurations fall in the upper half of this range. These investigations also noted relatively short latencies of 0.3 - 0.6ms as well as latencies

U.S. LIBRARY

greater than 1 ms. These latencies agree with those noted by Javel and colleagues (1987). Again, using pulse stimuli, Hartmann and colleagues also found strong phase locking if the interpulse interval was greater than 2ms, but noted that the strength of synchronization depended heavily upon current level. Strong phase locking to sinusoidal and pulsed stimulation in excess of 600 Hz has been reported (Hartmann, et al. 1984; van den Honert and Stypulkowski, 1987b; Javel et al, 1987) that was similar or slightly better than following rates seen for acoustic stimulation (e.g. Hartmann and Klinke, 1989; Javel, 1989; Joris and Yin, 1992). In the auditory cortex, phase locking was not recorded for stimulation rates above after about 40pps in close agreement with observations for acoustic stimulation (e.g. Schreiner and Urbas, 1988; Eggermont, 1991).

Using bipolar intracochlear radially-oriented electrodes and 100 $\mu$ s monophasic pulses presented at 25Hz, van den Honert and Stypulkowski (1987a) found that thresholds were always lowest in the auditory nerve population closest to the electrode. They also noted higher Q10 values or sharper tuning for a radial electrode configuration than for longitudinal electrode stimulation. Sharper spatial tuning curves were found for bipolar electrode stimulation over those of monopolar electrode stimulation (Hartmann, et al., 1984; van den Honert and Stypulkowski, 1987a). This is especially true if the fiber is in close proximity to the stimulating electrode. It can be assumed that this spatial preference for frequencies near the site of stimulation for a given electrode is maintained throughout the auditory pathway including the primary auditory cortex.

Rate/level data for auditory nerve fibers reveal steep functions in which increases in firing rate occur rapidly with only small increases in

JOSE LEBLANC

stimulus level that saturates at high levels, i.e. they are monotonic (van den Honert and Stypulkowski, 1987b). The firing rates often exceed 200 spikes/second within 6dB of threshold. This finding is also supported by Hartmann and colleagues (1984), who found that auditory nerve fibers respond monotonically to electrical stimulation reaching saturation at 6-12dB above threshold. The dynamic range in the cortex was found to be slightly smaller, usually between 3.5 to 10.5 dB. While some neurons responded with monotonic rate/level functions in the primary auditory cortex, many more revealed non-monotonic rate/level functions. Since acoustic stimulation reveals all strongly non-monotonic neurons to have smaller dynamic ranges due to inhibitory influences (Phillips, 1988), the difference between the dynamic range of the auditory nerve and cortex can be ascribed to inhibitory influences in central stations as well.

#### 4.3.2. Cochlear Nucleus

In two studies, the response characteristics of cochlear nucleus neurons to electrical cochlear stimulation were evaluated (Glass, 1983; Clopton and Glass, 1984) in guinea pigs. Animals were deafened with neomycin and implanted with two to four electrodes each separated by 1 mm. All recordings were done in the anteroventral cochlear nucleus. Thresholds for sinusoidal stimulation were between 74 and 174 $\mu$ A, comparable to those seen in auditory nerve fibers and inferior colliculus neurons of cats (van den Honert and Stypulkowski, 1987; Snyder et al., 1991). The lowest cortical thresholds were typically about 6 to 10dB higher than those for these other auditory stations. Dynamic ranges ranged from 2 to 15dB compared to 3.5 to 10.5dB in the auditory cortex. The smaller range for the cortical neurons may relate to the measurement criterion in that dynamic range was defined as the level difference

JOSE LIBRARY

between threshold and transition point versus cochlear nucleus measurements which were calculated as the difference between threshold and the level producing maximum firing rate. Clopton and Glass (1984) noted a very high degree of response synchrony to stimulation with single sinusoids and envelopes of multiple sinusoid stimuli. Other parameters studied in the cochlear nucleus are not directly comparable to those used in the cortical study.

#### 4.3.3 Inferior Colliculus

Previous studies of physiological responses of single units in the central nucleus of the inferior colliculus (ICC) to peripheral electrical stimulation (Merzenich and White, 1977; Snyder, et al., 1990, 1991) provide a basis for direct comparison for cortical neuronal responses using a similar electrical stimulation scheme. In these studies, adult experimental (neonatally deafened, implanted but not stimulated; neonatally deafened and chronically stimulated) and control animals (acutely deafened and implanted) were implanted with four to six off-set radial bipolar electrode pairs and stimulated with either three cycles of a 100Hz sinusoid or biphasic pulses, 0.2ms/phase delivered at 40pps. Since the animals in the present study most closely resemble the control animals in the ICC experiments, only those results will be compared.

##### 4.3.3.1 Response Types

ICC neurons responded with either sustained or onset responses to electrical stimulation using sinusoids at suprathreshold levels. Cortical responses to sinusoidal and pulse stimulation were limited to onset responses only. Cortical responses to high pulse rate stimuli also resulted

U.S. LIBRARY

exclusively in onset responses. Sustained or event-locked responses were seen, however, in cortical neurons using very low pulse rates (one second pulse trains presented 30 times). Sustained responses in ICC neurons were found to be near the location with the lowest threshold, were non-monotonic, and had relatively shorter latencies. While the spatial distribution of sustained responses was not obtained in the cortex, most neurons (single and multiple units) were able to follow low (8-10Hz) repetition rates with no clear relationship between this capacity and non-monotonicity. acoustic studies of the inferior colliculus have revealed a close relationship between response latency and ability to follow repetitive stimuli in a sustained fashion (Langner, et al., 1987). A similar relationship has been demonstrated in this study for the auditory cortex for electrical as well as acoustic stimulation.

#### 4.3.3.2 Threshold

Average minimum thresholds for ICC neurons in acutely implanted animals ranged from -10 to 17dB re 100 $\mu$ A (mean minimum threshold 140 $\mu$ A or 3dB). While this range overlaps with threshold ranges observed for some electrode pairs in some cases for the auditory cortex (see Table 9), ICC thresholds are generally lower than those found in AI (mean minimum thresholds 200-350 $\mu$ A or 6-11dB). This overall threshold difference may be due to several factors including: 1) differences in the number of electrodes and electrode configurations; 2) differences in electrode placement due to carrier length and width differences; 3) differences in inhibitory mechanisms at these two auditory stations. However, preliminary data comparing the lowest thresholds found in the cortex and in the ICC of the same animal (case 163) show that threshold values were essentially the same. An additional cortical case in which

U.S. LIBRARY

Implantation was with an electrode type that was used in most ICC experiments by Snyder and colleagues (1990, 1991) also showed the same threshold range as in all other cortical experiments. This evidence suggests that influences from the electrode design may not be the sole contributor to the difference between IC and cortical thresholds. An additional contribution may arise from the fact that the area with the lowest acoustic thresholds is responsively quiet for effectively broad-band electrical stimulation and, therefore, disallows the potentially lowest thresholds to emerge. Alternative electrical stimulation paradigms that would allow spatially more focal and/or temporally more dispersed stimulation may result in lower thresholds in the central sector of AI.

Inferior colliculus neurons showed greatest sensitivity in animals that had been neonatally deafened and were unstimulated. This finding was also observed in one cortical control case in which an animal had been deafened at birth and acutely implanted at three years of age and mapped (K33). This greater sensitivity in neonatally deafened animals is not well understood since it is known that very few spiral ganglion cells remain in these cases (Leake and Hradek, 1988). One theory postulated by Snyder and colleagues (1991) is that when only a small number of myelinated dendrites remain in neonatally-deafened animals, perhaps a preferential current path for the excitation of the remaining neural elements occurs thereby increasing the efficiency of the coupling to the spiral ganglion cells. Alternatively, Snyder and colleagues postulate that a form of denervation hypersensitivity is created similar to that of autonomic and somatic motoneurons following chronic peripheral and central lesions resulting in lower response thresholds.

JOSE LIBRARY

#### 4.3.3.3 Rate/Level Functions

Most single units in the ICC responded with an increased discharge rate when stimulated electrically, however, some units responded with a suppression of ongoing spontaneous activity. The latter case was not seen for cortical units in this sample. In terms of rate/level functions, most ICC units increased their firing rate monotonically with increases in stimulus intensity until responses saturated at 6 to 10dB above threshold. Only some collicular neurons showed non-monotonic functions whereby maximum firing rate was reached at 2-6dB above threshold (dynamic range), but decreased sometimes to 0 with further increase in stimulus intensity. The opposite proportions were observed for cortical neurons in which the majority show non-monotonic rate/level functions for electrical stimulation. Even using a stringent criteria of  $-1\%/dB$  as 'confidently non-monotonic', non-monotonic cortical rate/level functions are still 45% and 40% for the radial and longitudinal electrode pairs, respectively. The standard deviation of the dynamic range of cortical neurons (combined for monotonic and non-monotonic functions) was 3.5 to 10.5 dB for cortical neurons thereby essentially overlapping the range for both monotonic and non-monotonic ICC responses.

#### 4.3.3.4 Latency

Inferior colliculus neurons and primary auditory cortical neurons had similar responses to electrical stimulation in terms of onset latency, i.e. onset latency was influenced by stimulus intensity and stimulating electrode location. The latency response of the same neuron to different electrode pairs varied by as much as 5-10 ms in the ICC depending upon the response type. In the cortex, a small but significant mean minimum

U.S. LIBRARY

latency difference was seen between the radial and longitudinal electrode pairs. A larger, significant difference was observed between the electrical conditions and acoustic stimulation in the cortex. The range of minimum latencies in the ICC was 4-8ms and in the cortex 8-12ms (one standard deviation from the mean). Some of this difference is to be expected due to conduction time and the different number of synapses involved in the transmission to the two structures. However, other mechanisms may contribute to this difference as well, e.g. inhibitory contributions may be larger in the cortex and, thus, extend the latent period.

In contrast to acoustic stimulation, a relatively large number of 'inhibitory rebound' responses in ICC neurons to electrical stimulation were observed with latencies between 40ms and as much as 180ms, termed 'late responses' (Snyder, et al., 1991). Although inhibitory rebound responses in the auditory cortex have been described (Schreiner and Joris, 1988; Eggermont, 1992) and are fairly common for acoustic stimulation, only a small number of these responses were observed in this study with electrical stimulation. This relative absence of inhibitory rebounds suggests that these late responses are not only determined by the strength and duration of inhibitory processes but may also reflect the strength of appropriately timed feedback from other cortical areas. It is possible that this feedback is out of balance due to the different timing and excitatory/inhibitory balance evoked by electrical stimulation.

Among the conclusions from the ICC studies is that response properties to electrical stimulation in terms of latency distributions and diversity of rate/level functions are quite similar to those found in other studies of acoustic stimulation. While this finding, in general, is corroborated in the

U.S. LIBRARY

primary auditory cortex, there are many differences between ICC and primary auditory cortical neurons in their response to electrical stimulation. First, cortical neurons event-lock to low frequency stimuli, but unlike ICC neurons, they do not follow relatively higher frequency stimuli with sustained responses. Only onset responses were observed in the cortex. Secondly, cortical thresholds are typically higher than ICC thresholds. Lastly, most cortical neurons show non-monotonic rate/level functions while most ICC neurons reveal mostly monotonic rate/level functions. These differences in response behavior between AI and ICC neurons reflect a different balance between several underlying mechanisms, which may reside in sequencing differences between excitatory and inhibitory events, i.e. spread of excitation or synchronization of electrical input may have a greater impact on the excitatory/inhibitory sequence in the cortex than in the ICC thereby suggesting more and stronger inhibitory influences present in the cortex. Therefore, ICC neurons event-lock to higher stimulus frequencies, exhibit slightly lower thresholds, and display generally monotonic rate/level functions - all indicative of relatively weaker inhibitory influence.

#### 4.3.3.5 Spatial Tuning

Threshold measurements in the ICC as a function of depth, using peripheral electrical stimulation as previously described, resulted in V-shaped spatial tuning curves with the location of maximum sensitivity or 'best location' found at the tip of the curve confirming the findings by Merzenich and White (1977) and Snyder, et al. (1990). The location of the tip varied in depth depending upon the pure tone stimulus or the stimulating electrode location. This variation in best location in depth is consistent with the known cochleotopic organization of the ICC such that a

U.S. LIBRARY

tonotopic gradient is seen over successively deeper frequency band lamina (Merzenich and Reid, 1974; Roth, et al., 1978; Schreiner and Langner, 1988). Units with lower CFs are located more dorsally and units with higher CFs are located more ventrally. Once a "best location" was determined for a given electrode, stimulation of an adjacent electrode measured at that same, best location, resulted in a higher threshold. These findings are comparable to the preferential spatial tuning observed in primary auditory cortex. Stimulation of the longitudinal electrode pair resulted in the lowest thresholds for both the ICC and the cortex and resulted in very broad or absent spatial tuning.

Electrical stimuli presented at a given cochlear location at threshold resulted in restricted areas of excitation at a tonotopically appropriate depth within ICC (determined by acoustic stimulation of the ipsilateral ear). The area of excitation broadened with increases in stimulus intensity. The ICC results of the present study and that of Snyder and colleagues (1990) revealed comparable spatial tuning of approximately 1 octave at 6dB above minimum threshold. The spatial tuning is expressed in terms of the underlying frequency organization since the spatial dimension of basilar membrane, inferior colliculus, and cortex differ significantly. The mean width of spatial tuning in the auditory cortex ranged from 0.92 octaves for the most apical pair to 0.61 octaves for the most basal pair. Whereas the sharpness of tuning for the most apical pairs is similar to that seen in the inferior colliculus, the more basal pairs appear to be more narrowly tuned. However, the statistical reliability of these data is fairly weak, mostly due to a very noisy distribution of the threshold curves compared to the inferior colliculus data. Single and multiple unit data of cortical response distributions indicate, in general, a fairly large scatter of response properties in neighboring positions, making it more difficult to

UCSF LIBRARY

discern global spatial gradients (e.g. Imig et al., 1990; Schreiner et al., 1992; Schreiner and Sutter, 1992). An increase in sharpness of tuning with frequency is known to occur for acoustic tuning (Phillips and Irvine, 1981), however, it is thought to be related to the width of the traveling wave envelope. The relationship between this acoustic finding and electrical spatial tuning is unclear. Acoustic studies have found that the sharpness of frequency tuning varies along the dorsal-ventral extent of AI with the sharpest tuning in the center of AI and progressively broader tuning toward the dorsal and ventral ends of AI (Schreiner and Mendelson, 1990). In an attempt to provide a comparative analysis, the spatial tuning was measured at four different dorsal-ventral sectors of AI, i.e. along a ventral, central, and two dorsal strips. A weak statistical trend was seen that showed the narrowest tuning in the center of AI, in accordance with the acoustic distribution.

Spatial tuning curves obtained in the auditory nerve revealed an average width of 0.37 octaves for pure radial orientation of the bipolar electrodes and 1.2 octaves for longitudinally oriented electrodes separated by approximately 2mm (van den Honert and Stypulkowski, 1987a). Since these measurements were made 10dB above threshold, they may represent a slight overestimation of the bandwidth compared to the 6dB measurements for cortex and colliculus. However, the spatial tuning curves of auditory nerve fibers have very steep slopes, resulting in only small differences between these two measurement criteria. The global average of cortical tuning bandwidth was 0.77 octaves for an average lateral shift of electrode contacts for a radial pair of 0.5mm. From the auditory nerve data one can extrapolate that the spatial bandwidth for an electrode spacing of 0.5mm should be approximately 0.6 octaves. This is in reasonable agreement with the cortical tuning bandwidths actually

U.S. LIBRARY

obtained in the present study. Since the average tuning bandwidth in the ICC is approximately one octave, these comparisons suggest that narrower tuning in the primary auditory cortex may be more a consequence of processing than the projection pattern.

#### **4.4 Implications for Cochlear Implant Design and Performance**

One purpose of this study was to begin to ascertain whether aspects of the representation of electrical cochlear stimulation in the primary auditory cortex can aid in our understanding of potential deficits in the speech processing of implant patients and how to overcome these deficits with more appropriate stimulation paradigms. Many findings of this study reflect properties and consequences of electrical stimulation already known from studies of the auditory nerve, cochlear nucleus, and the inferior colliculus, e.g. minimum thresholds, dynamic ranges, spatial tuning, or are directly related to the functional organization of the auditory cortex as seen with acoustic stimulation, e.g. non-monotonicity, temporal repetition behavior. There is, however, one new finding that may directly bear on our understanding of the perceptual consequences of cochlear implant stimulation and the performance of cochlear implant patients with complex stimuli, most notably speech. In every studied animal, the central portion of AI was unresponsive to peripheral electrical stimulation or showed highly elevated response thresholds. The contribution of physiological responses in the central region of the primary auditory cortex to the understanding of speech has yet to be determined. However, it is clear that the neurons in this region respond differently to both acoustic and electrical stimulation than in the dorsal and ventral regions of AI. When stimulated acoustically with tonal stimuli, these neurons respond with low thresholds, sharp tuning, and

JOSEF LIBRARY

generally non-monotonic rate/level functions. Stimulation with broad-band acoustic stimuli has also revealed markedly lower firing rates in central AI (Schreiner and Mendelson, 1990). An interesting response characteristic of these neurons is that their thresholds increase in the presence of background noise (Phillips and Cynader, 1985). Therefore, central AI neurons provide fine frequency resolution at relatively low signal-to-noise ratios, and maintain the threshold-to-noise relationship so that threshold is adjusted just above the noise level. These response characteristics might be fundamentally important in speech feature detection and classification.

Although we might consider the overall responses of these neurons to broad-band acoustic stimulation to be relatively subdued, electrical stimulation results in an even further degradation in response strength from those of acoustic stimulation. That is, peripheral electrical stimulation results in neuronal responses in this central region that reveal a pattern of high thresholds, relatively long latencies, and low firing rates. An analysis of these composite responses suggests strong inhibition that significantly restricts or eliminates the native physiological response mechanisms underlying the responses of central AI neurons. One explanation for this strong inhibition lies in the balance of excitatory/inhibitory responses that favors the inhibitory influences as stimulus intensity increases due to the coherent temporal pattern of electrical stimulation.

The manifestation of profound inhibitory effects in central AI suggested by the results of the present study for electrical stimulation may play a role in explaining why some cochlear implant patients never understand open speech or why others do not understand open speech for

U.S. LIBRARY

some time after implantation. In particular, since a strongly coherent temporal excitatory pattern of peripheral electrical stimulation appears to result in a stronger engagement of inhibition than for acoustic stimulation, it can be speculated that the success or failure of cochlear implant patients in open speech understanding bears some relationship to the temporal characteristics of the stimulus. In addition, the spectral characteristics of the stimulus may also be of importance. In particular, cortical neurons event-lock only to low frequency stimuli while ICC neurons responding to sinusoidal stimuli were found to follow relatively higher frequency stimuli with sustained responses. In addition, acoustic nerve studies have shown that radial bipolar electrode configurations result in a sharply tuned, local response, with thresholds that are lowest for neurons closest to the stimulation site.

With the above factors in mind, it seems important that stimulating electrodes should be bipolar and as purely radial as possible to secure a relatively discrete stimulus locale. In this manner, spectral representation may be maintained in a discrete fashion as well as minimizing the inclusion of inhibitory influences with narrow spatial stimulation. Another possible enhancement of electrical stimuli may lie in the realization of less temporal synchrony that could circumvent strong inhibitory influences and, thereby, increase the probability of a greater contribution of excitatory input to AI. Some evidence for the enhancement of open speech understanding with non-simultaneous pulses was found in cochlear implant patients (Wilson, et al., 1991), although the underlying mechanisms for this enhancement are still unclear. Since it appears to be prudent to limit the spread of excitation and the high temporal synchronicity resulting from a single electrode, one stimulation scheme might entail non-simultaneous electrode stimulation using stimuli with a

U.S. LIBRARY

less steep onsets than the pulse stimuli used in the present study. Such stimuli may include ramped pulses or sinusoidal stimuli.

An interesting speculation is that without alterations in present cochlear implant stimulation electrodes and speech processing schemes, the mechanism that allows for the conversion of distorted speech percepts into meaningful stimuli may result from compensatory excitatory mechanisms that eventually emerge and ultimately override confounding organizational features, e.g. initially strong inhibitory influences. Evidence for plasticity in the response for primary auditory neurons has been obtained by lesion studies (Robertson and Irvine, 1990; Harrison et al., 1991), classical conditioning studies (Weinberger, et al., 1984; Diamond and Weinberger, 1989) and operative conditioning studies (Recanzone, et al., 1993) for the frequency organization of AI. For individuals who experience immediate open speech understanding, it may be that the neural inputs are so limited in number and location that little inhibition is engaged. This, coupled with a coherent memory for sound, may allow them good open speech understanding that also improves over time.

The present animal studies represent initial steps in determining the central representation of peripheral electrical stimulation and provide preliminary hypotheses that may have some bearing on cochlear implant patient performance in open speech understanding. Future experimental directions should concentrate on the evaluation of the efficacy of electrode designs and the consequences of multi-channel stimulation coding strategies in central auditory representations. In particular, investigations should be undertaken to evaluate the hypothesis that a balance of excitatory/inhibitory influences is differentially engaged in AI using acoustic versus electrical stimulation by modifications in the

UOBI LIBRARY

temporal characteristics of the applied stimuli. In addition, studies that evaluate physiological response behaviors and distributions in chronically stimulated animals should be initiated to address the question of why many cochlear implant patients improve in their speech understanding over time.

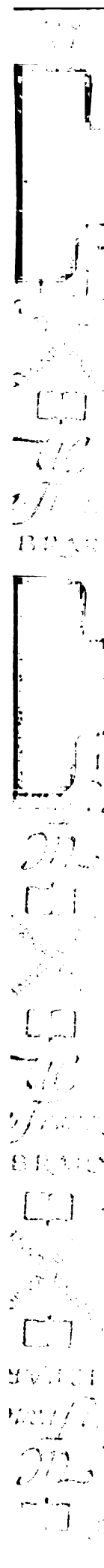
#### **4.5 Summary and Conclusions**

The responses of primary auditory cortical neurons to peripheral electrical stimulation reveal a threshold pattern that supports the maintenance of tonotopicity in AI. In addition, a non-uniformity in the electrical threshold distribution across the ventral-dorsal extent of AI has also been demonstrated. A comparison of known and duplicated physiological response distributions for acoustic stimulation with the distribution of the ventral-dorsal electrical threshold has been undertaken, revealing relationships that may have a critical bearing on the performance of cochlear implant patients immediately after implantation and over time.

A two-pronged approach was used in the present study whereby, initially, physiological responses of single units were measured in terms of response strength, latency, and temporal precision. Although spatial distributions were not determined for these single unit responses, a second phase of this study involved single and multiple unit mapping across the caudal-rostral center of AI with electrical and acoustic stimulation in the same animal. From the synthesis of the data from these two response measurement formats emerges a comprehensive picture of the representation of electrical stimulation in primary auditory cortex in terms of neuronal behavior and its spatial distribution.

U.S. LIBRARY

Parametric evaluation of single neuron responses and comparison of the spatial distributions for acoustic and electrical stimulation support the same conclusions regarding the physiological response behavior of primary auditory cortical neurons. It has been suggested that there may be a differential contribution of excitatory/inhibitory influences at given cortical locations such that the central region of AI has a relatively stronger inhibitory influence than the dorsal and ventral regions. The nature of stronger inhibition has been demonstrated to entail a progressively earlier onset of inhibitory mechanisms with increasing level. Using peripheral electrical stimulation, a highly synchronous excitatory pattern is effected that is temporally coherent and relatively widely spread across the nerve. This temporally coherent electrical stimulation may engage preexisting inhibitory mechanisms in central AI resulting in strong and early inhibition such that little response activity can be recorded from the central region of AI for this stimulus mode. These results may provide useful information applicable to future cochlear implant electrodes designs as well as in speech processing strategies that would allow better access to neuronal responses in central AI and, therefore, lead to greater open speech understanding immediately after implantation.



UCSF LIBRARY

## 5. BIBLIOGRAPHY

Bilger, R.C., Black, F.O., Hopkinson, N.T., Myers, E.N., Payne, J.L., Stenson, N.R., Vega, A., and Wolf, R.V. (1977). Evaluation of subjects presently fitted with implanted auditory prostheses. *Ann. Otol. Rhinol. Laryngol.* 86 (Suppl. 38):1-176.

Brugge, J.F. and Merzenich, M.M. (1973). Responses of neurons in auditory cortex of the macaque monkey to monaural and binaural stimulation. *J. Neurophysiol.* 36:1138-1159.

Clopton, B.M. and Glass, I. (1984). Unit responses at cochlear nucleus to electrical stimulation through a cochlear prosthesis. *Hearing Research* 14:1-11.

Dankowski, K., Mc Candless, G. and Smith, L. (1988). How does a percutaneous multichannel multielectrode cochlear implant work. *Rocky Mountain Journal of Communication Disorders* 3:21-23.

Diamond, D.M. and Weinberger, N.M. (1976). Classical conditioning rapidly induces specific changes in frequency receptive fields of single neurons in secondary and ventral ectosylvian auditory cortical fields. *Brain Research* 372:357-360.

Diamond, D.M. and Weinberger, N.M. (1989). Role of context in the expression of learning-induced plasticity of single neurons in auditory cortex. *Behav. Neurosci.* 103:471-494.

Disterhof, J.F. and Stuart, D.K. (1976). Trial sequence of changed unit

UCSF LIBRARY

activity in auditory system of alert rat during conditioned response acquisition and extinction. *J. Neurophysiol.* 39:266-281.

Djourno, A. and Eyries, C. (1957). Prothese auditive par excitation electrique a distance du nerf sensoriel a l'aide d'un bobinage inclus a demeure. *Presse Med.* 35:14-17.

Dowell, R.C., Mecklenburg, D.J. and Clark, G.M. (1986). Speech recognition for 40 patients receiving multichannel cochlear implants. *Arch. of Otolaryngol.* 112:1054-1059.

Doyle, P.J., Pijl, S., and Fraser, J.N. (1991). The cochlear implant: a comparison of single-channel and multichannel results. *The J. of Otolaryngol.* 20:204-208.

Eggermont, J.J. (1991). Rate and synchronization measures of periodicity coding in cat primary auditory cortex. *Hearing Research* 56:153-167.

Eggermont, J.J. (1992). Stimulus induced and spontaneous rhythmic firing of single units in cat primary auditory cortex. *Hearing Research* 61:1-11.

de Ribaupierre, F., Goldstein, M.H. and Yeni-Komishian, G. (1972). Cortical coding of repetitive acoustic pulses. *Brain Research* 48:205-225.

Finley, C.C., Wilson, B.S. and White, M.W. (1989). Models of neuron responsiveness to electrical stimulation. In: *Cochlear Implants-Models of the Electrically Stimulated Ear*, J.M. Miller and F.A. Spelman (Eds.), Springer-Verlag (pp.55-96).

JOSE LIBRARY

Gantz, B.J., Tye-Murray, N. and Tyler, R.S. (1989). Word recognition performance with single-channel and multichannel cochlear implants. *The Am. J. of Otol.* 10:91-94.

Glass, I. (1983). Tuning characteristics of cochlear nucleus units in response to electrical stimulation of the cochlea. *Hearing Research* 12:223-237.

Greenwood, D.D. (1961). Critical bandwidths and the frequency coordinates of the basilar membrane. *J. Acoust. Soc. Am.* 33:1344-1356.

Greenwood, D.D. (1974). Critical bandwidth in man and some other species in relation to the traveling wave envelope. In: *Sensation and Measurement*, H.R. Moskowitz and J.C. Stevens (Eds.), Reidel (pp.231-239).

Hari, R., Pelizzone, M., Makela, J.P., Hallstrom, J., Huttunen, J. and Knuutila, J. (1988). Neuromagnetic responses from a deaf subject to stimuli presented through a multichannel cochlear prosthesis. *Ear and Hearing* 9:148-152.

Harrison, R.V., Nagasawa, A., Smith, D.W., Stanton, S. and Mount, R.J. (1991). Reorganization of auditory cortex after neonatal high frequency cochlear hearing loss. *Hearing Research* 54:11-19.

Hartmann, R., Topp, G. and Klinke, R. (1984). Discharge patterns of cat primary auditory fibers with electrical stimulation of the cochlea. *Hearing Research* 13:47-62.

Hartmann, R., Topp, G. and Klinke, R. (1987). Single fiber recordings from

U.S. LIBRARY

the cat auditory nerve with electrical stimulation of the cochlea at different stimulation places. *Ann. Otol. Rhinol. Laryngol.* 96 (Suppl. 128): 30-31.

Hartmann, R. and Klinke, R. (1989). Response characteristics of nerve fibers to patterned electrical stimulation. In: *Cochlear Implants-Models of the Electrically Stimulated Ear*, J.M. Miller and F.A. Spelman (Eds.), Springer-Verlag (pp.135-160).

Herzog, H., Lamprecht, A., Kuhn, A., Roden, W., Vosteen, K., and Feinendegen, L.E. (1991). Cortical activation in profoundly deaf patients during cochlear implant stimulation demonstrated by H<sub>2</sub><sup>15</sup>O PET. *J. of Computer Assisted Tomography* 15:369-375.

Hoke, M., Pantev, C., Luetkenhoener, B., Lehnertz, K. and Suerth, W. (1989). Magnetic fields from the auditory cortex of a deaf human individual occurring spontaneously or evoked by stimulation through a cochlear prosthesis. *Audiology* 28:152-170.

House, W.F. and Urban, J. (1973). Long term results of electrode implantation and electronic stimulation of the cochlea in man. *Ann. Otol. Rhinol. Laryngol.* 82:504-17.

Imig, T.J. and Adrian, H.O. (1977). Binaural columns in the primary field (AI) of auditory cortex. *Brain Research* 138:241-257.

Imig, T.J., Irons, W.A. and Samson, F.R. (1990). Single-unit selectivity to azimuthal direction and sound pressure level of noise bursts in cat high-frequency primary auditory cortex. *J. Neurophysiol.* 63:1448-1466.

JOSE LIBRARY

Javel, E., Tong, Y.C, Shepherd, R.K. and Clark, G.M. (1987). Responses of cat auditory nerve fibers to biphasic electrical current pulses. *Ann. Otol. Rhinol. Laryngol.* 96 (Suppl. 128): 26-30.

Javel, E. (1989). Acoustic and electrical encoding of temporal information. In: *Cochlear Implants-Models of the Electrically Stimulated Ear*, J.M. Miller and F.A. Spelman (Eds.), Springer-Verlag (pp.247-295).

Jenkins, W.M., Merzenich, M.M., Ochs, M., Allard, T.T. and Guic-Robles, E. (1990). Functional organization of primary somatosensory cortex in adult owl monkeys after behaviorally controlled tactile stimulation. *J. Neurophysiol.* 63:82-104.

Joris, P.X. and Yin, T.C. (1992). Responses to amplitude-modulated tones in the auditory nerve of the cat. *J. Acoust. Soc. of Am.* 91:215-232.

Kiang, N.Y.S. and Moxon, E.C. (1972). Physiological considerations in artificial stimulation of the inner ear. *Ann. Otol.* 81:714-730.

Kitzes, L.M., Farley, G.R. and Starr, A. (1978). Modulation of auditory cortex unit activity during the performance of a conditioned response. *Experimental Neurol.* 62:678-697.

Langner, G., Schreiner, C.E. and Merzenich, M.M. (1987). Covariation of latency and temporal resolution in the inferior colliculus of the cat. *Hearing Research* 31:197-201.

Langner, G. and Schreiner, C.E. (1988). Periodicity coding in the inferior colliculus of the cat. I. Neuronal mechanisms. *J. Neurophysiol.*

U.S. LIBRARY

60:1799-1822.

Leake, P.A. and Hradek, G. (1988). Cochlear pathology of long term neomycin induced deafness in cats. *Hearing Research* 33:11-34.

Le Scao, Y., Robier, A., Baulieu, J.L., Beutter, P. and Pourcelot, L. (1992). Cortical perfusion response to an electrical stimulation of the auditory nerve in profoundly deaf patients: study with technetium-99m hexamethylpropylene amine oxime single photon emission tomography. *Eur. J. Nucl. Med.*19:283-286.

Liberman, M.C. (1982). The cochlear frequency map for the cat: labeling auditory nerve fibers known characteristic frequency. *J. Acoust. Soc. Am.* 72:1441-1449.

Luxford, W.M. and Brackmann, D.E. (1985). The history of cochlear implants. In: *Cochlear Implants*, Roger F. Gray (Ed.), College Hill Press, Inc. (pp.1-26).

Mendelson, J.R., Schreiner, C.E., Sutter, M. and Grasse, K. (1993). Functional topography of cat primary auditory cortex: representation of frequency modulation. *Exp. Brain Research* (in press).

Merzenich, M.M. and Reid, M.D. (1974). Representation of the cochlea within the inferior colliculus of the cat. *Brain Research* 77:397-415.

Merzenich, M.M., Knight, P.L. and Roth, G.L. (1975). Representation of the cochlea within primary auditory cortex in the cat. *J. Neurophysiol.* 38:231-249.

UCSF LIBRARY

1000 PARNASSUS AVENUE, SAN FRANCISCO, CALIFORNIA 94143-1102

Merzenich, M.M. and White, M. (1977). Cochlear implant: The interface problem. In: *Functional Electrical Stimulation*, F.T. Hambrecht and J. B. Reswick (Eds.), Decker (pp.321-339).

Merzenich, M.M., Kaas, J.H., Wall, J.T., Nelson, R.J., Sur, M. and Felleman, D.J. (1983a). Topographic reorganization of somatosensory cortical areas 3B and 1 in adult monkeys following restricted deafferentation. *J. Neurosci.* 10:33-55.

Merzenich, M.M., Kaas, J.H., Wall, J.T., Nelson, R.J., Sur, M., and Felleman, D.J. (1983b). Progression of change following median nerve section in the cortical representation of the hand in areas 3b and 1 in adult owl and squirrel monkeys. *J. Neurosci.* 10:639-665.

Merzenich, M.M., Nelson, R.J., Stryker, M.P., Cynader, M.S., Shoppmann, A. and Zook, J.M. (1984). Somatosensory cortical map changes following digital amputation in adult monkey. *J. Comp. Neurol.* 224:591-605.

Michelson, R.P. (1971). The results of electrical stimulation of the cochlea in human sensory deafness. *Ann. Otol. Rhinol. Laryngol.* 80:914-919.

Middlebrooks, J.C., Dykes, R.W. and Merzenich, M.M. (1980). Binaural response-specific bands in primary auditory cortex (AI) of the cat: topographical organization orthogonal to isofrequency contours. *Brain Research* 181:31-48.

Oonishi, S. and Katsuki, Y. (1965). Functional organization and integrative mechanism on the auditory cortex of the cat. *Jap. J. of Physiol.* 15:342-365.

JOSE LIBRARY

Owens, E., Kessler, D.K. and Raggio, M.W. (1983). Results for some patients with cochlear implants on the Minimal Auditory Capabilities (MAC) Battery. In: *Cochlear Protheses-An International Symposium*, C. Parkins and S. Anderson (Eds.), The New York Academy of Sciences (pp.443-450).

Owens, E., Kessler, D.K., Raggio, M.W. and Schubert, E.D. (1985). Analysis and revision of the Minimal Auditory Capabilities (MAC) Battery. *Ear and Hearing* 6:280-287.

Parkins, C.W. (1989). Temporal response patterns of auditory nerve fibers to electrical stimulation in deafened squirrel monkeys. *Hearing Research* 41:137-168.

Phillips, D.P. and Irvine, D.R.F. (1981). Responses of single neurons in physiologically defined primary auditory cortex (AI) of the cat: frequency tuning and responses to intensity. *J. Neurophysiol.* 45:48-58.

Phillips, D.P., Orman, S.S., Musicant, A.D. and Wilson, G.F. (1985). Neurons in the cat's primary auditory cortex distinguished by their responses to tones and wide-spectrum noise. *Hearing Research* 18:73-86.

Phillips, D.P. and Cynader, M.S. (1985). Some neural mechanisms in the cat's auditory cortex underlying sensitivity to combined tone and wide-spectrum noise stimuli. *Hearing Research* 18:87-102.

Phillips, D.P. and Hall, S.E. (1986). Spike-rate intensity functions of cat cortical neurons studied with combined tone-noise stimuli. *J. Acoust. Soc. Am.* 80:177-187.

U.S. LIBRARY

Phillips, D.P. and Hall, S.E. (1987). Responses of single neurons in cat auditory cortex to time-varying stimuli: linear amplitude modulations. *Exp. Brain Res.* 67:479-492.

Phillips, D.P. (1988). Effect of tone-pulse rise time on rate-level functions of cat auditory cortex neurons: excitatory and inhibitory processes shaping responses to tone onset. *J. Neurophysiol.* 59:1524-1539.

Phillips, D.P., Hall, S.E. and Hollett, J.L. (1989). Repetition rate and signal level effects on neuronal responses to brief tone pulses in cat auditory cortex. *J. Acoust. Soc. Am.* 85:2537-2549.

Phillips, D.P. and Sark, S.A. (1991). Separate mechanisms control spike numbers and inter-spike intervals in transient responses of cat auditory cortex neurons. *Hearing Research* 53:17-27.

Prieto, J.J. and Winer, J.A. (1992). Organization of GABAergic neurons and axon terminals in cat primary auditory cortex. *Soc. Neurosci. Abstr.* 22:434.1.

Rasmussen, D.D. (1982). Reorganization of raccoon somatosensory cortex following removal of the fifth digit. *J. Comp. Neurol.* 205:313-326.

Reale, R.A. and Imig, T.J. (1980). Tonotopic organization in auditory cortex of the cat. *J. Comp. Neurol.* 192:265-291.

Recanzone, G.H., Allard, T.T., Jenkins, W.M. and Merzenich, M.M. (1990). Receptive field changes induced by peripheral nerve stimulation in SI of adult cats. *J. Neurophysiol.* 63:1213-1225.

JOSE LIBRARY

Recanzone, G.H., Merzenich, M.M. and Schreiner, C.E. (1993). Plasticity of frequency representation in the primary auditory cortex following discrimination training in adult owl monkeys. *J. Neurosci.* (In press)

Rees, A. and Møller, A.R. (1987). Stimulus properties influencing the responses of inferior colliculus neurons to amplitude-modulated sounds. *Hearing Research* 27:129-143.

Robertson, D. and Irvine, D.R.F. (1989). Plasticity of frequency organization in auditory cortex of guinea pigs with partial unilateral deafness. *J. Comp. Neurol.* 282:456-471.

Roth, G.L., Aitkin, L.M., Andersen, R.A. and Merzenich, M.M. (1978). Some features of the spatial organization of the central nucleus of the inferior colliculus of the cat. *J. Comp. Neurol.* 182:661-680.

Schindler, R.A. and Kessler, D.K. (1987). The UCSF/Storz cochlear implant: patient performance. *The Am. J. of Otol.* 8:247-254.

Schindler, R.A. and Kessler, D.K. (1989). State of the art of cochlear implants-the UCSF experience. *The Am. J. of Otol.* 10:79-83.

Schreiner, C.E. and Cynader, M.S. (1984). Basic functional organization of second auditory cortical field (All) of the cat. *J. Neurophysiol.* 51:1284-1305.

Schreiner, C.E. and Joris, P.X. (1986). Intrinsic oscillations in the primary auditory cortex of cats. In: *IUPS Satellite Symposium on Hearing*, University of California, San Francisco, (p. 81).

UCSF LIBRARY

Schreiner, C.E. and Urbas, J.V. (1988). Representation of amplitude modulation in the auditory cortex of the cat. II. Comparison between cortical fields. *Hearing Research* 32:49-64.

Schreiner, C.E. and Langner, G. (1988). Periodicity coding in the inferior colliculus of the cat. II. Topographical organization. *J. Neurophysiol.* 60:1823-1840.

Schreiner, C.E., Mendelson, J.R., Grasse, K. and Sutter, M.L. (1988). Spatial distribution of basic response properties in cat primary auditory cortex. *Assoc. Res. Otolaryngol. Abstr.* 11:36.

Schreiner, C.E. and Mendelson, J.R. (1990). Functional topography of cat primary auditory cortex: distribution of integrated excitation. *J. Neurophysiol.* 64:1442-1459.

Schreiner, C.E. and Sutter, M.L. (1992). Topography of excitatory bandwidth in cat primary auditory cortex: single-neuron versus multiple-neuron recordings. *J. Neurophysiol.* 68:1487-1502.

Schreiner, C.E., Mendelson, J.R. and Sutter, M.L. (1992). Functional topography of cat primary auditory cortex: representation of tone intensity. *Exp. Brain Research.* (In press)

Shamma, S.A., Fleshman, J.W. and Wiser, P.R. (1992). Organization of response areas in primary auditory cortex in the ferret: spectral organization columns. *J. Neurophysiol.* (In press)

JOSE LIBRARY

Simmons, F.B. (1966). Electrical stimulation of the auditory nerve in man. *Arch. Otolaryngol.* 84:2-54.

Snyder, R.L., Rebscher, S.J., Cao, K., Leake, P.A. and Kelly, K. (1990). Chronic intracochlear electrical stimulation in the neonatally deafened cat. I: Expansion of central representation. *Hearing Research* 50:7-34.

Snyder, R.L., Rebscher, S. J., Leake, P.A., Kelly, K. and Cao, Keli (1991). Chronic intracochlear electrical stimulation in the neonatally deafened ear. II: Temporal properties of neurons in the inferior colliculus. *Hearing Research* 56: 246-264.

Spivak, L.G. and Waltzman, S.B. (1990). Performance of cochlear implant patients as a function of time. *J. Speech and Hearing Research* 33:511-519.

Suga, N. (1977). Amplitude-spectrum representation in the Doppler-shift processing area of the auditory cortex of the mustached bat. *Science* 196:64-67.

Suga, N. (1988). Neuroethology and speech processing: complex-sound processing by combination-sensitive neurons. In: *Auditory Function- Neurobiological Bases of Hearing*, G.M. Edelman, W.E. Gall, W.M. Cowan (Eds.), John Wiley & Sons (pp.672-720).

Sutter, M.L. and Schreiner, C.E. (1991). Physiology and topography of neurons with multi-peaked tuning curves in cat primary auditory cortex. *J. Neurophysiol.* 65:1207-1226.

UCSF LIBRARY

Sutter, M.L. and Schreiner, C.E. (1993). Topography of sensitivity and sharpness of intensity tuning in cat primary auditory cortex: single-neuron versus multiple-neuron recordings. (In preparation)

Thielemeir, M.A. (1983). Status and results of the House Ear Institute cochlear implant project in adults. In: *Cochlear Implants*, R.A. Schindler and M.M. Merzenich (Eds)., Raven Press (pp.455-460).

Thompson, R.F., Patterson, M.M. and Teyler, T.J. (1972). The neurophysiology of learning. *Annual Review of Psychology* 23:73-104.

van den Honert, C. and Stypulkowski, P.H. (1984). Physiological properties of the electrically stimulated auditory nerve. II. Single fiber recordings. *Hearing Research* 14:225-243.

van den Honert, C. and Stypulkowski, P.H. (1987a). Single fiber mapping of spatial excitation patterns in the electrically stimulated auditory nerve. *Hearing Research* 29:195-206.

van den Honert, C. and Stypulkowski, P.H. (1987b). Temporal response patterns of single auditory nerve fibers elicited by periodic electrical stimuli. *Hearing Research* 29:207-222.

Vureck, L.S., White, M., Fong, M. and Walsh, S.M. (1981). Optoisolated stimulators used for electrical evoked BSER. *Ann. Otol. Rhinol. Laryngol.* 90 (Suppl. 82): 21-24.

Weinberger, N.M., Hopkins, W. and Diamond, D.M. (1984). Physiological plasticity of single neurons in auditory cortex of the cat during acquisition

JOSE LIBRARY

of the pupillary conditioned response: I. Primary field (AI). *Behav. Neurosci.* 98:171-188.

Weinberger, N.M. and Diamond, D.D. (1987). Dynamic modulation of the auditory system by associative learning. In: *Auditory Function - Neurobiological Bases of Hearing*, G.M. Edelman, W.E. Gall, and W.M. Cowan (Eds.), John Wiley & Sons (pp.485-512).

Wilson, B.S., Finley, C.C. and Lawson, D.T. (1989). Representations of speech features with cochlear implants. In: *Cochlear Implants-Models of the Electrically Stimulated Ear*, J.M. Miller and F.A. Spelman (Eds.), Springer-Verlag (pp.339-376).

Wilson, B.S., Finley, C.C., Lawson, D.T., Wolford, R.D., Eddington, D.K. and Rabinowitz, W.M. (1991). Better speech recognition with cochlear implants. *Nature* 352:236-238.

Woolsey, C.N. and Walzl, E.M. (1942). Topical projection of nerve fibers from local regions of the cochlea to the cerebral cortex of the cat. *Bulletin of The Johns Hopkins Hospital*, 71:315-344.

Zeng, F.G. and Shannon, R.V. (1992). Loudness balance between electric and acoustic stimulation. *Hearing Research* 60:231-235.

UCSF LIBRARY

197950

JOSE LIBRARY

UCSF LIBRARY

FOR REFERENCE

NOT TO BE TAKEN FROM THE ROOM



CAT. NO. 23 012



609993



3 1378 00609 9934

